



Terms and Conditions of Use of Digitised Theses from Trinity College Library Dublin

Copyright statement

All material supplied by Trinity College Library is protected by copyright (under the Copyright and Related Rights Act, 2000 as amended) and other relevant Intellectual Property Rights. By accessing and using a Digitised Thesis from Trinity College Library you acknowledge that all Intellectual Property Rights in any Works supplied are the sole and exclusive property of the copyright and/or other IPR holder. Specific copyright holders may not be explicitly identified. Use of materials from other sources within a thesis should not be construed as a claim over them.

A non-exclusive, non-transferable licence is hereby granted to those using or reproducing, in whole or in part, the material for valid purposes, providing the copyright owners are acknowledged using the normal conventions. Where specific permission to use material is required, this is identified and such permission must be sought from the copyright holder or agency cited.

Liability statement

By using a Digitised Thesis, I accept that Trinity College Dublin bears no legal responsibility for the accuracy, legality or comprehensiveness of materials contained within the thesis, and that Trinity College Dublin accepts no liability for indirect, consequential, or incidental, damages or losses arising from use of the thesis for whatever reason. Information located in a thesis may be subject to specific use constraints, details of which may not be explicitly described. It is the responsibility of potential and actual users to be aware of such constraints and to abide by them. By making use of material from a digitised thesis, you accept these copyright and disclaimer provisions. Where it is brought to the attention of Trinity College Library that there may be a breach of copyright or other restraint, it is the policy to withdraw or take down access to a thesis while the issue is being resolved.

Access Agreement

By using a Digitised Thesis from Trinity College Library you are bound by the following Terms & Conditions. Please read them carefully.

I have read and I understand the following statement: All material supplied via a Digitised Thesis from Trinity College Library is protected by copyright and other intellectual property rights, and duplication or sale of all or part of any of a thesis is not permitted, except that material may be duplicated by you for your research use or for educational purposes in electronic or print form providing the copyright owners are acknowledged using the normal conventions. You must obtain permission for any other use. Electronic or print copies may not be offered, whether for sale or otherwise to anyone. This copy has been supplied on the understanding that it is copyright material and that no quotation from the thesis may be published without proper acknowledgement.

**Biological Investigations of Novel 1,8-
Naphthalimide Compounds and the Design
and Synthesis of Pyridine Based Polyamides**

By

Daniel Ómar Frímannsson

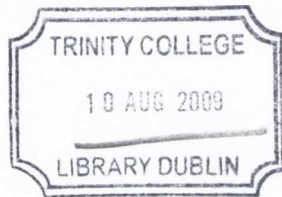
October 2008



**University of Dublin
Trinity College**

**Based on the research carried out under the direction of Prof. Thorfinnur
Gunnlaugsson and Prof. Mark Lawler**

*A thesis submitted to the School of Chemistry, University of Dublin, Trinity
College in fulfillment of the requirements for the degree of Doctor of
Philosophy.*



THOSIS
8785

Declaration

This thesis is being submitted for the degree of Doctor of Philosophy in the University of Dublin, Trinity College Dublin and has not been submitted before for any degree or examination in this or any other University. Except where acknowledgment is given, all work described is original and carried out by the author alone. Permission is granted so that the Library may lend or copy this thesis upon request. This permission covers only single copies made for study purposes, subject to normal conditions of acknowledgement.

)
son

...But I can't do this all on my own,
No, I know I'm no Superman...
Lazlo Bane; Scrubs Theme Song

Acknowledgements

First of all, I would like to thank my friends and supervisors, Prof. Thorri Gunnlaugsson and Prof. Mark Lawler for giving me the opportunity to work in such a great research environment. I have learnt a lot from you the last four years. My greatest lesson was something you both agreed on; “it does not matter, it is always going to be last minute.”

I would like to thank my two research groups that have always welcomed me, even though they did not see me for a month at a time. Firstly, the Lawler research group that included the hypoxia working people, Laura and Lynn and the methylation (smethylation) subgroup with Therese (Smurf) and Antoinette. Also, big thanks to Lisa, Jackie, Ruth, Prerna and Linda for all their help and company. Huge thanks to Tony, who guided me through the wonders of cell culture and related worlds. Thanks a million for all your help. Lastly, I would like to thank my good friend Elaina, for all your help and great company through these four years; we have finally made it!

Secondly, huge thanks to the Gunnlaugsson research members, both former and present. Big thanks to Ann-Marie, Joe, Andrew, Celine, Lisa, Eoin, Flo, and Lin for all their help when I was starting. The “first-years”, Laura and Elaine for doing some last minute changes and good vibes. Brian and Sam for all their help making tea and reading over my chapters. Thank you Rob, for reading my chapters and boosting up my confidence by allowing me trash you at football. Big thanks to Christophe and Jen for your enormous help during the preparation of this thesis, now you guys behave! I would like to thank the post-docs of the group (in no special order...or what?), Cidalia, Aline, Steve, Celia and Emma for all their help, especially Emma that corrected this thesis nearly three times. I would like to thank the original “first-years” Doireann (JD), Rebecca and Claire for your great stories over the years and all the great laughs you gave me! You are great! Thanks Niamh for all your help coping with stress meanwhile writing this thesis. I still cant believe that we are printing out and it is 3 am. Finally, I would like to thank my greatest friends, Sally (Big Mama) and Gary (Vanilla Bear) for all the fun we had, the great nights and the adventures. I will never forget those moments with you, such as the Aussie rules match (where I shook the hand of the Irish president) and all those long weekends with the Ryan family.

Thanks to all the technical and administrative staff in the School of Chemistry; John, Manuel, Martin, Fred, Patsy, Brendan, Peggy, Tom, Teresa, Corinne, Helen, Maria and Tess.

Finally I would like to thank my parents and grandparents for all their support over the years. Eins og ég hef alltaf sagt, þá er þetta bara eitt af þeim fáu skrefum sem við höfum öll tekið saman, alveg frá því að ég datt í sjóinn í Hafnarfirðinum hérna í gamla daga.

I also want to thank my sister Andrea and my brother Bjarki for being there for me when I needed it the most. Héðan í frá vil ég verða kallaður doktor, doc eða doktorinn. Ég hugsaði til ykkar á hverjum degi síðan ég flutti út.

Finally, thank you Una for all your understanding over the last four years. Without you by my side, I would never ever managed to finish this work. There have been so many funny moments we have shared over these last years here in Ireland. Það eru búnar að vera svo frábærar og skemmtilegar minningar þessi seinustu ár og ég bara trúi ekki að við séum loksins að verðar alvöru doktorar.

Abbreviations

APL	Acute Promyelocytic Leukemia
A	Adenine
Bpy	Bipyridine
<i>ct</i> -DNA	Calf Thymus DNA
δ	Chemical shift
CHCl ₃	Chloroform
CML	Chronic Myelogenous Leukemia
CD	Circular Dichroism
<i>J</i>	Coupling constant
C	Cytosine
DCM	Dichloromethane
DNA	Deoxyribonucleic Acid
DMAP	4-(N, N-dimethylamino)pyridine
DMF	Dimethylformamide
d	doublet
dd	double doublet
Eq.	Equivalents
EtOH	Ethanol
G	Guanine
Hz	Hertz
HPLC	High Performance Liquid Chromatography
HCl	Hydrochloride Acid
IR	Infrared
MgSO ₄	Magnesium Sulphite
m.p.	Melting Point
MeOH	Methanol
m	Multiplet
MTT	3-(4,5-dimethylthiazol-2-yl)-2,5-diphenyl tetrazolium bromide
NAT2	<i>N</i> -acetyltransferase 2
NMR	Nuclear Magnetic Resonance
ppm	Parts Per Million
PBS	Phosphate buffered saline

KMnO ₄	Potassium permanganate
q	quartet
ROS	Reactive Oxygen Species
s	singlet
H ₂ SO ₄	Sulphuric acid
Boc	<i>tert</i> -butoxycarbonyl
T _m	Thermal Melting
THF	Tetrahydrofuran
T	Thymine
Topo I	Topoisomerase I
Topo II	Topoisomerase II
t	triplet
Uv	Ultraviolet
λ	Wavelength

Summary

This thesis entitled “Biological Investigations of Novel 1,8-Naphthalimide Compounds and the Design and Synthesis of Pyridine Polyamides” is divided into six chapters. Chapter 1, the introduction focuses on the basic cellular mechanisms, such as growth and programmed cell death and their connection to cancer. Furthermore, the different means of inhibiting the growth of cancer cells is discussed, followed by examples of organic compounds that have been synthesised with that in mind. Special focus will be given to the genetic material, DNA and agents that have been designed to interact with it.

Chapter 2 describes the biological investigations of a series of peptide based 1,8-naphthalimide conjugates. The different structural components of these systems were compared and it was shown that the 4-nitro-1,8-naphthalimide conjugates were substantially more potent against the growth of HL-60 cells, an acute promyelocytic leukemia cell line. In addition, these compounds were shown to induce apoptosis after 24 hours incubation. However, flow cytometry analysis of the cellular uptake and fluorescent microscopy studies indicated that these compounds underwent a transformation within cells, resulting in less cytotoxic activity after 48 hours.

Chapter 3 details the results of biological studies carried out on three novel Tröger's base 1,8-naphthalimide possessing different amino side chains. These compounds were shown to be rapidly entered HL-60 cells and were shown to localise in the nucleus of these types of cells within 24 hours of incubation. These Tröger's bases were shown to have similar cytotoxicity as their 4-amino-1,8-naphthalimide precursors and results indicated that the pK_a of the corresponding amino side chains were shown to be highly influential in their biologic activity. Cell cycle analysis and topoisomerase inhibition studies indicated that the biological activity exerted by Tröger's base derivatives possibly involved the binding to DNA and the subsequent inhibition of the Topoisomerase I and II enzymes.

Chapter 4 describes the biological examination of a series of Ru(II)-1,8-naphthalimide conjugates and their evaluation as potential photodynamic therapy agents. These agents were entered cells according to flow cytometry and were shown to mainly localise within the nucleus. Cytotoxicity studies showed that these compounds were relatively non-toxic in the dark. However upon photoactivation their cytotoxicity was dramatically increased. Further studies into the mechanism of action of these compounds revealed that these complexes induced a G₂/M arrest and lead to the loss of the

mitochondrial membrane potential, possibly arising from the production of reactive oxygen.

Chapter 5 describes work towards synthesising the polyamides based on the pyridine amino acid structure is described. The synthesis of the pyridine amino acid and the corresponding di-peptide were proven successful as demonstrated by X-ray crystallography. In addition, these pyridine units were found to react with numerous moieties, which could improve the water solubility and the DNA binding affinity with DNA. Finally, characterisation of these compounds is presented in Chapter 6 along with the detailed experimental procedure that were employed during the course of this PhD work.

Table of Contents

Acknowledgements	i
Abbreviations	ii

Chapter 1 - Introduction

Introduction	1
Causes and Cure of Cancer	1
<i>The Loss of Cell Growth Control</i>	3
<i>Evasion of Cell Death</i>	6
Cancer Classification	12
Cancer Treatment	14
<i>Chemotherapy</i>	14
<i>Targeting the Genetic Material</i>	17
<i>Covalent Binding</i>	21
<i>Intercalation Interaction</i>	22
<i>Electrostatic Interaction</i>	25
<i>Hydrogen Bonding Interaction</i>	26
Conclusion	29
Work Described in This Thesis	30

Chapter 2 – The Biological Examination of Peptide Based 1,8-Naphthalimides

Introduction	32
<i>Previous Work From the Gunnlaugsson Research Group</i>	35
<i>The Work Described in This Chapter</i>	39
Cellular Uptake and Localisation Studies of 47-51	41
<i>Cellular Uptake Studies Using Flow Cytometry</i>	41
<i>Localisation Studies on 48-50 Using Fluorescent Microscopy</i>	46
<i>Summary</i>	49
The Cytotoxic Activity of 47-51 Against HL-60 Cells	49
Investigation of the Mechanism of Cell Death Exerted by 47-51	54
<i>Investigation of the Cell Morphology After Treatment With 47-51</i>	54
<i>Detection of DNA Fragmentation Induced by 47-51</i>	58
<i>Summary</i>	60
Cell Cycle Analysis	60
Topoisomerase I and II Activity Studies	65
Conclusion and Future Studies	68

Chapter 3 – Biological Evaluation of 1,8-Naphthalimides Containing Tröger's Bases

Introduction	71
<i>Tröger's Base Analogues as Targets of DNA</i>	72
<i>Design of 1,8-Naphthalimides Based Tröger's Base</i>	74
Analysis of Cellular Uptake and Localisation of 68-70	76
<i>Uptake Studies of 68-70 Using Flow Cytometry</i>	76
<i>Localisation Studies of 68-70 Using Confocal Microscopy</i>	83
<i>Summary</i>	80

Cytotoxicity Studies 65-70	83
Cell Cycle Analysis and Investigation of the Mode of Cell Death Induced by 65-70	87
<i>Cell Cycle Studies of HL-60 Cells Treated With 65-70</i>	87
<i>Cell Morphology Investigation After Treatment With 65-70</i>	90
<i>Summary</i>	92
The Effects of 68-70 on Topo I and II Activity	93
<i>Topo I Investigations</i>	96
<i>Topo II Investigations</i>	99
<i>Summary</i>	100
Conclusion and Future Studies	100

Chapter 4—Biological Evaluation of Ru(II)-1,8-Naphthalimide Conjugates as PDT Agents

Introduction	103
<i>The design of Ru(II)-1,8-Naphthalimide Conjugates as PDT agents</i>	106
<i>Objectives of Current Studies</i>	107
Analysis of Cellular Uptake and Localisation of 74-77	108
<i>Cellular Uptake Studies Using Flow Cytometry</i>	108
<i>Cellular Localisation studies of 74-77</i>	111
<i>Summary</i>	113
Cytotoxicity and Phototoxicity of 74-77	113
Formation of ROS in Cells after Treatment with 74-77	119
The Effects on the Cell Cycle after Treatment with 74-77	122
Changes in the Mitochondrial Membrane Potential Induced by 74-77	125
Conclusion and Future Studies	129

Chapter 5-The Synthesis of Pyridine Based Minor Groove Binders

Introduction	131
<i>The Objectives of This Research</i>	133
The Synthesis Pyridine Building Blocks	135
<i>Synthesis of an Amino Protected Pyridine Carboxylic Acid Derivatives</i>	135
<i>Synthesis of a Carboxylic Acid Protected Pyridine Amine Derivatives</i>	138
<i>Summary</i>	140
Pyridine Polyamide Synthesis and Investigations	141
<i>The Synthesis of a di-peptides and Symmetrical Tri-peptides</i>	141
Conclusion and Future Studies	155

Chapter 6-Experimental	158
Chapter 7-References	176
Appendix 1	183
Appendix 2	206
Appendix 3	213
Appendix 4	216

1 Introduction

1.1 Introduction

Cancer is a generic term used to describe more than 200 diseases that can affect different parts of the human body. With an estimated 3.2 million new cases and 1.7 million deaths each year, cancer remains an important public health problem in Europe.¹ Due to the strong association between age and cancer, it is predicted that these numbers will continue to rise.² The above numbers are especially relevant to Ireland, because according to a study carried out by Berino *et al.*³, Irish cancer patients have about a 50% survival rate. This only underlines the urgency for a better understanding of the disease, which will lead to improved drugs and increased survival rates.

This *Thesis* will discuss the synthesis and biological activity of four novel types of compounds that might improve the selectivity and potency of the current anticancer treatment. The first three approaches were inspired by the 1,8-naphthalimide chromophore and its potential to interact with the genetic material. Firstly, amino acids were introduced to enhance the selectivity of the 1,8-naphthalimide unit, while the introduction of a Tröger's base structural unit to the 1,8-naphthalimide chromophore reinforced its binding capacity to the genetic material. These approaches have been extensively reviewed within the Gunnlaugsson group, in the PhD theses of Phelan⁴, Hussey⁴, Gillespie⁵ and Veale.⁶ The third approach involved novel photodynamic therapy agents, based on the ruthenium(II)-1,8-naphthalimide conjugates. These conjugate systems were constructed of units that were known to interact with the genetic material, as will be discussed later in this chapter. The last approach discussed in this *Thesis*, involved the synthesis of pyridine polyamides. This work was inspired by the binding selectivity of natural products, such as netropsin as will be discussed in detail in this chapter.

Furthermore, this chapter will deal with cell proliferation and its connection to cancer along with the involvement of the genetic material in the cause of cancer. Examples of different modes of binding to the genetic material will be given and the history and development of relevant compounds will be discussed in detail. However, in order to understand how cancer occurs and the possible ways to intervene, it is important to describe the structure of cells and their cellular processes.

1.2 Causes and the Cure of Cancer

The mechanism by which cancer arises is generally considered to be as a result of changes to the genome, *i.e.* point mutations, gene amplifications, chromosomal deletions

and translocations.⁷ These changes may lead to abnormal regulation (over or under activation of genes), failure of expression of genes, or alteration of a gene, ultimately affecting the cell function. This transformation is passed on from an individual cell to its progeny, leading to cell accumulation.

There are two different aspects to the connection between cancer and the genome. The first type includes inherited defects, called germline mutations, which increase cancer susceptibility. These neoplasm only count for about 1-2% of total cancers and approximately 50 forms of hereditary cancers have been reported.⁸ Examples of hereditary cancers include *retinoblastoma* and *xeroderma pigmentosum*. The second group involves changes of the genetic material that occur over time due to both environmental carcinogens and spontaneous degeneration. These changes are called somatic mutations and the outcome depends on the severity of these changes and the accuracy of the physiological repair progress. Severe damage is followed by cellular death, while a repair follows non-lethal damage. This repair might introduce a mutation, which may influence the cell's behavior. The mutated cell and its descendants become more susceptible to subsequent mutations and could gradually accumulate enough damage so that the normal cell growth control is perturbed.

There are several lines of evidence that tumor formation is a multi-step process and each step represents a genomic alteration that drives the transformation of normal human cells into highly malignant derivatives.⁸⁻¹⁰ In addition, pathological analyses have revealed lesions that represent intermediate steps in transformation from a normal human cell into invasive cancer.^{11,12} Furthermore, Hanahan *et al.*¹³ proposed six capabilities that is shared by most cancer cell types;

- **limitless replicative potential,**
- **sustained angiogenesis tissue,**
- **invasion and metastasis,**
- **self-sufficiency in growth signals,**
- **insensitivity to anti growth signals,**
- **evasion of programmed cell death.**

Cellular proliferation is normally controlled by external factors, among which the most important are growth factors and hormones.¹⁴ However, most cancer cells have

overcome the need for growth factors or have become resistant to anti-growth signals and as a result, cancer cells grow in an unregulated manner. This loss of cell growth control occurs when mutations arise in two broad families of genes that regulate growth; proto-oncogenes that produce an oncogene with a dominant gain of function and tumor suppressor genes, which leads to a recessive loss of function. This will be discussed in detail in the next section.

1.2.1 The Loss of Cell Growth Control

Cell growth has two components, proliferation and differentiation.¹⁴ Differentiation is the sum of all the processes by which a cell in a developing organism achieves a special set of structural and functional characteristics that distinguishes the progeny cells from their parent cells.⁷ In a developing tissue, normal cells have a short life after they reach maturity. On the contrary, differentiation is frequently arrested in malignant cells.¹⁴ Differentiation arrest affects cancer cells at different points along the maturity pathway and this will impact the tumor growth, especially if the arrest occurs before the cell loses its ability to multiply. If cancer cells stay immature and divide, cells may grow more rapidly and the tumor may become more aggressive.¹⁴ The control of differentiation is not fully understood but there are indications that differentiation is controlled, at least partly, by proto-oncogenes.¹⁴

Cell proliferation is a complex cellular process that is regulated with a balance between growth stimulating and growth suppressing factors.¹⁵ Each dividing cell must go through a specific sequence of events that concludes with the production of two daughter cells. These series of events are collectively termed the cell cycle, which is depicted in Figure 1.1. While extended reviews have been published on the mode of the cell cycle,^{16,17} a few key features will be described herein and will be referred to later in this *Thesis*. The major phases of the cell cycle are **G₀**, **G₁**, **S**, **M** and **G₂** (Figure 1.1). Resting cells are in **G₀** phase and in order to divide (and enter **G₁** phase), they must be induced by external growth factors. In contrast to **G₁**, the **S** phase proceeds without growth factors. The amount of enzymes involved in genome duplication increases in the beginning of the **S** phase and they move from the cytoplasm where they are synthesised, to the nucleus where genome is duplicated. After the genetic material has been duplicated, cells enter the **G₂** phase where proteins necessary for mitosis are synthesised. Finally, the **M** phase (mitosis) is subdivided into four main stages; **prophase**, **metaphase**, **anaphase** and **telophase** (Figure 1.2).¹⁸

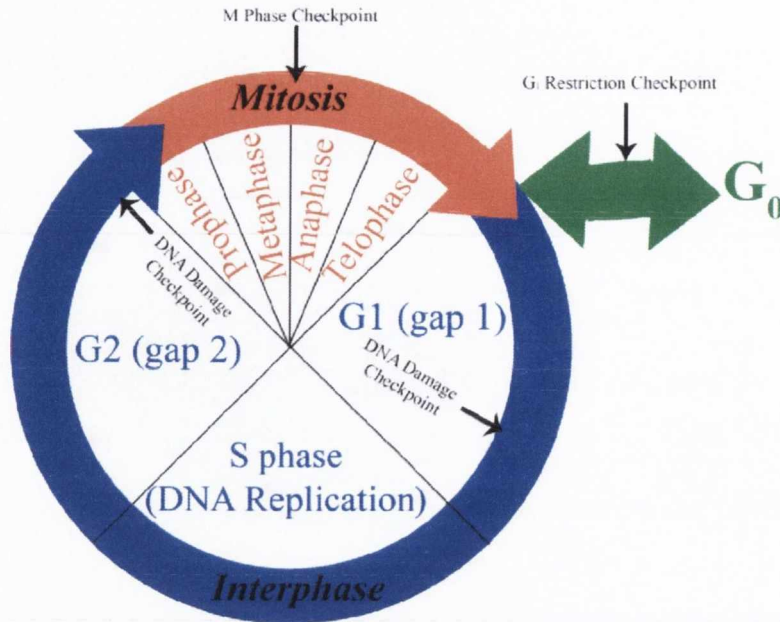


Figure 1.1 A schematic representation of the cell cycle. Resting cells (G_0) are stimulated by external growth factors to enter the G_1 phase. Upon adequate levels of growth signals, the cell will proceed in G_1 . The genome of the cell undergoes the first examination before entering S phase where the DNA is duplicated. After the genetic material has been duplicated, cells enter G_2 , where the genome undergoes the second examination. Finally, during the four stages of mitosis the chromosomes condense, align and separate, leading to cell division. The M phase checkpoint ensures that the chromosomes are correctly aligned.

During **prophase**, the chromosomes have condensed and are visible as two identical coiled filaments; the *sister chromatids* that are held together by a *centromer* (Figure 1.2 **B**). The nuclear membrane starts to disintegrate and *centrioles*, which are responsible for organising a network of microtubules, move apart to opposite poles. Microtubules radiate from each centriole, forming *asters* (Figure 1.2 **C**). These radiating microtubules, together with associated proteins are named the *spindle* and during **metaphase**, the spindle connects the centrioles to the centromers of the condensed chromosomes (Figure 1.2 **D**). These spindle fibers catalyse the movement of the sister chromatids to the equatorial plane of the cell. In early **anaphase**, the sister chromatids separate at their centromers and migrate to the opposite poles of the cell (Figure 1.2 **E**). The cell elongates and starts to pinch at the center (Figure 1.2 **F**). In **telophase**, the chromosomes start to uncoil and become less condensed. The nuclear membranes starts to form and surround the two sets of daughter chromosomes (Figure 1.2 **G**). Simultaneously, there is division of the cell cytoplasm and separation (cytokinesis) of the two daughter cells (Figure 1.2 **H**).

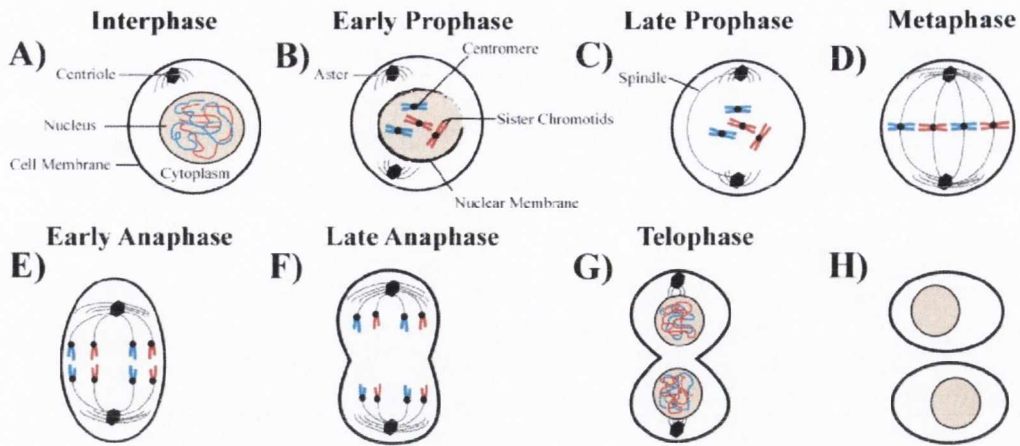


Figure 1.2 The stages of mitosis. *A) Prior to mitosis, the genome has been replicated. B) In early prophase, the centrioles divide and start to move toward the opposite poles of the cell. The chromosomes begin to condense and the nuclear membrane starts to disaggregate. C) Chromosome condensation is complete. The centrioles are situated at the opposite poles. D) During metaphase, the chromosomes align in the equatorial plane and their centromeres are attached to the spindle fibers. E) The centromeres split, donating one copy of each chromosome to each daughter cell. Simultaneously, the cell elongates. F) The chromosomes have almost reached their respective poles and the cell membrane begins to pinch at the center. G) New membranes form around the daughter nuclei and the chromosome uncoil. Cytokinesis is nearly complete and the spindle fibers disappear. H) Upon completion of cytokinesis, the cell enters the G_1 phase of the cell cycle and proceeds again around the cycle.*

The events that regulate the cell cycle are called checkpoints and are based upon pathways and feedback mechanisms that ensure that a phase of the cell cycle does not begin until the preceding phase has been completed. There are four major checkpoints in the cell cycle; the G_1 restriction checkpoint and the genome damage checkpoints in G_1 and G_2 and the M phase checkpoint (Figure 1.1). The G_1 restriction checkpoint is activated upon inadequate levels of growth factors and the cell reverts back to G_0 . This restriction control point is defective in cancer cells, allowing them to continue growing under conditions that keep normal cells in G_0 .¹⁹ The genome damage checkpoints causes a delay in either G_1 or G_2 that prevents the cell from entering the next phase until the damage has been repaired. Several oncogenes have been implicated in these checkpoint mechanisms, among them the tumor suppressor genes, *p53* and *ataxia telangiectasia gene*, *ATM*.^{11,12} In addition, if the damage has not been rectified during this delay, the cells progress into the next phase with the damage, resulting in mutations that can lead to cancerous growth.²⁰ The M phase checkpoint ensures that the segregation is carried out correctly and the

chromosomes are correctly aligned. Mutations of mitotic checkpoint genes are found in cancers, causing severe damage to daughter cells.²¹

As mentioned above, activated checkpoints give the cell time to repair any damage to the genome, but if the damages is not soon corrected the cells will initiate *programmed cell death* or *apoptosis*, as will be discussed in the following section. This mechanism will prevent any mutations to be carried on to progeny cells.¹⁴ However, cancer cells have found a way to circumvent this programmed death mechanism, resulting in cell accumulation that is characteristic for tumor progression.¹³

1.2.2 Evasion of Cell Death

Programmed cell death was first observed in 1971 and was named *apoptosis*.²² This mechanism has now been accepted as the major mode of *programmed cell death*, which normally occurs during the development and aging of a cell and as a homeostatic mechanism to maintain cell population in tissues.²³ Other modes of programmed cell death have recently been described, such as *pyroptosis* and *autophagy*.²⁴

The alternative to programmed cell death is *necrosis*, which is a process that is caused by interference of the energy supply of the cell or direct damage to cell membranes. Necrosis results in cell swelling and chromatin dissolution (karyolysis) whereas apoptosis involves cell shrinkage, chromatin condensation (pyknosis) and nuclear fragmentation (karyorrhexis) as explained schematically in Figure 1.3 and Table 1.1, respectively. These two types of cell death are both mechanically and morphologically different but there is evidence of a considerable amount of overlap between them.^{24,25}

Table 1.1 Comparison of morphological features of apoptosis and necrosis.

Apoptosis	Necrosis
<i>Energy dependant</i>	<i>Energy independant</i>
<i>Cell Shrinkage</i>	<i>Cell Swelling</i>
<i>Pyknosis and karyorrhexis</i>	<i>Karyolysis</i>
<i>Intact cell membrane</i>	<i>Disrupted cell membrane</i>
<i>Cytoplasm retained in apoptotic bodies</i>	<i>Cytoplasm released</i>
<i>No inflammation</i>	<i>Inflammation</i>

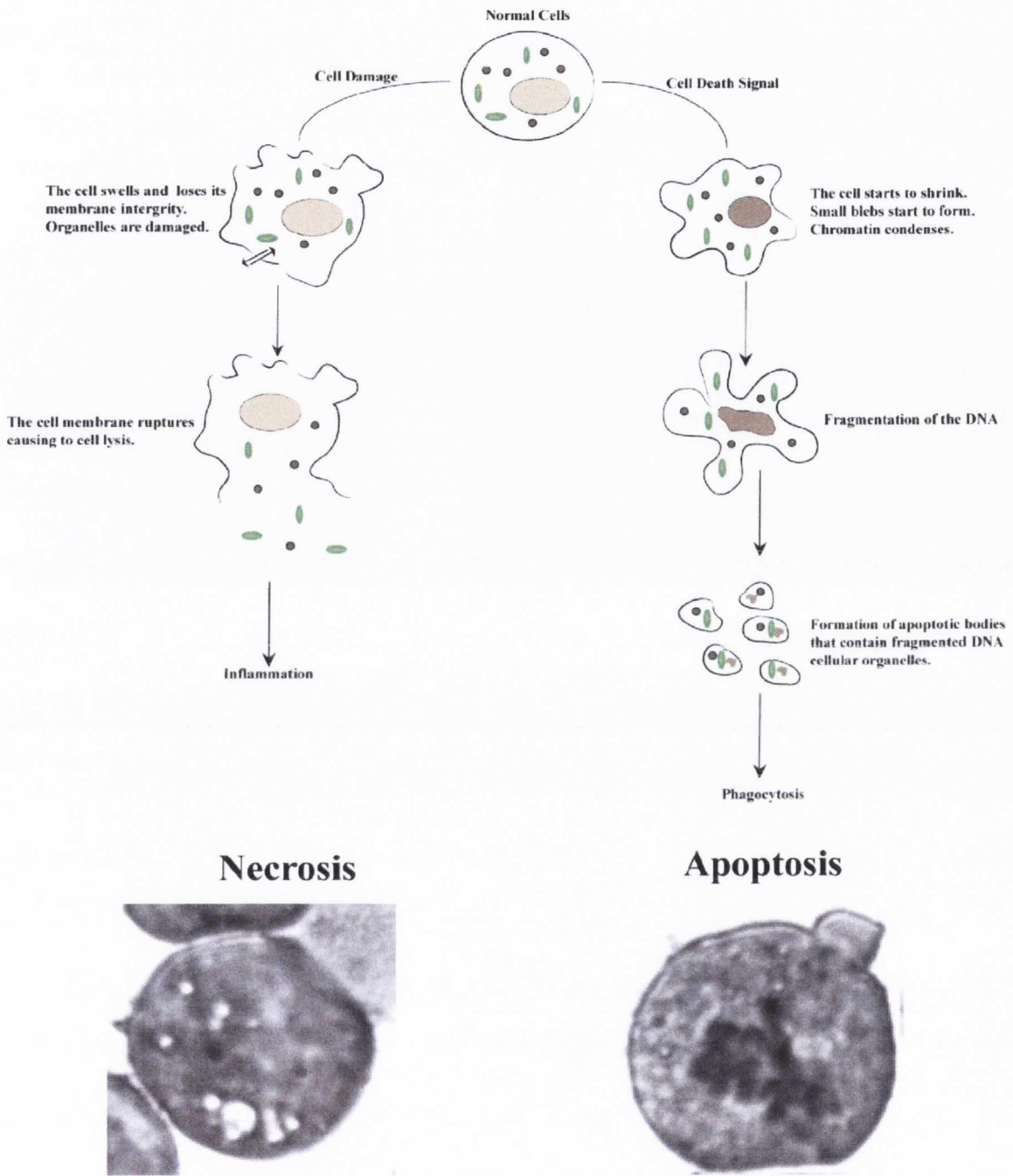


Figure 1.3 *The morphological characteristics of necrosis and apoptosis. Necrosis involves swelling and the subsequent breakdown of the cell membrane, leading to the leakage of intracellular proteins into the cytoplasm, ultimately causing inflammation. Apoptosis on the other hand involves cell shrinkage and programmed fragmentation of the cell in to apoptotic bodies that are taken up by neighboring cells or macrophages. Below are examples of a necrotic and apoptotic cell.*

In a dying cell, adenine triphosphate (ATP) depletion has been shown to be the major impicator of the fate of the cell. A cell undergoing necrosis follows an energy-independent

mode of cell death.²⁶ A sudden decrease in ATP production would result in the diminished activity of proteins and ion pumps found in the cytoplasm and cytoplasmic membrane, respectively. As a result, death channels in the cell membrane allow the influx of anions (*i.e.* Cl⁻) into the cytoplasm.²⁷ When the plasma membrane becomes open to electrolytes and low molecular weight solutes, only high molecular weight molecules exert osmotic force.²⁸ Consequently, the concentration of high molecular weight molecules, for instance proteins, is higher inside the cell than on the outside. As a means of withholding the osmotic pressure, water moves into the cell, causing it to swell. This swelling, one of characteristics of necrosis, will continue until the plasma membrane ruptures and the cell organelles will leak into the surrounding tissue, causing inflammation (Figure 1.3).²⁸ The above inability to maintain the plasma membrane permeability also leads to a disruption of other membranes within the cell, for instance the lysosomes that release their contents into the cytoplasm, causing karyolysis.²⁹ Necrotic cell death has little or no implication in tumor formation but there is some evidence that drugs that induce necrotic cell death might selectively target cancer cells.^{30,31}

In comparison to necrosis, apoptosis is an energy-dependant process where the integrity of organelles, such as the lysosomes is maintained. During the process, the cell will start to form irregular bulges, called blebs, that eventually separate from the cell forming apoptotic bodies (Figure 1.3).^{23,24,29} These apoptotic bodies contain portions of the cytoplasm and eventually undergo phagocytosis by macrophages and neighboring cells.³² In contrast to necrosis, this leads to a non-inflammatory response, which is one of the hallmarks of apoptosis.²³

The biochemical mechanism of apoptosis involves two main pathways; the **extrinsic death receptor pathway** and the **intrinsic mitochondrial mediated pathway**. The extrinsic pathway is activated by specific external signals, whereas the intrinsic pathway can be triggered by different insults, such as growth factor deprivation, hypoxia, genotoxic injury.⁷

The extrinsic signaling pathway involves death receptors that are transmembrane proteins and members of the tumor necrosis factor receptor (TNFR) gene superfamily.³³ The best-characterised death receptors are CD95 (also called Fas) and TNFR-1 that are activated by corresponding trimeric ligands. Upon extra-cellular binding, three receptors will crosslink and form a cluster (Figure 1.3).³³⁻³⁷ The cytoplasmic sequences of the above receptors form a bundle, termed the *death domain*, which binds to an adapter protein (*i.e.* Fas-associating protein with death domain, FADD).³⁸ This adapter molecule contains

effector domains that recruit inactive **cysteine-dependant aspartate-directed proteases** (caspases).

Caspases are categorised into two groups; **initiator** (*i.e.* caspase-8 and -9) and **executioner** caspases (*i.e.* caspase-3, -6, -7).³⁹⁻⁴¹ Caspases are widely expressed in an inactive pro-enzyme form and are activated by proteolytic cleavage. Once activated, caspases can activate other pro-caspases, thereby amplifying the apoptotic signal, causing rapid cell death.⁴¹

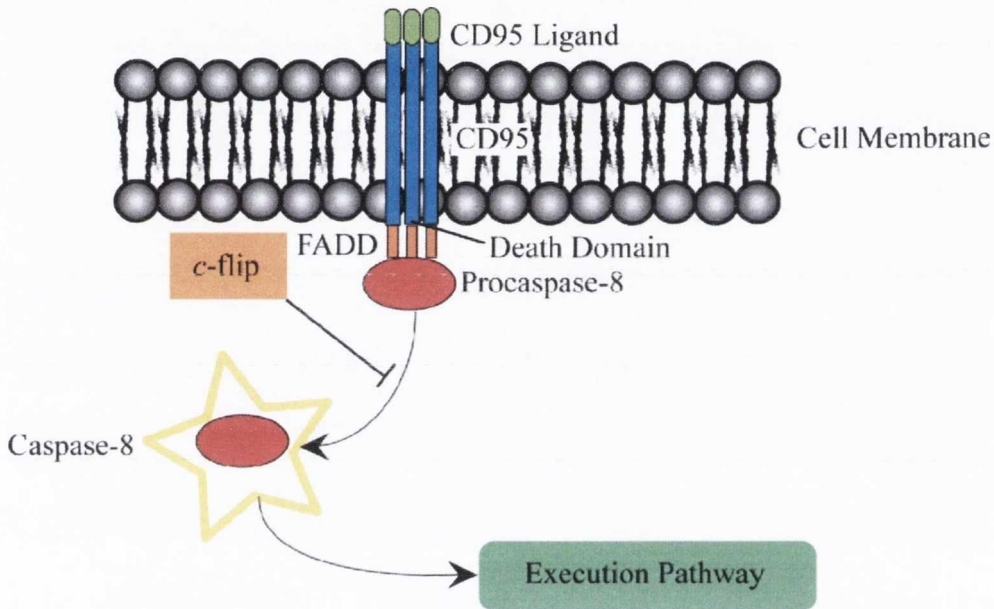


Figure 1.4 Schematic drawing of the external death-receptor pathway. Upon activation of the CD95 by the corresponding trimeric ligand, the cytoplasmic sequences of CD95 construct the death domain. This bundle binds to the adapter protein FADD that recruits and stimulates the activation of pro-caspase-8, which in turn can be inhibited by *c-flip*.

The intrinsic pathway involves the activation of an initiator caspase, caspase-8 or a caspase-8-like protease such as caspase-10. It is not known to date how many initiator caspases are needed, however it has been assumed that they cleave and activate downstream caspases called executioner caspases, leading to the final stages of apoptosis. This last stage is common to both the extrinsic and intrinsic pathway and will be discussed later in this section.

Tumorigenic disruptions in the extrinsic pathway occurs less frequently than in the intrinsic pathway.⁴² Nevertheless, there are examples of mutation in the death receptors^{43,44} and downstream regulators such as *c-flip*, a caspase-8 mediator (Figure 1.4).⁴⁵ Overexpression of *c-flip*, has been documented in some cancers, prevents the activation of caspase-8 resulting in apoptosis evasion.⁴⁵

The other main apoptosis pathway, the intrinsic pathway, involves changes to the inner mitochondrial membrane, caused by cellular stress such as genotoxic injury. As a sensor for cellular stress, *p53* is a critical initiator of the intrinsic pathway and proteins that detect damage to the genetic material such as ATM, phosphorylate and stabilise *p53* directly (Figure 1.5).⁴⁶

p53 can initiate apoptosis by transcriptionally activating pro-apoptotic Bcl-2 family members (*i.e.* Bax and Bak) and repressing anti-apoptotic Bcl-2 proteins (*i.e.* Bcl-2 and Bcl-X_L) as depicted in Figure 1.5. It is believed that the main mechanism of action of the Bcl-2 family of proteins is *via* alteration of the mitochondrial membrane permeability, leading to a loss of mitochondrial membrane potential and subsequent release of pro-apoptotic proteins such as cytochrome *c* and Caspase activated DNase (CAD) as shown in Figure 1.5 and Figure 1.6, respectively.^{23,47-49}

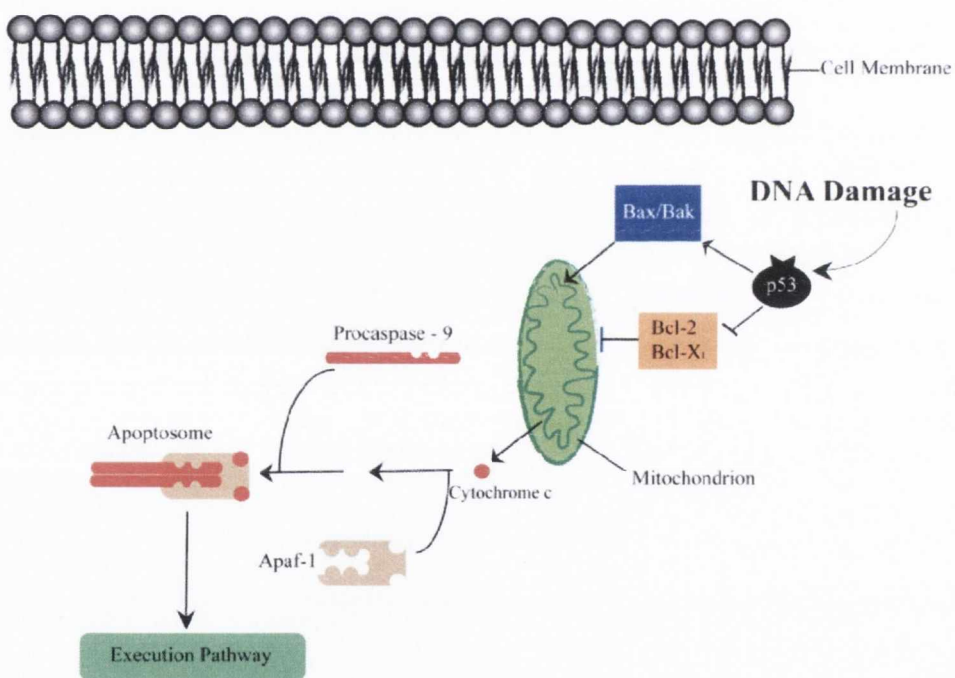


Figure 1.5 Schematic drawing of the internal mitochondrial pathway. The intrinsic pathway is activated by different stimuli such as DNA damage, resulting in the activation of the tumor suppressor gene, *p53*. The loss of the mitochondrial membrane potential, via the activation of the pro-apoptotic Bcl-2 family members (Bax, Bak) leads to the release of cytochrome *c*. This step can be inhibited by the anti-apoptotic members of the Bcl-2 family of apoptotic regulators (Bcl-2, Bcl-X_L). Together with Apaf-1 and pro-caspase 9, cytochrome *c* will form the apoptosome complex.

Cytochrome *c* is normally situated between the inner and outer membrane of the mitochondria and is traditionally associated with the electron transport chain. Once apoptosis is activated, cytochrome *c* is translocated into the cytoplasm, where it binds to the apoptosis protease factor-1 (Apaf-1) (Figure 1.5).⁵⁰ This leads to a transformational change in the structure of Apaf-1, leading to an open and active conformation of Apaf-1, allowing Apaf-1 to oligomerise. This oligomer recruits an inactive initiator caspase, pro-caspase-9, forming a complex termed an apoptosome.^{51,52} The clustering of pro-caspase-9 in this manner leads to the activation of caspase-9 and the subsequent triggering of the execution pathway (Figure 1.5).^{47,51,52}

The extrinsic and the intrinsic pathway come together at the point of the **execution pathway**, considered the final stage of apoptosis (Figure 1.6).

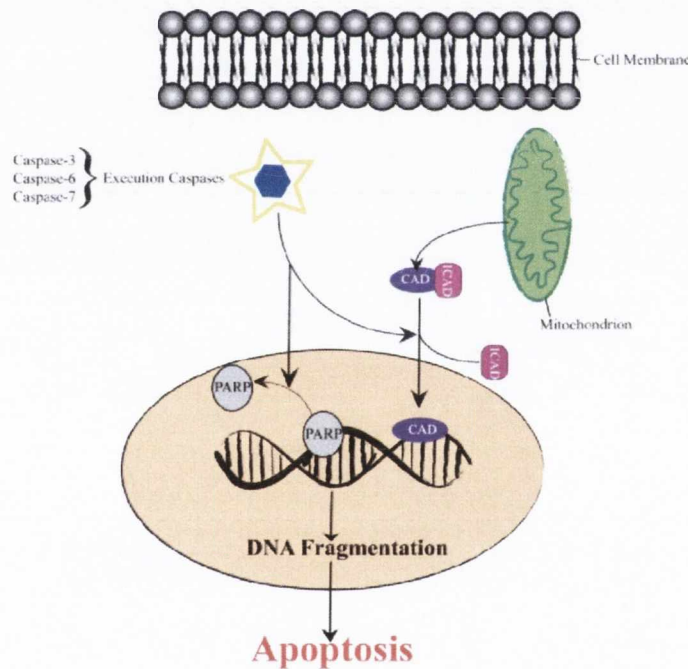


Figure 1.6 The execution pathway. The effector caspases from the intrinsic and the extrinsic pathway activate the execution caspases shown. The execution caspases lead to the activation and relocation of the CAD protein that activates the fragmentation of the genome. Execution caspases also deactivate the DNA repair protein, PARP to facilitate further breakdown of the genome.

The major components of this last stage are the executioner caspases that cleave various substrates, causing the morphological changes that distinguish apoptotic cell death, as discussed in the previous section.²³ These caspases include caspase-3, -7 and -6. Caspase-3 is thought to be the most important of the executioner caspases and it is

activated by all initiator caspases previously mentioned (caspase-8, -10 and -9).⁵³ Caspase-3 has numerous substrates, such as CAD, poly (ADP-ribose) polymerase (PARP) (Figure 1.6). CAD contains mitochondrial localisations signals that are cleaved upon entering the mitochondria, resulting in a mature protein, which is released into the cytoplasm upon the loss of the mitochondrial membrane potential. CAD is activated indirectly by Caspase-3 that cleaves and inactivates the inhibitor of CAD (ICAD).^{54,55} This allows the CAD to enter the nucleus, causing a two-step digestion of the genetic material, first fragmenting it into approximately 50 kb and then further into the characteristic 180 bp fragments. PARP, on the other hand, has a DNA repair function within the cell, fixing single-stranded DNA nicks. When caspase-3 enters the nucleus, it deactivates PARP, facilitating the DNA fragmentation by CAD.

Disruption of the intrinsic pathway is extremely common in cancer. Indeed, the *p53* tumor suppressor gene is the most frequently mutated gene in human tumors.⁵⁶ Moreover, functional mutations or altered expression of *p53* downstream effectors such as the Bcl-2 pro- or anti-apoptotic family members (*i.e.* Bax, Bak and Bcl-2, respectively) or upstream regulators (*i.e.* ATM), occurs in human cancers.⁴⁶

Cell proliferation and differentiation are highly regulated in cells and mutations that disrupt these regulation pathways have been detected in tumor cells. For most solid tumors (*i.e.* colon, lung, breast and prostate) mutations in multiple pathways are required to produce an invasive carcinoma.⁸ However, as discussed in the next section, single genetic defects can lead to specific types of cancers, for example chronic myelogenous leukemia (CML) and acute promyelocytic leukemia (APL).

1.3 Cancer Classification

From a histological standpoint there are hundreds of different types of cancer. They are grouped into five major categories based on their tissue origin:

- **Sarcoma:** the cancer of the supportive or connective tissue
- **Carcinoma:** the cancer of epithelial tissue
- **Myeloma:** the cancer of the plasma cells of the bone marrow
- **Leukemia:** the cancer of the blood marrow
- **Lymphoma:** the cancer of glands or nodes of the lymphatic system.

Carcinomas account for approximately 90% of human cancer, whereas, leukemias and lymphomas account for 8% of malignancies in humans.²¹ Leukemia is the cancer of the cells of the blood and blood forming tissues, such as the bone marrow, resulting in high levels of abnormal or immature blood cells. There are several types of leukemia, which are classified by the cell lineage that gives rise to the disease, either *lymphoid* or *myeloid*. Although histological examination is often sufficient to determine the leukemia type, gene expression microarrays are now able to classify patients on the basis of molecular genetic profile, drug sensitivity and prognosis.⁵⁷

A variety of chromosomal abnormalities occur in various leukemias, the classical example being the *Philadelphia chromosome* in **chronic myelogenous leukemia** (CML). CML is a hematological stem cell disorder characterised by excessive proliferation of cells of the myeloid lineage.⁵⁸ CML is caused by a chromosomal translocation between chromosome 9 and 22 resulting in an abnormal chromosome named the Philadelphia chromosome and leads to the formation of a fused protein named Bcr-Abl (Figure 1.7).⁵⁹

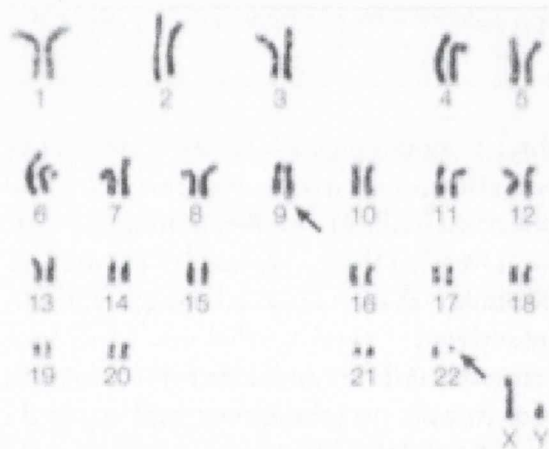


Figure 1.7 Karyotype from a CML patient. The arrows indicate the 9;22 translocation and the otherwise normal karyotype.⁷

The fusion of the Bcr sequence to the Abl protein, results in the aberrant activity and altered subcellular localisation of the Abl protein tyrosine kinase, promoting cell survival and proliferation through several intracellular signal transduction pathways.

Although most oncogenes stimulate cell proliferation, the oncogenic activity of some transcription factors result from inhibition of cell differentiation. As an example, retinoid acid induces differentiation in a variety of cancer types by diffusing through the plasma membrane and binding to intracellular receptors that serves as transcriptional regulatory

molecules. Mutated form of the retinoic acid receptor can act as an oncogene in proteins, as seen in acute promyelocytic leukemia (APL).⁶⁰

APL is associated with chromosomal translocations involving the retinoic acid receptor alpha (RAR α) locus on chromosome 17 and one of five different partner genes.^{60,61} The most common and the most studied fusion gene in APL is PML-RAR α , associated with a translocation between the long arms of chromosome 15 and 17.^{60,61} The two genes PLM and RAR α are fused together, leading to the transcription of a fusion product PML-RAR α . The fusion protein PML-RAR α arrests differentiation by abnormal RAR α activity and alters nuclear biology and natural apoptosis through an abnormal PML protein.⁶¹ Patients suffering from CML or APL have been successfully treated with a Bcr-Abl tyrosine kinase inhibitors and all-trans retinoic acid (ATRA), respectively. However, as discussed in the next section, patients often experience relapse due to resistance to these drugs.

1.4 Cancer Treatment

Surgery, radiation and chemotherapy are the main options for a patient diagnosed with cancer. Treatment may involve one or even a combination of these methods depending on the type and the location of the cancer, as well as the age and general health of the patient.

Chemotherapy offers the greatest potential for advancing the current treatment strategy. Recent advantages in the molecular biology of cancer have become increasingly important for the whole process of drug discovery and development, including the identification and validation of new cancer drug targets and improving molecular screens for the discovery of new candidate drugs, ultimately leading to more specific drugs with enhanced clinical efficacy.⁶² Furthermore, new ways to intervene against cancer are being discovered and new technologies are now used in combination with chemotherapy. A relevant example is photodynamic therapy that will be discussed in detail in *Chapter 4*.

1.4.1 Chemotherapy

Chemotherapy is the use of cytotoxic compounds to kill or inhibit the growth of cancer cells. The oldest class of chemotherapeutic agents is alkylating agents that originated from the Second World War when military doctors noticed that soldiers exposed to nitrogen mustard died from bone marrow destruction. This observation led to the

development of more effective alkylating agents that blocked DNA synthesis and cell division, ultimately leading to apoptosis. Although these compounds showed efficacy, they lacked specificity resulting in dramatic side effects. Examples of different classes of chemotherapeutic agents are given in Table 1.2.

Table 1.2 Common chemotherapy agents and their mechanism of action.

Type	Mechanism of Action
<i>Alkylating Agents</i>	<i>Directly damage the genetic material</i>
<i>Antimetabolites</i>	<i>Interfere with replication and transcription</i>
<i>Anthracyclines</i>	<i>Interfere with enzymes involved in replication</i>
<i>Targeting Agents</i>	<i>Target a mutated version of a specific protein</i>
<i>Hormonal Agents</i>	<i>Restrict the growth of cancer cells by either prevent the use of or the formation of specific hormones</i>
<i>Differentiating Agents</i>	<i>Force cancer cells to differentiate</i>

The discovery of oncogenes meant that small molecules could target a specific gene or its gene product that was responsible for the disease.^{63,64} One of the most successful molecules for targeting oncogenic proteins is Glivec **1**, which is used to treat patients with CML. Glivec **1**, was developed by Novartis and was shown to inhibit the activity of Bcr-Abl (Figure 1.8 A).⁶⁵

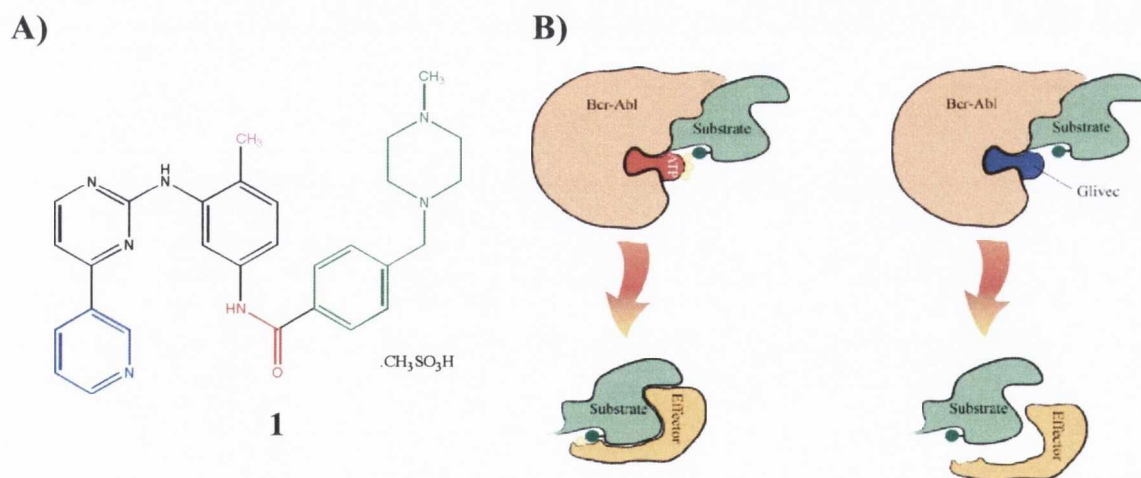


Figure 1.8 The structure and mechanism of Glivec, 1. **A)** The chemical structure of 1. **B)** Mechanism of inhibition of Bcr-Abl by 1. Left panel, the Bcr-Abl protein phosphorylates the substrate, which in turn interacts and activates downstream effector proteins. Right panel, 1 is bound to the ATP binding pocket. The substrate is not phosphorylated and can no longer interact with the effector protein.

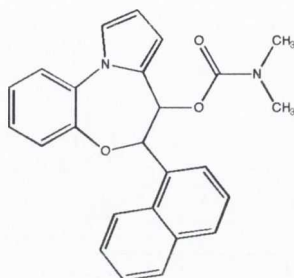
The lead compound for the development of **1** was the 2-phenylamino pyrimidine (showed in black in Figure 1.8 A) and it was identified through screening of compounds that had kinase activity.⁶⁵ Further, strong inhibition of serine/threonine kinases was obtained from derivatives bearing the 3'-pyridyl (blue in Figure 1.8 A) group at the 3'-position of the pyrimidine. The presence of an amide group (red in Figure 1.8 A) on the phenyl ring provided inhibitory activity against tyrosine kinases, such as Bcr-Abl. The key observation of the structure-activity relationship, was that the presence of the methyl group at position 6 at the diaminophenyl group (purple in Figure 1.8 A) completely abolished serine/threonine kinase inhibitory activity but retained or even enhanced the activity against tyrosine kinases.⁶⁵ The methyl group was shown to hinder the rotation around the amine bond, leading to a preferred conformation that was specific for tyrosine kinases. Finally, the attachment of a *N*-methyl piperazine moiety (green in Figure 1.8 B) markedly increased the solubility and the oral availability.⁶⁵

In healthy cells, protein kinases bind ATP, leading to a conformation change of the protein kinases, from the open and inactive state, to the closed and active one. The downstream substrate binds to the active protein that phosphorylates the substrate (Figure 1.8, B left panel). Glivec **1** occupies the ATP pocket of the Bcr-Abl with high selectivity (Figure 1.8, B right panel), thereby inhibiting the substrate phosphorylation process.⁶⁶

The approach of targeting an oncogenic protein is highly promising but it suffers from several drawbacks. Firstly, because of the complexity of cancer, it is highly unlikely that only one oncogene is responsible for cancer progression.⁶⁷ It is more likely that more than one oncogene needs to be targeted to successfully treat cancer. Secondly, resistance to **1** develops over time in almost every treated patient and furthermore, different mechanisms of resistance exist. In some cases, genomic amplification of the Bcr-Abl gene and the overexpression of the protein are observed.^{68,69} These complications are usually overcome by increasing the drug dosage. Another mechanism of resistance is the mutation of the Bcr-Abl gene. The most frequent mutations involve amino acids that are situated in the ATP binding pocket of the protein and thus decrease the affinity of **1** or in some cases inhibit binding.^{70,71} This has also been shown to occur in all patients treated with ATRA, the commonly used treatment for APL.⁷² The observed resistance to ATRA was likely to be related to the feedback mechanism aimed at reducing ATRA concentrations in the organism.⁷³

Despite the aforementioned drawbacks, this approach of specifically targeting responsible oncogenes has shown encouraging clinical responses. In addition, second-

generation tyrosine kinases are being tested in patients with reoccurring disease and compounds with different mechanism of action are being tested alongside Glivec, such as the microtubule targeting agent, pyrrole-1,5-benzoxazepine (PBOX)-6, **2**.^{74,75}

**2**

Nevertheless, due to the genetic instability shown in cancer and the fact that some cancer etiologies are unknown, the genetic material remains one of the main targets for cancer chemotherapy.

1.4.1.1 Targeting the Genetic Material

The genetic material contains valuable information for normal cell maintenance. As discussed in previous sections, cell replication is kept under strict control to ensure that each daughter cell receives an intact copy of the genetic material, failure of which could lead to cell death or cancer. The major advantage of targeting genetic material directly arises from the fact that cancer is a complex disease where not only the genetic variability differs between cancer types but also between different patients with the same type of cancer. In addition, the complete sequencing of the genome has helped the search for small molecular drugs that could interact specifically to with genetic material.

The genetic material of the cell is often referred to as *deoxyribonucleic acid* (DNA). DNA is composed of two polynucleotide strands that are held together by weak, noncovalent interactions, namely hydrogen bonds. The strands are composed of two types of heterocyclic bases that are connected with a negatively charged sugar phosphate group. The two types of heterocyclic bases consist of the bigger purines—**adenine (A)** and **guanine (G)** and the smaller pyrimidines—**cytosine (C)** and **thymine (T)** (Figure 1.9). The strands have an anti-parallel orientation; the base at the 5' end of one strand is paired with a corresponding base at the 3' end of the other strand. The origin of the specificity of base pairing is the possible hydrogen bonding between the bases. According to the Watson–Crick base pairing rules, **A** on one chain is paired with **T** on the other chain while **G** is paired with **C**, as illustrated in Figure 1.9.⁷⁶

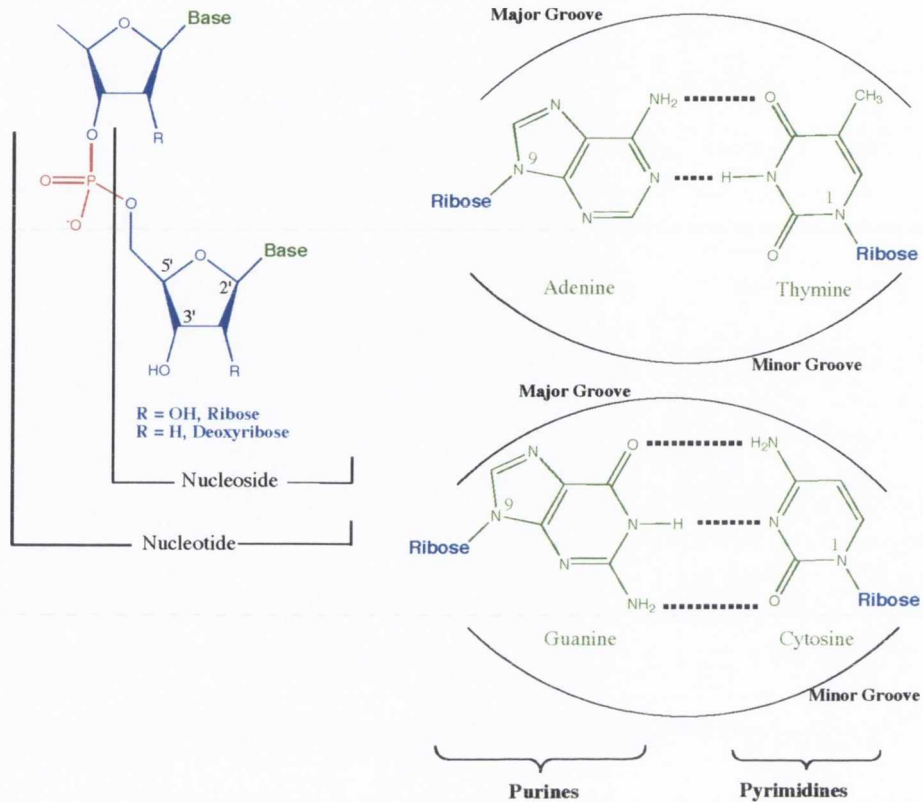


Figure 1.9 The basic building blocks of DNA.

Many different structures of DNA have been resolved but their biological role is mostly unknown.⁷⁷ The most common structure, B-DNA is characterised by a wide and shallow major groove and deep and narrow minor groove (Figure 1.9). As discussed in *Section 1.4.1.1.4*, it is through these grooves that external agents, such as proteins and drugs can interact with the DNA molecule.⁷⁷

Each base pair exposes a system of hydrogen bond donors and acceptors, producing a small part of the genetic code. The edge of the major groove can distinguish between all four possible base pairs (Figure 1.9). This allows proteins to specifically recognise a DNA sequence without opening and thereby disrupting the DNA helix. The information in the minor groove is less useful for distinguishing between base pairs because the hydrogen bonding and accepting system can not discriminate between **A:T** and **T:A** nor **C:G** and **G:C**. Moreover, the narrow minor groove cannot fit the amino acid side chains of proteins comfortably, unlike the wider major groove.

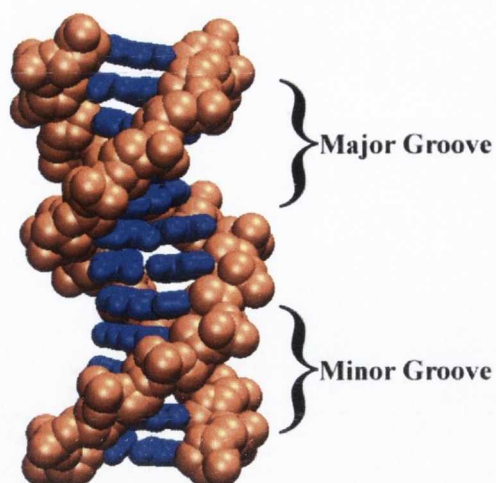


Figure 1.10 The common B-form of DNA. The positions of the major and minor groove are indicated. The phosphate backbone is shown in orange and the base pairs are in blue.⁷⁸

During replication and transcription, the DNA double helix needs to be separated to allow macromolecular complexes to access the DNA. These processes require the local unwinding of the DNA double helix. This local strain leads to the overwinding of surrounding regions or to supercoiling. The degree of supercoiling is determined by a special set of enzymes called topoisomerases that are classified into two classes, topoisomerase I and topoisomerase II, based on their mode of action of cleaving DNA. **Topoisomerase I** (Topo I) catalyses the relaxation of supercoiled DNA, which is a thermodynamically favorable process (Figure 1.11). Topo I creates a single-stranded DNA nick and binds covalently to the 3'-phosphate of the DNA thereby liberating the 5'-hydroxyl to generate a strand break.

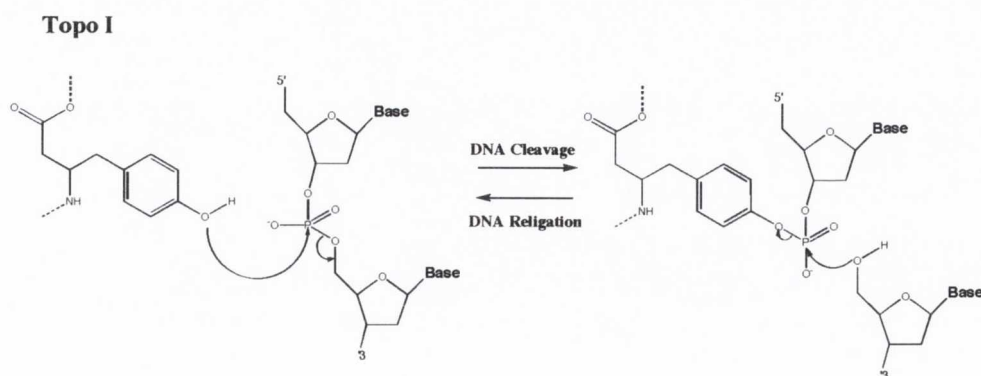


Figure 1.11 Topo I mediated DNA cleavage and ligation. A hydroxyl group of a tyrosine inside the binding cavity of the Topo I attacks a phosphate group on one strand of the DNA backbone to form a phosphodiester linkage between the enzyme and DNA, cleaving the strand and releasing a free 5'-hydroxyl group.

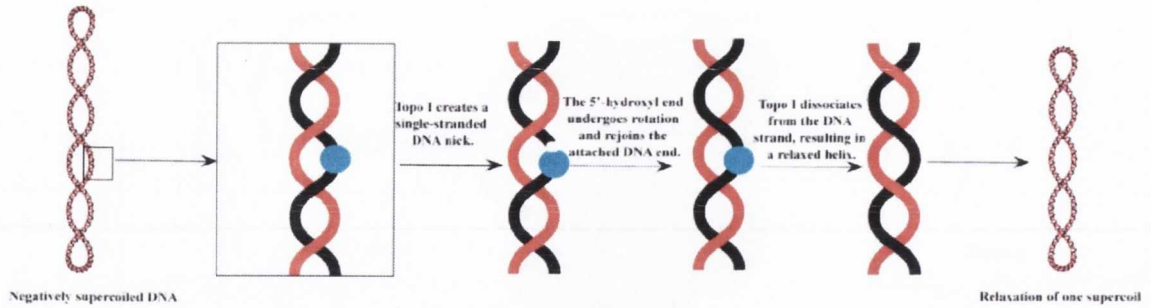


Figure 1.12 Topoisomerase I mechanism. On binding to DNA, Topo I cleaves one strand of the DNA duplex. The cleaved strand rotates around the uncleaved strand in a controlled manner and the reaction is completed by religation of the cleaved strand.

The detached DNA strand undergoes rotation and rejoins the cleaved DNA by nucleophilic attack of the 5'-hydroxyl group to the phosphotyrosine linkage in the Topo I active site. This releases the strain of one supercoiling (Figure 1.12).

Supercoiling is catalysed with the second class of topoisomerase, **topoisomerase II** (Topo II) that actively creates a double-stranded DNA break (Figure 1.13).¹⁸ Topo II is a dimeric protein that consists of two subunits, topoisomerase II α and II β . These subunits bind to one double helix, the **gate segment** (G-segment). Upon binding to ATP, Topo II undergoes a conformational change that triggers the cleavage of the G-segment and the subsequent passage of the **transported segment** (T-segment) through the DNA strand break, ultimately leading to religation of the T-segment.

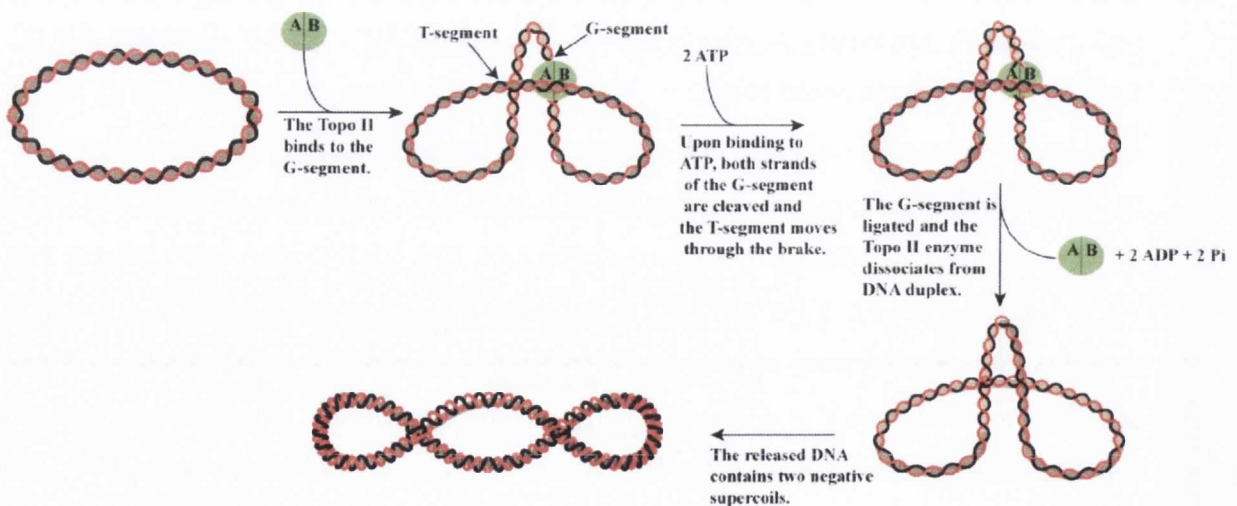


Figure 1.13 Topo II mechanism. Topo II protein binds first to the G-segment and cleaves the DNA duplex upon binding to ATP. Simultaneously, Topo II binds to the additional DNA duplex, the T-segment that moves through the break in the G-segment and out of the enzyme. The enzyme dissociates from the DNA duplex and the released DNA with two additional negative supercoils.

Depending on the type of DNA interactions, compounds can either block the access of enzymes such as Topo I and Topo II or they distort the DNA helix so that enzymes can not bind. The interactions between a drug and DNA can be categorised into:

- **covalent interaction,**
- **intercalating interactions,**
- **electrostatic interactions,**
- **groove binding interactions.**

The binding of small molecules to DNA can involve one or a combination of these types of interactions. Each of these interactions will be discussed and examples of each binding mode will be discussed in the following sections.

1.4.1.1.1 Covalent Binding

Nitrogen mustard, **3** was one of the first chemotherapy agents used for the treatment of cancer and cisplatin, **4** was the first platinum based anti-cancer drug in clinical use (Figure 1.14 A). The mechanism of action by covalent binders is generally similar. For example, **4** is a bifunctional binder, forming two covalent bonds with DNA. First, **4** specifically forms monofunctional adducts with G residues at the N7 position.

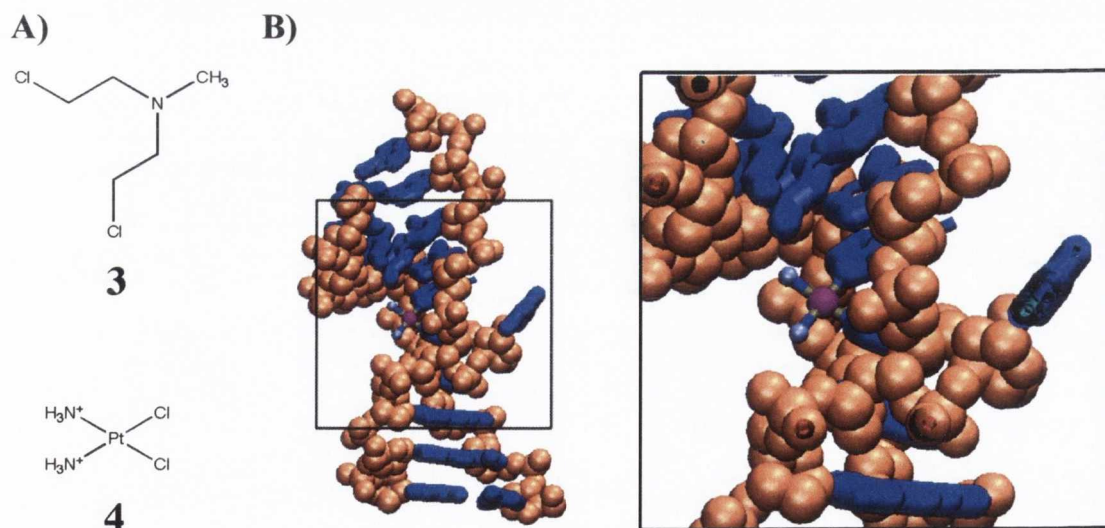


Figure 1.14 The covalent binding agents. **A)** The chemical structure of nitrogen mustard, **3** and cisplatin, **4**. **B)** Crystal structure of interstrand crosslinking of **3**. The DNA backbone is shown in orange, the bases in blue, platinum metal in purple and the nitrogen atoms in **4** in sky blue.⁷⁹

These monofunctional adducts distort DNA in a sequence-dependant manner and also unwind the duplex but on the other hand they only negligibly affect replication.^{80,81} The monofunctional adducts subsequently form an intrastrand or interstrand crosslink between adjacent purine residues, with a strong preference for **G** over **A**.⁷⁷ This leads to a considerable change in the secondary structure of DNA, causing a kink in the helix (Figure 1.14 **B**)

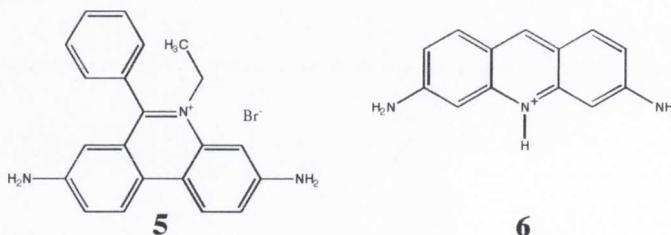
With regards to the cell cycle, studies have revealed that **3** triggers G₂ phase arrest, as expected by the changes in DNA structure, ultimately leading to apoptosis.^{82,83} However, as discussed in *Section 1.3*, the mechanism of apoptosis is highly complex, with multiple pathways that need to be explored for a full understanding of how **3** triggers apoptosis.⁸⁴

1.4.1.1.2 Intercalating Interactions

There are numerous types of well-known DNA intercalators, such as ethidium bromide **5** and proflavin **6**, which were among the first anti-cancer agents to be discovered. Early studies by Lerman *et al.*⁸⁵ showed that aminoacridines such as **6** increased the length of DNA and locally unwound the DNA double helix. Later, Waring *et al.*^{86,87} described the interaction between DNA and ethidium bromide **5** using UV/Vis spectroscopy. These pioneering studies lead the way for the design of intercalators as chemotherapeutic agents.

According to the classical model of intercalation, the DNA double helix lengthens by 3.4 Å, the thickness of a typical aromatic ring system. This base pair separation distorts the torsion angle of the phosphodiester bonds the helical axis to unwind. The extent of these changes are dependant on the intercalator molecule and the DNA sequence.⁸⁸

In general, intercalators show low DNA sequence specificity. Simple intercalators like **5** show a slight preference to 5'-pyrimidine-purine-3' and especially **C:G** steps.⁸⁹ This preference is thought to arise from the lower energy required to disrupt this sequence compared to others.⁹⁰



Another factor governing the binding is the “neighboring exclusion rule” that states that intercalators can, at most, bind at alternate possible binding sites on DNA, giving a maximum of one intercalator, every second site.^{88,91} Intercalation can affect the biological

properties of DNA, inhibiting or influencing the interaction between DNA and associated proteins in essential cellular processes, including replication and transcription, leading to apoptosis. An example of DNA intercalators are the **1,8-naphthalimides**.

Among the first 1,8-naphthalimides that showed biological activity were mitonafide, **7** and its 4-amino derivative amonafide, **8** (Figure 1.15 A). These compounds were shown to intercalate DNA and induce DNA strand breaks in the HL-60 cells, an APL cell line.⁹²⁻⁹⁴ These results suggested that **7** and **8** could be topoisomerase-targeting drugs, as was later shown by Hsiang *et al.*⁹⁵ This study also showed that the positively charged quaternary nitrogen in the side chain is essential for cytotoxic activity, and that the side chain interacts sterically with the active site of Topo II. Furthermore, the substitution at position 3 in the naphthalic ring instead of 2 or 3 gave optimal results.⁹⁶

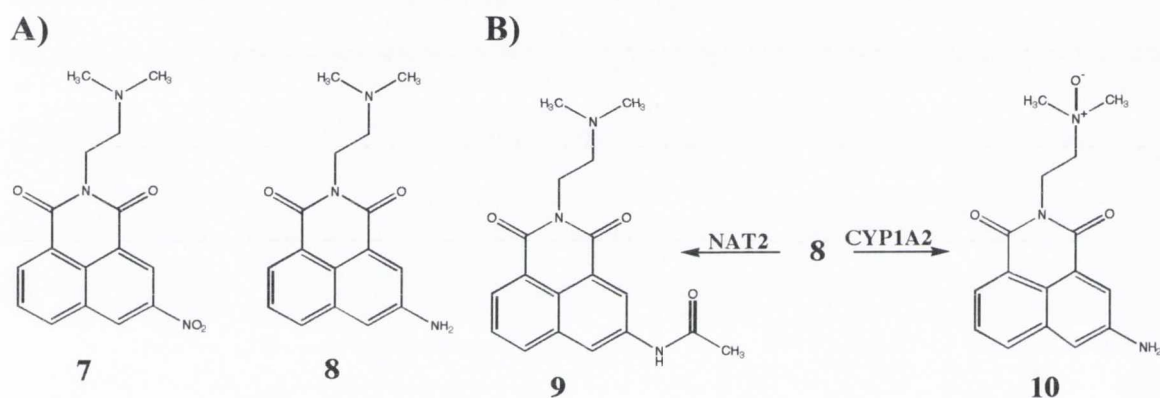


Figure 1.15 The intercalating agents. A) The chemical structures of mitonafide, **6** and amonafide, **7**. B) Metabolism of amonafide to *N*-acetyl-amonafide and *N'*-oxide-amonafide.⁹⁷

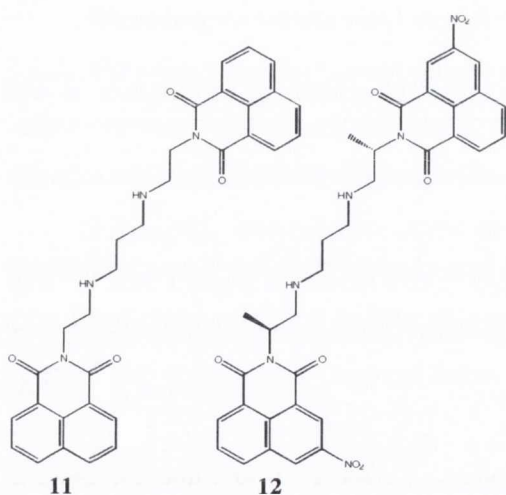
Both these 1,8-naphthalimide compounds went into clinical trials but **7** was withdrawn from further clinical development because of severe side effects that were associated with central neurotoxicity and the lack of efficacy in solid tumors. The 3-nitro substitution appeared to be responsible for this toxicity.⁹⁸

In comparison, **8** has completed several Phase I and II trials but its clinical development was hampered by highly variable and unpredictable toxicity that was thought to arise from the pharmacogenic properties of the drug. The drug was shown to undergo extensive metabolism *in vitro* by *N*-acetyltransferase 2 (NAT2), forming the metabolite *N*-acetyl-amonafide, **9** and also by CYP1A2 that leads to the formation of *N'*-oxide-amonafide **10** (Figure 1.15 B).⁹⁷ The *N*-acetyl-amonafide metabolite **9** displayed similar *in vitro* toxicity to **8**, while **10** was inactive and is rapidly cleared from the cell.⁹⁹ Most

compounds that are less effective in patients are fast acetylators because drugs usually lose their activity by the addition of an acetyl group. Furthermore, metabolism by CYP1A2 leads to the exportation of drugs from cells. In the case of **8**, the acetyl group retains its toxicity and inhibits CYP1A2 metabolism, leading to a higher exposure of more toxic compounds for longer periods in fast acetylators than in slow acetylators.⁹⁹ As a result, two pharmaceutical companies grouped patients into slow or fast acetylators and then appropriately reduced the clinical dose of the compound. Xanafide® made by Xanthus Pharmaceutical, an *L*-malate salt derivative of **8** has shown significant activity in secondary acute myeloid leukemia, both as monotherapy and in combination with cytarabine, an antimetabolite.¹⁰⁰ Furthermore, Quinamed (Chemgenex), a dihydrochloride salt derivative of **8**, is currently in Phase II studies as a treatment for fast acetylator patients that are suffering from prostate, ovarian or breast cancer and have shown no response to chemotherapy.

To improve the activity of 1,8-naphthalimide derived drugs, bisintercalating agents were developed based on the structural features of **7** and **8**. Among the several bisnaphthalimides synthesised by Braña *et al.*¹⁰¹, the non-substituted compound, **11** was shown to be the most active in preclinical trials (Figure 1.16 A).

A)



B)

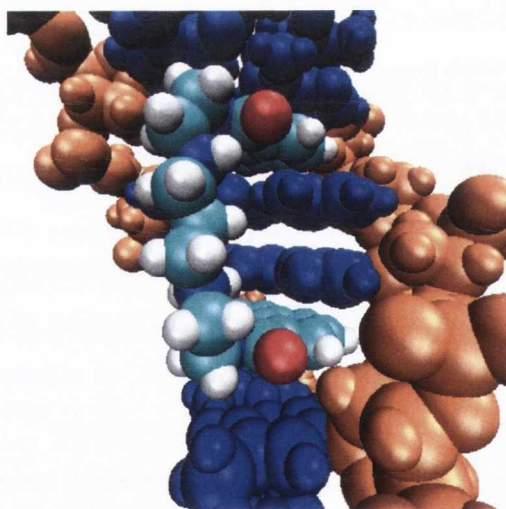
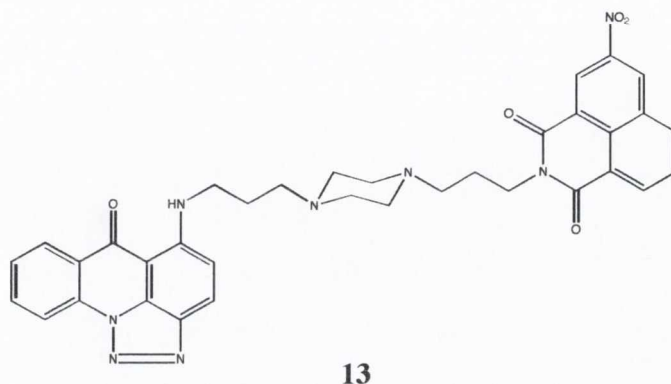


Figure 1.16 The bisnaphthalimide derivatives. A) The chemical structures of LU 79553, **11** and DMP-840, **12**. B) The mechanism of binding of **11** to DNA.¹⁰²

This compound was named **LU 79553** as the free base or **elinafide** as the dimethanesulfonate derivative. Because of the absence of a substitution group, **11** did not show the severe toxicity like **7** nor the extensive metabolism of **8**. A symmetrical nitro derivative, DMP-840 **12** was later shown to be a Topo II poison, stabilising the cleavage

complex, in the same way as its precursors, **7** and **8**.¹⁰³ Recently, Michejda *et al.*¹⁰⁴ reported the synthesis of an unsymmetrical bifunctional antitumor agent **13** that included the 1,8-naphthalimide chromophore as a structural unit.

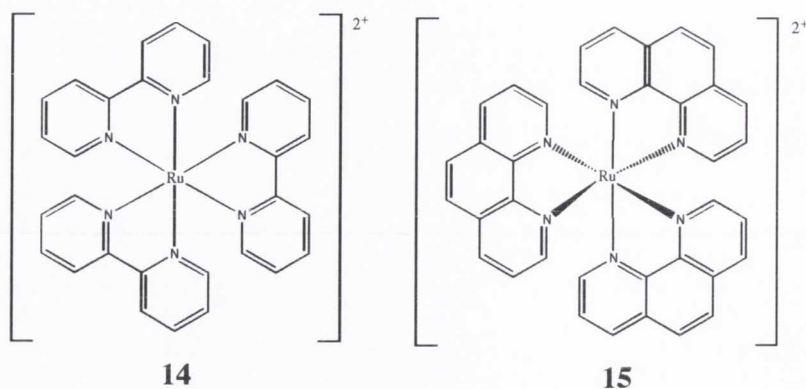


This compound showed potency against the APL cell line, HL-60 and was shown to induce apoptosis after 72 hours of treatment. The authors postulated that **13** was bound to DNA by intercalation of only one of the aromatic residues while the other aromatic moiety and the linker would reside in the minor groove. Furthermore, the biological activity was believed to arise from the interaction of the DNA-compound complex with critical DNA binding proteins, causing unreparable DNA damage and the subsequent activation of *p53* tumor suppressor gene.¹⁰⁵

1.4.1.1.3 Electrostatic Interactions

DNA is a polyelectrolyte due to the broad electronegative cloud that surrounds the polyphosphate backbone. In aqueous solutions, metal ions such as Na^+ and Mg^{2+} are the most common electrostatic binders. Binding to the backbone of the DNA is non-specific and weak. Proteins interact through the grooves of the DNA but cationic residues such as arginine, can form hydrogen bonds with the phosphate oxygens. There are few reports of synthetic agents that specifically target this area of DNA. However, as discussed in the next section, small molecules have cationic groups to potentially increase water solubility and direct the molecules to DNA.

A relevant example of an ionic binder is **Ruthenium-tris (2,2'-bipyridine)** ($\text{Ru}(\text{bpy})_3^{2+}$), **14** that was shown to mainly bind through ionic interactions on the outside of DNA.¹⁰⁶ Due to the weak binding to DNA, **14** was shown to be nontoxic to a series of human tumor cell lines.¹⁰⁷



Barton *et al.*^{108,109} revealed that complexes with extended heteroaromatic ligands, such as Ruthenium-Tris (1,10-phenanthroline) **15** involved a mixture of binding modes, namely intercalation and electrostatic interactions. These observations were later disproven, when Satyanarayana *et al.*¹¹⁰ suggested that the previous unwinding of the helix, was attributed to partial non-classical intercalation, resulting in a kink in the helix. The photophysical properties of Ruthenium based complexes and their potential as photoreactive reagent for DNA will be discussed in detail in *Chapter 4*.

1.4.1.1.4 Hydrogen Bonding Interactions

As discussed in *Section 1.4.1.1*, the formation of two distinct grooves in the double helical structure is highly important for biological processes such as replication and transcription. It is through these grooves, that DNA interacting proteins achieve DNA sequence recognition by forming specific hydrogen-bond contacts to the edges of the base pairs. This raises the possibility of designing compounds that would bind a specific DNA sequence and thereby inhibit the activity or the transcription of a specific gene.

The hydrogen bonding and accepting system in the major groove can discriminate between all the base pairs of DNA (Figure 1.9). In addition, the major groove is wider so it is more likely to accept large macromolecules like proteins or single RNA strands. Although the first demonstration of a triple helix formation of DNA dates back to 1957,¹¹¹ it was not until 1987 that Moser *et al.*¹¹² showed that oligoribonucleotides could form specific triple helix complexes at pH, temperature and salt concentration similar to a living cell.¹¹² Furthermore, these oligonucleotides were shown to inhibit DNA binding proteins and modulate transcription in cell-free systems.^{113,114} However, these high molecular weight oligomers suffered from several limitations. They were restricted to homopurines in the target sequence and their poor cellular uptake restricted testing in cell culture.¹¹⁵ Due to aforementioned drawbacks, targeting the minor groove with small synthetic molecules has

proven more successful and this area of research is highly active today. Examples include the natural product netropsin, **14** and its close relative distamycin, **15** (Figure 1.17 A).

Netropsin **14** was shown to bind A:T rich sequence, through NMR studies and X-ray crystallography analysis (Figure 1.17 B).¹¹⁶⁻¹¹⁸ This compound formed a 1:1 complex in the minor groove by forming a hydrogen bond between the NHs of the carboxamides and the N-3 in the case of A or the O-2 in the case of T. This preference for A:T is reinforced by the steric repulsion formed between the aromatic hydrogen of the *N*-methylpyrrole ring and the NH₂ of the G:C base pair. Finally, the cationic ends sit tightly in the minor groove, binding to the outermost base pair in the sequence.^{116,119}

Distamycin **15** showed similar binding, but in addition to forming a 1:1 complex, it also showed the formation of an anti-parallel 2:1 complex.¹²⁰ The formamido group was later shown to strongly induce the formation of this 2:1 complex.¹²¹

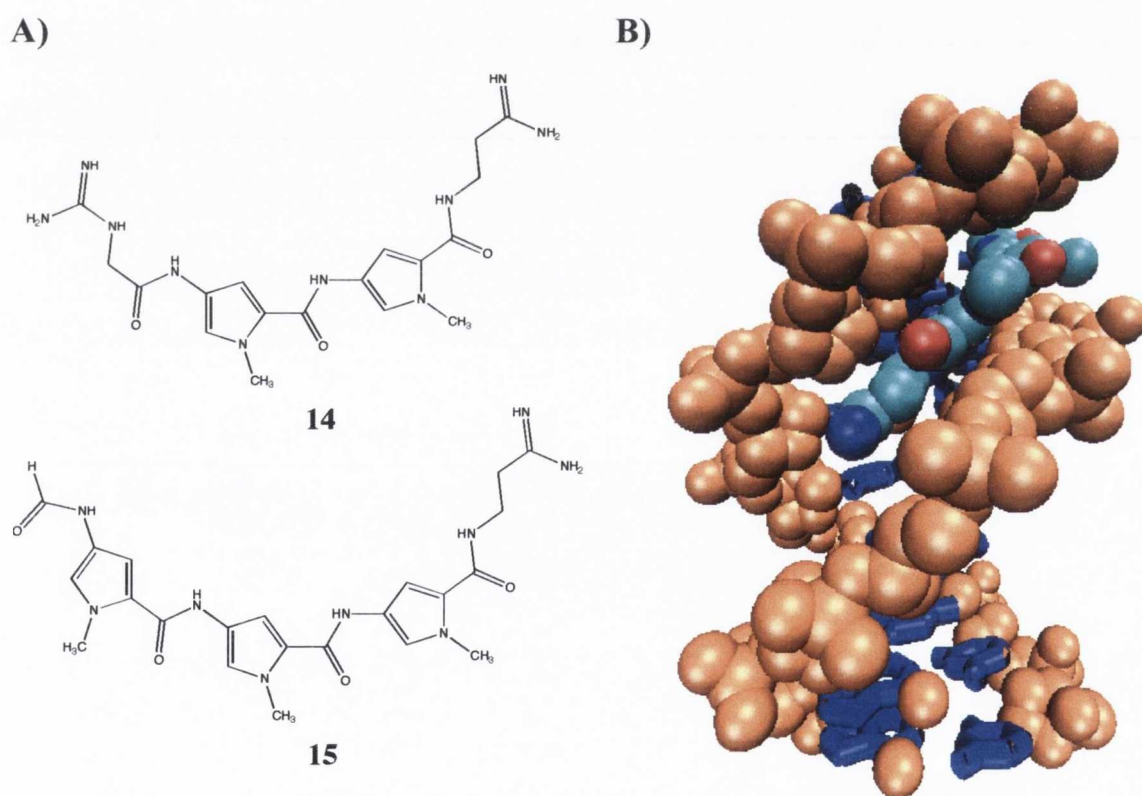


Figure 1.17 The natural minor groove binders. **A)** The chemical structures of netropsin **14** and distamycin **15**. **B)** The binding mechanism of **14** to DNA.¹¹⁶ Carbon molecules are shown in cyan, nitrogen atoms in blue and oxygen atoms in red.

The discovery that the minor groove was able to host two molecules proved a turning point in the field of DNA recognition because it raised the possibility of recognising all of the base pairs, instead of only being able to discriminate between A:T

and G:C as was originally thought.¹²² This discovery led to the development of other minor groove binding agents and in the late-1990s, Dervan *et al.*¹²³⁻¹²⁷ proposed a “four base pair code” that used synthetic ligands, namely amide linked pyrroles, imidazoles and 3-hydroxypyrroles (Figure 1.18 A). The *N*-methylimidazole **17**, put less steric strain on G:C base pairs and offered a lone pair of electrons that could accept a hydrogen bond from the NH₂ group of G. The 3-hydroxypyrrole **18** had an exocyclic hydroxy group that protruded into the floor of the minor groove, only to fit in between the cleft of A:T base pairs. Furthermore, this hydroxy group preferred to lie opposite T, not A.^{123,125} Corresponding polyamides made from **16-18** were shown to bind in a 1:1 complex but in high concentrations, they formed a side-by-side anti parallel 2:1 complex (Figure 1.18 B and C).¹²⁵

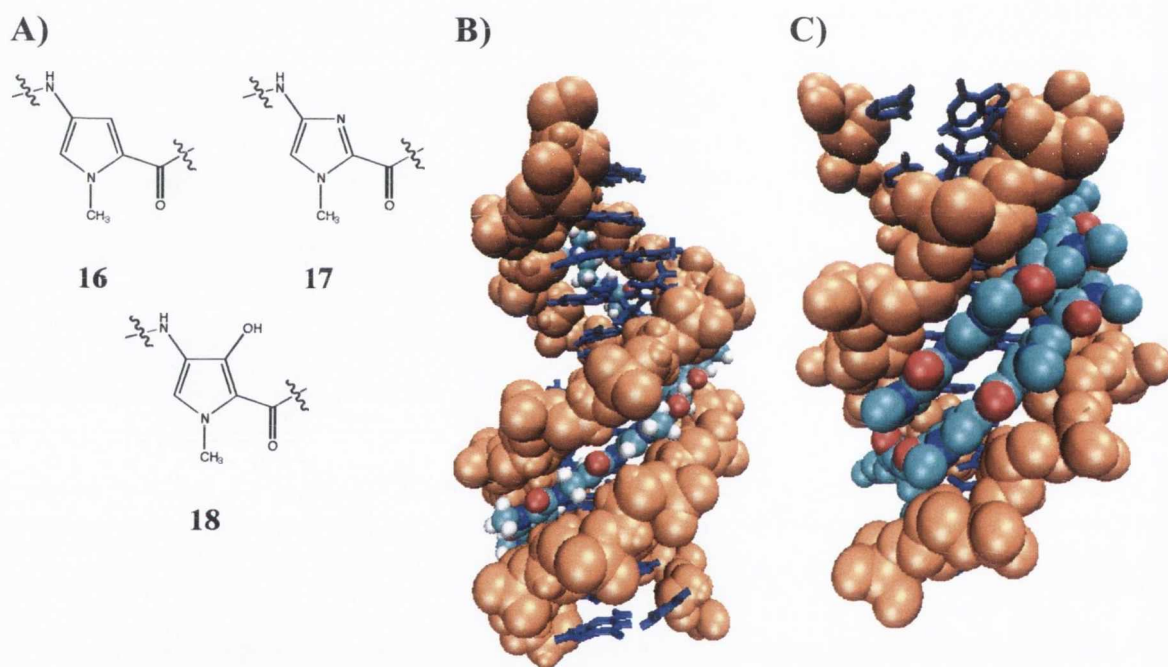
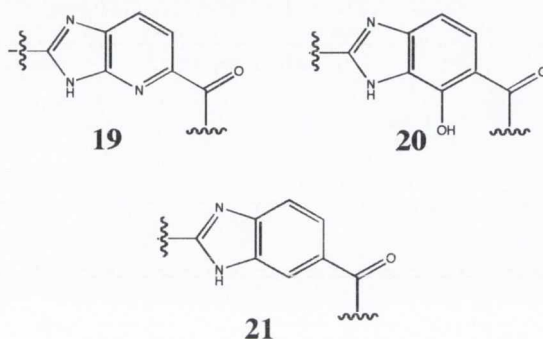


Figure 1.18 The synthetic minor groove binders. A) The structures of the aromatic amino acids synthesised by Dervan *et al.*¹²³⁻¹²⁷ B) The 1:1 complex to DNA formed by a β -alanine linked polyamide.¹²⁸ C) The 2:1 complex formed by two polyamides.¹²⁵

These polyamides have been successfully used to bind specific sequences *in vitro*, such as the hypoxia response element (HRE) sequence. Solid tumors contain regions of very low oxygen concentrations (hypoxia). Under these conditions, the heterodimeric hypoxia inducible factor 1 (HIF-1) complex binds to the HRE sequence, ultimately leading to the expression of hypoxia inducible proteins such as VEGF.^{129,130} Inhibition of VEGF

has shown to be sufficient to inhibit tumor growth in model systems.¹³¹ These results showed that polyamides could disrupt the binding of HIF-1 to the HRE sequence. Furthermore, polyamides were localised in the nuclei of cultured cells with no deleterious effects on growth or replication rates.¹³⁰

Due to the instability of the 3-hydroxypyrrole and the overcurvature of the *N*-methylpyrrole, the search for other binding motifs continued and ultimately led to the incorporation of 5-6 bicyclic benzimidazole structures **19-21**.¹³²⁻¹³⁴



These systems showed increased binding affinity and specificity to their 5-membered counterparts due to an increased degree of rigidity and a curvature that suited the inherent curvature of the DNA helix.

1.5 Conclusion

Cancer research has revealed that cancer is a disease involving dynamic changes to the genome that cause deregulation of important processes such as cell proliferation and programmed cell death. The basic biology of cancer has led to the development of approaches that target the molecular abnormality found in specific types of cancer, such as the use of Glivec **1** for the treatment of CML. Although **1** has improved the life expectancies of CML patients, cancer cells acquire resistance to the drug, which has led to the generation of a group of second-generation inhibitors.

Due to the observed resistance of targeting drugs such as **1**, DNA interacting agents have gained considerable attention. These small molecules inhibit cellular processes, thereby forcing the cell to examine the subsequent damage and to initiate programmed cell death. The mechanisms of action shown by these drugs have been thoroughly studied and many drugs are now in clinical trials such as Quinamed®, a dihydrochloride salt of amonafide **7**.

As discussed in previous sections, modern cancer chemotherapy agents suffer from several drawbacks, such as lack of DNA sequence specificity, cellular resistance and

cancer cell specificity. To improve the efficacy of modern cancer drugs, a major collaborative effort from many fields of science is needed.

1.6 Work Described in This Thesis

The objective of this multidisciplinary PhD is to address the issue of DNA sequence specificity by four novel means. The first class of compounds discussed in *Chapter 2*, are novel peptide functionalised 1,8-naphthalimides. The general structures of these compounds are shown in Figure 1.19 A.

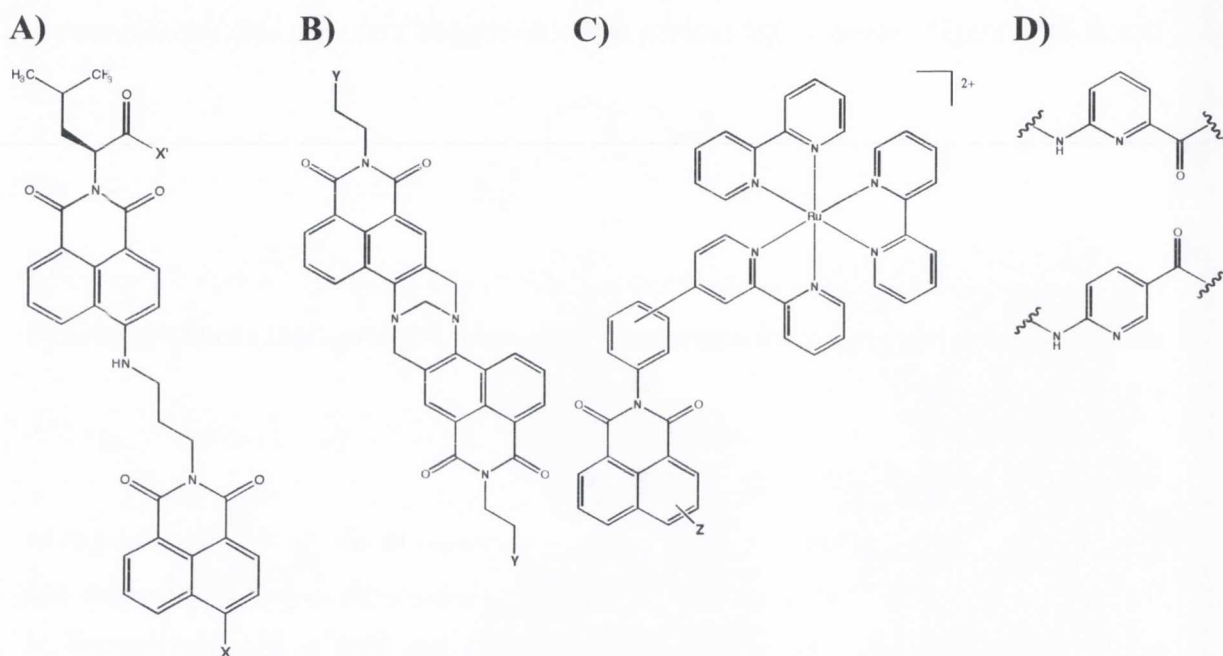


Figure 1.19 General structures of compounds discussed in this Thesis. **A)** The peptide-based 1,8-naphthalimides. **B)** The 1,8-naphthalimide incorporated Tröger's bases. **C)** The Ruthenium Tris(Bipyridine) connected 1,8-naphthalimide. **D)** Pyridine amino acids.

This approach is based on the inherent intercalation property of the 1,8-naphthalimide unit and the recognition feature of peptides. The compound's cytotoxic activity and mechanism of action in leukemic cells will be evaluated using standard biological assays and fluorescent microscopy. This work was done in collaboration with Dr. Gillian Hussey, Dr. Celine Blais and Dr. Tony McElligott.

In *Chapter 3*, a series of Tröger's base compounds that have incorporated 1,8-naphthalimide units are described (Figure 1.19 B). These compounds have been shown to bind tightly to DNA in a cell-free system.⁶ Their ability to induce cell death and their

effects on the topoisomerase enzyme family will be compared to the activity of their precursors. This work has been done in collaboration with Dr. Emma Veale.

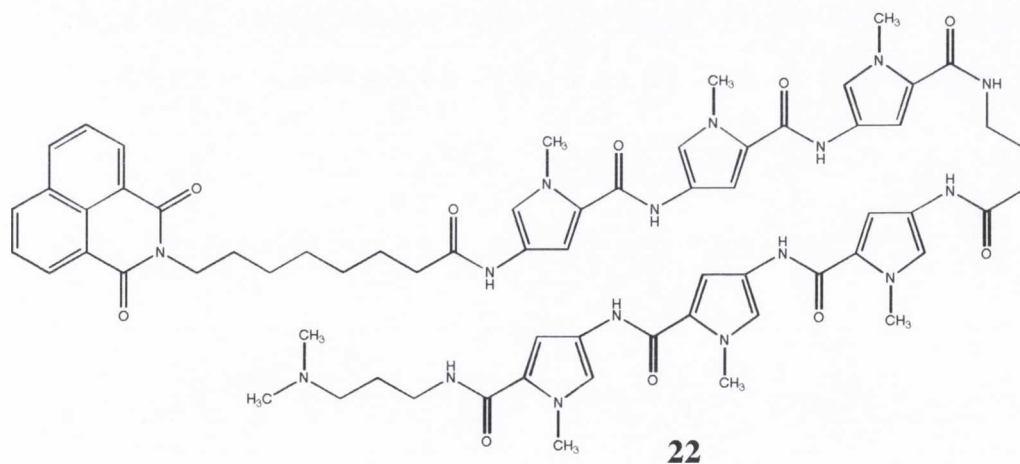
In *Chapter 4*, the biological evaluation of a series of novel photodynamic therapy agents will be discussed. The ruthenium tris(bipyridine), depicted in Figure 1.19 **C** have been shown to bind DNA by intercalation in a cell-free system and induce DNA cleavage by photoinduction.^{135,136} Their cellular uptake and their mechanism of action will be investigated. This work was done in collaboration with Dr. Gary James Ryan.

In *Chapter 5*, the synthesis of a pyridine minor groove binder will be described. This approach is based on work described in *Section 1.4.1.3*. The pyridine unit shown in Figure 1.19 **D** would be an interesting addition to the aromatic amino acids, mentioned in previous sections, because of its size and curvature. Finally, in *Chapter 7* general experimental procedures are outlined.

2 The Biological Examination of Peptide Based 1,8-Naphthalimides

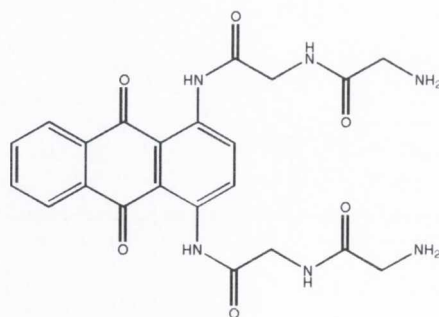
2.1 Introduction

As discussed in *Chapter 1*, the potential of small molecules that target DNA in a sequence specific manner, has long been realised and has had major implications in medicine, as well as for basic research. Such DNA targeting compounds must satisfy a certain criteria before being considered effective in treating human diseases. For example, they must be actively taken up by cells, while surviving the biochemically active environment within the cells, and reach their intended target. Furthermore, targeting of the genome requires both selective interactions and high affinity for specific DNA sequences. One way of achieving this is by combining the effects of different DNA binding modes, such as **intercalation**, **electrostatic** and **hydrogen bonding interactions** in a single molecular target, as discussed in *Section 1.4.1.1*. To date several excellent examples have been published that attempted to achieve this, one example is that of Lee *et al.*¹³⁷ who combined the intercalation effect of the 1,8-naphthalimide chromophore with the groove binding effect of pyrrole-imidazole polyamides, giving conjugate **22**. Ethidium bromide displacement studies showed that the 1,8-naphthalimide moiety of **22** intercalated into DNA upon binding. In addition, DNase I footprinting, thermal denaturation (T_m), circular dichroism (CD) and surface plasma resonance (SPR) studies established that sequence selective binding to a Topo II gene promoter regulatory sequence was driven by the pyrrole-imidazole portion of **22**, in a similar manner as explained in *Section 1.4.1.1.4*.¹³⁷



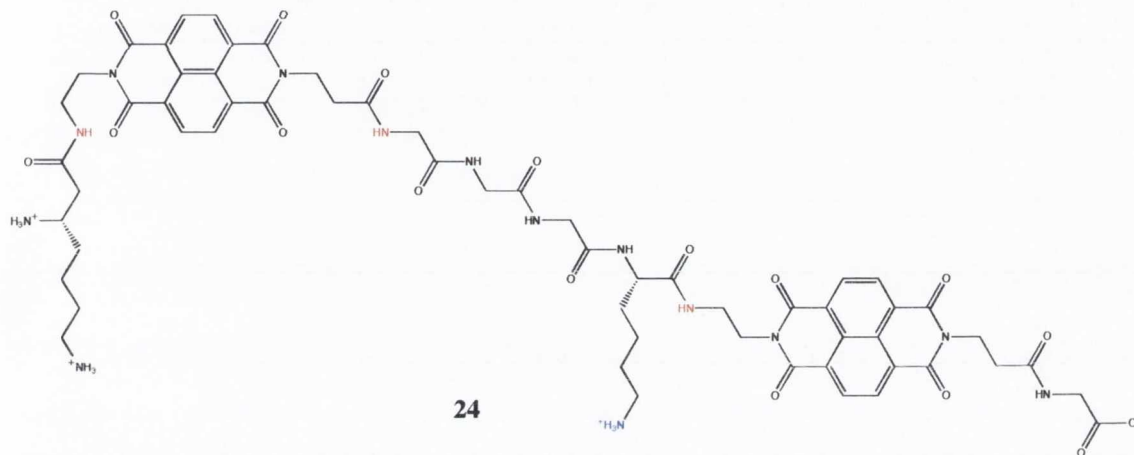
The above example demonstrated that selective DNA targeting is possible and in the last decade, the design and synthesis of novel sequence specific DNA binding agents has received considerable interest.¹¹⁵ It is well known that the precise recognition of defined DNA sequences in biological systems is mediated by enzymes and proteins having

appropriate structural motifs for DNA recognition.⁷⁷ Proteins employ their amino acid residues to form hydrogen bonds to DNA bases, where the amino acid residues are found to bind different bases, depending on the structure of the DNA sequence and are often able to bridge two stacked bases by forming hydrogen bonds between both parts. Despite this level of complexity, some success has been achieved by using synthetic peptides containing zinc finger motifs as mimics of the naturally occurring DNA binders.¹³⁸ The recognition element of naturally occurring peptides also has been used, in conjunction with intercalating moieties to achieve selective DNA targeting, as in the case of **23**, which was developed by Palumbo and coworkers.¹³⁹ Fluorescent spectroscopy investigations on calf thymus DNA (*ct*-DNA) suggested that the presence of glycine in the second position of **23** improved the specificity to cytosine and guanine base pairs (**C:G**) when compared to a lysine derivative, which distributed more evenly along the nucleic acid backbone. The authors speculated that the electrostatic contribution of the lysine side chains interacted non-specifically with the phosphate groups of the DNA backbone, leading to low specificity. Moreover, the *D*-isomers of these anthraquinone derivatives showed stronger affinity than *L*-isomers to DNA, indicating a possible advantage for the design of new drugs.¹³⁹ Furthermore, these compounds were tested for activity against human tumor cells, such as the APL cell line, HL-60. The toxicity was shown to correlate with the nature of the amino acid in the side chain rather than the number of amino acids in the side chain.¹³⁹ Importantly, **23** exhibited a moderate interference with the Topo II-DNA cleavable complex, stimulating double strand breaks. This topic will be discussed in Section 2.6 of this chapter.

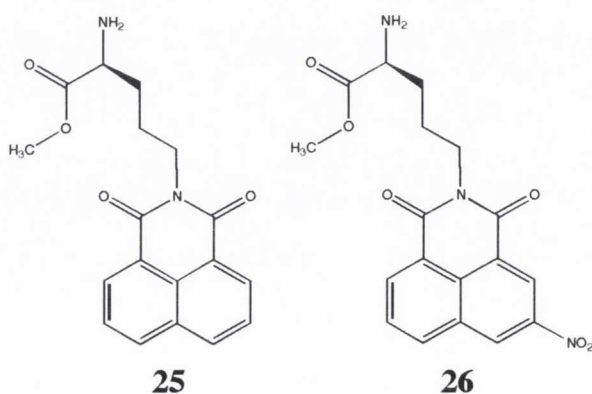
**23**

Another example of the use of chromophores conjugated to a peptidyl chain is that of Iverson *et al.*¹⁴⁰ who further showed that the peptide bis intercalator **24** binds DNA by intercalation, or more specifically, by the threading of the naphthalene diimide *via* the

major groove, in a similar manner to that of the bis 1,8-naphthalimides **11** and **12**, discussed in *Chapter 1*. In this example, the naphthalene diimide parts showed a preference for the binding to **G:G** steps, which was possibly enhanced through the formation of specific hydrogen bonds between the amide N-H groups (shown in red) and the oxygen of guanine. Furthermore, the NH_3^+ (shown in blue) from the lysine residue was folded towards the negatively charged phosphate backbone of DNA, thus improving the DNA recognition and the overall strength of the binding.



Other examples of a peptide intercalator includes the *L*-lysine based 1,8-naphthalimides **25-26** that showed high DNA cleavage efficiency and selectivity upon photoirradiation.¹⁴¹ While the specificity for the **5'-G-G-3'** cleavage of **25** was not fully explained by Saito *et al.*¹⁴¹, they speculated that an electron transfer occurred from the mostly electron-rich **G-G** step, to the photoexcited 1,8-naphthalimide **25**, and that this was the first step of the photooxidative destruction of the guanine base. Moreover, a single strand cleavage was observed by **25**, which was thought to result from the oxidation of the guanine base.

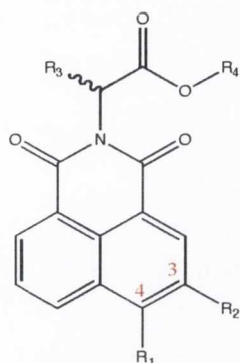


In comparison, the 3-nitro 1,8-naphthalimide **26**, was shown to be able to photonic double stranded DNA, preferentially at the location of thymine (T) residues. The selectivity exhibited by **26** was thought to arise from a hydrogen abstraction from the methyl group of the thymine, by the photoexcited nitro group of **26**.

These few examples show that the combination of naturally occurring amino acids and peptides with intercalating chromophores is a highly attractive mean of gaining site specific targeting of DNA. With this in mind, the Gunnaugsson group has developed a large library of compounds based on the combination of the 1,8-naphthalimide structure and amino acids, or short peptides. As discussed in *Section 1.4.1.1.2* in *Chapter 1*, the 1,8-naphthalimide compounds have been shown to possess cytotoxic properties against various human cancer cells,⁹³ and they that can easily be modified to allow introduction of various different conjugates; which could in principle tune the cytotoxicity of these compounds. Furthermore, the amino substituted 1,8-naphthalimides are highly fluorescent in the visible region ($\lambda_{\text{max}} \sim 550 \text{ nm}$) with high quantum yields, rendering molecules that could act as sensors. These characteristics are ideal for designing a bifunctional chemotherapeutic agent that potentially could be used simultaneously to visualise cancer cells and exert therapeutic effects on cancer cells. This chapter describes the biological investigations of a group of these bifunctional peptide based 1,8-naphthalimide compounds. However, a short summary of the studies that were carried out in the Gunnaugsson group on various families of 1,8-naphthalimide structures is detailed in the next section.

2.1.1 Previous Work from the Gunnaugsson Research Group

In the pursuit of enhanced selectivity and stronger binding affinity to DNA, the Gunnaugsson research group are involved in the design and modification of the 1,8-naphthalimide chromophore using the recognition elements of amino acids.^{4-6,142} To date, several hundred mono 1,8-naphthalimide conjugates have been synthesised, using solution phase peptide chemistry. The basic structures comprises of a nitro, chloro, bromo or amino 1,8-naphthalimide chromophore that are substituted either at the third or the fourth position of the aromatic ring as shown in Figure 2.1. These 1,8-naphthalimide chromophores are connected to an α amino acids such as glycine, *L*-alanine, leucine, phenylalanine and lysine. Their synthesis are described in the thesis of Dr. Hussey⁴ and Dr. Phelan¹⁴², respectively.



Compound	R ₁	R ₂	R ₃	R ₄	EC ₅₀ (μM)
27	H	NO ₂	H	CH ₃	29.8
28	NO ₂	H	H	CH ₃	4.10
29	H	NO ₂	<i>L</i> -CH ₃	CH ₃	61.5
30	H	NO ₂	<i>D</i> -CH ₃	CH ₃	91.0
31	NO ₂	H	<i>L</i> -CH ₃	CH ₃	2.24
32	NO ₂	H	<i>D</i> -CH ₃	CH ₃	2.81
33	H	NO ₂	<i>L</i> -CH ₂ CH(CH ₃) ₂	CH ₃	24.7
34	NO ₂	H	<i>L</i> -CH ₂ CH(CH ₃) ₂	CH ₃	2.34
35	NH ₂	H	<i>L</i> -CH ₂ CH(CH ₃) ₂	CH ₃	22.0
36	H	NO ₂	<i>L</i> -CH ₂ Ph	CH ₃	19.2
37	NO ₂	H	<i>L</i> -CH ₂ Ph	CH ₃	1.95
38	NH ₂	H	<i>L</i> -CH ₂ Ph	CH ₃	33.0

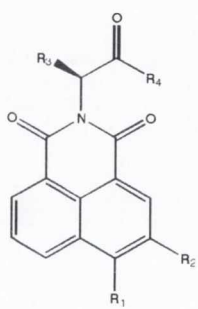
Figure 2.1 The basic structure of the peptide based mono 1,8-naphthalimides 27-38 and their corresponding EC₅₀ values. Examples of peptide based mono 1,8-naphthalimide derivatives synthesised by Gunnlaugsson *et al.*^{4,142} The generic structure is shown along with EC₅₀ value obtained after 24 hours treatment in HL-60 cells. The EC₅₀ value refers to the concentration of a compound, which induces a response halfway between the baseline and the maximum.

In collaboration with Prof. Lawler and Dr. McElligott in the Institute of Molecular Medicine, St. James' Hospital, these peptide-based 1,8-naphthalimides were screened for cytotoxic activity in the **HL-60** cell line that was originally derived from a patient suffering from an acute promyelocytic leukaemia and a selection of the most active compounds underwent further screening in the CML cell line, **K562**. From these results, Gunnlaugsson *et al.* established that:

- An amino acid with a large side group was preferred in the first position.
- *L*-amino acids were preferred over *D*-amino acids.
- The nitro substituted 1,8-naphthalimides were the most active (e.g. 28, 31, 32, 37).
- A substitution at the 4th position of the 1,8-naphthalimide chromophore was preferred over the 3rd position.

As shown in the table in Figure 2.1, these results are in contradiction to the structure and activity analysis (SAR) published by Braña *et al.*⁹³, where they concluded that substitution at position 3 of the 1,8-naphthalimide gave optimal cytotoxic activity against various cancer cell lines. Furthermore, Braña *et al.*⁹³ deduced that the presence of a basic terminal group in the side chain was essential for cytotoxic activity. Although peptide derivatives 27-38 lack the terminal nitrogen in their structure, they generally showed only

ten-fold decrease in activity compared to the reference compound, mitonafide **7** that had been previously been developed by Braña *et al.*⁹³ as was discussed in Section 1.4.1.1.2 in Chapter 1. The introduction of dimethylamine in a terminal position of the peptide derivatives, resulted in diminished activity in all cases expect for the 3-nitro alanine derivative **39** as summarised in Figure 2.2.



Compound	R ₁	R ₂	R ₃	R ₄	EC ₅₀ (μM)
29	H	NO ₂	CH ₃	OCH ₃	61.5
31	NO ₂	H	CH ₃	OCH ₃	2.24
33	H	NO ₂	CH ₂ CH(CH ₃) ₂	OCH ₃	24.7
34	NO ₂	H	CH ₂ CH(CH ₃) ₂	OCH ₃	2.34
39	H	NO ₂	CH ₃	NHCH ₂ CH ₂ N(CH ₃) ₂	11.5
40	NO ₂	H	CH ₃	NHCH ₂ CH ₂ N(CH ₃) ₂	5.76
41	H	NO ₂	CH ₂ CH(CH ₃) ₂	NHCH ₂ CH ₂ N(CH ₃) ₂	75.7
42	NO ₂	H	CH ₂ CH(CH ₃) ₂	NHCH ₂ CH ₂ N(CH ₃) ₂	3.23

Figure 2.2 Analysis of the effect of the dimethylamine group on cytotoxic activity against HL-60 cells. The generic structure is shown along with different constituents and corresponding EC₅₀.

These results further suggested that the peptide based 1,8-naphthalimides behave in a different way to mitonafide **7** and amonafide **8**. This research is still ongoing and the PhD work described herein involved the cytotoxicity screening of novel 1,8-naphthalimide derivatives against the HL-60, K562 and HeLa cell lines, examples of which are shown in Figure 2.3. These novel 1,8-naphthalimide derivatives contain modifications of peptide side group or the substitution group as shown for EV273 and RD069, respectively. However, due to the considerable time it would take to discuss individual compounds and for the sake of keeping context, the results from these screenings and structures of numerous different 1,8-naphthalimide derivatives can be found in Table A1.1 in Appendix 1 and will be referred to throughout this section.

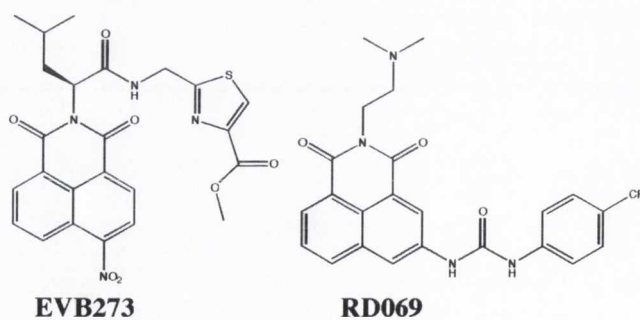


Figure 2.3 Examples of novel 1,8-naphthalimide derivatives being developed by the Gunnlaugsson research group.

Three new series of bis intercalating agents were also designed within the Gunnlaugsson group by using the structural features of the lead mono 1,8-naphthalimide derivatives. The first series consisted of so-called “head to head” linked 1,8-naphthalimides as exemplified by the symmetrical **43** and the unsymmetrical **44** shown in Figure 2.4. These compounds were shown to be the most cytotoxic derivatives in preliminary testing, having EC_{50} values of 3.46 μ M and 4.58 μ M, respectively. As for the mono 1,8-naphthalimides, the 4-nitro 1,8-naphthalimides were the most active members of this family.

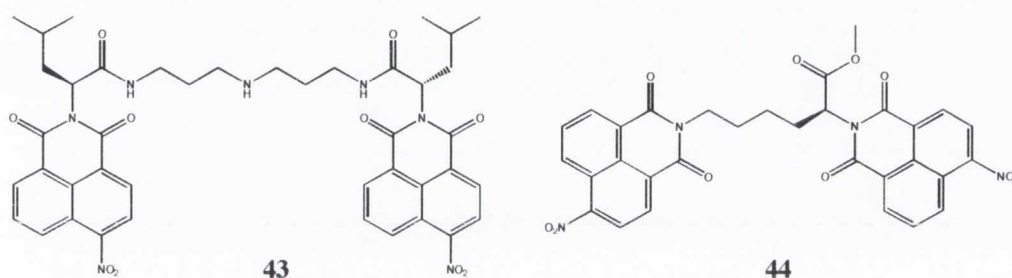


Figure 2.4 The most active “head to head” family members developed by Dr. Hussey.⁴

The second family developed by Dr. Gillespie, involved the linkage from the 4-position of the 1,8-naphthalimide chromophore, as shown in Figure 2.5 and was called the “tail to tail” family. These compounds were a part of the investigations that were carried out during this PhD work and their results and structures are shown in Appendix 1. The aminoalkyl derivative **45** showed comparable activity to that of the “head to head” bis 1,8-naphthalimide ($EC_{50} = 2.7 \mu$ M) analogue in HL-60 cells. While, the hexyl bridged naphthalene diimide linked 1,8-naphthalimides **46**, displayed considerable activity against HL-60 cells ($EC_{50} = 31.6 \mu$ M) the shorter chain analogues such as, pentyl and propyl displayed less activity in this cell line.

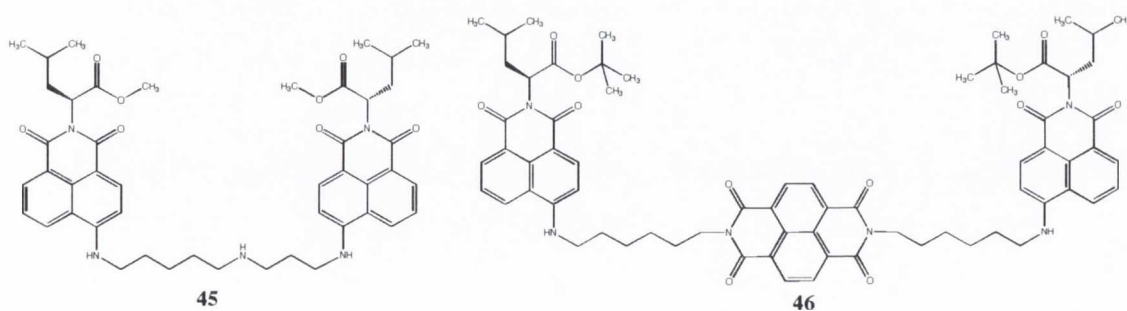


Figure 2.5 Examples of the “tail to tail” family developed by Dr. Gillespie.⁵

Furthermore, fluorescent microscopy studies suggested that **46** was localised in the nucleus in HL-60 cells after 24 hours incubation. However, these compounds were shown to suffer from water insolubility that might affect their cytotoxic activity. Gillespie concluded in her PhD thesis that these naphthalene diimide analogous operated *via* an alternative-binding mode to their mono 1,8-naphthalimide precursors⁵, where the binding mechanism was thought to involve the treading of the naphthalene diimide part of the molecule and the subsequent groove binding of the two 1,8-naphthalimide groups.

The third series consisted of “*head to tail*” linked 1,8-naphthalimides, which were developed as potential visualising agents that possessed cytotoxic activity. These compounds showed the same trend as observed for the mono 1,8-naphthalimides and the “*head to head*” 1,8-naphthalimides, i.e. the cytotoxic activity was maximised when, i) the nitro group was in the fourth position and ii) a large group was situated in the side chain of the amino acid. Furthermore, the toxicity of these compounds was maximised when a three-carbon bridge separated the two 1,8-naphthalimide chromophores.

2.1.2 The Work Described in This Chapter

As examples throughout this section have shown, this PhD involved the cytotoxic screening of numerous different 1,8-naphthalimide compounds that were synthesised by the various members of the Gunnlaugsson research group. However, it was decided to investigate the mechanism of action of a relatively small group of molecules in an attempt to elucidate information about their mechanism of action. These compounds were chosen for comprehensive biological investigations because of their different structural components and photophysical abilities. The work described in this chapter discusses the anti cancer toxicity of the water soluble mono 1,8-naphthalimide **47** developed by Dr. Hussey⁴ and the novel “*head to tail*” bis 1,8-naphthalimides, **48-51** developed by Dr. Blais, a former postdoctoral fellow in the Gunnlaugsson group.¹⁴³ These compounds are shown in Figure 2.6. The bis 1,8-naphthalimides were developed to integrate two important factors for cancer therapeutics, their luminescence within cells and cytotoxicity. As described in *Section 1.4 of Chapter 1*, surgery is one of the main options for a patient diagnosed with cancer and therefore, the fluorescence arising from the excitation of the 4-amino 1,8-naphthalimide of **48-50** could possibly be used to visualise cancer cells, which would improve the results from surgery. Furthermore, patients also show sign of reoccurring disease after surgery, however studies have shown that by treating the patient with therapeutic drugs after surgery dramatically increases the life expectancy of the

patient.¹⁴⁴ Therefore, by incorporating a second 1,8-naphthalimide chromophore in these compounds, might possibly give these molecules cytotoxic potential.

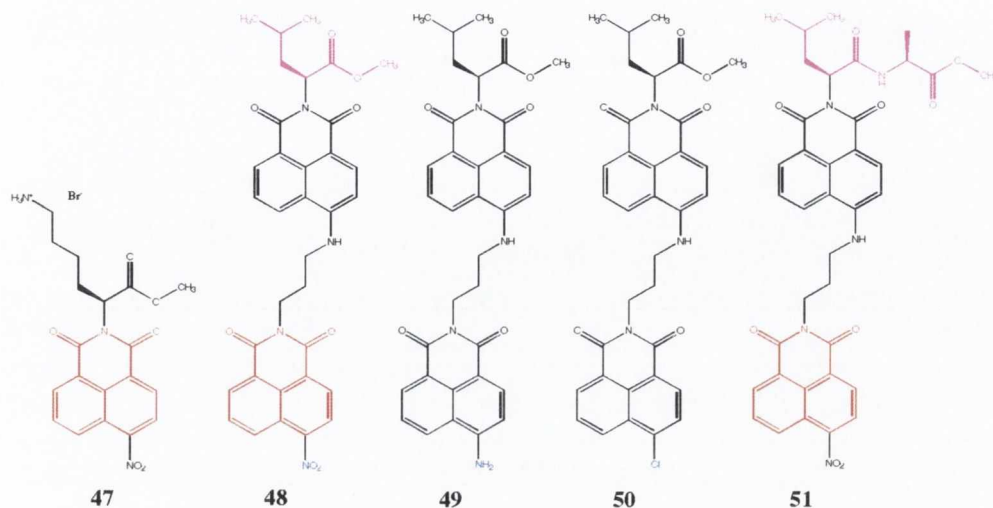


Figure 2.6 The peptide 1,8-naphthalimides 47-50. Red indicates the comparison between the mono 1,8-naphthalimide 47 and the bis 1,8-naphthalimides 48 and 51. Blue demonstrates the different constituent and purple represents the comparison between a mono peptide and a di-peptide.

The first objective was to determine the uptake of these peptide derivatives by flow cytometry. The bis 1,8-naphthalimides **48-51** were insoluble in water and therefore, they had to be dissolved in DMSO. The investigation into the cellular uptake was important to establish if the lipophilicity of these compounds hinder absorbance by cells. The fluorescence arising from the excitation of the 1,8-naphthalimide chromophore was used to determine the uptake and as well the localisation of the peptide derivatives **48-50** within the cell. The localisation studies indicated the primary site of localisation within cells and gave information about the potential these compounds had as visualising agents. This is discussed in detail in *Section 2.2*.

The second objective of this investigation was to compare the cytotoxic activity between the different derivatives, the mono 1,8-naphthalimide **47** to the activity of the bis 1,8-naphthalimides **48** and **51** against the acute promyelocytic leukaemia cell line, HL-60 by using an *MTT assay*, which will be discussed in detail in *Section 2.3* in this chapter. In addition, the activity of the amino, chloro and nitro substituents were compared and finally the leucine connected 4-nitro-1,8-naphthalimide **48** was compared to the leucine-alanine connected 4-nitro-1,8-naphthalimide di-peptide **51**.

The third objective was to determine the mode of cell death (**apoptosis** or **necrosis**) induced by **47-51** using classical apoptosis assays and if any difference in both mode and

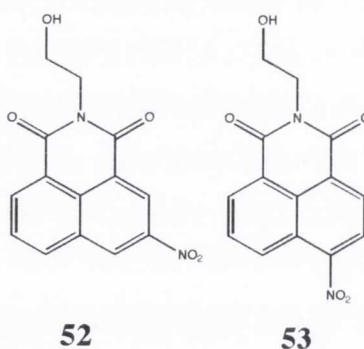
activity could be correlated with a distinct structural component depicted in Figure 2.6. The result from these investigations will be discussed in *Section 2.4*.

The fourth objective was to investigate the inhibitory activity of the peptide 1,8-naphthalimides against the Topo I and II enzymes in a cell free system. As described in *Chapter 1*, these enzymes have been shown to be the major targets of the classical 1,8-naphthalimides such as mitonafide **7** and amonafide **8**. The *Section 2.5* will deal with the results from these studies. The investigations into the biological activity of the 1,8-naphthalimide derivatives **47-51** begin with the uptake studies, as these studies were the first step in determining if these compounds reached the insides of the cells.

2.2 Cellular Uptake and Localisation Studies of 47-51

2.2.1 Cellular Uptake Studies Using Flow Cytometry

To date, there are few reports of the uptake of 1,8-naphthalimides derivatives by mammalian cells.^{94,145,146} The uptake of amonafide **8** was investigated by using *high performance liquid chromatography* (HPLC) and its uptake was shown to be rapid with apparent intracellular saturation achieved in 30 minutes.⁹⁴ Later, Hodgekiss *et al.*¹⁴⁶ reported the synthesis and corresponding biological activity of potential fluorescent markers for hypoxic cells, which were based on the 3-nitro- and 4-nitro-1,8-naphthalimide chromophores, such as derivatives **52** and **53**, respectively.



The uptake of **52** was determined by extracting the surviving fraction of **52** from the cell medium and calculating the concentration by HPLC.¹⁴⁵ The authors concluded that the preferential fluorescence in hypoxic cells observed by **52** arose from bioreduction of the nitro group. However, the 4-nitro derivative **53** showed strong and similar fluorescence in both hypoxic and oxic cells. The fluorescence within cells was studied using a combination of fluorescent microscopy and flow cytometry.¹⁴⁶

Flow cytometry is a technique that measures and analyses multiple physical characteristics of a single particle, normally cells, as they flow in a fluid stream through a beam of light.¹⁴⁷ These characteristics are determined using an “optical to electric” coupling system that records how a cell scatters incident laser light and emits *fluorescence*.¹⁴⁷ Light scattering occurs when a particle deflects an incident light, the extent depends on the physical properties of a particle, namely its size and internal complexity. The flow cytometry can read up to 10,000 cells in approximately a minute, thereby giving a good approximation of the characteristics and morphology of the overall cell population. *Forward light scatter* (FCS) is proportional to the size of the cell and measurement of mostly diffracted light and is detected just off the axis of the incident light beam in the forward direction by a photodiode detector (Figure 2.7 A).¹⁴⁷

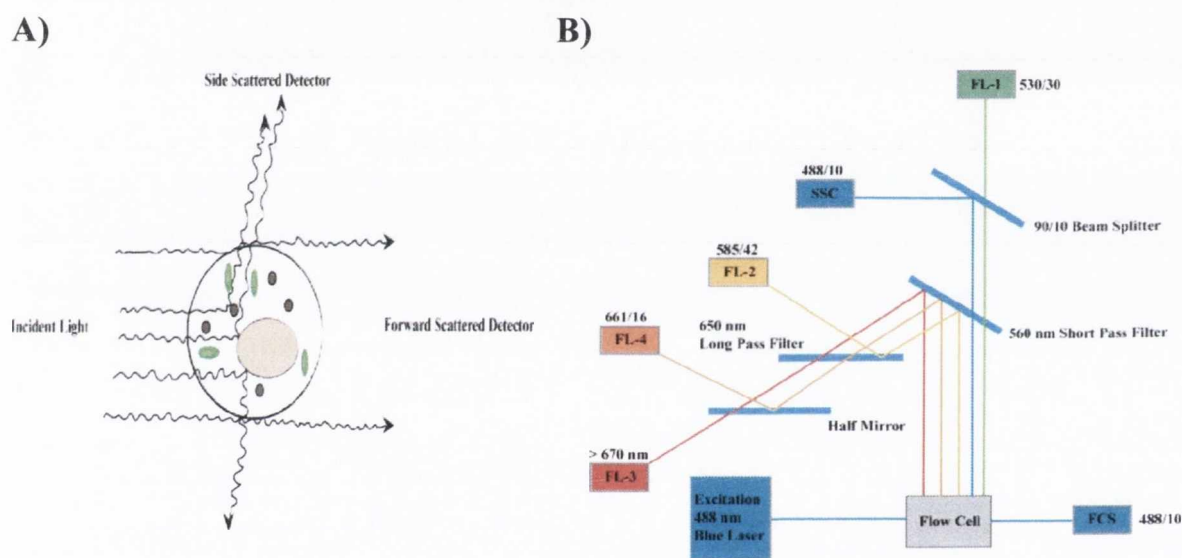


Figure 2.7: The parameters of flow cytometry. A) The light scattering properties of a cell. **B)** The optical setup of the FACScalibur flow cytometer.¹⁴⁷

In contrast, *side scattered light* (SSC) is proportional to the internal complexity. SSC is a measurement of a reflected light that occurs at any interface within the cell where the refractive index changes (Figure 2.7 A). By plotting the FCS against the SSC cells can be discriminated on the basis of their morphological appearance, *i.e.* their size and condensation, which can be used to distinguish apoptotic cells from the live cell population because the hallmarks of apoptosis involved cell shrinkage and nuclear condensation, as discussed in *Section 1.2.2* in *Chapter 1*. In addition to the investigation into the cell morphology, the major application of the flow cytometry involves fluorescence detection. Numerous fluorophores can be used to detect various events within the cell, such as the

analysis of the cell cycle and detection of the mitochondrial membrane potential, that will be discussed in detail in *Section 2.5* and *Section 4.5*, respectively. Furthermore, an argon laser that is commonly used in flow cytometry can be used to excite more than one fluorescent compound, offering the potential of simultaneously investigating two or more events within cells. The filters and optical mirrors for the flow cytometry system used throughout this Thesis is shown in Figure 2.7 **B**. As already discussed, the compounds **47-51** have been shown to be fluorescent and hence it was decided to utilise the aforementioned flow cytometry system to establish the uptake of these compounds by cells. Similar investigations have been used to detect fluorescence from **52** and **53** within cells and Barton and coworkers have used this assay to investigate the uptake of Ru(II) complexes.^{146,148}

For the studies described herein, HL-60 cells were treated with compounds **47-51** at 0.5 μM concentration over different periods, ranging from 30 minutes to 24 hours and then washed with *phosphate buffered saline* (PBS) to minimise nonspecific binding to the external part of the cell membrane. After this treatment, the FCS versus SSC chart was recorded of investigated cells and the results were used to discriminate between live and viable cells from apoptotic cells and non-cellular debris. The live cell population corresponds to the accumulation of dots shown in Figure 2.9 **A**, where cellular debris are shown to possess both lower FCS and SSC. The live population was gated so that only cells in this region were included in the analysis of fluorescence emission arising from **47-51** and importantly, this would prevent particles of the 1,8-naphthalimide compounds **47-51** to influence the results. This was believed to be necessary due to the insolubility of these compounds in water. To detect the fluorescence emission of untreated and treated cells, the *FL-2 channel* of the flow cytometry system shown in Figure 2.7 **B** was used. Investigations were carried out in triplicate and the results from these additional sets of experiments were shown to be identical within experimental error and can be found in *Figure A1.1* in *Appendix 1*. However, an example of a result obtained from these investigations is shown in Figure 2.8 **B** for HL-60 cells treated with the 4-nitro-1,8-naphthalimide compound **47**. The solid purple peak represents the auto fluorescence from cells that have been left untreated. As depicted in Figure 2.7 **B**, 30 minutes incubations with compound **47** lead to a shift in fluorescent intensity, that indicated the rapid uptake of this compound and furthermore suggested that **47** was within cells after treatment. The example shown in Figure 2.8 **B** shows that the 4-nitro derivative **47** was absorbed by HL-60 cells after 30 minutes of incubation and the fluorescent intensity decreased over time.

Although there might be numerous reasons for this behaviour, these results can be explained by the fact that **47** might be transferred out of cells, leading to decreased concentration with the cells and therefore less detected fluorescence intensity.

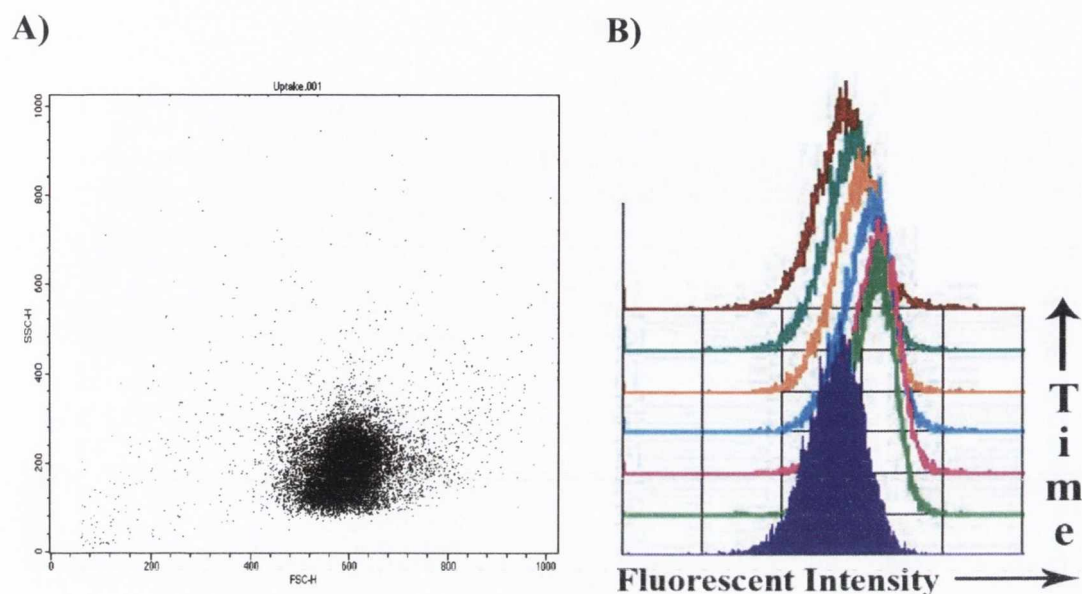


Figure 2.8 An example of results from cell uptake studies. **A)** The FSC v.s. SSC printout showing the population of viable cells. **B)** The plot of emitting fluorescence intensity from HL-60, as determined by flow cytometry cells in absence (—) and in presence of **47** (0.5 μ M) after 30 min. (—), 60 min. (—), 3 hours (—), 6 hours (—), 9 hours (—) and 24 hours (—).

In addition, these results could also indicate that **47** might not be stable in the condition used for cell incubation. When compared to the bis 1,8-naphthalimides, **47** showed less shift in fluorescence from untreated cells than the 4-nitro bis 1,8-naphthalimide derivatives **48** and **51**, which are shown in Figure 2.9 **A** and **B**, respectively. These observations suggest that the substantial difference in fluorescent intensity between **47** and **48-51** resulted from the incorporation of the 4-amino 1,8-naphthalimide into the structure of **48** and **51**, as was discussed in Section 2.1.2. As a result, the limited range of excitation at 488 nm by the flow cytometry system would only manage to excite a small population of **47** due to the low absorbance at this wavelength, while the 4-amino 1,8-naphthalimide of **48** and **51** would be excited to a larger extent. Furthermore, these results could also be explained by the fact that **47** is charged and the lipid bilayer of the cell membrane is impermeable to charged molecules.¹⁴⁹ Interestingly, treatment with compound **48** and **51** for 9 hours resulted in the appearance of an additional new fluorescence peak, which was of lower intensity than the original peak as can be shown in Figure 2.9. As in

the case of **47**, this could suggest that **48** and **51** were not stable at the conditions used for cell culture. These results could also suggest that **48** and **51** must be transformed into different molecules that emitted less fluorescence than the original compounds.

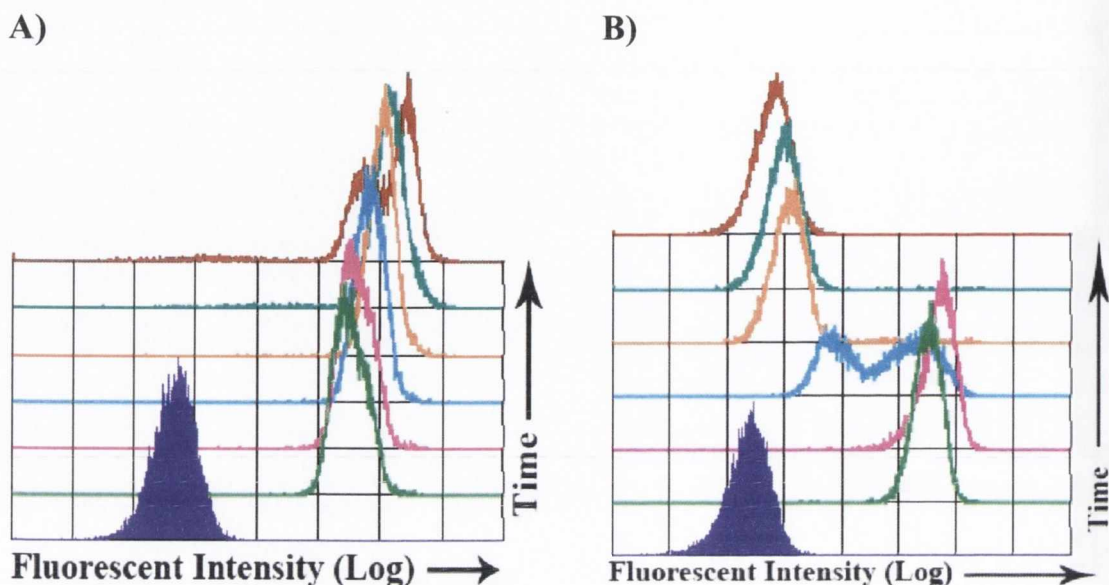


Figure 2.9 Histograms of the emitting fluorescence intensity from HL-60 cells. Cells treated with **A)** **48** ($0.5 \mu\text{M}$), **B)** **51** ($0.5 \mu\text{M}$) for 30 min. (—), 60 min. (—), 3 hours (—), 6 hours (—), 9 hours (—) and 24 hours (—). Untreated cells are shown as a solid purple peak. These graphs are representative of three separate experiments.

When investigating the possible modification of these structures of **48** and **51** that could explain this behaviour, several possible explanations were introduced. First, the common 4-nitro group in their structure had been shown to be metabolised in cells in hypoxic environment,¹⁴⁶ however the assay condition described herein involved normal oxygen levels. Furthermore, to induce such a decrease in fluorescent intensity, the nitro group would have been completely removed from the 1,8-naphthalimide chromophore and such a behaviour has not been reported to our knowledge. Secondly, these compounds possess a secondary amino group at the fourth position of the peptide-linked 1,8-naphthalimide chromophore. The observed decrease in fluorescent intensity might have occurred from the binding of **48** and **51** through a hydrogen bonding interaction involving the lone pair of the secondary amino group.

As shown in Figure 2.10 **A** and **B**, the bis 1,8-naphthalimides **49** and **50** showed less fluorescent intensity when compared to **48** and **51** and furthermore, they did not show similar behaviour as to that observed for **48** and **51**, respectively. There are several plausible explanations for the observed difference between the 4-nitro 1,8-naphthalimide

derivatives **48** and **51** and the 4-chloro- and 4-amino-1,8-naphthalimide derivatives **49** and **50**. Firstly, these results could suggest that the 4-nitro group is responsible for the transformation within cell, nevertheless the delayed appearance of an additional peak for **49** and **50** can not be ruled out at this point. Furthermore, the absence of additional fluorescent peaks for **49** and **50** might be indicative of the importance of the 4-nitro group for binding to a cellular target either indicating the lack of binding to a cellular target by **49** and **50** or the delayed binding of **48** and **51**. However, further studies are needed to confirm these observations.

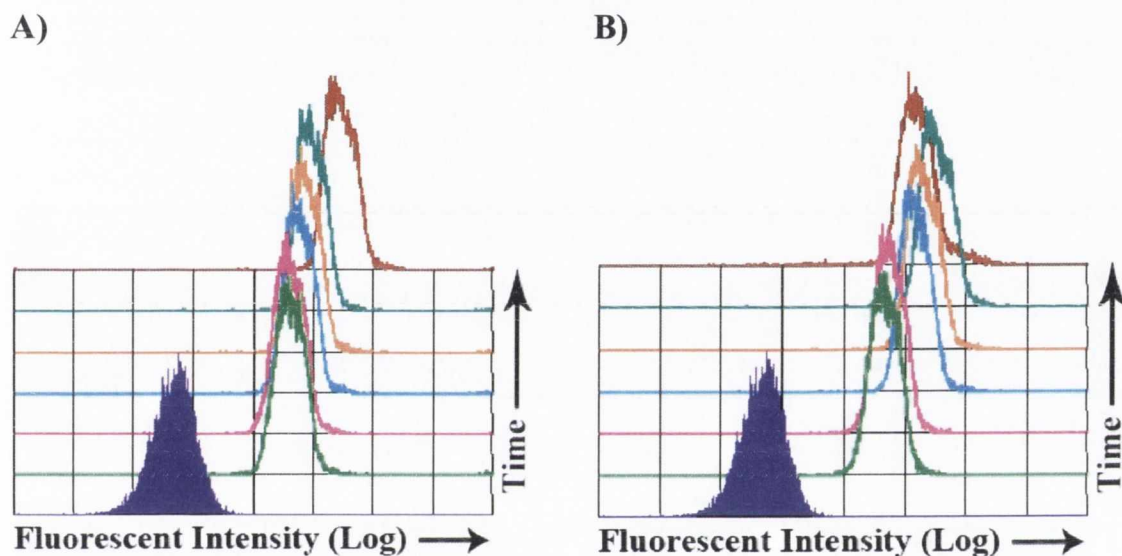


Figure 2.10 Histograms of the emitting fluorescence intensity from HL-60 cells. Cells treated with **A**) **49** ($0.5 \mu\text{M}$), **B**) **50** ($0.5 \mu\text{M}$) for 30 min. (—), 60 min. (—), 3 hours (—), 6 hours (—), 9 hours (—) and 24 hours (—). Untreated cells are shown as a solid purple peak. These graphs are representative of three separate experiments.

To summarise, compounds **47-51** were shown to enter cells after 24 hours. However, it was unknown where these compounds would localise and for that reason, it was suggested to utilise fluorescent microscopy to determine the effects of different 1,8-naphthalimide substituents on the localisation of the compounds. In addition, these investigations would also confirm the results obtained from flow cytometry, that **47-51** were indeed taken up by cells. The results from these studies are described in the next section.

2.2.2 Localisation Studies on **48-50** using Fluorescent Microscopy

As described in the last section, the results from the uptakes studies suggested that compounds **47-51** were rapidly absorbed by HL-60 cells. In addition, the 1,8-naphthalimide

chromophore has been shown to be an DNA intercalator and thus would localise in the nucleus to exert its cytotoxic activity.⁹³ For that reason, it was decided to use the inherent fluorescent properties of the 1,8-naphthalimide chromophore to determine the localisation of these drugs. Moreover, compounds **48-50** were chosen for these studies, to investigate the effects from different substituents in the 4-position of the 1,8-naphthalimide chromophore.

The nitro, amino and chloro derivatives **48**, **49** and **50**, respectively, were incubated with HL-60 cells at 37 °C in the presence of 5% CO₂ for 3 hours and 24 hours. Before analysing these cells under the fluorescent microscopy, the nucleus was counterstained with Hoechst 3342 stain, a known DNA minor groove binder that emits fluorescence in a different wavelength to the 1,8-naphthalimide compounds **48-50**. The cells were then washed with PBS to remove particles of **48-50** and to minimise nonspecific binding to the external side of the cell membrane. The 1,8-naphthalimide derivatives **48-50** and Hoechst 3342 were excited by a mercury lamp at 465-495 nm and 340-380 nm wavelengths, respectively and their fluorescence was detected by 515-555 nm and 435-485 nm detectors for the 1,8-naphthalimide derivatives **48-50** and the Hoechst 3342, respectively. The overlays of resulting images after 3 hours and 24 hours treatment are shown in Figure 2.11.

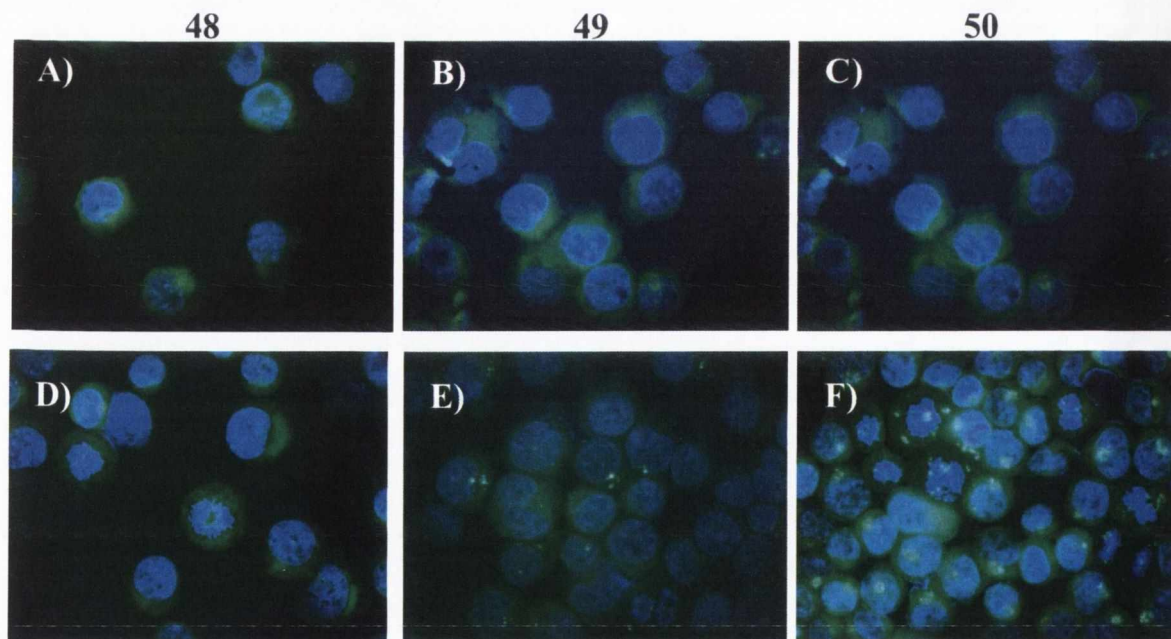


Figure 2.11 Overlaid fluorescent images of HL-60 cells incubated with **48-50** and Hoechst 3342 stain. HL-60 cells were incubated with **A, D) 48** (1.0 μ M, green), **B, E) 49** (1.0 μ M, green) and **C, F) 50** (1.0 μ M, green) for 3 hours and 24 hours, respectively. Cells were then counterstained with a nuclear dye, Hoechst 3342 (0.5 μ M, blue) for 15 minutes before analysing under a fluorescent microscope. Figures are shown at 40 \times magnification.

These results confirmed that **48-50** were taken up by HL-60 cells after 3 hours and furthermore, that these compounds were mainly situated within the cytoplasm after 24 hours incubation, in contrast what had been reported earlier for other 1,8-naphthalimides.⁹³ As shown in Figure 2.11 **E** and **F**, the amino derivative **49** and the chloro derivative **50** accumulated in distinct loci within the cells after 24 hours, while the nitro derivative **48** did not show any formation of these specific spots. In addition, compounds **47** and **51** did not show any loci formations as can be see from *Figure A1.2* in *Appendix 1*. Furthermore, these spots were absent from cells after 3 hours treatment with **49** and **50**.

Consequently, it was decided to co-stain for well-known organelles in the cytoplasm: the mitochondrion, the lysosomes and the golgi apparatus, respectively. An example from these investigations is shown in Figure 2.12 for the localisation studies of lysosomes and in addition the resulting images of other organelles can be found in *Figure A1.3* in *Appendix 1*.

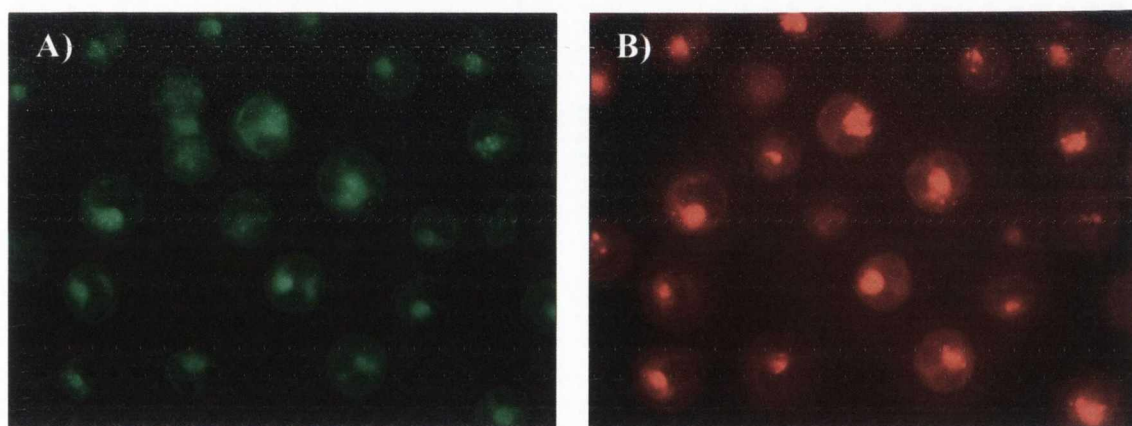
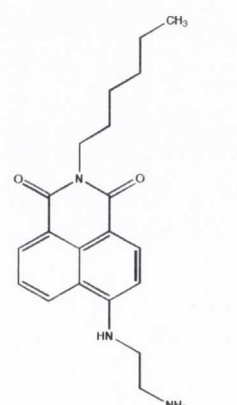


Figure 2.12 Colocalisation studies using fluorescent microscopy. HL-60 cells were incubated with **A**) **49** (1.0 μ M, green) for 24 hours. Cells were then counterstained with **B**) a lysosomal stain, LysoTracker Red (50 nm, red) for 15 minutes before investigating under a fluorescence microscopy. Figures are shown at 60 \times magnification.

The result indicated that **49** and **50** were localised in the lysosomes after 24 hour incubation and furthermore, their fluorescent intensity was believed to be higher than in the cytoplasm. The possible reasons of this observation could be that these compounds accumulated in a smaller enclosed area and therefore the concentration is higher within the lysosomes than in the bigger cytoplasm. Furthermore, these compounds could possible be broken down by the acidic hydrolases that are situated in the lysosomes.



InstantLyso LLT-1

Similar behaviour has been reported with a close analogue of the peptide derivatives, InstantLyso LLT-1, a 1,8-naphthalimide derivative that is used to stain lysosomes.⁵⁰ In addition, these investigations could suggest that the **49** and **50** are secreted out by the lysosomal vesicular secretory pathway, as has been shown with a fluorescent labelled cisplatin **4**,¹⁵¹ which was discussed in *Section 1.4.1.1.1* in *Chapter 1*.

2.2.3 Summary

The results from the flow cytometry indicated the rapid uptake of the bis 1,8-naphthalimide derivatives **47-51**. Furthermore, the uptake studies revealed a difference between the nitro derivatives **48** and **51** and the amino and chloro derivatives **49** and **50**, respectively that involved the formation of an additional fluorescent peak, which had less fluorescent intensity to the original peak. The possible explanations for the observed difference between these molecules were believed to involve the nitro group at the fourth position of the 1,8-naphthalimide, either through binding to a cellular target or transformation of these molecules within cells. The fluorescent microscopy studies confirmed that these compounds were indeed being absorbed by HL-60 cells. In addition, the 4-amino and the 4-chloro derivatives **49** and **50**, respectively were shown to be localised within the lysosomes after 24 hours incubation. These results indicated that **49** and **50** were exported out of the cells after 24 hours. Although the 4-nitro derivatives did not show the formation of these spots, further incubation periods will be needed to fully confirm this observation. However, these results have established that these compounds can cross the cell membrane and localise in the cytoplasm, potentially exerting biological activity through binding and inhibition to the proteins in the cytoplasm. Therefore, it was decided to determine the cytotoxicity of **47-51** against HL-60. In addition, these investigations might be used to correlate with the results discussed in this section, where a substantial difference from both flow cytometry and fluorescent microscopy studies was observed between different substituents of the 1,8-naphthalimide chromophore. The results for the cytotoxic investigation are described in the next section.

2.3 The Cytotoxic Activity of 47-51 against HL-60 cells

As discussed in *Section 1.4.1.1.2* in *Chapter 1*, amonafide **8** was sent to the National Cancer Institute (NCI) for screening and evaluation, where it showed considerable activity against P388 and L1210 leukemia models. A different study suggested that **8** was active against the APL cell line, HL-60 by colony-formation assay. For that reason, it was

decided to determine the cytotoxicity of compounds **47-51** against these types of cells. The cytotoxic activity of the peptide based 1,8-naphthalimides **47-51**, previously discussed was measured using an MTT colorimetric assay. The assay uses the yellow 3-(4,5-dimethylthiazol-2-yl)-2,5-diphenyl tetrazolium bromide (MTT) salt **54**, that undergoes a biotransformation in metabolically active cells to form the purple formazan **55** (Figure 2.13).¹⁵² The formazan **55** is solubilised and the resulting colored solution is quantified using a scanning multi-well spectrophotometer (ELISA reader). The amount of the purple formazan correlates directly to the number of metabolically active cells.¹⁵²

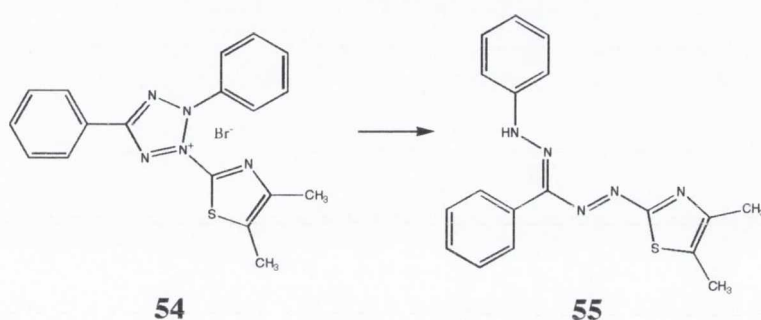


Figure 2.13 Metabolisation of MTT **54** to formazan **55** by viable cells.

The assay was performed according to the drug US National Cancer Institute (NCI) 60 human tumor cell line screening model.¹⁵³ The procedure involved inoculating the HL-60 cells into a 96 well plate followed by incubation at 37 °C, in the presence of 5% CO₂ for 24 hours before they were treated with **47-51** to maintain log-phase growth. At the time of treatment, the cell population was measured by the MTT assay. After 24 or 48 hours incubation, the absorbance reading from each well was used to calculate the percentage growth inhibition at each of the concentration levels using equations 2.1 or 2.2,

$$Ti \geq Tz, (Ti - Tz) / (C - Tz) \times 100\% \quad (\text{Eq. 2.1})$$

or

$$Ti < Tz, (Ti - Tz) / Tz \times 100\% \quad (\text{Eq. 2.2})$$

where **Ti** is the absorbance from wells that holds treated cells, **Tz** is the absorbance from cells at the time of treatment and **C** is the absorbance from cells that were treated with corresponding vehicles, dimethylsulphoxide (DMSO) in the case of **48-51**, and RPMI medium in the case of **47**. Each concentration was done in quadruplicate and experiments were repeated three times. For comparison purposes, cells were also treated with the

reference compound **7**. Three dose-responsive parameters were calculated for each of the 1,8-naphthalimide derivatives tested:

- The growth inhibition of 50% (**GI₅₀**) that corresponds to the drug concentration needed to inhibit 50% of growth compared to vehicle treated cells.
- The total growth inhibition (**TGI**) that corresponds to the concentration needed to inhibit 100% of growth compared to vehicle treated cells.
- The 50% lethal dose **LD₅₀** that indicates the concentration needed to reduce the number of cells by 50% compared to vehicle treated cells.

Compounds **47-51** and the reference compound **7** were tested using the above procedure. The resulting cytotoxicity profile shown in Figure 2.14 was obtained after 24 hours incubation. From Figure 2.14 and Table 2.1 it can be seen that, the mono derivative **47** (in red) was needed in the highest concentration to induce 50 % growth inhibition and is in fact three times less active than the bis 1,8-naphthalimide **50** (2.50 μM vs. 0.342 μM) which was found to be the most active of the compounds tested. It was also shown to be considerably less active than the corresponding nitro derivatives **48** and **51**.

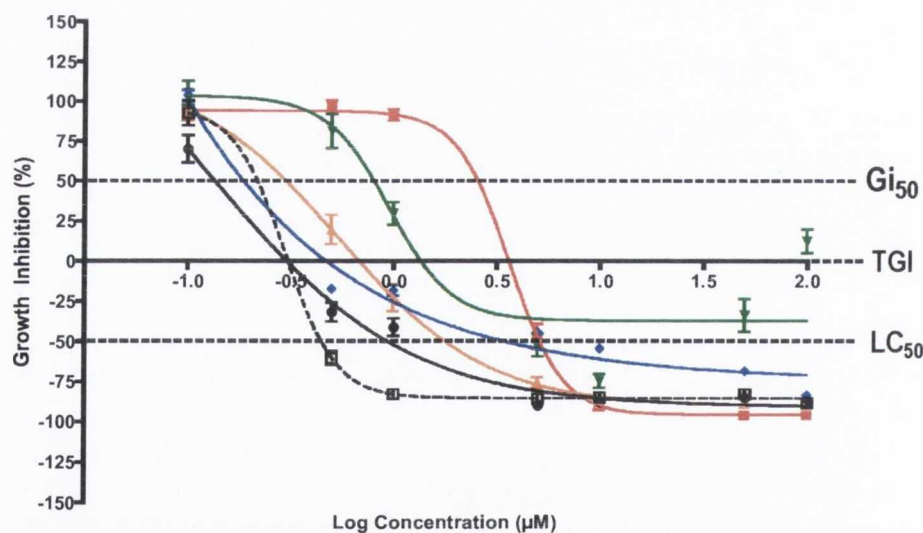


Figure 2.14 *In vitro* cytotoxic activity against HL-60 cells after 24 hours treatment. HL-60 cells were treated with **7** (□), **47** (■), **48** (▲), **49** (▼), **50** (◆) and **51** (●) for 24 hours before being analysed by MTT assay as described in text. The dotted lines indicate the position three dose-responsive parameters (**GI₅₀**, **TGI** and **LC₅₀**) on the graph. Values shown are means \pm standard errors of three independent experiments.

This result indicated that the incorporation of an additional 1,8-naphthalimide unit contributed substantially to the cytotoxicity exerted by these compounds, as in the case of the bis 1,8-naphthalimides **11** and **12**, which were discussed in *Section 1.4.1.1.2* in *Chapter 1*. Furthermore, these results correlate well with the results from our previous uptake studies that suggested that **47** suffered from poor uptake by HL-60 cells. An interesting observation was made by comparing the effects the different substituents of the 4-position of the 1,8-naphthalimide has on growth inhibition (GI_{50}). For instance, the chloro derivative **50** was shown to be twice as active as the nitro analogue **48** (0.188 μ M versus 0.342 μ M) and four times more active than the amino analogue **49** (0.188 versus 0.804). However, the chloro derivative and the nitro derivative **50** and **51** had the most effects on the growth of HL-60 cells and they showed similar ability to inhibit growth as the reference compound **7**. Furthermore, the investigation into the effects of the amino acids had on cell growth, revealed that **51** possessing an additional alanine amino acid, was nearly twice as active as its leucine analogue **48**. Together, these results demonstrated that minor structural alterations gave rise to significant changes in activity of these bis 1,8-naphthalimide systems.

Table 2.1 GI_{50} and LD_{50} values for the reference compound **7** and the novel peptide 1,8-naphthalimides **47-51** after 24 hours treatment. The values represent the means of three separate experiments, each done in quadruplicate (\pm standard errors). Values mentioned in the text are highlighted with a red color.

	7	47	48	49	50	51
GI_{50}	0.179 (± 0.05)*	2.50 (± 0.47)	0.342 (± 0.09)	0.804 (± 0.14)	0.188 (± 0.01)	0.138 (± 0.02)
LD_{50}	0.365 (± 0.13)*	5.05 (± 0.82)	1.88 (± 0.65)	> 100	3.81 (± 0.87)	0.960 (± 0.14)

* Mean and standard errors calculated from only two experiments.

Although, the chloro group was shown to be the most active against cell growth, when effects from different substituents on the cell reduction (LD_{50}) were compared, the results revealed that the nitro derivatives **48** and **51** were shown to reduce the cell population as shown in Table 2.1. These results highlighted the importance of the nitro group to the cytotoxic effects that these compounds have on HL-60 cells. Furthermore, the nitro derivatives **47**, **48** and **51** were shown to be the only compounds that induced nearly 100% cell killing after 24 hours. As shown in Figure, 2.14 and Table 2.1, the amino

derivative **49** was shown to have an LD₅₀ value higher than 100 μM. However, it was believed that **49** was suffering from the lack of solubility at higher concentrations, that would lead to decreasing concentration of **49** in solution.

The results from fluorescent microscopy studies that were discussed in the last section suggested that **48** and **49** were possibly exported out of the cell, and flow cytometry studies also indicated that the nitro group was involved in binding or being chemically transformed in the cell. Therefore, it was decided to treat HL-60 cells for 48 hours and compare the cytotoxic effects to the 24 hours treatment. The results for the 48 hours treatment are shown in Table 2.2. These results suggested that the cytotoxic activity of **47-51** was considerably decreased after 48 hours of incubation, while the reference compound **7** retained its cytotoxic ability. In fact, the activity decreased by at least a factor of two or greater for all of the peptide based 1,8-naphthalimides **47-51**. Although, there was no obvious trend deduced from these results, the LD₅₀ values after 24 hours and 48 hours exhibited for the 4-nitro derivatives **47, 48** and **51**, showed a minimal decrease in cytotoxic activity compared to the amino or chloro derivatives **49** and **50**, respectively. This observation correlated well with the results from fluorescent microscopy studies, where **49** and **50** were shown to localise in the lysosomes and were possibly exported out of the cell. However, the exportation of the nitro derivatives could not be excluded until further investigations are carried out. Furthermore, the decrease in cytotoxic potential might result from the instability of these compounds at the conditions used for cell culture. This was in agreement with the flow cytometry observations.

Table 2.2 Gi₅₀ and LD₅₀ values for the reference compound **7** and the novel peptide 1,8-naphthalimides **47-51** after 48 hours treatment. The values represent the means of three separate experiments each done in quadruplicate (± standard errors). Values mentioned in the text are highlighted with a red color.

	7	47	47	48	49	50
Gi₅₀	0.126 (±0.02)	4.47 (±0.38)	0.815 (±0.24)	1.12 (±0.25)	0.424 (±0.04)	0.464 (±0.13)
LD₅₀	0.149 (±0.05)*	6.58 (±1.32)	3.42 (±0.67)	> 100	25.3 (±0.95)	1.40 (±0.42)

* Mean and standard errors calculated from only two experiments.

In summary, the peptide 1,8-naphthalimides **47-51** showed cytotoxic activity in HL-60 cells and were comparable to the cytotoxicity exerted by the classical 1,8-naphthalimide

7. However, the cytotoxicity of the peptide derivatives **47-51** decreased after 48 hours, indicating that the cells overcome the toxicity from the peptide 1,8-naphthalimides. These results further suggested that these compounds are exported out of the cell after 24 hours, as was discussed in *Section 2.2*. However, since the cytotoxicity against HL-60 cells was established, it was decided to investigate the mechanism that **47-51** exerted.

2.4 Investigation of the Mechanism of Cell Death Exerted By **47-51**

As discussed in *Chapter 1*, necrotic cell death results in the release of intracellular content and causes inflammation in the tissue. In contrast to necrosis, apoptosis or programmed cell death, results in the disposal of cell debris that is engulfed by neighboring cells and macrophages. Furthermore, apoptosis is the consequence of a series of precisely regulated events that are frequently altered in cancer cells. Therefore, induction of apoptosis provides the opportunity for selective clinical intervention and to minimise the effects on surrounding cells. The basic differences between apoptosis and necrosis, which were discussed in *Section 1.2.2* of *Chapter 1*, underscore the reason why apoptosis is a more desirable target mechanism for the induction of cell death in tumor cells.

The classical 1,8-naphthalimides, such as amonafide **7**, have been shown to induce apoptotic cell death in HL-60 cells by propidium iodide staining for sub-G₁ content analysis (discussed in *Section 2.5*) and by DNA fragmentation.¹⁵⁴ Amonafide **7** was shown to induce 10% apoptosis in HL-60 cells at 10 µmol/L by sub-G₁ staining and triggered DNA fragmentation in a dose-dependant manner.¹⁵⁴

To determine if compounds **47-51** were causing cells to die by necrosis or apoptosis, two different experimental methods were used, namely the investigation of the cell morphology and the detection of the DNA ladders. These methods and the results from these studies will be described in detail in the next two sections.

2.4.1 Investigation of the Cell Morphology After Treatment With **47-51**

First, cell morphology was used to determine the primary mode of cell death. This method is based on the morphological difference between apoptosis and necrosis, which was discussed in *Section 1.2.2* of *Chapter 1*. The procedure involves treating cells and subsequently spinning them down onto a glass slide. The cells are then fixed with 90% ethanol and then the cytoplasm is stained with haematoxylin and the nucleus is stained with eosin. The cells are then analysed by microscopy and apoptotic cells were counted based on the appearance of the nucleus and the membrane integrity. An example of a field of

view is shown in Figure 2.15, where an apoptotic and a necrotic cell are indicated. The image shows HL-60 cells that were treated with **47** at 5 μM concentration for 24 hours. In our investigation, the HL-60 cells were treated with compounds **47-51** at three different concentrations, 0.5, 1 and 5 μM for 24 and 48 hours, respectively. For comparison purposes, cells were also treated with our reference compound **7**.

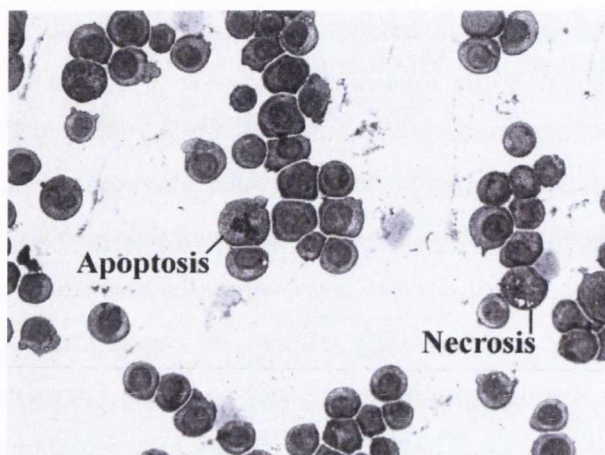


Figure 2.15 The morphology of HL-60 cells. An apoptotic cell is indicated, with the nucleus highly fragmented. The necrotic cell shows the karyolysis and the corresponding cell swelling.

Importantly, the morphological features of apoptosis, such as cell shrinkage, chromatin condensation, nuclear fragmentation and the appearance of apoptotic bodies, were largely absent from the vehicle treated cells, but were visible in the cells after treatment with compounds **47-51**. As shown in Figure 2.16, cells treated with **51** were significantly reduced after 24 hours treatment when compared to the vehicle treated cells (DMSO).

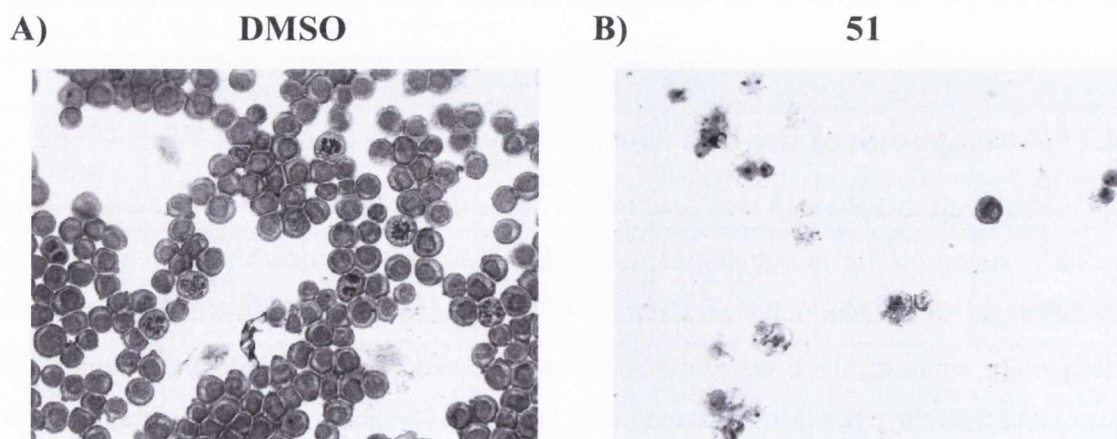


Figure 2.16 Comparison between vehicle treated HL-60 cells and cells treated with **51**. HL-60 cells were incubated with **A)** vehicle (1% DMSO) or **B)** **51** (5.0 μM) for 24 hours.

Furthermore, the treated cells are dark and condensed and there is more evidence of apoptotic bodies. The 4-nitro derivative **48** showed similar reduction in cell number compared to vehicle treated cells, although not to the same extent as **51**. The results from **48** and **51** correlated well with the results from the cytotoxicity studies discussed in Section 2.3, where these compounds demonstrated the lowest LD₅₀ values, which indicated their potential to reduce cells in culture. The chloro derivative **50** showed the formation of cell shrinkage and condensed nucleus but again they were less exhibited from the 4-nitro derivatives **48** and **51**. However, compounds **47** and **49** showed little or no effect on either cell number or cell morphology. The resulting images of the morphology of treated cells with compounds **48-50** can be found in Figure A1.4 in Appendix 1. When the morphological changes in HL-60 cells that had been treated with **47-51** for 24 hours were analysed, the 4-nitro derivatives **48** and **51** showed the highest percentage of apoptosis of the five compounds at 5 μ M, with an average of 66% and 41%, respectively, as shown in Figure 2.17 A. These results further confirm the cytotoxic potential of these compounds that was revealed in the cytotoxicity studies in Section 2.3. Interestingly, treatment with the 4-chloro derivative **50** at 5 μ M concentration exhibited only 18% apoptosis after 24 hours treatment.

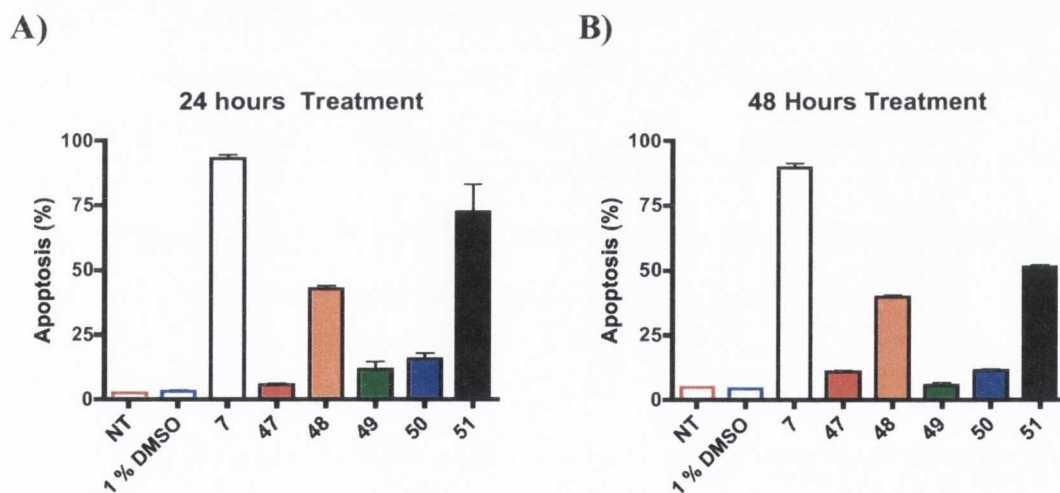


Figure 2.17 Morphological changes in HL-60 cells by treatment of peptide derivatives 47-51 after **A)** 24 hours treatment, **B)** 48 hours treatment. The percentage of apoptosis induced by 1 % DMSO (□), 7 (1.0 μ M, □), 47 (5.0 μ M, ■), 48 (5.0 μ M, ■), 49 (5.0 μ M, ■), 50 (5.0 μ M, ■) and 51 (5.0 μ M, ■). Untreated cells are shown as □. Each graph represents the results of three separate experiments.

This result contradicted the result obtained from the cytotoxicity studies, where it was shown that **50** showed the most effect on the growth of HL-60 cells and was shown to

have a LD₅₀ value of 3.81 μM after 24 hours treatment. Therefore, the result obtained for **50** were indicative of a different mechanism of cellular death induced by this compound. Compounds **47** and **49** showed the least apoptosis at 5 μM concentration of the five compounds tested, with an average of 5% and 11%, respectively. As shown in Figure 2.17 A, the reference compound **7** induced 93% apoptosis at 1 μM concentration after 24 hours treatment. However, when **47-51** were tested at the same concentration, the 4-nitro derivative **51** showed the highest percentage of apoptosis, with an average of 18%. Furthermore, 24 hours treatment at 0.5 μM concentration with **47-51** revealed similar trend, with **51** exhibiting the highest apoptosis induction with an average 9% apoptosis. The resulting graphs for 1 μM and 0.5 μM concentration are presented in Figure A1.5 A and C, respectively.

As discussed in Section 2.3, the toxicity studies indicated that **47-51** were exported out of cells and thus showed less cytotoxic activity after 48 hours treatment. Therefore, it was decided to determine the extent of apoptosis after 48 hours and compare those results to the 24 hours treatment. The results from the 48 hours treatment are shown in Figure 2.17 B. Interestingly, as with the toxicity studies discussed in Section 2.3, the percentage of apoptosis in these studies was shown to be less after 48 hours treatment with **47-51** at 5 μM concentration, in comparison to the 24 hours incubation. These results further suggested that **47-51** lost their ability to induce cell death and reduce cell number after 48 hours treatment. As suggested in Section 2.2 and Section 2.3, this indicated the exportation of **47-51** or the instability of these compounds under the conditions used for cell culture. Further testing at lower concentration of 1 μM and 0.5 μM, only resulted in a lower percentage for apoptosis, confirming that these compounds induce apoptosis in a concentration dependant manner. The result for these studies can be found in Figure A1.5 B and D for 1 μM and 0.5 μM concentration, respectively.

In this section, it was established that **47-51** induced apoptosis in HL-60 cells after 24 hours incubation. Moreover, the 4-nitro bis 1,8-naphthalimide derivatives **48** and **51** showed the highest induction of apoptosis. These results further confirmed the importance of the 4-nitro group to the cytotoxic potential. To further confirm that apoptosis was indeed the preferred mode of cell death induced by **47-51**, a method based on the detection fragmented DNA by agarose gel electrophoresis was used, the results of which are discussed in next section.

2.4.2 Detection of DNA Fragmentation Induced by 47-51

As discussed in *Section 1.2.2* in *Chapter 1*, caspases-3 indirectly activates CAD by cleaving an inhibitor of CAD, namely ICAD.^{54,55} Upon activation, CAD relocates to the nucleus, causing a two-step digestion of the nuclear material, first by fragmenting it into approximately 50 kb fragments and then further into multiples of 180 bp fragments. This fragmentation can be seen as a “ladder” when the DNA is extracted from treated cells and analysed on an ethidium bromide stained agarose gel.

As discussed in *Section 2.4.1*, **47-51** induced apoptosis in HL-60 cells at 5 μM concentrations after 24 hours treatment. However, to confirm if these compounds would indeed induce apoptosis, it was decided to investigate the effects of **47-51** at a higher concentration, namely 10 μM . The results from these investigations shown in *Figure 2.18* revealed that the treatment with compounds **47-51** for 24 hours at 10 μM concentration lead to the formation of DNA ladders. This also indicates that these compounds induce apoptosis at this concentration.

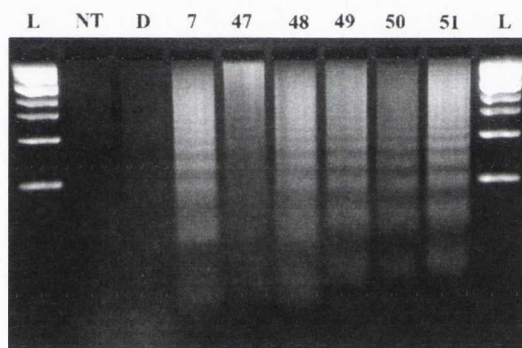


Figure 2.18 DNA fragmentation induced by **47-51** at 10 μM concentration. HL-60 cells were incubated with peptide derivatives **47-51** (10 μM), the reference compound **7** (10 μM) and 1% DMSO (Lane D). Untreated cells are shown in lane labelled NT and lane L contained 1 kb DNA ladder.

However, no conclusions could be drawn from these results about the extent of apoptosis induced by each of the compounds or the effects from different structural parts. Therefore, it was decided to investigate lower concentrations, to determine the minimum concentration that would be required to induce apoptotic activity by these compounds. For these studies, HL-60 cells were treated with **47-51** at 1, 5 and 10 μM concentrations for 24 hours. Cells were also treated with Etoposide **58**, which is a known inducer of apoptosis, to be used as a positive control and the reference compound **7** at 1 and 5 μM concentrations to compare to that of **47-51**. The resulting agarose gels are shown in *Figure 2.19, A and B*,

respectively. These results show that the bis 1,8-naphthalimides **48-51** all induced the formation of DNA laddering at 5 μM concentration. Furthermore, they also showed that 24 hours treatment with compounds **48-51** at 1 μM treatment did not lead to the formation of fragmented DNA.

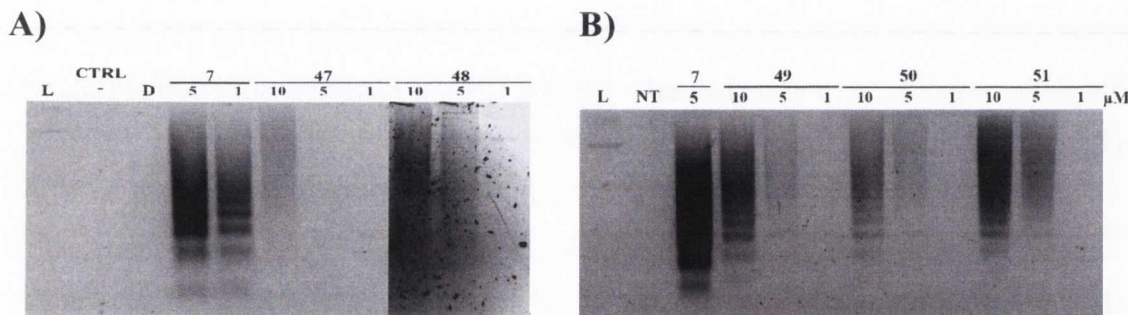


Figure 2.19 DNA fragmentation induced after 24 hours treatment with 47-51. HL-60 cells were incubated with peptide derivatives 47-50 (10, 5 and 1 μM), the reference compound 7 (5 and 1 μM) and 1% DMSO (Lane D). Cells were also treated with 58 (100 μM) as a positive control. Untreated cells are shown in lane labelled NT and lane L contained 1 kb DNA ladder.

These observations contradicted the results from the cell morphology investigations that were discussed in the last section. There, it was found out that compounds **48** and **51** showed 14% and 18% apoptosis, respectively. The reason for the absence of DNA fragmentation was possibly due to the loss of DNA after extraction from the cells. Treatment with **47** at 10 μM concentrations showed the induction of DNA ladders, while they were shown to largely ineffective at 5 μM concentration as was shown in the cell morphology studies, which were discussed in Section 2.4.1.

As discussed in Section 1.2.2, the activation of caspases in apoptosis leads to the cleavage of PARP. For that reason, it was decided to investigate the status of PARP by western blot studies. The results from this study can be seen in Figure 2.20.

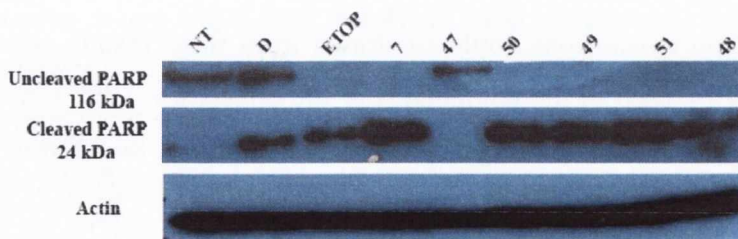


Figure 2.20 Western blot analysis of PARP status after 24 hours treatment with 47-51. HL-60 cells were treated with 10 μM concentrations of 47-51 and the reference compound 7. Cells were also treated with 58 (50 μM), which is a known inducer of apoptosis. Lane NT represents untreated cells, while the Lane D shows the effect of 2% DMSO on cells.

Although only preliminary, these results showed that the treatment with bis 1,8-naphthalimides **48-51** at 10 μM concentration induced PARP cleavage and, therefore its deactivation after 24 hours. However, treatment with compound **47** at the same concentration, only showed the presence of uncleaved PARP after 24 hours. This supported the studies that were discussed in this section, where **47** was shown to induce less apoptosis.

2.4.3 Summary

In this section, it was established that **47-51** all induced apoptosis to some extent after 24 hours treatment at a concentration as low as 5 μM . Furthermore, the results showed that the 4-nitro derivatives **48** and **51** induced the highest percentage of apoptosis compared to the other bis 1,8-naphthalimides. This has further confirmed the importance of the nitro group in relation to cytotoxicity. However, to further investigate the mechanism of action induced by **47-51**, it was decided to investigate the effects these compounds had on the cell cycle. The results from these studies will be discussed in the following section.

2.5 Cell Cycle Analysis

As mentioned in *Section 1.2.1 in Chapter 1*, the cell cycle is a complex process that is involved in the growth and proliferation of cells and especially in the regulation of DNA damage repair. The cell cycle is often deregulated in cancer due to alterations in either oncogenes or tumor suppressor genes that impact the regulation of the cell cycle. Therefore, the effect on the cell cycle is regarded an important factor in anti cancer drug design. Furthermore, Hodgekiss *et al.*¹⁴⁵ reported that the formation of double strand breaks in DNA after treatment with the reference compound **7** that lead to the activation of the G_2 damage checkpoint as was discussed in *Section 1.2.1 in Chapter 1*. This delayed the cell cycle and prevented the cell from entering the next phase until the damage had been repaired or initiated apoptosis if the DNA damage was too severe. For this reason it was decided to investigate the effects of 24 hours treatment with **47-51** on the cell cycle. Furthermore, these investigations would also be able to confirm the results from the last section, where it was found that **47-51** induced apoptosis after 24 hours treatment.

The cell cycle analysis assay is based on the detection of the varying amount of DNA in the various different cell cycle phases. As discussed in *Section 1.2.1 in Chapter 1*, the G_1 phase has an equivalent amount of DNA while the G_2 phase has double the amount of genetic material as shown in Figure 2.21. However, cells that are synthesising DNA

during the S phase will have a DNA content ranging from one copy to two copies of the genetic material and moreover, cells that have not undergone cytokinesis in the M phase contain twice the amount of DNA within the same cellular membrane and therefore they are counted along with cells in the G₂ phase.

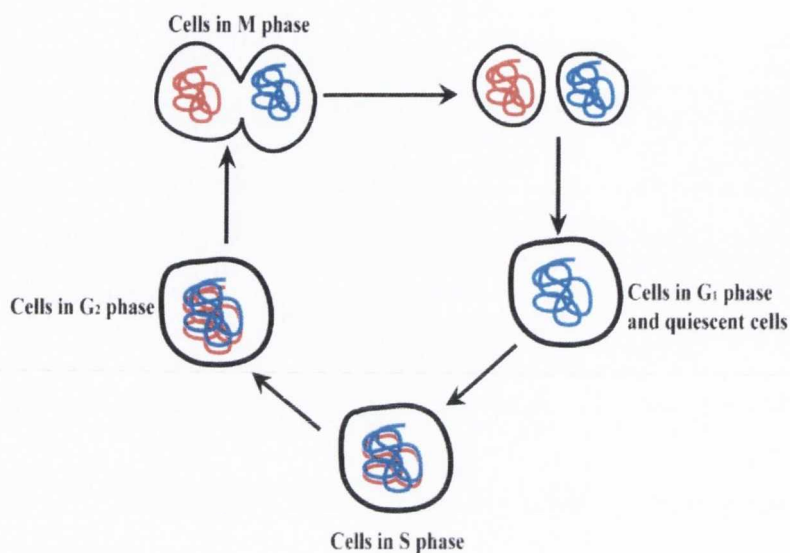


Figure 2.21 The amount of DNA in each phase of the cell cycle. Quiescent and cells in G₁ phase of the cell cycle will have one copy of the genome, while the cells in G₂ will have two copies. Since the cells in the S phase are synthesising DNA, they will contain between one and two copies of the genome. Cells in the M phase will have 2 copies of the genome within one cell before cytokinesis. The flow cytometry can not discriminate between a cell in G₂ and a cell in M phase that has not undergone cytokinesis, as described in the text.

Additionally, the extent of apoptosis can be detected from the presence of apoptotic bodies that contain fragmented DNA, leading to the formation of a G₁-like sub-population. Furthermore, propidium iodide **56**, which is shown in Figure 2.22 A, is a fluorescent DNA intercalator that is commonly used for the determination of the amount of DNA. The fluorescent intercalator **56** is excited at 488 nm and its fluorescence is found to be proportional to the amount of DNA. When **56** is bound to DNA, its fluorescence emission maximum is 617 nm and therefore it can be detected by FL-2 or FL-3 channels of the flow cytometry system, which is depicted in Figure 2.6 of this chapter. Finally, the flow cytometry then sorts the cells based on their fluorescent intensity, resulting in a plot of the intensity against the cell number or counts. An example of such a plot is shown in Figure 2.22 B for cells that were untreated for 24 hours. As shown in Figure 2.22 B, most of the studied cells are in the G₁ phase. This is expected since this phase has been shown to be the longest phase of the cell cycle.¹⁷ Furthermore, the plot clearly shows the different amount

of DNA in the S phase, with the fluorescent intensity ranging over a longer stretch. The cells in G₂ and the M phases are sorted together by the flow cytometry because of reasons already discussed. As indicated on the plot in Figure 2.22 **B**, there are only few cells or particles situated in the sub-G₁ phase, which contains cells that have less than one copy of the genetic material. This can be explained by the fact that this plot is obtained from untreated cells that are not undergoing apoptosis.

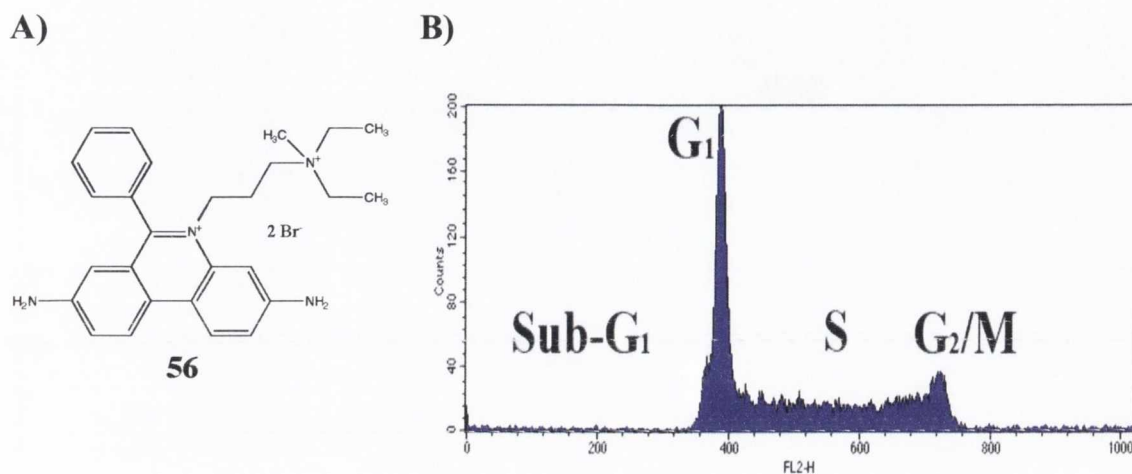


Figure 2.22 An example of experimental output from a cell cycle analysis. Each phase of the cell cycle is indicated.

For the investigation of the effects **47-51** had on the cell cycle, HL-60 cells were treated with compounds at three different concentrations (5.0, 1.0 and 0.5 μM) for 24 hours before being analysed by flow cytometry. Resulting plots for each of the concentrations were combined to further visualise the effects of increasing concentration. The results obtained for compounds **47** and **51** are shown in Figure 2.23 **A** and **B**, respectively. The corresponding results for **48-50** can be found in Figure A1.6 in Appendix 1. Furthermore, these analyses were done in triplicate for reproducibility and the results from the other two sets of experiments can be found in Figure A1.7 in Appendix 1. In addition, the percentage of cells in each phase was determined from these plots to quantify the effects these compounds had on each of the cell cycle phases. These results are summarised in Table 2.3. As shown in Figure 2.23 **A**, the mono 1,8-naphthalimide **47** induced an G₂/M arrest after 24 hours treatment at 5.0 μM concentration, which indicated that **47** behaved in similar manner to the reference compound **7**.

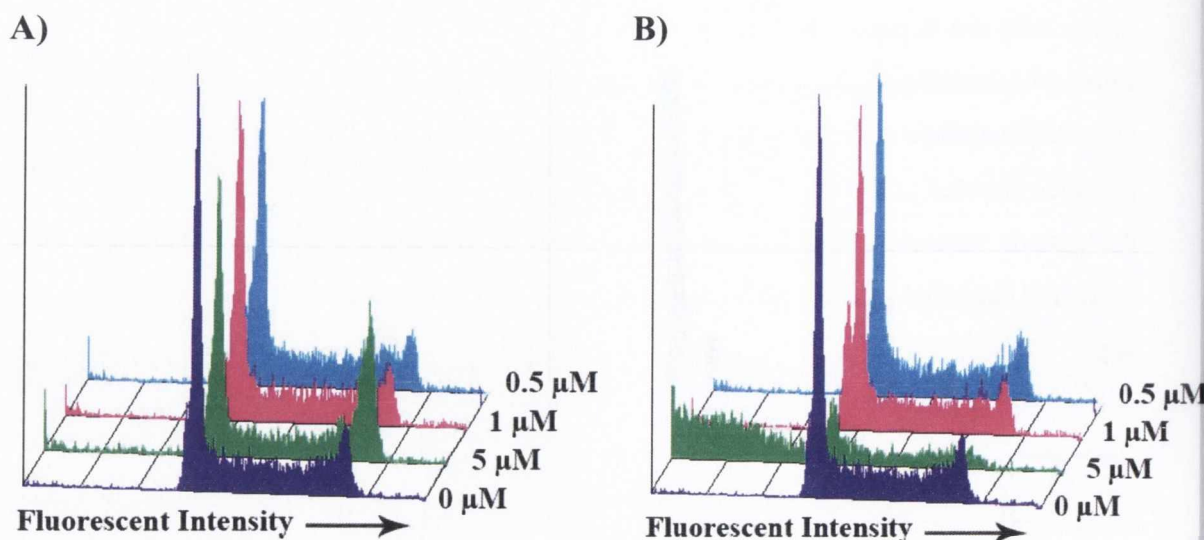


Figure 2.23 Examples of cell cycle effects induced by peptide derivatives **47** and **51**. HL-60 cells were treated with **A)** **47** and **B)** **51** for 24 hours before analysis on the flow cytometry. The solid purple histogram represents untreated cells. Other colors are indicative of concentrations, 5.0 μM (■), 1.0 μM (■) and 0.5 μM (■). Each picture represents three separate experiments.

However, this only resulted in a small increase of cells in pre-G₁ compared to vehicle treated cells. This confirmed the cellular morphology and DNA fragmentation studies that were discussed in *Section 2.4*, where it was found that 24 hours treatment with **47** only resulted in minimal induction of apoptosis. However as shown in **Figure 2.23 B**, the 4-nitro bis 1,8-naphthalimide **51** was not shown to induce a G₂/M arrest at 5 μM concentration and similar results were obtained after treatment with **48-50** at the same concentration. These results can be found in *Figure A1.6* and *Figure A.17* in *Appendix 1*. These studies suggested that these compounds do not induce G₂/M cell cycle arrest after 24 hours treatment. However, these results might also be indicative of an early arrest in HL-60 cells treated with **48-51**. Treatment with the 4-nitro derivatives **48** and **51** resulted in the induction of apoptosis by 74% and 56%, respectively as shown in *Table 2.3*. These results further confirmed the importance of the 4-nitro group to the toxicity of these compounds as was suggested from the analysis of the cytotoxicity, cell morphology and DNA fragmentation studies, which were discussed in previous sections. Furthermore, these results supported the hypothesis of the early arrest of the cell cycle by these compounds. Interestingly, the treatment with the 4-amino and the 4-chloro derivatives **49** and **50**, respectively, showed only limited induction of apoptosis, as demonstrated in *Table 2.3*. This correlated well with the results from *Section 2.4*, where **49** and **50** showed low levels

of apoptosis. Furthermore, these results also confirmed that the high cytotoxicity exerted by **50** was possibly a consequence of a different cell death than apoptosis.

Table 2.3 The effect of 24 hours treatment to each phase of the cell cycle. The novel peptide 1,8-naphthalimide derivatives 47-51 were tested at 5.0 μM concentration while the reference compound **7** was tested at 1.0 μM . The values represent the means of three separate experiments (\pm standard errors). Values mentioned in the text are indicated by a red color.

	Pre-G ₁	G ₁	S	G ₂ /M
<i>NT</i>	4.23 (\pm 1.24)	40.5 (\pm 4.07)	36.2 (\pm 5.13)	13.9 (\pm 1.73)
<i>1 % DMSO</i>	8.46 (\pm 4.50)	39.2 (\pm 5.60)	36.16 (\pm 4.16)	12.3 (\pm 1.97)
7	76.3 (\pm 10.8)	5.48 (\pm 4.81)	12.8 (\pm 6.16)	1.25 (\pm 0.90)
47	13.8 (\pm 7.03)	22.0 (\pm 2.80)	27.2 (\pm 3.67)	29.3 (\pm 6.44)
48	73.7 (\pm 6.98)	5.17 (\pm 3.65)	7.18 (\pm 3.59)	2.80 (\pm 0.15)
49	24.3 (\pm 1.25)	23.7 (\pm 2.63)	36.2 (\pm 4.99)	9.40 (\pm 3.58)
50	17.4 (\pm 6.08)	32.8 (\pm 4.69)	36.4 (\pm 6.14)	12.0 (\pm 2.23)
51*	55.5 (\pm 7.68)	11.1 (\pm 3.50)	14.7 (\pm 2.95)	10.0 (\pm 5.03)

*Results of two independent experiments.

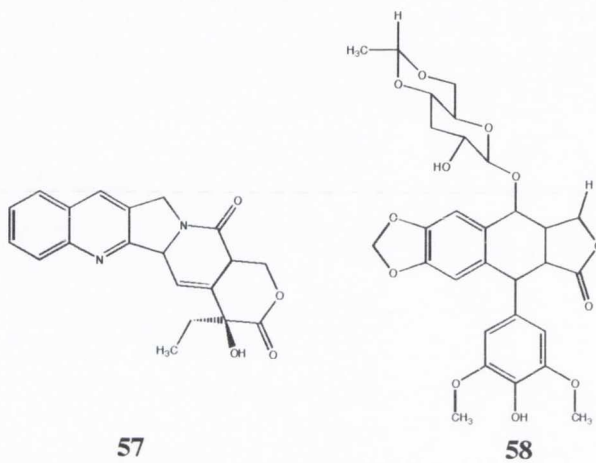
To summarise, the mono 1,8-naphthalimide **47** was shown to induce G₂/M cell cycle arrest. Furthermore, the bis 1,8-naphthalimide derivatives did not induce an arrest in any of the cell cycle phases, nevertheless the 4-nitro derivatives **48** and **51** show considerable increase in apoptosis. The lack of any arrest in the cell cycle along with the initiation of apoptosis suggested either that these compounds would not interfere with the cell cycle or that the cell cycle arrest was an early event after treatment with **48** and **51**. The 4-amino and 4-chloro derivatives **49** and **50**, showed limited extent of apoptosis, which indicated a different mechanism of cells death being initiated after treatment with these compounds. These results were in correlation with the results from the cell morphology investigations, which were discussed in the last section.

As discussed in Section 1.4.1.1.2 in Chapter 1, the reference compound **7** has been shown to induce a G₂/M arrest by introducing double strand breaks into the DNA.¹⁵⁵ Moreover, **7** was also shown to interrupt the DNA strand reactions by Topo II and inhibiting the breakage and reunion reaction of the enzyme, which was discussed in Section 1.4.1.1 in Chapter 1. Consequently, it was decided to investigate the effects **47-51** on Topo I and Topo II enzymes. The results from this investigation will be discussed in the next section.

2.6 Topoisomerase I and II Activity Studies

As discussed in *Chapter 1*, the topoisomerase family modulates DNA superhelicity. Topo I relaxes supercoiled DNA by introducing a single stranded nick in the DNA substrate while the Topo II enzyme creates supercoiling by forming a double-stranded DNA nick.¹⁸ Both enzymes are involved in DNA repair, replication and in transcription.

Two general classes of topoisomerase interacting compounds have been described; the topoisomerase poison and the catalytic inhibitors. Two well-known topoisomerase poisons include Camptothecin **57** and Etoposide **58** for used for Topo I and II, respectively.



These particular drugs interrupt the breakage and reunion reaction of the enzymes, resulting in the accumulation of the topoisomerase-DNA covalent intermediate, ultimately leading to apoptosis. The catalytic inhibitors act by blocking the overall catalytic activity of the enzyme or blocking the access to the DNA.¹⁵⁶ The basis for the mechanistic screening of topoisomerase inhibitors is the detection of different kinds of DNA complexes by agarose gel electrophoresis. In the presence of only Topo I, the half-life of the nicked intermediate is relatively short. However, the Topo I poisons stabilise the intermediate and lead to an increase in nicked and open circular DNA as shown in Figure 2.24 A. In the presence of a catalytic inhibitor of Topo I, the relaxation activity is inhibited, leading to unchanged DNA products. These different DNA products can be separated by agarose gel electrophoresis, as the different forms migrate at different rates through the gel (Figure 2.24 B). The supercoiled DNA is the most compact of the three forms, thereby it migrates fastest and furthest through the gel. The relaxed form, which is circular and bulky follows the supercoiled form and finally the nicked open circular migrates to the least extent.

Ethidium bromide or SYBr green, are known fluorescent intercalators that are used to detect DNA in agarose gels.

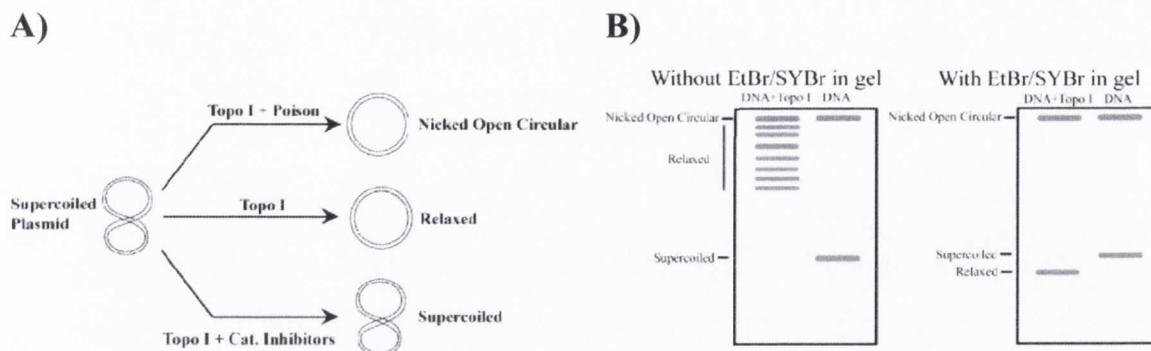


Figure 2.24 Interpretation of the Topo I assay. **A)** The formation of different complexes by topoisomerase inhibitors. **B)** Schematic of a resulting gel.

Moreover, by including a fluorescent intercalator in the running buffer and gel, the relaxed DNA may be better resolved from nicked open circles. Demonstrating Topo I activity is easier to achieve by excluding ethidium bromide in the gel and therefore, normally reactions are run on two separate gels; one with ethidium bromide and one without ethidium bromide in the gel. Similarly, the effect on Topo II activity can be determined by agarose gel electrophoresis as shown in Figure 2.25. The analysis of the Topo I and II assays will be referred back to throughout this Thesis.

As mentioned in *Chapter 1*, mitonafide **7** and amonafide **8** have been shown to intercalate between the base pairs of DNA and the side chain was shown to interact sterically with the Topo II enzyme active site.⁹⁴ Although compounds **47-51** had been shown to mainly situated in the cytoplasm by fluorescent microscopy as was discussed in *Section 2.1.2*, it was decided to investigate the effects these compounds had on the activity of these compounds in a cell-free system.

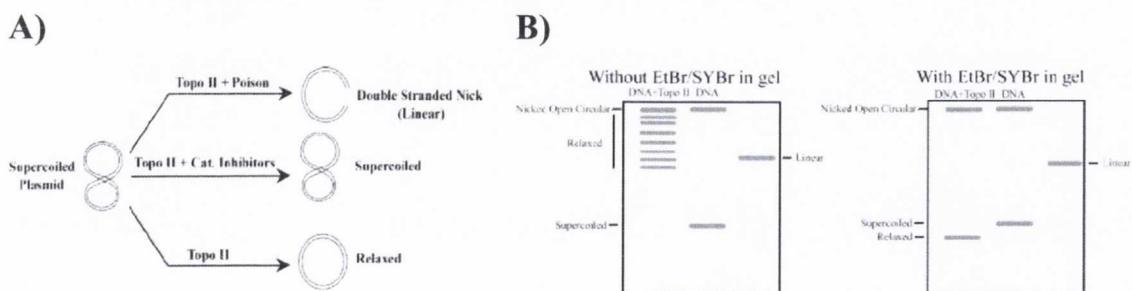


Figure 2.25 Interpretation of the Topo II assay. **A)** The formation of different complexes by topoisomerase II inhibitors. **B)** Schematic of a resulting gel.

These investigations were carried out using **47-51** at three different concentrations (25, 10 and 1 μM). The corresponding reactions were also run in the absence of the topoisomerase enzyme, to investigate the effect these compounds had on the supercoiled plasmid. Firstly, their activity against Topo I was investigated and the resulting gel obtained in the absence of EtBr/SYBr green is shown in Figure 2.26. Furthermore, the corresponding gel that was run in presence of EtBr/SYBr green can be found in *Figure A1.8* in *Appendix 1*. These results indicated that the relaxation activity of Topo I was uninhibited in the presence of **47-51** at the concentrations tested.

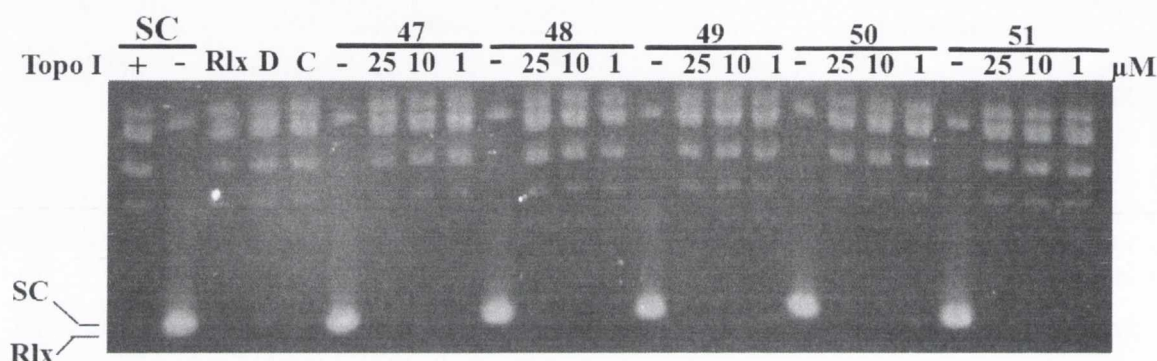


Figure 2.26 The effect on Topo I in the absence of EtBr/SYBr green. Compounds **46-50** were incubated with a supercoiled plasmid (0.5 μg) and Topo I (5 units), at three different concentrations (25, 10 and 1 μM) as indicated above each lane. Lanes labelled - represent reactions done in the absence of Topo I. Lane D represents the effects of 1% DMSO and Rlx indicates the position of the relaxed DNA. Lane C represents the effects of a Topo I poison (Camptothecin, 100 μM) and finally the Topo I, + and Topo I, - represents the reactions done in presence and in absence of Topo I, respectively.

Furthermore, these compounds did not seem to interact with the bases of the DNA plasmid even when analysed at a concentration of 25 μM . This was observed where only the DNA plasmid was incubated in the presence of **47-51** (Lanes labelled - in Figure 2.26). If these compounds were to intercalate, the supercoiled plasmid would have migrated slower and a difference would have been seen from the lane where only the plasmid was run in the absence of Topo I. These results, along with to the result obtained from the EtBr/SYBr green containing gels as shown in *Figure A1.8* in *Appendix 1*, indicated the non-intercalating nature of these compounds and furthermore, that these compounds did not affect the activity of Topo I in a cell free system.

Investigations using **47-51** were also performed on Topo II by using the same experimental procedures as for Topo I. As before, compounds **47-51** were tested at three different concentrations, 25, 10 and 1 μM . These results were shown to be inconclusive

possibly due to the inactivity of the enzyme or the bad quality of the plasmid. However, they implied that compounds **47-51** had no effect on the cleaving activity of the Topo II enzyme at these concentrations. Furthermore, these results emphasised that **47-51** do not in fact interact to DNA at these concentrations. These resulting gels from these analysis can be found in *Figure A1.9* and *Figure A1.10* in *Appendix 1*.

In summary, the novel peptide based 1,8-naphthalimide derivatives **47-51** did not inhibit the activity of the topoisomerase family at these concentrations or stabilise the cleavage intermediate. Further, the results from both Topo I and II substantially show that **47-51** did not effect the migration of DNA on an agarose gel. This strongly indicated that these compounds do not intercalate DNA at a concentration of 25 μ M.

2.7 Conclusion and Future Studies

In this chapter, the biological effects of the novel peptide based 1,8-naphthalimides **47-51** were investigated. These compounds showed rapid uptake by HL-60 cell by using flow cytometry as was discussed in *Section 2.2*. Furthermore, these studies revealed that the treatment with the 4-nitro substituted 1,8-naphthalimides **48** and **51**, respectively resulted in the formation of a distinct peak, that showed less fluorescent intensity. Although this behaviour could not be explained, it was suggested that these compound were metabolised within the cells. Further studies will be needed to elucidate the exact consequence of this behaviour. Other derivatives did not show the same behaviour, however longer incubation times might be need for the biotransformation of the 4-amino and the 4-chloro derivatives **49** and **50**, respectively to occur. Therefore, the transformation of the other derivatives cannot be ruled out at this point.

The fluorescent microscopy studies that were discussed in *Section 2.2.1*, revealed that compounds **48**, **49** and **50** were mainly localised in the cytoplasm after 3 hours. Interestingly, the 4-chloro and the 4-amino derivatives **49** and **50** accumulated within distinct loci after 24 hours incubation, however the nitro derivative **48** does not show any formation of similar spots after 24 hours. Further co-localisation studies investigations suggested that these spots within the cell were in fact lysosomes.

As discussed in *Section 2.3*, the 4-nitro derivatives **48** and **51** were shown to be highly toxic after 24 hours along with the 4-chloro derivative **50**. These results reveal the importance of the nitro group to the cytotoxic mechanism and especially in regard to previous results that indicated exportation of the 4-amino and 4-chloro derivatives **49** and **50**. However, the cytotoxic activity was less after 48 hours incubation for all of the peptide

derivatives while the reference compound, mitonafide **7** retained its cytotoxic activity against the cell lines over the course of 48 hours.

As discussed in *Section 2.4*, compounds **47-51** were shown to induce apoptosis by DNA fragmentation and by investigating the morphological changes that were associated with apoptosis. The nitro derivatives **47** and **50** were the most potent inducers of apoptosis after 24 hours. These results correlated well with the cytotoxicity studies and further confirmed the importance of the nitro group to cytotoxicity exerted by these compounds. These studies also indicated that the 4-chloro derivative **50** induced apoptosis to a small extent. However, it was suggested that this compound triggered activation of a different mode of death. The amount of apoptosis was shown to be less after 48 hours, supporting the previous investigations, where it was shown that the cytotoxic activity decreased after 48 hours.

Results obtained from the cell cycle analysis in *Section 2.5*, showed that the mono 1,8-naphthalimide **47** induced G₂ arrest after 24 hours at 5.0 μM and that there was no indication of a similar arrest induced by the bis 1,8-naphthalimides **48-51**. However, these analyses are only a “snapshot” of the treatment after 24 hours and therefore the cell cycle arrest might be an earlier event. These studies also showed that the nitro derivatives **48** and **51** exhibited the greatest extent of apoptosis after 24 hours treatment and these results correlated well with the cytotoxicity studies and the cell morphology investigation that suggested that the nitro group did significantly improve cytotoxicity.

As discussed in *Section 2.6*, compounds **47-51** did not show any effect on the cleavage activity of the topoisomerase enzymes, Topo I and II. Although inconclusive, these results indicated a different mechanism of action by **47-51** compared to the reference compound **7**, an observation that was in an agreement with the fluorescent microscopy investigations, where **48-50** were shown to be mainly located in the cytoplasm, not the nucleus.

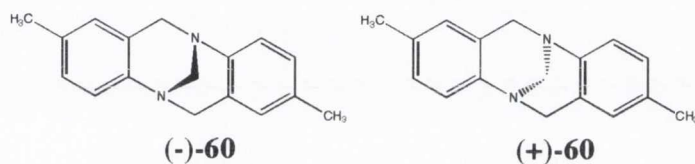
To summarise, the nitro substituted 1,8-naphthalimide derivatives **48** and **51** showed the most activity against the APL cell line, HL-60. These derivatives are suspected to transform within cells after 24 hours and form a metabolite that decreases the cytotoxic activity; ultimately showing diminished activity after 48 hours. Future work could be directed towards finding the exact mechanism of apoptosis exerted by these compounds by using western blotting studies. Also, for the further development of peptide based 1,8-naphthalimides, the metabolite and the mechanism of biotransformation will be investigated.

After establishing the cytotoxicity of **47-51**, the next steps were to investigate related compounds, namely the Tröger's base 1,8-naphthalimides. These compounds were designed to enhance the DNA binding and consequently, to improve the cytotoxic activity against HL-60 cells. The results from this work will be discussed in *Chapter 3*.

**3 Biological Evaluation of 1,8-Naphthalimides
Containing Träger's Bases**

3.1 Introduction

The Tröger's base **60**, was discovered by Julius Tröger and is a chiral cleft-containing molecule with a C_2 axis of symmetry, which is provided by two bridgehead stereogenic nitrogen atoms.¹⁵⁷ Although it was synthesised and purified in 1885, it was not until 1935, that Spielman successfully determined the correct structure of **60**.¹⁵⁸ Later, Wilcox *et al.*¹⁵⁹ reported the three-dimensional structure of **60** that showed the formation of two enantiomers that had dihedral angles between the planes of the aromatic rings of 92.8° and 97.4° , or almost perpendicular to each other, creating a V-shaped molecule. The dihedral angle between the aromatic rings has since been shown to range from 81° - 104° depending on the nature of the substituents on the rings.¹⁵⁷



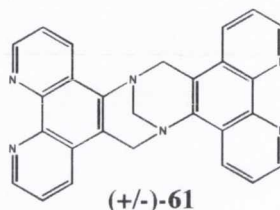
Because of its structural properties and chirality, the Tröger's base skeleton has been extensively used in the field of supramolecular chemistry, specifically in molecular recognition.¹⁶⁰ The geometry of the Tröger's base unit gives rise to molecules that have a helical shape, which can be either similar or opposite to the helicity of DNA.¹⁶¹ This is highly promising for the development of novel DNA probes and DNA interacting drugs.

In this chapter, the design and the biological activity of novel 1,8-naphthalimide containing Tröger's bases will be discussed. A detailed discussion on the synthesis and the DNA affinity as determined by using UV/Vis and fluorescent measurements of these novel compounds were described in the PhD thesis of Dr. Veale.⁶ However, this chapter will deal with the results from the investigation of the biological activity of the novel 1,8-naphthalimides containing Tröger's base compounds, such as their cellular uptake and their cytotoxic effect against HL-60 cells. Furthermore, the cytotoxicity of the 4-amino-1,8-naphthalimide precursors will be compared to the corresponding Tröger's base derivatives. The effect on the cell cycle exerted by these compounds will also be investigated along with their ability to induce apoptosis. Finally, because the 1,8-naphthalimide compounds such as **7** and **8** have been shown to affect the activity of topoisomerase enzyme, studies will be carried out to determine if the Tröger's base containing 1,8-naphthalimides show similar behavior. However, first some recent examples of the DNA binding affinity of

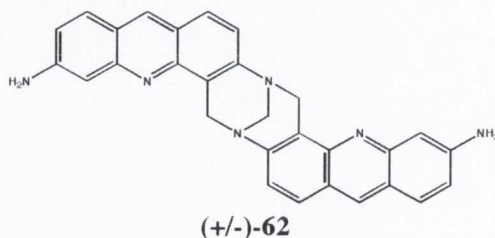
various Tröger's bases systems will be discussed, followed by the development and rationale behind the novel 1,8-naphthalimide containing Tröger's bases.

3.1.1 Tröger's Base Analogues as Targets of DNA

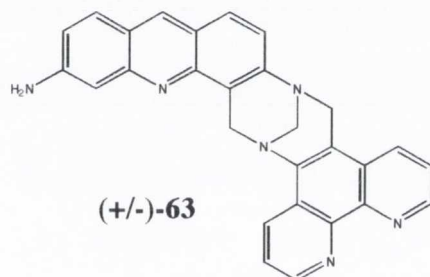
Although the chiral and structural properties of the Tröger's base unit has been known for some time, there are only a few reports on the utility of Tröger's bases for the recognition of DNA. Chiral recognition of DNA using the Tröger's base unit was first achieved by Yashima *et al.*¹⁶² by the development of the (1,10-phenanthroline) containing Tröger's base **61**. The racemic mixture of **61** was shown to interact with DNA using circular dichroism spectroscopy (CD). Furthermore, a copper (I) complex of **61** was shown to cleave DNA, converting a covalently closed circular plasmid to open circular DNA.



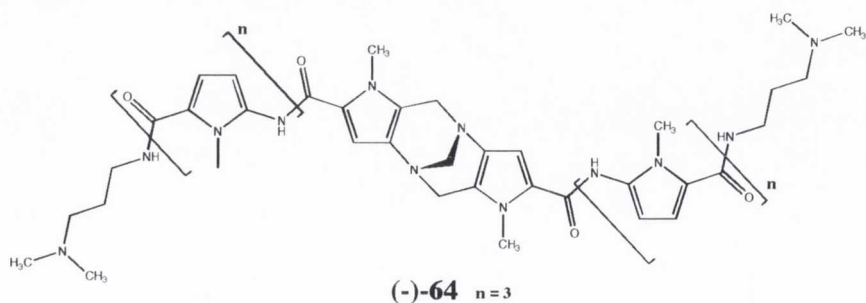
Following this, Demeunynck *et al.*¹⁶³ reported the synthesis of an symmetric acridine containing Tröger's base **62** whereby the (-)-enantiomer showed preferential binding to B-DNA by liquid-liquid partition studies. These results were later confirmed by thermal denaturation (T_m) studies of DNA in the presence of the different isomers of **62**. However, neither isomers inhibited the relaxation activity of Topo I or II, indicating that these compounds did not bind to DNA through an intercalation mechanism. Furthermore, compound **62** did not affect the methylation of N7-guanine residues of DNA, suggesting that the ligand interacted within the minor groove of the DNA. Although the exact binding mode of **62** with DNA could not be elucidated, because of the symmetric structure of this molecule, the authors concluded that the sequence specificity shown by the (-)-isomer using DNAase I footprinting assays was possibly due to the local structure of the recognised DNA sequence rather than its base pair sequence.



To provide further insight into the binding mode of **62** with DNA, Bailly *et al.*¹⁶⁴ reported the synthesis of an asymmetric acridine-phenanthroline based Tröger's base **63** and studied its interaction with DNA using various biochemical and biophysical methods. UV/Vis spectroscopy and T_m studies revealed that **63** interacted with DNA. Furthermore, CD and electric linear dichroism (ELD) studies suggested that the acridine ring of **63** intercalated between the DNA base pairs, while the phenanthroline ring resided in one of the grooves. Hence, the phenanthroline ring was expected to be responsible for the sequence selectivity binding and it was suggested that the triplet sequence 5'-GTC-3':5'-GAC-3 might be the optimal binding site for **63**. In contrast to compound **62**, this compound was shown to inhibit the relaxation activity of Topo I at high concentrations ($>10 \mu\text{M}$), most likely due to the intercalative binding of the ligand into DNA. Furthermore, the authors observed an increased production of nicked DNA molecules by Topo I, suggesting that the ligand acted as a Topo I poison as discussed in Section 1.4.1.1. However, **63** did not show any inhibitory effect on the Topo II in similar experiments.



Recently, the synthesis of distamycin analogues with an incorporated Tröger's base skeleton has been reported.¹⁶⁵ As discussed in Section 1.4.1.1.4, distamycin **15** and its analogues can bind DNA as monomers in the minor groove as well as anti-parallel dimers. DNA binding agents such as **64** were developed to improve the fit of the dimer into the minor groove and more importantly to give the agents enantio-selective capabilities through the concave structure of the Tröger's base.



The most effective Tröger's base derivative in this study, (-)-**64** showed less affinity and selectivity to **A:T** sequences and increased affinity to **G:C** sequences when compared to **15**. Furthermore, the authors speculated that dramatic changes in the induced ECD at high concentrations of (-)-**64** resulted from a two-step binding mode to DNA and that (-)-**64** interacted with DNA either through i) one of the *N*-methyl pyrrole peptide arms and a partial contact of the Tröger's base unit to the minor groove of DNA or ii) through the terminal segments of both *N*-methyl pyrrole peptide arms only.

In summary, the aforementioned studies have shown that the incorporation of the Tröger's base structural unit into DNA targeting drugs, could potentially lead to an enhanced binding affinity and enantioselective recognition of DNA. Consequently, the Gunnlaugsson group developed 1,8-naphthalimide based Tröger's base derivatives in the pursuit of further improving the DNA binding affinity shown by 1,8-naphthalimides.

3.1.2 Design of 1,8-Naphthalimides Based Tröger's Base

As discussed in *Chapter 1* and *Chapter 2*, amonafide **8** has been shown to act as a Topo II poison, forming double strand breaks. The formation of double strand breaks in the DNA caused an G₂/M arrest in the cell cycle, which ultimately resulted in apoptosis.¹⁶⁶ Furthermore, the toxicity against Topo II has been shown to involve the side chain of **8**, which is a basic terminal group that is separated from the 1,8-naphthalimide chromophore by two methylene units. However, as discussed in *Section 1.4.1.1.2*, the key issue for **8** has been dose-limiting myelosuppression, which has been linked to the metabolism of the 3-amino group on the 1,8-naphthalimide ring.⁹⁷

With this in mind, Dr. Veale designed the 1,8-naphthalimide containing Tröger's base derivatives **68-70** (Figure 3.1) that were easily synthesised from the 4-amino-1,8-naphthalimide precursors **65-67**.⁶ The side chains of compounds **68-70** were expected to have similar cationic properties to **8** and they were anticipated to be positively charged at physiological pH (pH 7.4) contributing both water solubility and stronger interaction with the negatively charged polyphosphate backbone of DNA. Furthermore, the toxicity that had been shown to be associated with the metabolism of **8**, was expected to be minimised by the incorporation of the Tröger's base structural unit. A detailed discussion of the photophysical properties of **68-70** and their DNA binding interactions can be found in the PhD thesis of Dr. Veale.⁶ However, in the interest of the reader of this *Thesis*, a short summary of the DNA binding affinity of these compounds is necessary to emphasise the importance of their further development.

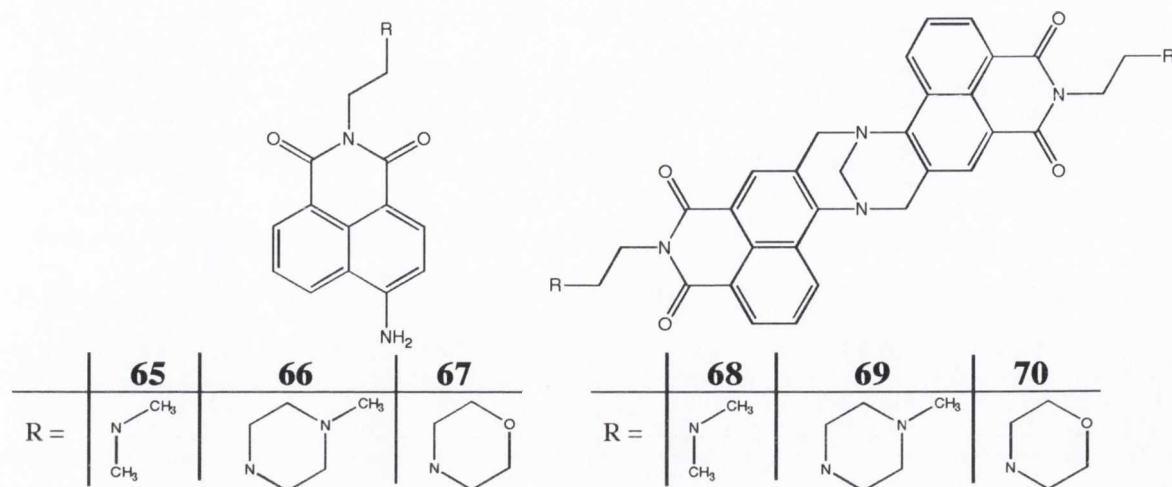


Figure 3.1 Structures of the 4-amino-1,8-naphthalimide **65-67** and the Tröger's base derivatives **68-70**.

The 1,8-naphthalimide Tröger's bases **68** and **69** were found to have pK_a values of 8.7 and 8.2, respectively thus being protonated within the physiological pH range (pH 6-8). However, it was found that **70** had a pK_a value of 6.2 and thus it was not expected to be fully protonated at physiological pH. This was shown to be an important factor in the DNA binding affinity of **70**.

The DNA binding interaction of the Tröger's base derivatives **68-70** to *ct*-DNA were studied using UV/Vis and fluorescence spectroscopy, T_m and CD studies. As shown in Table 3.1, compounds **68** and **69** showed impressive binding to DNA by UV/Vis and fluorescence spectroscopy studies while the binding of **70** to DNA was shown to be weaker. The results indicated an unorthodox bimodal binding mode, which was thought to arise from both the electrostatic binding of the amino group of the protonated side chains with the negatively charged phosphate backbone and minor groove binding.

Table 3.1 Summary of DNA binding properties exhibited by **68-70**.⁶

	68	69	70
^(a) K _b (M ⁻¹)	7.40 x 10 ⁶	4.24 x 10 ⁶	0.79 x 10 ⁶
^(b) n	1.70	1.51	0.48
^(c) C ₅₀ (μM)	0.38	0.625	10
^(d) T _m (°C)	N.D.	> 88	> 75

^(a)The binding constants (K_b) as determined from absorbance data in 10 mM phosphate buffer, pH 7.4. ^(b)The number of nucleotides occluded by a bound ligand (n) as determined from fluorescence data in 10 mM phosphate buffer, pH 7.4. ^(c)The C₅₀ values from an ethidium bromide displacement assay, representing the concentration of compound to displace 50% of the ethidium bromide. Error ± 10%. ^(d)The T_m values thermal denaturation studies. For comparison, the *ct*-DNA was shown to melt at 68 °C. N.D means not determined.

Moreover, when compared to their precursors **65-67**, the Tröger's base derivatives exhibited much greater affinity for DNA. The results from ethidium bromide displacement studies confirmed the reoccurring trend throughout the DNA binding studies that **68** had the strongest binding affinity to DNA, while **70** showed the weakest.

Although UV/Vis titrations studies with polynucleotides consisting of poly(dA:dT) or poly(dG:dC) did not reveal any sequence specificity by **68** and **69**, corresponding fluorescence studies indicated that **69** had a binding preference to poly(dA:dT) over poly(dG:dC) and furthermore, these studies suggested that **68** and **69** interacted differently with G:C sequences in comparison to A:T sequences, which was confirmed later by carrying out ethidium bromide displacement assays. Further investigations into the mode of binding were carried out using T_m and CD studies and it was shown that compounds **68** and **69** were superior to their precursors **65** and **66** in stabilising DNA towards thermal denaturation, indicating stronger DNA interaction by the Tröger's base analogues. Moreover, these results suggested that **68** and **69** bind by intercalation or within the grooves of the DNA helix. Although CD experiments were inconclusive due to the racemic mixtures of Tröger's base derivatives, the results indicated that **68-70** enhanced the chirality of DNA upon binding. Further discussions and explanations into the theory and nature behind any of the photophysical results have been thoroughly discussed in the PhD thesis of Dr. Veale.⁶

The work described in this chapter involves the biological testing of **68-70** against HL-60 cells. The primary objective was to compare the toxicity of these molecules to their precursors **65-67** by MTT proliferation assay and cell cycle analysis. The second objective was to investigate and compare the effects of the different cationic substituents in the imide-attached side chain on the uptake by HL-60 cells, as well on apoptosis induction capabilities and Topo I and Topo II inhibition. The results of these studies will be discussed in the following sections.

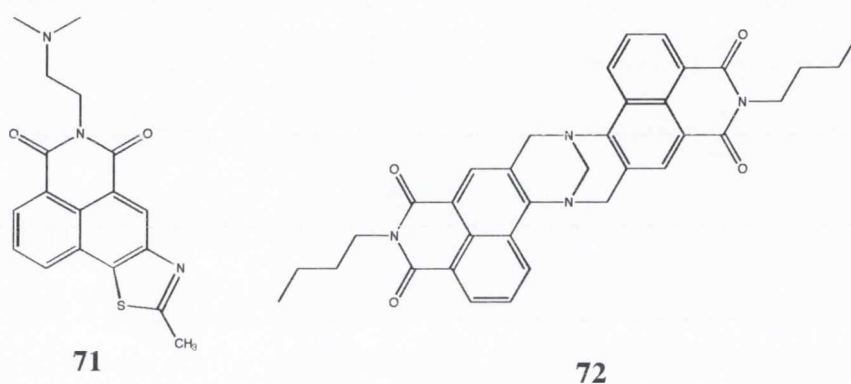
3.2 Analysis of Cellular Uptake and Localisation of 68-70

3.2.1 Uptake Studies of 68-70 Using Flow Cytometry

As mentioned in *Section 2.2*, there are few reports that describe the uptake of 1,8-naphthalimide compounds by cancer cells.^{94,145,146} To date, the exact mechanism by which these types of compounds are absorbed by cells is unknown. However, although a number of routes exist for absorption of drugs through membranes and tissues, transport by passive

diffusion is the most common.¹⁸ To be absorbed by this route, drugs need to be sufficiently lipophilic to penetrate the lipid cores of membranes but not so lipophilic that they get stuck within the membrane. Furthermore, the ionisation status (pK_a) has been shown to affect the lipophilicity and render molecules water solubility.¹⁸

A report by Qian *et al.*¹⁶⁷ showed that the extent of protonation significantly affected the ability of 1,8-naphthalimide molecules, such as **71** to pass through the lipophilic membranes. Moreover, it was shown that a lower degree of protonation was desirable for cell penetration but a higher degree favoured stronger DNA binding. Therefore, when these two factors were effectively compromised, higher cytotoxicity against tumour cells was observed.¹⁶⁷



Recently, Deprez and coworkers reported the synthesis of an alkyl based 1,8-naphthalimide Tröger's base, such as **72** that was insoluble in water.¹⁶⁸ However, compounds **68-70** contain a protonated amino terminus, which improves water solubility and thus affects the lipophilicity of these compounds. To investigate the effects of the protonation to cell absorption, the uptake of these compounds by cells was studied using flow cytometry as described in Section 2.2 of Chapter 2. Briefly, HL-60 cells were treated with **68-70** for different time periods, varying from 30 minutes to 24 hours. Compounds were tested at 1 μ M concentration to limit cell death and loss of cells. After different time periods, the cells were centrifuged and washed twice with ice cold PBS to remove particles of compounds and molecules that would be bound on the surface of each cell. The FL-2 channel was used to detect the fluorescence arising from **68-70**, according to the flow cytometry system that was described in Figure 2.8 in Chapter 2. The resulting plots of the fluorescent intensity against time for **68-70** are shown in Figure 3.2. These investigations were repeated twice and the results from the repeated experiments can be found in Figure A2.1 in Appendix 2.

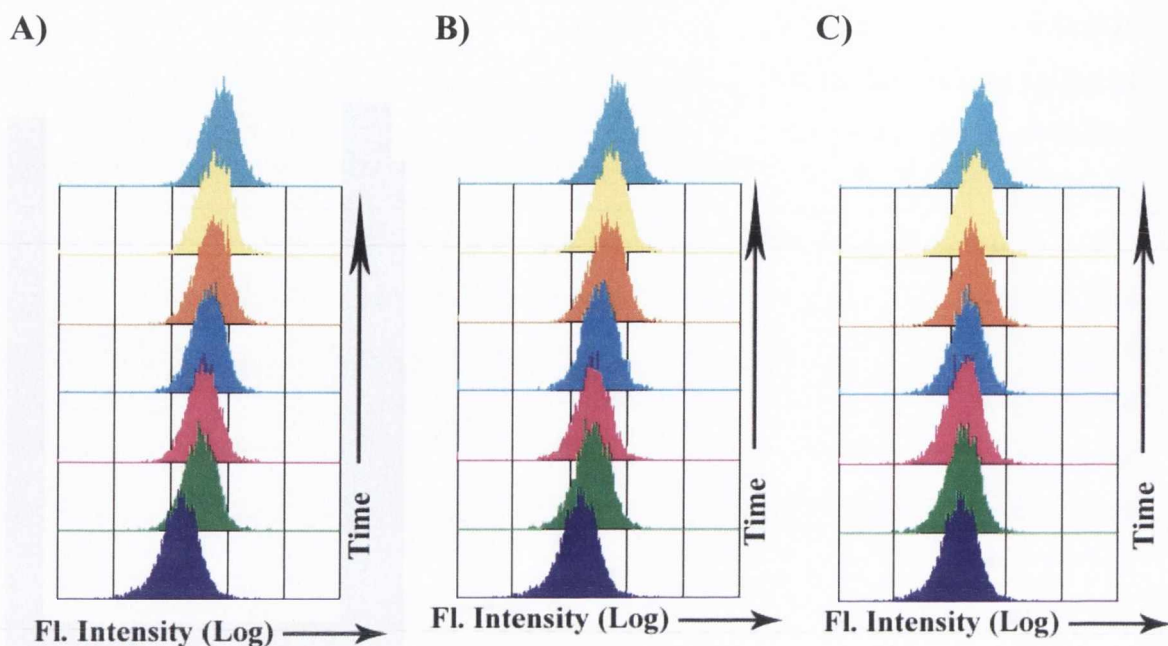


Figure 3.2 Plots of the emitting fluorescence intensity from HL-60 cells. Cells treated with **A**) **68** (1.0 μM), **B**) **69** (1.0 μM), **C**) **70** (1.0 μM) for 30 min. (■), 60 min. (■), 3 hours (■), 6 hours (■), 9 hours (■) and 24 hours (■). Untreated cells are shown as a solid purple peak. These graphs are representative of three separate experiments.

As shown in Figure 3.2, the Tröger's base derivatives **68-70** showed small shifts in fluorescence intensity compared to the autofluorescence arising from untreated cells. This can be explained by the fact that these compounds have an absorbance maximum at 381 nm in 10 mM phosphate buffer.⁶ Therefore, upon excitation at 488 nm, possibly only a small population of molecules is excited, resulting in less detected fluorescence. However, as shown in Figure 3.3, the time-dependant uptake becomes obvious, when the maximum fluorescent intensity from each peak is plotted against time for **68-70**. As shown in Figure 3.3, the dialkylaminoethyl substituted Tröger's base **68** exhibited the most rapid cellular uptake, with nearly 85% being accumulated by the three-hour mark. This percentage was calculated from the average fluorescence maximum when the compounds reach saturation and the maximum intensity at a specific time period. Similarly, the *N*-methyl piperazine analog **69** showed 80% uptake recorded after three hours, whereas **70**, which contains a morpholine moiety as the terminal of the side chain, showed the slowest uptake by reaching 85% accumulation after 6 hours. The possible reason for the difference between the Tröger's bases might be explained by looking at the extent of their protonation.

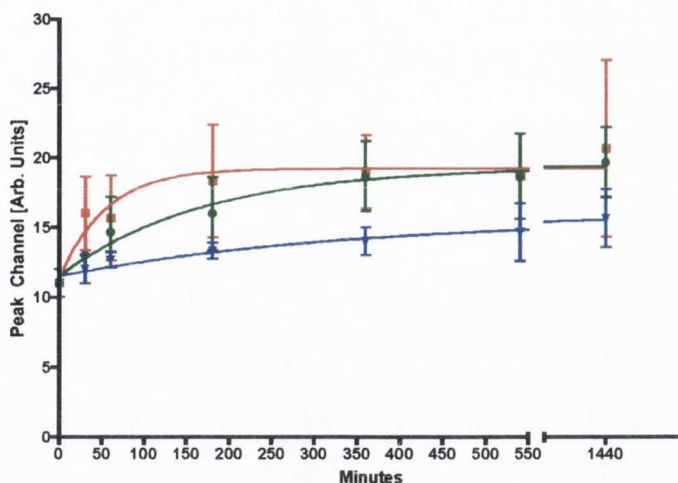


Figure 3.3 Cellular uptake of 68-70 by HL-60 cells. HL-60 cells were treated with **68** (■, 1.0 μ M), **69** (●, 1.0 μ M) and **70** (▼, 1.0 μ M) for various times at 37 °C in the presence of 5% CO₂. Each point on the graph represents a mean from three separate experiments (\pm SD).

As discussed previously, **70** has a pK_a value of 6.2 and thus is expected to mainly exist in the unprotonated form at physiological conditions (pH 7.4). Hence, the significant lack of cellular uptake of **70** maybe attributed to its insolubility in water at physiological pH. Therefore, the concentration of **70** was less in solution at the time of treatment, which resulted in less detected fluorescence intensity. However, the *N*-methyl piperazine Tröger's base **69** and the dimethylamine derivative **68** showed a more rapid uptake than **70**. As already discussed, **68** and **69** are protonated at pH 7.4, which is believed to lower their lipophilicity. Consequently, these results suggest that the protonated side chains of **68** and **69** render these molecules sufficiently enough lipophilicity to cross the cell membrane and to remain water soluble at the conditions used for cell culture. These results confirm the importance of the pK_a values to the cellular uptake observed by these types of compounds.

In summary, compound **68-70** were shown to enter HL-60 cells after 30 minutes and had fully accumulated in the cells after 24 hours incubation. These results also indicated that pK_a was important for the uptake of these compounds, since the fully protonated compounds **68** and **69** showed higher fluorescent intensity within the cells than the unprotonated compound **70**. After establishing that these compounds entered HL-60 cells, it was decided to determine the localisation of these compounds within cells by confocal microscopy. The results from these investigations are described in the next section.

3.2.2 Localisation Studies of 68-70 Using Confocal Microscopy

As discussed in *Section 2.2.2*, 1,8-naphthalimide compounds such as **7** and **8** have been shown to intercalate within the DNA base pairs and for that reason they are suggested to localise in the nucleus of cultured cells.¹⁶⁶ The investigations into the localisation of **68-70** would be important to confirm the results that were obtained from the cellular uptake studies in *Section 3.2.1*, where it was shown that these compounds were situated within cells after 24 hours. Furthermore, these studies would be indicative of the mechanism of cytotoxicity.

Confocal and fluorescent microscopy were used to investigate the localisation of **68-70** within HL-60 cells. Briefly, cells were incubated with **68-70** at 10 μ M concentration for 24 hours at 37 °C in the presence of 5% CO₂ and then washed with PBS and spun to a glass slide and allowed to dry. The cells were then fixed with 90% ethanol and a coverslip was mounted onto the slide, to conserve the fluorescence and the morphology of the cells before they were analysed under a confocal microscope. The results from these studies are depicted in Figure 3.4.

As shown in Figure 3.4, compound **68-70** were all localised within the cells after 24 hours. These results confirmed the cellular uptake results that were discussed in *Section 2.2.1*. Furthermore, as shown in Figure 3.4 **F** these results indicated that **70** was localised to a more extent in the cytoplasm than the nucleus after 24 hours. However, Figures 3.4 **B** and **D** for **68** and **69**, respectively indicated that the protonated derivatives were more localised in the similar or same region as to the nucleus. These results suggested that these compounds could potentially reach the nucleus and interact with DNA, in a similar manner as had been shown by **7** and **8**. Furthermore, as shown from the bright field images in Figure 3.4 **A**, **C**, **E**, the morphology of these cells suggested that **68** and **69** were potentially more cytotoxic than **70**. The cells that were treated with **68** and **69** were condensed and formed blebs at the surface of the cell membrane. In contrast, cells treated with **70** exhibited intact membrane integrity and a larger cytoplasm compared to **68** and **69**. The difference in behaviour between these compounds could be explained by the results from the uptake studies, which indicated that the low water solubility of **70**, resulted in a less concentrated solution. For that reason, the cells are exposed to less concentration of **70**, which substantially affects the cytotoxicity of this compound.

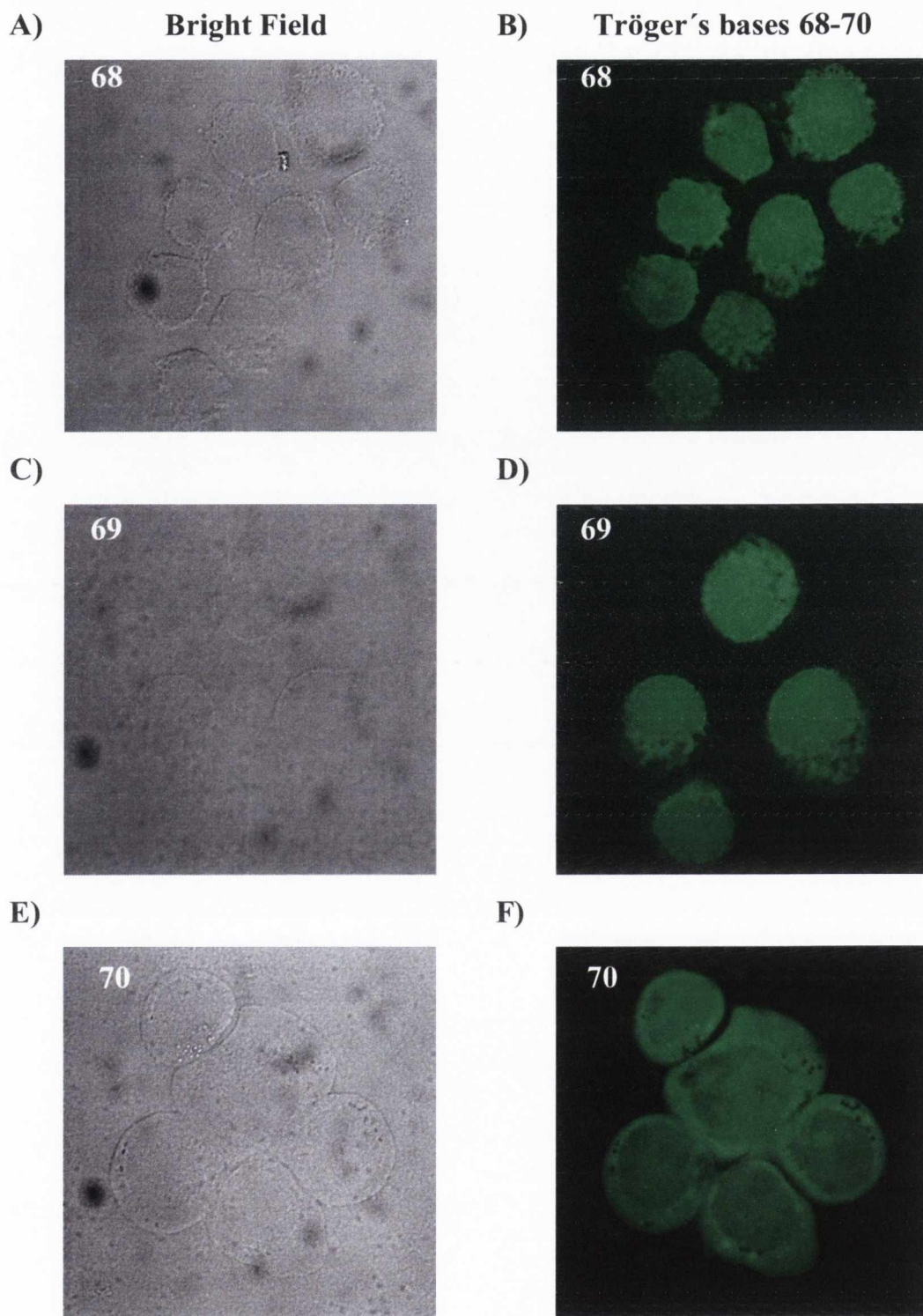
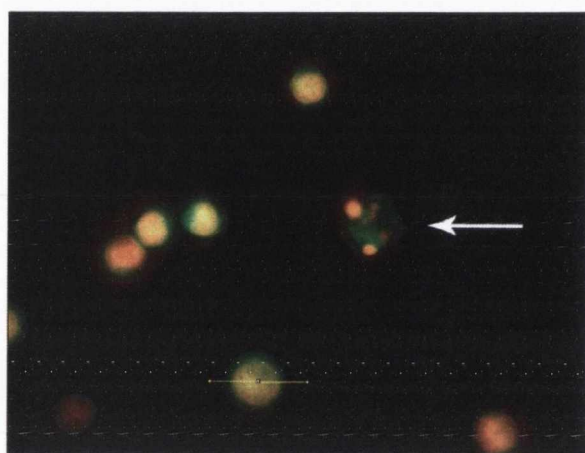


Figure 3.4 Confocal images of HL-60 cells incubated with 68-70 (10 μ M) for 24 hours. Prior to visualisation, excess compound was washed off by rinsing the cells with PBS. Cells were then spun to a glass slide, fixed and a coverslip was mounted onto the slide. Compounds were excited by a 488 nm argon laser and 500-530 nm bandpass filter was used to detect the fluorescence. The slides were investigated at x63 magnification.

To further investigate the localisation of these molecules, **68** was incubated with HL-60 cells for 24 hours and after fixation the cells were counterstained with a known fluorescent intercalator, propidium iodide **53**, which was discussed in *Section 2.5* in *Chapter 2*. This compound is also known to bind to RNA and thus, the cells were treated with RNase, preventing any RNA staining. The cells were then investigated by using fluorescent microscopy. The results are shown in Figure 3.5, with the corresponding transcellular overlay of fluorescence.

A)



B)

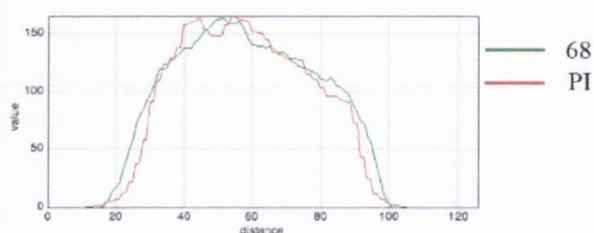


Figure 3.5 *Fluorescent images of HL-60 cells incubated with 68 (10 μ M) for 24 hours.* **A)** *The cells were fixed with 95% EtOH before they were counterstained with propidium iodide 53 (ex. 540 \pm 25 nm, Em >610 nm) for 15 minutes and treated with RNase. Compound 68 (green) was excited with a mercury lamp (Ex 465-495 nm) and its fluorescence was detected using a filter cube (515-555 nm). The arrow indicates an apoptotic cell. **B)** *Longitudinal transcellular overlay of fluorescence intensity of 68 and propidium iodide.**

As shown in Figure 3.5 **B**, these investigations revealed that **68** was mainly localised in the same region as propidium iodide after 24 hours treatment, confirming that **68** was situated in the nucleus. Furthermore, as indicated in Figure 3.5, the presence of **68** in apoptotic bodies indicated that **68** was still bound to the DNA, even after the fragmentation and furthermore, these results also indicated that **68** induced cellular death, possibly apoptosis.

3.2.3 Summary

Compounds **68-70** have been shown to enter HL-60 cells after 24 hours. The dimethylamine derivative **68** showed the most rapid uptake, while the morpholine

derivative **70** was taken up to the least extent. The reason for the poor uptake shown by **70** was believed to arise from its poor water solubility, as it has a p*K*_a value of 6.2. However, **68** and **69** have p*K*_a values of 8.6 and 8.2, respectively. As discussed in the beginning of this section, the p*K*_a values are shown to affect the water solubility and the lipophilicity of related molecules such as **71**. These results suggested that the p*K*_a of **68** and **69** rendered the molecules a perfect balance between water solubility and lipophilicity for cellular uptake.

The Tröger's bases **68** and **69** were shown to localise in the nucleus of HL-60 cells after 24 hours treatment, while **70** was mainly situated in the cytoplasm. Moreover, co-localisation studies with a known DNA intercalator confirmed that **68** was, in fact situated in the nucleus after 24 hours treatment. These observations were important to confirm that **68-70** could reach their proposed cellular target, namely the DNA. From these results, it was deemed necessary to investigate the effects these compounds had on the growth of HL-60 cells and furthermore, to compare them to the precursors **65-67**. The results and observations will be discussed in the following section.

3.3 Cytotoxicity Studies of 65-70

As discussed in *Chapter 1* and *Chapter 2*, the toxicity of 1,8-naphthalimides has been thoroughly investigated, in particular compound **8**, which was shown to induce apoptosis by forming double strand breaks.⁹⁴ Furthermore, the toxicity was shown to be maximised when the 1,8-naphthalimide unit was separated by a spacer that consisted of two methylene units and a dimethylamine at the end position. In addition, the *N*-methyl piperazine moiety showed decreased cytotoxic activity against HeLa cells compared to the dimethylamine derivative and the morpholine was shown to be the least active. Furthermore, as discussed in *Section 1.4.1.1.2*, the promising cytotoxicity of mono 1,8-naphthalimides such as **8**, lead to the design of bis 1,8-naphthalimides **11** and **12**, which exhibited increased cytotoxicity when compared to their mono precursors. For that reason, it was decided to compare the toxicity of the 4-amino-1,8-naphthalimide precursors **65-67** to the corresponding Tröger's bases **68-70**, to compare the mono 1,8-naphthalimide derivatives to the bis 1,8-naphthalimide Tröger's base derivatives. These investigations were necessary to determine the effect of the Tröger's base unit and the effect of the importance of the cationic group at the terminus of their side chain.

The MTT proliferation assay was conducted as described in *Section 2.2* of *Chapter 2*. Briefly, HL-60 cells were incubated for 24 and 48 hours with either **65-70** or vehicle

(RPMI medium) at 37 °C in the presence of 5% CO₂. Each experiment was carried out in quadruplicate and stock solutions of **65-70** (1 mM) were made up in cell medium. After a certain incubation period, the amount of metabolically active cells was quantified using the MTT assay and it was compared to vehicle-treated cells using *Equations 2.1* or *Equation 2.2* in *Chapter 2*. The cytotoxic parameter, Gi₅₀, TGI and LD₅₀ were calculated from the aforementioned equations. The concentration of compound was then plotted against the growth percentage and the resulting graph for 24 hours treatment with **65-70** is shown in *Figure 3.5*. The corresponding cytotoxicity parameters, Gi₅₀, TGI and LD₅₀ are given in *Table 3.2*.

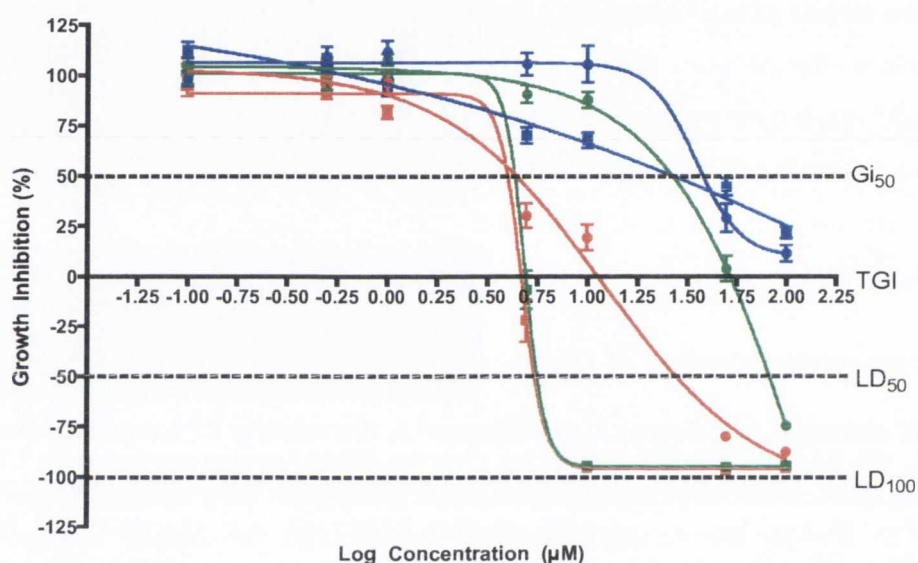


Figure 3.6: Cytotoxicity profile after 24 hours. HL-60 cells were incubated with **65** (●), **66** (●), **67** (●), **68** (■), **69** (■) and **70** (■) at 37 °C in the presence of 5% CO₂ for 24 hours before determining the amount of metabolically active cells by MTT assay. The cytotoxicity parameters (Gi₅₀, TGI, LD₅₀ and LD₁₀₀) are indicated on the graph. Each point on the graph represents the mean from three separate experiments, each done in quadruplicate (±SEM).

As shown in *Table 3.2*, the introduction of the Tröger's base skeleton into the 1,8-naphthalimide chromophore resulted in an increase in the cytotoxic potential after 24 hours treatment. Although the growth inhibition is similar to that of **65** and **68**, there is a marked difference between the 50% growth inhibition exerted by the *N*-methyl piperazine derivatives, **66** and **69** (Gi₅₀ values of 28.0 µM and 4.35 µM, respectively). These results are in an agreement with the DNA binding studies conducted by Dr. Veale, where it was

showed that the Tröger's base **68-70** derivatives exhibited higher binding affinity compared to the precursors **65-67**.

Table 3.2: Summary of cytotoxicity values (μM) for 65-70 after 24 hours incubation with HL-60 cells. Each value represents a mean calculated from three independent experiments, all done in quadruplicate (\pm SEM). Values mentioned in the text are indicated by a red colour.

	65	66	67	68	69	70
GI₅₀	4.83 (\pm 1.39)	28.0 (\pm 6.17)	35.8 (\pm 8.80)	3.35 (\pm 0.920)	4.35 (\pm 0.301)	25.5 (\pm 6.70)
TGI	11.6 (\pm 2.59)	51.5 (\pm 7.02)	> 100	4.15 (\pm 0.822)	4.88 (\pm 0.279)	> 100
LD₅₀	27.7 (\pm 4.23)	80.9 (\pm 4.12)	> 100	5.21 (\pm 0.540)	5.50 (\pm 0.284)	> 100

As shown in Table 3.2, compound **68** completely inhibited the growth of HL-60 cells at a two-fold lower concentration than the corresponding 1,8-naphthalimide precursor **65** (TGI values of 4.15 μM and 11.5 μM , respectively). Furthermore, the *N*-methyl piperazine derivative **69** induced a complete growth inhibition at a concentration that is ten times lower than the corresponding 4-amino-1,8-naphthalimide derivative **66** (TGI values of 4.88 μM and 51.5 μM , respectively). The Tröger's bases **68** and **69** exhibited a considerable increase in 50% cell reduction over their precursors and in addition, **68** and **69** reduced the cell population completely at a considerable lower concentration than their precursors **65** and **66**, respectively. This is indicated in Figure 3.5, by the cytotoxicity parameter LD₁₀₀, the concentration of a compound that will give 100 % cell reduction compared to vehicle-treated cells. These results highlighted the importance of the Tröger's base skeleton on the cytotoxicity potential shown by **67-70**. In addition, the morpholine derivatives **67** and **70** showed an apparent lack of cytotoxicity. These results correlated well with the uptake and fluorescent studies that were discussed in Section 3.2, where it was shown that possibly due to solubility reasons, the concentration of **70** was believed to be less in solution than expected. This further suggested the significance of the p*K*_a values of these compounds to their uptake and cytotoxicity.

As shown in Table 3.3, the Tröger's base derivatives **68** and **69** retained their cytotoxic ability after 48 hours treatment. They were also shown to be more cytotoxic than the corresponding 4-amino-1,8-naphthalimide derivatives **65** and **66** after 48 hours. These results show that the growth of the HL-60 cells had recovered after 48 hours treatment with **70**, suggesting that the inhibition is not enough to sustain the cytotoxic effects for 48 hours.

Table 3.3: Summary of cytotoxicity values (μM) for 65-70 after 48 hours incubation with HL-60 cells. Each value represents a mean calculated from three independent experiments, all done in quadruplicate (\pm SEM).

	65	66	67	68	69	70
GI₅₀	4.58 (\pm 0.323)	34.7 (\pm 1.47)	> 100	4.76 (\pm 0.031)	4.99 (\pm 0.394)	> 100
TGI	10.4 (\pm 0.426)	56.5 (\pm 2.29)	> 100	5.43 (\pm 0.378)	5.16 (\pm 0.488)	> 100
LD₅₀	23.3 (\pm 0.664)	80.7 (\pm 4.83)	> 100	6.32 (\pm 0.939)	6.17 (\pm 0.632)	> 100

In addition to these results, **65-70** were also tested for cytotoxicity against the chronic myeloid leukaemia (CML) cell line, K562. This cell line is known for its resistance to drugs, resulting from the expression of the chimeric Bcr-Abl protein discussed in *Section 1.3* in *Chapter 1*.¹⁶⁹ As for the studies on HL-60 cells, **68** was shown to be the most cytotoxic with an EC₅₀ value of 5.53 μM . The *N*-methyl piperazine derivative **69** was three times less active than **68** (17.0 μM vs. 5.53 μM), whereas **70** was shown to be inactive at 100 μM concentration. These results were in agreement with studies done on etoposide **58** in these cells lines, where it was shown that treatment with **58** induces more apoptosis in HL-60 cells than K562 cells, possibly due to the apoptosis suppressing role of the Bcr-Abl protein.¹⁷⁰ The results from the cytotoxicity investigation against the growth of K562 cells can be found in *Table A2.1* in *Appendix 2*.

In summary, the introduction of the Tröger's base skeleton into the 1,8-naphthalimide chromophore resulted in an increase in the cytotoxic activity of **68-70** against HL-60 cells in comparison to their precursors **65-67**. These results correlated well with the results obtained from the uptake studies, where **68** showed the most rapid uptake. Additionally, the morpholine analogue **70**, which showed the least uptake, only had a minimal effect on the growth of the HL-60 cells, further indicating that the p*K*_a was important for the biological cytotoxicity of these compounds. Furthermore, Tröger's bases **68** and **69** completely inhibited the growth at a much lower concentration than **65** and **66** and more importantly, the toxic ability is sustained over 48 hours treatment.

As already discussed in *Section 2.1* in *Chapter 2*, amonafide **8**, a 3-amino substituted analogue of the 1,8-naphthalimide precursors **65-67** was found to induce double stranded breaks *in vitro*, leading to an arrest in G₂/M phase of the cell cycle and the induction of programmed cell death (apoptosis).¹⁶⁶ Therefore, it was deemed necessary to study the effects that **65-70** would exert on the cell cycle.

3.4 Cell Cycle Analysis and Investigation of the Mode of Cell Death Induced by 65-70

3.4.1 Cell Cycle Studies of HL-60 Cells Treated With 65-70

As discussed in *Section 3.1.1*, amonafide **8** has been shown to induce apoptosis in human cancer cells.¹⁶⁶ The mechanism of action has been shown to involve the formation of double strand breaks, resulting from Topo II inhibition. This arrested the cell cycle in one of their DNA checkpoints, namely G₂ as was discussed in *Section 1.2.1* of *Chapter 1*. The G₂ checkpoint is activated upon different stimuli, such as DNA damage. The arrest allows the cell to undergo examination of the extent of the DNA damage and to decide whether to repair the damage or to initiate apoptosis. Therefore, investigation into the effects compounds **65-70** have on the cell cycle could suggest the mechanism by which these compounds act and their ability to induce apoptosis.

Cell cycle analysis was performed on HL-60 cells as described in *Section 2.5* of *Chapter 2*. Briefly, cells were incubated for 24 and 48 hours with compounds **65-70** at three different concentrations (1, 5 and 10 μ M). Cells were then washed, and their DNA stained with propidium iodide **56** before analysing the cell population on the flow cytometry. The fluorescent intensity was plotted against the concentration of **65-70** and the corresponding plots for 24 hours treatment are shown in Figure 3.7. Each plot is representative of three separate reproducible experiments and the results from the additional sets of experiments can be found in *Appendix 2, Figure A2.2*. Furthermore, the population of each phase after 10 μ M treatment was determined and the means along with the standard errors are shown in Table 3.4 and Table 3.5 for 24 and 48 hours treatments, respectively.

As shown in Figure 3.7, these compounds did not induce apoptosis to a large extent at these concentrations after 24 hours treatment, which could be indicative of a different mechanism of cell death being induced. Firstly, the morpholine derivative **67** only induced 4% apoptosis (pre-G₁) after 24 hours treatment whereas the corresponding Tröger's base **70** induced 2.6%, as shown in Table 3.4. Furthermore, these compounds did not induce an arrest in any of the cell cycle phases. These results correlated well with the analysis from cytotoxicity studies in *Section 3.3*, where it was shown that the morpholine derivatives **67** and **70** showed only minimal effects on the cell growth after 24 hours treatment. The *N*-methyl piperazine based 1,8-naphthalimide **66** and the corresponding Tröger's base **69** did

not arrest the cells in G₂/M phase of the cell cycle and these compounds were shown to induce apoptosis similar to that of vehicle-treated cells. These results indicated that these compounds exerted their cytotoxicity without interfering with the cell cycle.

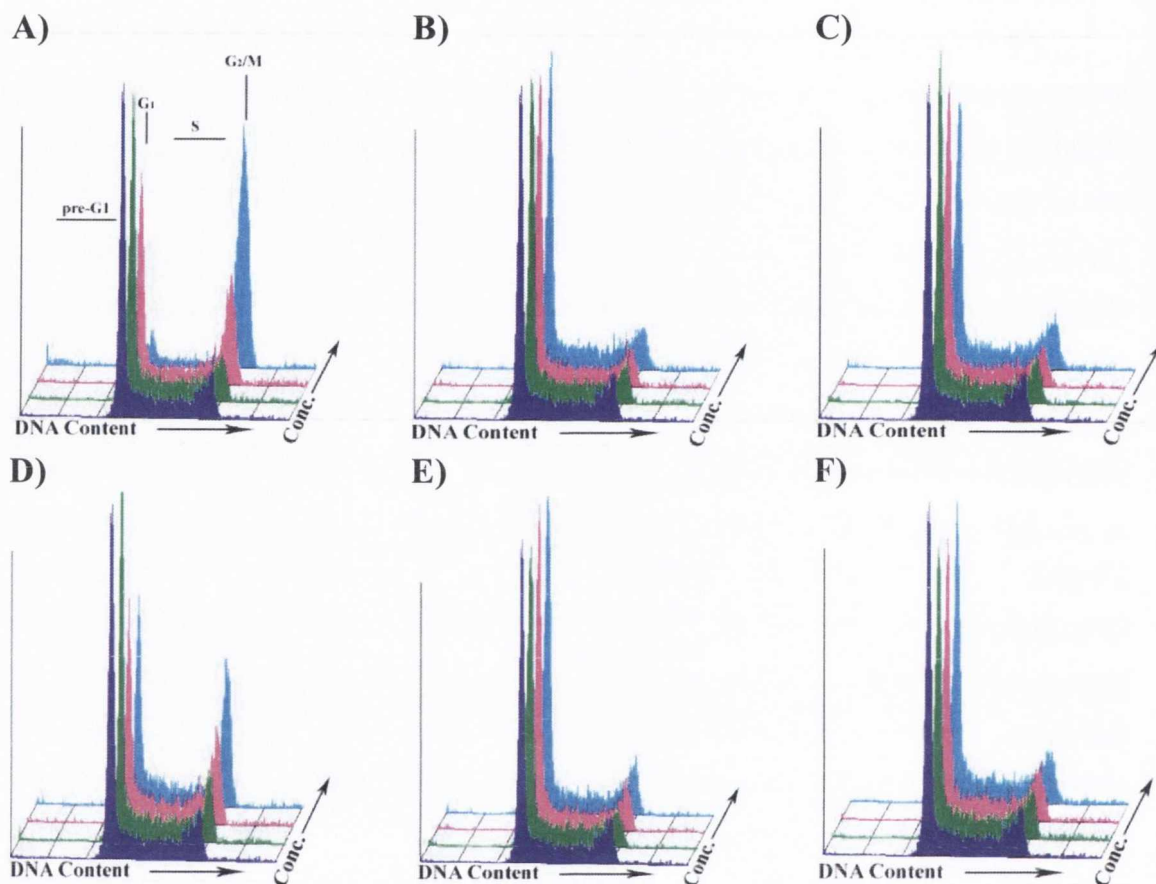


Figure 3.7: Cell cycle analysis of precursors 65-67 and Tröger's bases 68-70 after 24 hours treatment. HL-60 cells were incubated with A) 65, B) 66, C) 67, D) 68, E) 69 and F) 70 at three concentrations 1.0 μM (■), 5.0 μM (■) and 10 μM (■) for 24 hours. The vehicle-treated cells are shown as a purple solid peak.

The dimethylamine 1,8-derivatives **65** and **68** showed considerable effects on the cell cycle after 24 hours at 10 μM concentration. The 4-amino-1,8-naphthalimide **65** was shown to block cells in the G₂/M phase of the cell cycle, by nearly three times as much compared to vehicle-treated cells (14.9%→40.9% as shown in Table 3.4). The corresponding Tröger's base **68** showed similar capabilities to block cells in the G₂/M phase of cell cycle (14.9%→41.3%). These results indicated that the dimethylamine moiety in the side chain of these compounds is important for the induction of apoptosis, which also correlated well with the toxicity studies discussed above, where it was shown that these

compounds were highly cytotoxic, exhibiting GI_{50} values of 4.83 μM and 3.35 μM for **65** and **68**, respectively. Furthermore, the observed G_2/M arrest was in agreement with the investigation into the mechanism of apoptosis shown by **8**, where it was shown that the dimethylamine moiety was important for creating double stranded breaks in DNA.

Table 3.4: Cell cycle analysis of HL-60 cells after 24 hours treatment with 65-70 at 10 μM concentration. Values mentioned in the text are indicated by a red colour.

	Pre- G_1	G_1	S	G_2/M
NT	2.08 (± 0.411)	44.2 (± 2.67)	34.3 (± 2.30)	14.9 (± 1.14)
65	5.97 (± 2.55)	16.3 (± 6.39)	23.00 (± 4.98)	40.9 (± 8.65)
66	3.50 (± 0.856)	45.4 (± 3.09)	30.1 (± 1.32)	14.6 (± 1.20)
67	4.02 (± 1.18)	42.5 (± 1.15)	30.4 (± 1.40)	14.7 (± 0.695)
68	2.55 (± 0.709)	21.6 (± 8.02)	27.5 (± 7.50)	41.3 (± 13.4)
69	2.22 (± 0.224)	44.2 (± 1.68)	33.1 (± 2.07)	15.9 (± 0.885)
70	2.62 (± 0.059)	39.6 (± 2.23)	33.6 (± 1.67)	16.0 (± 0.233)

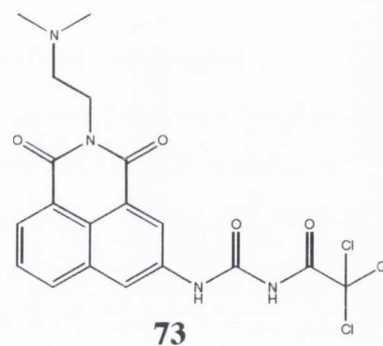
Despite the fact that **65** and **68** were shown to arrest the cell cycle, they only induced a minimal amount of apoptosis after 24 hours treatment. To further investigate this behaviour, HL-60 cells were treated for 48 hours at the same concentrations of compounds **65-70**. As before, each experiment was repeated twice for reproducibility and the resulting plots of the fluorescent intensity against concentration of compounds **65-70** can be found in *Appendix 2, Figure A2.3*. The summary from those results are listed in Table 3.5.

Table 3.5: Cell cycle analysis of HL-60 cells after 48 hours treatment with 65-70 at 10 μM concentration. Values mentioned in the text are indicated by a red colour.

	Pre- G_1	G_1	S	G_2/M
NT	9.63 (± 2.75)	50.7 (± 3.16)	27.3 (± 0.880)	7.76 (± 0.894)
65	12.5 (± 3.88)	24.9 (± 14.9)	15.1 (± 4.41)	40.9 (± 12.5)
66	5.33 (± 0.630)	55.6 (± 3.40)	28.3 (± 3.07)	5.96 (± 2.76)
67	4.78 (± 1.13)	49.6 (± 0.593)	31.8 (± 1.24)	8.01 (± 0.937)
68	4.45 (± 1.04)	52.2 (± 4.29)	21.5 (± 0.844)	16.6 (± 0.312)
69	4.23 (± 0.642)	54.8 (± 4.48)	27.1 (± 2.01)	7.25 (± 1.12)
70	2.96 (± 0.807)	46.6 (± 4.73)	32.1 (± 0.897)	9.87 (± 0.936)

These results further show that the cell cycle was largely unaffected by treatment with the morpholine and *N*-methyl piperazine derivatives **66-67** and **68-69**, respectively. In contrast, the corresponding Tröger's base derivative **68** only arrested twice as many cells in the G₂/M phase compared to the vehicle-treated population (16.6% vs. 7.76%). These results further indicated a decrease in the amount of arrested cells after 48 hours when compared to 24 hours treatment (16.6% and 41.3%, respectively). Although these results could not be fully explained, they seem to suggest that the HL-60 cells have ability to overcome the arrest induced by **68**. Furthermore, the 4-amino-1,8-naphthalimide derivative **65** showed similar ability to arrest cells in G₂/M after 48 hours as was shown for 24 hours treatment (40.9% and 40.9%, respectively). This further suggested that the Tröger's base unit might be responsible for the apparent decrease in arrested cells after 48 hours treatment with **68**. The possible explanation for this difference between **65** and **68** was believed to involve the difference of binding to DNA. As discussed in *Chapter 1*, a cell cycle checkpoint is activated upon DNA damage, which delays the cell cycle and allows the cell to examine the extent of the DNA damages.¹⁴ The cell initiates apoptosis if the damage is severe, however if the damage is negligible, the DNA damage is repaired. Therefore, these results indicate that the treatment with **68** results in less DNA damage than **65**.

The apparent lack of apoptosis after 48 hours treatment by **65-70** indicated a different mode of cell death being initiated after treatment. Kiss *et al.*¹⁷¹ have reported similar observations, which suggested that 1,8-naphthalimide derivatives such as **73** induced autophagy in a prostate cancer cell line, PC-3. Therefore, it was deemed necessary to investigate further the mechanism of death induced by **65-70**, by inspecting the cellular morphology of treated cells. The results from that study will be discussed in the next section.



3.4.2 Cell Morphology Investigation After Treatment With 65-70

As discussed in the *Section 3.3*, compounds **65-70** were shown to be cytotoxic against HL-60 cells after 24 hours. However, the results from the cell cycle analysis suggested that these compounds induced a different mode of cell death to apoptosis. For that reason, the morphology of the treated cells were investigated using the cell morphology assay that was described in *Section 2.4* in *Chapter 2*. Briefly, HL-60 cells

were treated with **65-70** at three different concentrations (1, 5 and 10 μM) for 24 and 48 hours. The cells were then spun to a glass slide and stained with haematoxylin and eosin, which coloured the nucleus and cytoplasm, respectively. Apoptotic cells were distinguished by the hallmarks of apoptosis, such as condensed cells, fragmented nucleus and the blebbing from the cell membrane. The percentage of apoptosis cells from three different fields of view are plotted and the resulting graph for **65-70** at 10 μM concentration after 24 hours treatment is shown in Figure 3.8.

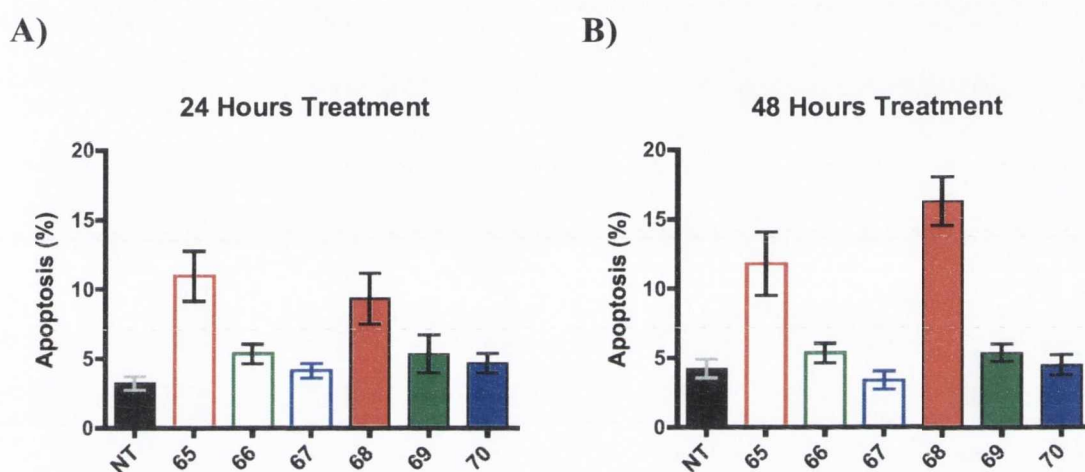


Figure 3.8 Morphological changes in HL-60 cells after 24 hours treatment with **65-70**. The percentage of apoptosis induced by **65** (10 μM , \square), **66** (10 μM , \square), **67** (10 μM , \square), **68** (10 μM , \blacksquare), **69** (10 μM , \blacksquare) and **70** (10 μM , \blacksquare). Untreated cells are shown as \blacksquare . Each graph represents three separate experiments.

The results shown in Figure 3.8 A, indicated that apoptosis is not induced to a large extent after 24 hours treatment with **65-70** at 10 μM concentrations. Treatment with the dimethylamine derivatives **65** and **68** showed the largest induction of apoptotic cells, about 11% and 9%, respectively. However, the piperazine derivatives **66** and **69** resulted only in about 5% apoptosis after 24 hours treatment, while the morpholine derivatives **67** and **70** induced minimal apoptosis or 4%. These results confirmed the results from the cell cycle analysis studies that were discussed in the last section, where it was shown that the dimethylamine derivatives **65** and **68** induced the highest percentage of apoptosis. However, the extent of apoptosis was different between the cell cycle analysis and the assay described in this section. This could be explained by the fact that the cell cycle analysis assay determines the percentage from ten thousand cells, while the cell morphology investigations only include three hundred cells. The results that were obtained

after 48 hours treatment indicated that the percentage of apoptotic cells increased over time, in correlation with the results obtained from the cell cycle analysis. Furthermore, the treatment at lower concentrations, such as 1 and 5 μM only resulted in lower apoptosis. However, the same trend was obtained for the lower concentrations as for the treatment at 10 μM applied, where the dimethylamine derivatives **65** and **68** were shown to induce apoptosis to the largest extent, followed by the *N*-piperazine derivatives **66** and **69** and then the morpholine derivatives **67** and **70**, which showed minimal induction of apoptosis. The results from the lower concentrations are shown in *Figure A2.4* in *Appendix 2*. Furthermore, the morphology of the cells did not indicate necrosis after 24 hours nor 48 hours, indicating an even different mode of cell death being induced, such as autophagy as was discussed above.

3.4.3 Summary

Compounds **66-67** and **69-70** were shown not to affect the cell cycle to a large extent and furthermore, only induce minimal amount of apoptosis after either 24 hours or 48 hours treatment. However, the dimethylamine derivatives **65** and **68** showed considerable arrest in the G_2/M phase after 24 hours and 48 hours treatment. Despite arresting the cells, there was no significant increase in apoptosis after treatment with these compounds and these results were confirmed by investigating the cellular morphology. The lack of apoptosis could be indicative of a different cellular death being induced, such as has been shown by **73**.¹⁷¹

In conclusion, both **65** and **68** induced G_2/M arrest in HL-60 cells in a similar manner as had already been shown with amonafide **8**.¹⁶⁶ It has been previously indicated that the observed G_2/M arrest induced by **8** was a result of the formation of DNA double strand breaks. Furthermore, the mechanism of the formation of double stranded breaks is thought to involve the intercalation of the 1,8-naphthalimide chromophore and the interaction of the dimethylamine side chain with the Topo II binding site, thereby inhibiting the ligation step of the Topo II as discussed in *Section 1.4.1.1* of *Chapter 1*. Therefore, it was considered necessary to investigate the activity of the Tröger's bases **68-70** against Topo I and Topo II enzymes. The results from these studies will be discussed in the following section.

3.5 The Effects of 68-70 on Topo I and II Activity

As discussed in *Section 1.4.1.1* and in *Section 2.6*, Topo I and Topo II are highly involved in the proliferation of cells and have been proposed as targets for anticancer drugs.¹⁷² Drugs that interact with DNA, such as mitonafide **7** and amonafide **8** have been shown to be involved in the catalytic inhibition of topoisomerase enzymes.^{94,95,173} It has also been suggested that the basic side chain of **7** and **8** interacts electrostatically with a tyrosine residue in the active site of the Topo II enzyme, which is responsible for DNA cleavage and ligation. This leads to an increasing lifetime of the corresponding topoisomerase-DNA complex, resulting in a halt in the G₂ phase as was discussed in *Section 3.4*.¹⁶⁶ Furthermore, compound **8** was also shown to effect the cleavage activity of Topo I.⁹⁴ This can be explained by the fact that **8** intercalates between the DNA base pairs and relaxes the plasmid. Therefore, the plasmid is already fully relaxed upon addition of the Topo I enzyme and thus no enzymatic activity is required from the enzyme. When the reaction is stopped, compound **8** leaves the DNA and the plasmid returns to its supercoiled state, resulting in a migration pattern that resembles untreated plasmid. Since the 1,8-naphthalimides **7** and **8** have been shown to affect the activity of topoisomerase enzymes, it was decided to investigate the effects **68-70** had on these enzymes. Furthermore, these investigations would also give an idea about the binding mechanism of these compounds and the effect of the incorporation of the Tröger's base unit to DNA.

3.5.1 Topo I Investigations

For these investigations, compounds **68-70** were tested at 1, 5 and 10 μM concentration in the same manner as described in *Section 2.6* of *Chapter 2*. Briefly, the plasmid was incubated with **68-70** in the presence or absence of Topo I at 37 °C and the corresponding plasmid products were then separated by an agarose gel electrophoresis. The guidelines for analysis of the Topo I gels can be found in *Figure 2.24* in *Chapter 2*. The resulting gels without SYBr are shown in *Figure 3.9 A* and *B* and the SYBr containing gels are shown in *Figure 3.10 A* and *B*.

As shown in *Figure, 3.9*, the gel in the absence of SYBr green suggested that **68-70** were Topo I inhibitors, which blocked the access of the enzyme to the DNA or the overall catalytic activity, resulting in a higher formation of supercoiled plasmid. Nevertheless, upon closer examination, the reaction in the absence of **68-70** showed similar amounts of the unreacted plasmid (Lane +, SC) as the reaction carried out in the presence of these

compounds. Therefore, these results were considered to be as being inconclusive, particularly because of the low formation of the relaxed plasmid, possibly due to the low reactivity of the enzyme.

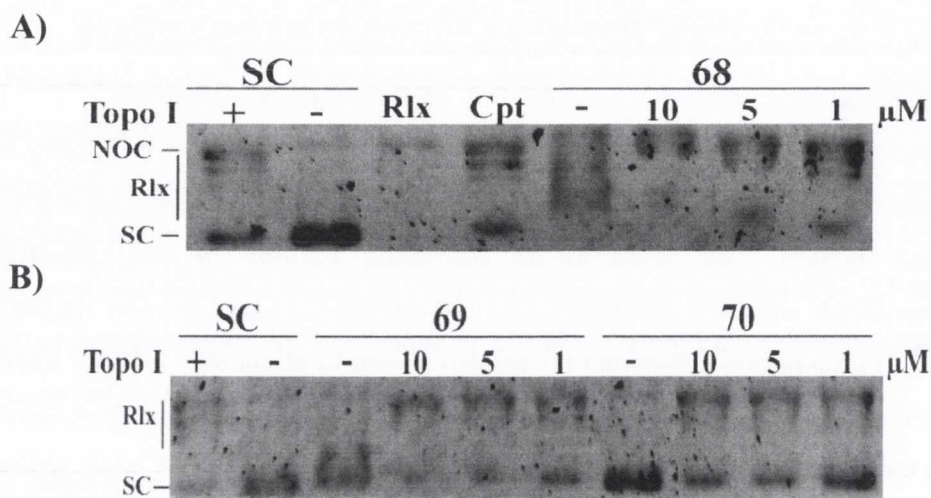


Figure 3.9: Topo I analysis of compounds 68-70 at 10, 5 and 1 μM concentrations in the absence of SYBr green. Compounds were incubated with a supercoiled plasmid (0.5 μg) and Topo I (5 units), at three different concentrations (10, 5 and 1 μM) as indicated above each lane. Lanes labeled - represent reactions done in the absence of Topo I. Rlx indicates the position of the relaxed marker. Lane Cpt represents the effects of a Topo I poison (Camptothecin, 100 μM) and finally the SC, + and SC, - represents the reactions done in the presence and in absence of Topo I, respectively.

The resulting gels in the presence of the SYBr green shown in Figure 3.10 A and B, indicated that these compounds did not behave like a Topo I poison, which would result in an increase of the amount of nicked open circular (NOC) plasmids after treatment. Furthermore, the results in the presence of SYBr green showed considerable amounts of unreactive supercoiled plasmid, confirming the low activity of the enzyme used. Although these results were inconclusive in terms of determining the effects of compounds 68-79 on the activity of the enzyme, they revealed that 68 caused a minimal decrease of the mobility of the supercoiled plasmid at 10 μM concentration. This was apparent by comparing the lanes where the plasmid was incubated with or without 68 in the absence of Topo I (Lane -, 68 and Lane -, SC, respectively). Compound 69 showed similar effects, however to a smaller extent. These results can be attributed to the lengthening of the plasmid, due to strong interactions between the plasmid and 68 and 69 at 10 μM concentration. This behaviour has been reported for compounds that interact with DNA, *i.e.* intercalators¹⁷⁴ as well as minor groove binders¹⁷⁵ and also with divalent cations such as Mg^{2+} .^{174,176} DNA

interacting compounds reduce the helical twist of the DNA plasmid and introduce partial relaxation to the plasmid, ultimately resulting in a less compact DNA.

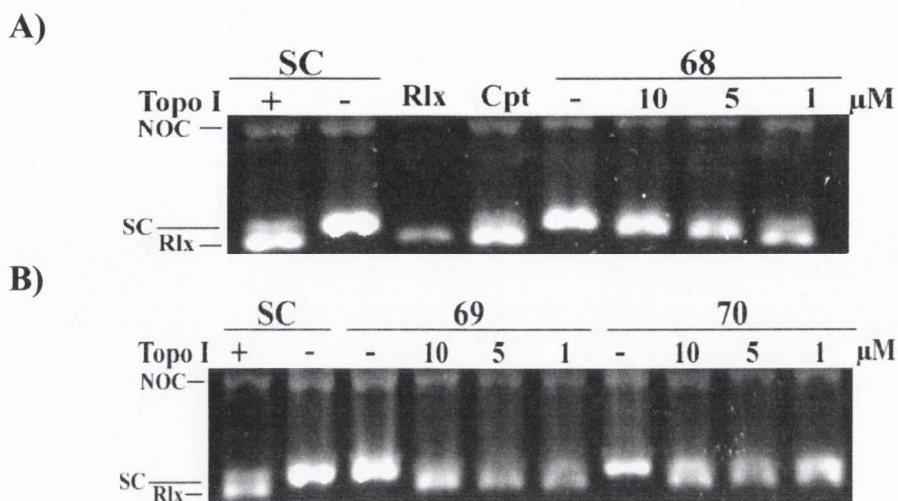


Figure 3.10 *Topo I* analysis of compounds **68-70** at 10, 5 and 1 μM concentrations in the presence of SYBr green. Compounds were incubated with a supercoiled plasmid (0.5 μg) and *Topo I* (5 units), at three different concentrations (10, 5 and 1 μM) as indicated above each lane. Lanes labeled - represent reactions done in the absence of *Topo I*. Rlx indicates the position of the relaxed marker. Lane Cpt represents the effects of a *Topo I* poison (Camptothecin, 100 μM) and finally the SC, + and SC, - represents the reactions done in the presence and in absence of *Topo I*, respectively.

In addition, similar behaviour has been reported by Andersson *et al.*⁹⁴, which showed that **8** induced DNA smearing at high concentrations (20 μM). The authors concluded that this behavior indicated significant alteration in the DNA charge and in the subsequent electrophoresis migration owing to the binding of **8** to DNA. For that reason, it was decided to investigate the effects higher concentrations of **68-70** had on the plasmid and the activity of the *Topo I*.

These investigations were carried out as described before however, concentrations of 12.5, 25 and 50 μM of **68-70** were used. The resulting gels ran in the absence of SYBr green as shown in Figure 3.11, whereas the gel ran in the presence of SYBr green can be found in Figure A2.5 in Appendix 2.

Firstly, these results indicated that **70** was inactive against *Topo I* at these concentrations, whereas, **68** and **69** showed a considerable inhibition effect on *Topo I* activity. The mechanism for **68** and **69** inhibition possibly involved the relaxation of DNA induced by these compounds that resulted in the migration pattern that resembled untreated DNA, similar to what has been shown by **8**.⁹⁴ Secondly, these results confirmed that **68** and **69** affected the mobility of the supercoiled plasmid, as was shown for the investigation into

the lower concentrations of **68-70**. The observed smearing of the plasmid after treatment with **68** was reproducible as shown in *Figure A2.6* in *Appendix 2*. These results strongly implied that **68** had considerable effect on the charge of the DNA, as was reported with high levels of **8**.

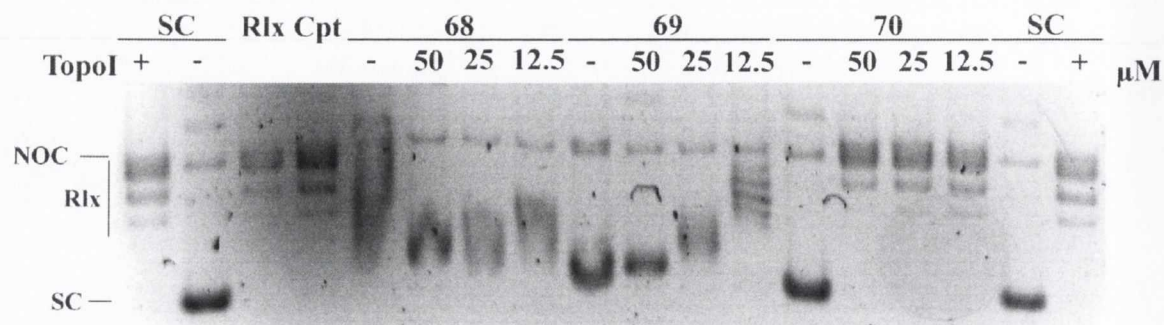


Figure 3.11 *Topo I analysis of compounds 68-70 at 50, 25 and 12.5 μM concentrations in the absence of SYBr green.* Compounds were incubated with a supercoiled plasmid (0.5 μg) and Topo I (5 units), at three different concentrations (50, 25 and 12.5 μM) as indicated above each lane. Lanes labeled - represent reactions done in the absence of Topo I. Lin indicates the position of the linear marker. Lane Cpt represents the effects of a Topo I poison (Camptothecin, 100 μM) and finally the SC, + and SC, - represents the reactions done in the presence and in absence of Topo I, respectively.

In summary, compounds **68** and **69** were shown to inhibit Topo I in a cell-free system, while compound **70** did not have any effect on the cleavage activity of Topo I. Furthermore, these results confirmed that **68** and **69** interacted with DNA and the nature of this interaction possibly involved electrostatic binding of these compounds to the negatively charged phosphate backbone of DNA. However, as described in the beginning of this section, 1,8-naphthalimide compounds have also been known to inhibit Topo II and thus, **68-70** were also tested against the Topo II enzyme. The results from these studies are discussed in the next section.

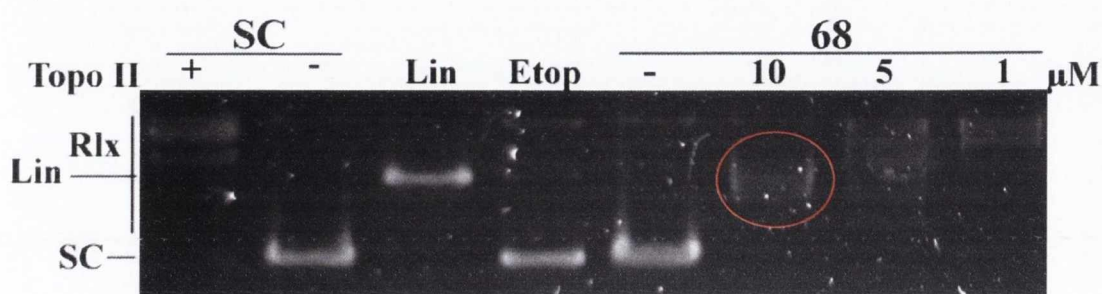
3.5.2 Topo II Investigations

Compounds **68-70** were tested according to the description in *Section 2.6* of *Chapter 2*. Similar to the Topo I investigation, compounds **68-70** were originally tested at lower concentrations, namely 1, 5 and 10 μM . The results obtained from these investigations are shown in *Figure 3.12* for the gel in the absence of SYBr green and *Figure 3.13* for the gel in presence of SYBr green.

As shown in *Figure 3.12* and *3.13*, the results from this study indicated that **69** and **70** were largely inactive in inhibiting Topo II at 10 μM concentration, neither inducing the

formation of linear plasmids or nicked open circular plasmids, which would be indicative of a double stranded or single strand breakage, respectively. Furthermore, the results shown in Figure 3.12 in the absence of SYBr green suggested that **68** induced the formation of linear DNA at 10 μM concentration (red circle). However, this behavior could also be explained by the fact that **68** interacted with the plasmid and affected its mobility, as was discussed in Section 3.5.1. In that case, the migration pattern could be similar to the linear DNA marker in the absence of SYBr green in the gel.

A)



B)

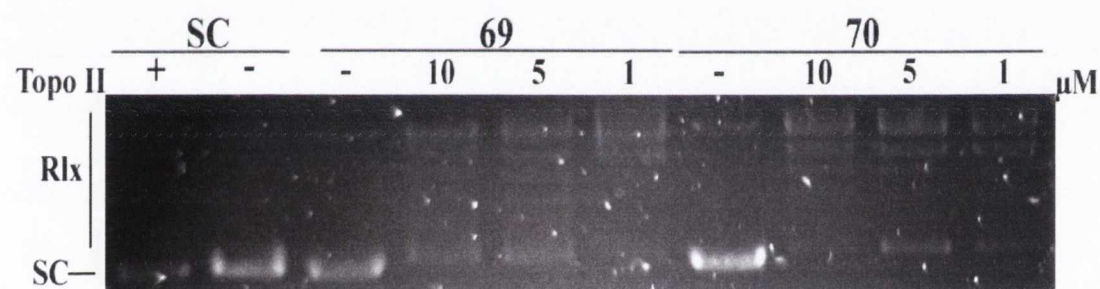


Figure 3.12 Topo II analysis of compounds **68-70** at 10, 5 and 1 μM concentrations in the absence of SYBr green. Compounds were incubated with a supercoiled plasmid (0.5 μg) and Topo II (5 units), at three different concentrations (10, 5 and 1 μM) as indicated above each lane. Lanes labeled - represent reactions done in the absence of Topo II. Lin indicates the position of the linear marker. Lane Etop represents the effects of a Topo II poison (Etoposide, 100 μM) and finally the SC, + and SC, - represents the reactions done in the presence and in absence of Topo II, respectively.

As shown in Figure 3.13, the corresponding gel that ran in presence of SYBr green showed that the linear plasmid was not induced by treatment of **68** at 10 μM concentration, indicating that this compound affected the mobility of the plasmid. These results were in agreement with the Topo I results that were discussed in Section 3.5.1, where 10 μM concentration of **68** was also shown to affect the migration pattern of the plasmid. Compounds **69** and **70** were shown to be inactive at these concentrations, similar to what was observed in Figure 3.10.

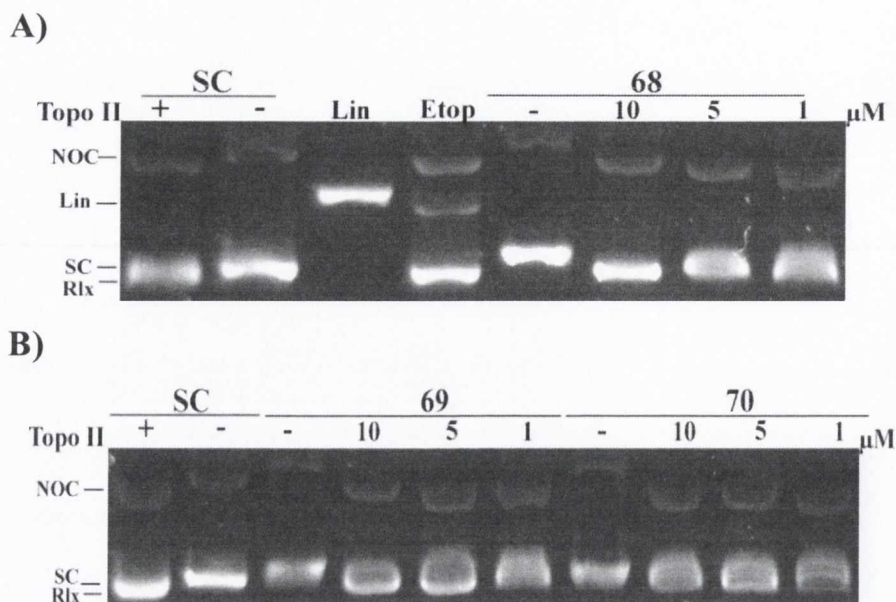


Figure 3.13 *Topo II* analysis of compounds **68-70** at 10, 5 and 1 μM concentrations in the presence of SYBr green. Compounds were incubated with a supercoiled plasmid (0.5 μg) and *Topo II* (5 units), at three different concentrations (10, 5 and 1 μM) as indicated above each lane. Lanes labeled - represent reactions done in the absence of *Topo II*. Lin indicates the position of the linear marker. Lane Etop represents the effects of a *Topo II* poison (Etoposide, 100 μM) and finally the SC, + and SC, - represents the reactions done in the presence and in absence of *Topo II*, respectively.

As for the *Topo I* analyses above, it was deemed necessary to investigate the effects of **68-70** at higher concentrations on the activity of *Topo II*. The assays were performed as described before, using 50, 25 and 12.5 μM concentration of **68-70** and each reaction was run with and without SYBr green in the gel. The results are shown in Figure 3.14 and Figure 3.15, respectively.

As shown in Figure 3.14, the morpholine derivative **70** showed little effect at these higher concentrations, with a minimal inhibition being observed at 50 μM . In addition, the mobility of the plasmid was unaffected, confirming the lack of interaction of this compound with DNA. The *N*-methyl piperazine derivative **69** effectively inhibited the *Topo II* enzyme when studied at a concentration of 25 μM , resulting in the appearance of untreated plasmid. Furthermore, the results indicated that the dimethylamine derivative **68** inhibited the *Topo II* enzyme at 12.5 μM , as the mobility of **68** has been extensively changed when compared to the supercoiled plasmid on its own. As previously stated for the *Topo I* analysis, the observed streaking of the bands is probably due to the strong DNA binding to **68**, possibly through electrostatic interactions. This streaking behaviour was reproducible as shown in Figure A2.6 in Appendix 2.

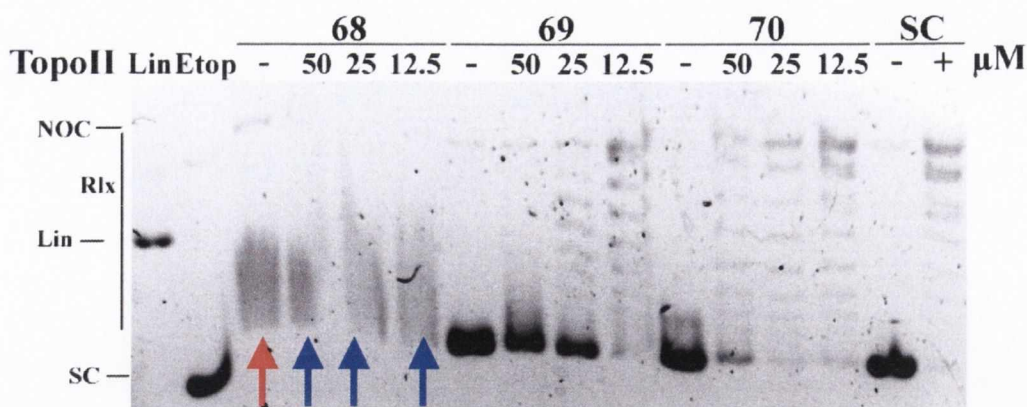


Figure 3.14: Topo II analysis of compounds 68-70 at 50, 25 and 12.5 μM concentrations in the absence of SYBr green. Compounds were incubated with a supercoiled plasmid (0.5 μg) and Topo II (5 units), at three different concentrations (12.5, 25 and 50 μM) as indicated above each lane. Lanes labeled - represent reactions done in the absence of Topo II. Lin indicates the position of the linear marker. Lane Etop represents the effects of a Topo II poison (Etoposide, 100 μM) and finally the SC, + and SC, - represents the reactions done in the presence and in absence of Topo II, respectively.

Although these gels were hard to interpret due to the streaking of the gels, the inhibition effects can be speculated when comparing the lane with **68** in the absence of Topo II (red arrow) to the lanes ran in the presence of **68** and Topo II (blue arrows). Moreover, the inhibition effect is more evident when examining the gel in presence of SYBr green in Figure 3.15.

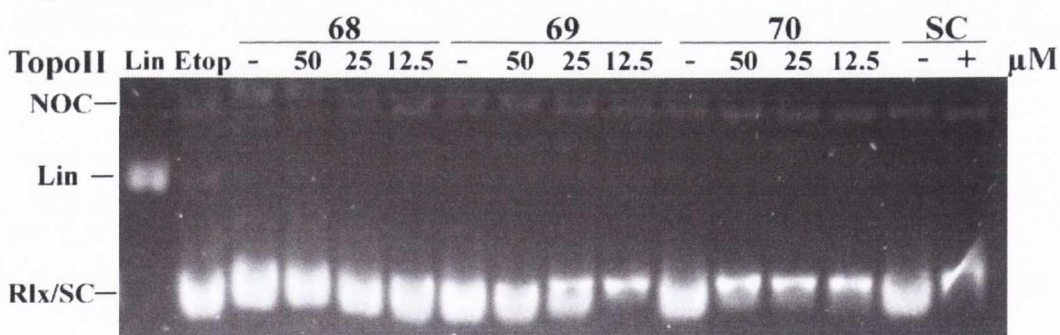


Figure 3.15 Topo II analysis of compounds 68-70 at 50, 25 and 12.5 μM concentrations in the presence of SYBr green. Compounds were incubated with a supercoiled plasmid (0.5 μg) and Topo II (5 units), at three different concentrations (12.5, 25 and 50 μM). Lanes labeled - represent reactions done in the absence of Topo II. Lin indicates the position of the linear marker. Lane Etop represents the effects of a Topo II poison (Etoposide, 100 μM) and finally the SC, + and SC, - represents the reactions done in the presence and in absence of Topo II, respectively.

In addition, as shown in Figure 3.15, an obvious similarity is observed between the lanes containing **68** and the lane with the unreactive plasmid, further indicating that **68** is

an effective inhibitor of DNA relaxation by Topo II. Figure 3.15 also confirms the partial inhibition showed at 25 μM concentration of **69** and the inactivity of **70**. Although **68-70** were shown to inhibit the catalytic activity of Topo II, they did not induce the formation of the linear or the nicked open circular plasmid products. These results indicated that these compounds interacted with the plasmid to exert their inhibition effects and not by directly inhibiting the enzyme as has been suggested previously for **7** and **8**.¹⁶⁶

3.5.3 Summary

The morpholine derivative **70** did not exhibit any inhibition effect on either of the topoisomerase enzymes. However, the *N*-methyl piperazine derivative **69** and the dimethylamine derivative **68** showed considerable activity against the topoisomerase enzymes. As discussed in *Section 3.1*, the acridine-phenanthroline based Tröger's base **63** was shown to fully inhibit the relaxation of DNA by Topo I at concentration higher than 10 μM . Similarly, the results described herein indicate that **68** and **69** completely inhibit the relaxation by Topo I at a concentration of 12.5 μM and 50 μM , respectively. Similar results were also obtained from the Topo II inhibition studies, which indicated that **68** and **69** were active at the same concentrations as for Topo I but **70** was inactive.

These results correlated well with the DNA binding studies discussed in the PhD thesis of Dr. Veale, where **68** exhibited the strongest binding affinity to DNA and **70** the weakest.⁶ This strong binding of **68** was confirmed by the Topo I and Topo II studies described in this section, where **68** affected the mobility of the supercoiled plasmid on an agarose gel at a considerably low concentration of 10 μM . Similar effects on the mobility of the plasmid has been shown by classical intercalators.¹⁷⁵ However, as discussed in the PhD thesis of Dr. Veale, compounds **68-70** are believed to bind DNA either through electrostatic interactions to the DNA backbone or by groove binding.⁶ The streaking effect observed by DNA after incubation with **68** indicated electrostatic binding to DNA, as already had been shown by **8** at higher concentrations.⁹⁴

3.6 Conclusion and Future Studies

The results from this chapter highlighted the significant cytotoxic potential of 1,8-naphthalimide containing Tröger's bases, such as **68-70**. These compounds exhibited rapid cellular uptake and improved cytotoxicity over their precursors **65-67** against the human cancer cell lines, HL-60 and K562. Furthermore, cellular localisation studies confirmed that **68-70** were absorbed by cells and furthermore, indicated that they were localised in the

nucleus after 24 hours. These results were especially important because as they showed that despite their positive charge, these compounds were able to reach their biological target *in vitro*, namely the genetic material.

The dimethylamine derivatives **65** and **68** were shown to be the most cytotoxic compounds against HL-60 cells, indicating the importance of the dimethylamine moiety in the side chain. Moreover, these results suggested that the pKa played a major role in the mechanism of cell death exerted by these compounds. Further investigations into the cell cycle showed that the cytotoxicity exerted by **65** and **68** resulted from a G₂/M arrest, as already has been shown by the 3-nitro-1,8-naphthalimide **8**. The apparent lack of apoptosis was confirmed by morphological examination and it was proposed that **68-70** induced a different mode of cell death, possibly autophagy as already reported for 1,8-naphthalimide derivatives, such as **73**. In addition, the amount of arrested cells after 48 hours treatment with **68** was shown to be less than was observed after 24 hours treatment. These results suggested that cells overcame the cell cycle arrest that was induced by **68** after 24 hours, implying that the Tröger's base unit might be responsible.

Compound **68** was shown to inhibit the activity of Topo I and II to the largest extent, while **70** was shown to be inactive against the topoisomerase enzymes. These results further confirmed the strong DNA interactions that had already been shown by Veale.⁶ Furthermore, the results suggested that **68** was electrostatically bound to DNA in a cell-free system. This correlated well with the cytotoxicity results, which indicated that pKa was an important factor for cytotoxicity and induction of apoptosis.

In conclusion, the binding behaviour of **8** was believed to involve intercalation of the 1,8-naphthalimide chromophore and the electrostatic binding of the protonated dimethylamine moiety in the side chain.⁹⁴ Therefore, the incorporation of the Tröger's base unit into these structures might possibly prevent these molecules from intercalating between DNA base pairs and consequently, the 1,8-naphthalimide containing Tröger's bases interact exclusively through electrostatic binding. This hypothesis could be used to explain the observed difference in the amount of G₂/M arrested cells, which was shown in the cell cycle studies described in *Section 3.4.1*, by the fact that intercalation induces more damage to the DNA than electrostatic interaction. Thus, arrested cells will initiate apoptosis upon treatment with 4-amino-1,8-naphthalimide **65** while cells that were arrested by the Tröger's base **68** initiate DNA repair and re-enter the cell cycle. Thus, future investigations will be directed at the detection of the DNA strand breaks in cultured cells and the activation of crucial members of the DNA repair mechanism. Furthermore, a time-

dependant investigation of the cell cycle and investigations into the different modes of cell death will be carried out.

The Gunnlaugsson research group has also utilised the 1,8-naphthalimide chromophore to develop novel Ru(II) probes and photoreagents for DNA. These potential photodynamic therapy agents have been shown to interact with DNA and to induce the formation of a nicked plasmid upon excitation. The principal behind photodynamic therapy and the biological evaluation of the of Ru(II) based 1,8-naphthalimides as photodynamic therapy agents will be described in *Chapter 4*.

4 Biological Evaluation of Ru(II)-1,8-Naphthalimide Conjugates as PDT agents

4.1 Introduction

As discussed in *Chapter 1*, conventional cancer therapies such as surgery, chemotherapy and radiation therapy have been proven clinically beneficial for patients. However, with improved technology, novel approaches are now being investigated to improve the efficacy of cancer treatment and to minimise side effects. One such approach that has received increasing attention in recent years is photodynamic therapy (PDT). PDT is a treatment that is based on two main components; a **photosensitising agent** and a **light source**, which are individually non-toxic, but when combined exert therapeutic effects against cancer cells. The treatment involves the administration of the photosensitising agent, which is generally absorbed by all the cells in the body. Some studies indicate that cationic photosensitisers accumulate to a greater extent in cancer cells than healthy cells, possibly because of the high affinity for cationic compounds exhibited by mitochondria in tumour cells.¹⁷⁷ A targeted light source whose wavelength matches the absorbance of the photosensitiser allows for localised activation of the agent, and thus specificity. The photophysics of the activation of the photosensitiser has been thoroughly investigated and is depicted in Figure 4.1.

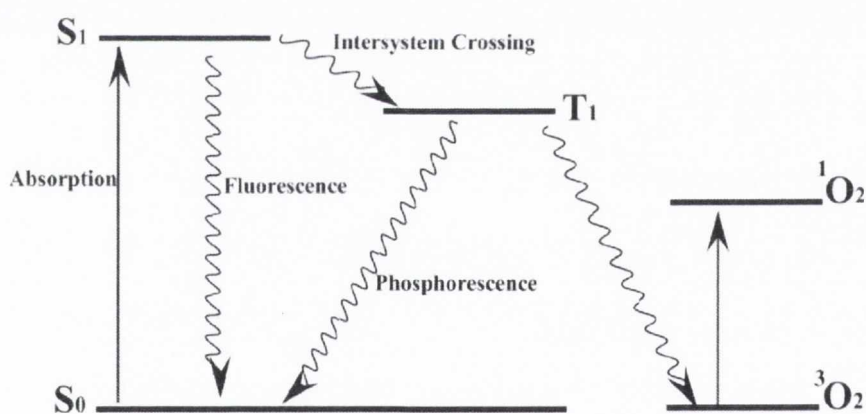


Figure 4.1 A qualitative energy level diagram explaining the activation of a PDT agent, leading to the formation of singlet oxygen.

Upon excitation, the photosensitiser absorbs energy from the light, resulting in population of the excited singlet state, which can decay directly back to the ground state emitting fluorescence. However, to exert therapeutic effects the singlet state must undergo an electron spin conversion to its triplet state. The triplet state may then undergo two different types of reaction as depicted in Figure 4.2.

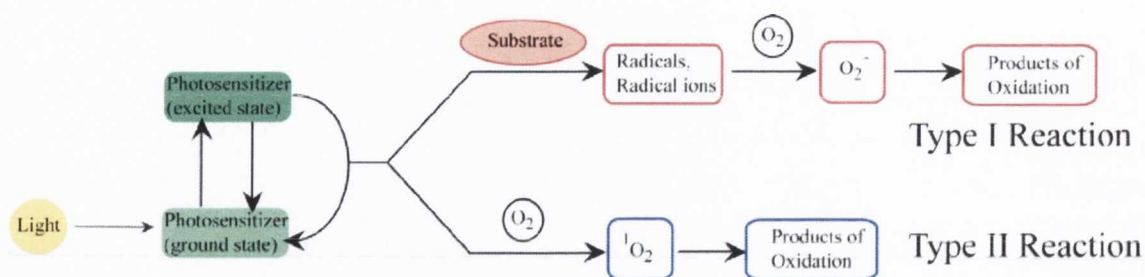


Figure 4.2 The Type I and Type II reactions induced by PDT.

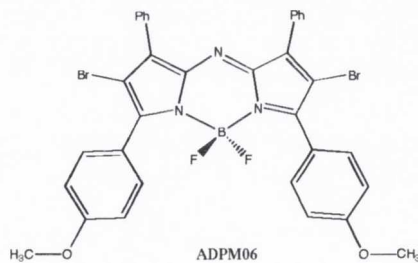
Firstly, the triplet state can react directly with a substrate, by proton or electron transfer, to form radicals or radicals ions, which ultimately react with oxygen to give oxygenated products (**Type I reaction**). Secondly, the excited triplet state can transfer its energy to ground state oxygen to form singlet oxygen, a highly reactive oxygen species (**Type II reaction**). In turn, this reactive oxygen form can react with many biological molecules such as lipids, proteins or nucleic acids, but this is limited to the closest vicinity because of its relatively short lifetime. Consequently, the localisation of the photosensitiser has been shown to be an important indicator of the mode of cell death induced by PDT.

There are a number of signaling pathways that can be induced upon excitation of a photosensitiser, which depends on their localisation. Most photosensitisers are shown to be lipophilic and for that reason they are mostly found in membrane bound organelles or in the cell membrane. A photosensitiser that is bound in the cell membrane is considered to induce a necrotic response upon photoactivation, as a consequence of the disruption of the cell membrane, which is followed by the corresponding lysis of the cell organelles. The full details of the mechanism of necrotic response to PDT has not been elucidated and numerous different signaling pathways have been suggested.^{178,179} Contrastingly, there is also some evidence that suggests that an apoptosis induction might occur from the irradiation of a membrane bound photosensitiser, resulting from the trimerisation of the death receptors, that were discussed in *Section 1.2.2* in *Chapter 1*. This leads to the activation of caspase-8, which in turn activates caspase-3, which is responsible for the activation of the final steps of the apoptotic process, resulting in fragmentation of the nuclear material.

Photosensitisers have also been shown to localise in the mitochondria, and upon excitation they initiate an apoptotic response by disrupting the mitochondrial membrane and causing the mitochondria to depolarise.¹⁸⁰ As discussed in *Section 1.2.2* in *Chapter 1*, the loss of the mitochondrial potential leads to the release of cytochrome c, which can form

a complex with Apaf-1 and pro-caspase 9, promoting the activation of caspase-9 and ultimately leading to activation of caspase-3.⁴⁷ Moreover, few photosensitisers have been shown to situate in the nuclear membrane, causing direct DNA damage, which is limited due to the very short life span of singlet oxygen.¹⁸⁰ For that reason, it is likely that the observed DNA damage by PDT is indirect or is limited to the part of the nuclear material that is situated very close to the nuclear membrane.¹⁸¹ Nonetheless, investigation into the direct DNA damage induced by PDT agents have been shown to include DNA strand breaks, DNA degradation and DNA-protein crosslinks.¹⁸¹ Furthermore, apoptosis has been shown to occur within 30 minutes following irradiation in a mouse lymphoma cell line, LY-R cell and it was concluded that DNA strand breaks were responsible for the apoptosis induction.¹⁸² Oleinick *et al.*¹⁸¹ showed that cells that possessed an active p53 gene induced higher levels of apoptosis than a p53-inactive cell line, which suggested that the cytotoxicity exerted by PDT varies between different cell types and particularly the p53 status of cells.

The first photosensitiser to be approved for clinical use was Photofrin®, which is a complex mixture of porphyrin monomers and oligomers, and has been used to treat various types of cancer, such as esophageal and cervical cancer.¹⁸³ Despite the proven clinical efficacy of Photofrin, it suffered from several drawbacks related to its photochemistry, including its low absorption at 630 nm, the wavelength that is usually used in the clinic. Consequently, higher light doses are required for tumor control, usually around 100-200 J/cm².¹⁸³ In addition, the therapeutic doses of Photofrin results in skin photosensitivity for 4-12 weeks.¹⁸³ The limitations of Photofrin treatment lead to the synthesis of many porphyrin and porphyrin-related compounds and some of them have entered clinical trials, such as the protoporphyrin IX.¹⁶⁹ However, the development of non-porphyrin based photosensitising agents has been considerably less extensive, despite the possibility of identifying compounds with improved efficacy, reduced side effects and easily modified structures. An example of novel non-porphyrin includes the BF₂-chelated tetaarylaxadiphyrromethanes such as **ADPM06** developed by O'Shea and coworkers.¹⁸⁴ With this in mind, the Gunnlaugsson research group has been investigating novel Ru(II)-1,8-naphthalimide conjugates as DNA probes and as DNA photocleaving agents. The synthesis and DNA binding investigations will be discussed in the next section.



4.1.1 The Design of Ru(II) 1,8-Naphthalimide Conjugates as PDT agents

As discussed in *Chapter 1*, synthetic molecules that could bind DNA in a sequence specific manner would be highly beneficial for the development of novel drugs that could regulate expression of specific proteins, or for different biological applications, such as regulators of expression¹¹⁵ or as DNA probes.¹⁸⁵ An example of a DNA binding system is the novel Ru(II)-1,8-naphthalimides conjugates **74-77** that were developed by Dr. Ryan, a former member of the Gunnlaugsson research group.¹³⁵ These compounds were developed as DNA probes and as can be seen in Figure 4.3. These systems consist of the 1,8-naphthalimide chromophore previously used in *Chapters 2* and *3*, respectively that was connected through an aromatic ring to a Ru(bpy)₃²⁺ core, through either a *para* or a *meta* arrangement, as shown for compound **74,76** and **75,77** respectively. Compounds **74-77** displayed significant emission enhancement upon binding to DNA and furthermore, these compounds were shown to bind DNA with high affinity by UV/Vis, fluorescent spectroscopy and CD spectroscopy, ethidium bromide displacement assays and T_m studies.¹³⁵ The wedged *meta* derivatives **76** and **77** were shown to bind to a higher degree to DNA than the linear *para* derivatives **74** and **75**, potentially due to greater complementarity in the shape of the complex to DNA. A summary from these investigations is shown in Table 4.1.

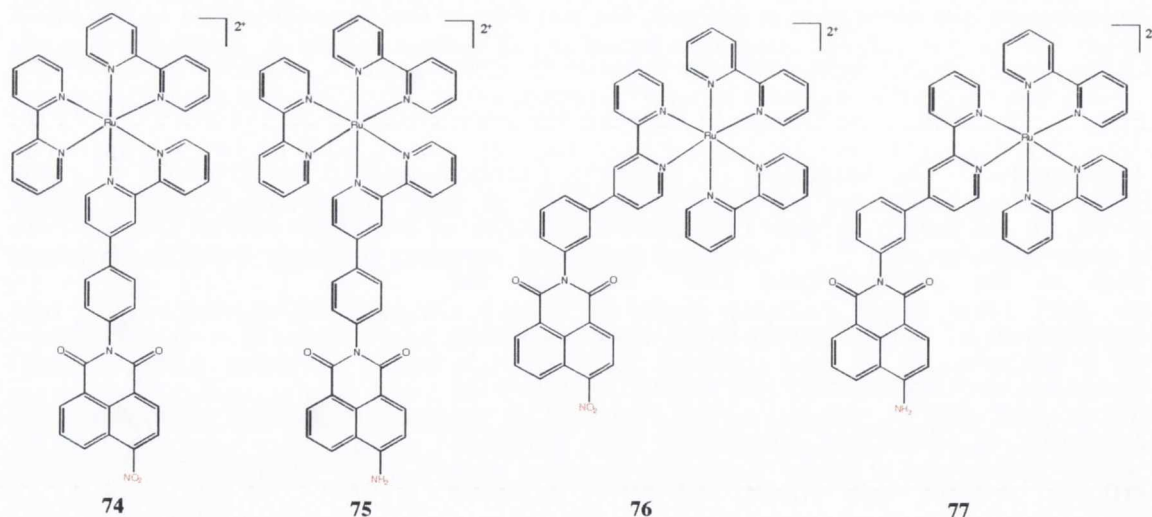


Figure 4.3 The Ru(II) based 1,8-naphthalimides **74-77** synthesised by Dr. Ryan.¹³⁵

Due to the excellent DNA binding ability of these systems and the fact that the different parts of these systems, the 1,8-naphthalimide chromophore and the Ru(bpy)₃²⁺ had individually been shown to cleave DNA upon photoactivation,^{141,186} Dr. Ryan decided to

investigate their ability to act as DNA photocleavers. The results from these investigations indicated that the substitution at the 1,8-naphthalimide moiety was important for the DNA photocleavage efficiency.¹³⁵ The nitro derivatives **74** and **76** exhibited similar cleavage abilities as Ru(bpy)₃²⁺ and only the *para* derivative **74** was shown to exert DNA damage in a Type II reaction manner, by forming singlet oxygen. The *meta* derivative **76** was believed to form another reactive oxygen species or directly oxidize the DNA bases. The amino derivatives **75** and **77** exhibited improved DNA photocleavage over the nitro derivatives, the mechanism of which was shown to involve the formation of singlet oxygen. Full details of this investigation can be found in the PhD Thesis of Dr. Ryan to which the reader is directed for more thorough explanation of the mechanism of photocleavage and photophysics of compounds **74-77**.¹³⁵

Table 4.1 Summary of DNA binding properties exhibited by 74-77.¹³⁵

	74	75	76	77
^(a) K_b (M⁻¹)	4.5 x 10 ⁶	3.0 x 10 ⁶	1.9 x 10 ⁷	1.1 x 10 ⁷
^(b) n	0.98	0.88	1.36	1.50
^(c) T_m (° C)	> 75	73	> 75	73
^(d) C₅₀ (M⁻¹)	5.2 x 10 ⁶	1.1 x 10 ⁷	2.6 x 10 ⁷	1.7 x 10 ⁷
^(e) % Form I	27	10	41	11

^(a) The binding constant as determined from absorbance data in 10 mM phosphate buffer, pH 7. ^(b) The number of nucleotides occluded by a bound ligand (*n*) as determined from absorbance data in 10 mM phosphate buffer, pH 7. ^(c) The *T_m* values from DNA thermal denaturation studies. ^(d) The binding constants derived from the ethidium bromide displacement assay. ^(e) The percentage of Form I pBR322 plasmid DNA upon 5 min. irradiation at > 400 nm as determined from photocleavage study.

4.1.2 Objectives of Current Studies

The work described in this chapter involves the biological testing of compounds **74-77** in K562 cells, to determine their potential as PDT agents. The CML cell line, K562 was chosen for its known resistance to drug treatment, which results from the expression of the chimeric Bcl-Abl protein and the absence of a functional p53 protein.¹⁸⁷ Several lines of evidence have shown that Bcr-Abl exerts its anti-apoptotic effects by blocking the mitochondrial release of cytochrome c and other pre-apoptotic inducers. Furthermore, as discussed in this section, the status of p53 has been shown to be an important factor for PDT agents, and this cell line has been used to determine the effect of ALA in preclinical models, a photosensitising agent that has now been approved for clinical use.¹⁶⁹ The first objective of this work was to determine if **74-77** were efficiently taken up by K562 cells

and to use the photophysical properties of these compounds to determine their localisation within cells. The results from these investigations will be discussed in Section 4.2. The second objective, which will be discussed in Section 4.3 was to investigate the cytotoxicity of these compounds in the dark and when irradiated with different doses of light. The third objective was to look into the mechanism of action exerted by **74-77** within these cells by using different methods, such as cell cycle analysis, the formation of reactive oxygen species (ROS) and the investigation of the mitochondrial membrane potential as discussed in Sections 4.4-4.6. However, the cell uptake investigation of **74-77** were the first step in determining if these compounds could cross the cell membrane and potentially reach their anticipated target, the nuclear material. The results from these investigations will be discussed in the next section.

4.2 Analysis of Cellular Uptake and Localisation of **74-77**

4.2.1 Cellular Uptake Studies Using Flow Cytometry

As discussed in Section 3.2 in Chapter 3, passive diffusion is the most common means of transportation of drugs into the cells and to be absorbed by such a transport mechanism, agents must be sufficiently lipophilic to cross the cell membrane.¹⁸ This is potentially the reason for relatively few reports of the activity of Ru(II) complexes against cultured cancer cells, despite their impressive photoreactivity to DNA in cell-free systems. Their charged characteristics are thought to affect their lipophilicity, which will limit their ability to cross the cell membrane. A study by Barton and Puckett¹⁸⁸ described the uptake of series of Ru(II) complexes into HeLa cells by flow cytometry. These Ru(II) complexes varied in charge, size and lipophilicity as shown in Figure 4.4. This study showed that complexes containing bigger and more hydrophobic ligands could enter cells, underlining the importance of lipophilicity and charge for efficient cellular uptake.

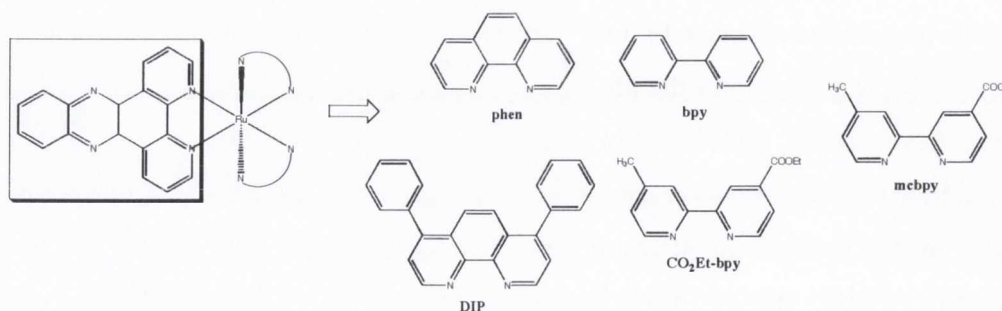


Figure 4.4 Ru(II) complexes that were studied by Barton and Puckett.¹⁸⁸

It was anticipated that the bifunctional nature of **74-77** comprising of both lipophilic 1,8-naphthalimide moiety and the hydrophilic Ru(bpy)₃²⁺ units would allow them to cross the cell membrane. Consequently, it was decided to study the uptake of these compounds by K562 cells using flow cytometry, in a similar manner as described in *Section 2.2* in *Chapter 2*. Briefly, K562 cells were incubated with vehicle (RPMI medium) or **74-77** at 1 μM concentration to minimise cytotoxicity and the loss of cells. At the time of analysis, cells were washed three times with cold PBS buffer, to remove particles of compounds and externally bound molecules. The fluorescence arising from these compounds was detected using the FL-3 channel in the flow cytometry system depicted in *Figure 2.6* in *Chapter 2*. Furthermore, the FCS vs. SSC dot plot was collected to exclude cellular debris from these results. The subsequent fluorescent intensities were plotted against time and the resulting plots are shown in *Figure 4.5*. Each experiment was conducted three times to show reproducibility and to minimise errors. The results from the repeated experiments can be found in *Figure A3.1* in *Appendix 3*.

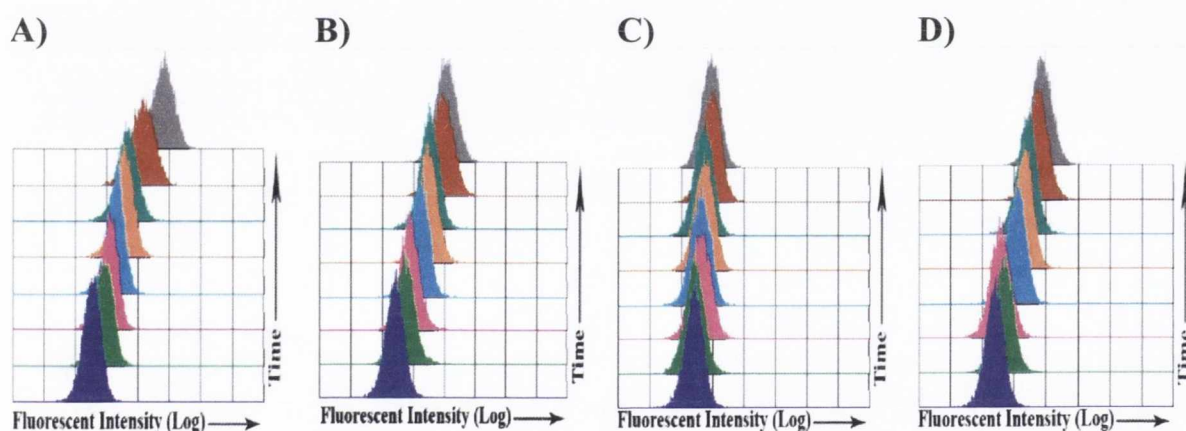


Figure 4.5 Plots of emitting fluorescence intensity from K562 cells. Cells were treated with **A)** **74** (1.0 μM), **B)** **75** (1.0 μM), **C)** **76** (1.0 μM) and **D)** **77** (1.0 μM) for 30 min. (■), 60 min. (■), 3 hours (■), 6 hours (■), 9 hours (■), 24 hours (■) and 48 hours (■). Untreated cells are shown as a solid purple peak. These plots are representative of three separate experiments.

As shown in *Figure 4.5*, these results indicated that **74-77** were absorbed by the K562 cells and their fluorescence increased steadily over time (30 minutes → 48 hours). The fluorescence was shown to increase after 30 minutes in all cases, except for the wedged 4-nitro derivative **76**. The plots in *Figure 4.5* also indicated that the wedged derivatives **76** and **77** had slower uptake at the early stages of the investigation (within one hour) and furthermore, cells treated with the linear derivatives **74** and **75** showed a gradual increase

of fluorescence that was time-dependant. This was indicative of importance of the structural difference between the linear and the wedged conformation for the uptake of these compounds.

As shown in Figure 4.6, the difference in emitted fluorescence becomes more evident when the maximum fluorescent intensity is plotted against time for 74-77. As depicted in Figure 4.6, the fluorescent intensity did not reach a plateau as was expected if the compounds would have fully accumulated in cells. These results indicated that these complexes crossed the cell membrane within 9 hours and were possibly located in the cytoplasm at that stage. Furthermore, the maximum fluorescence intensity was largely increased after 24 and 48 hours, which could be a consequence of a higher concentration within the cell or that these compounds are bound to a cellular target.

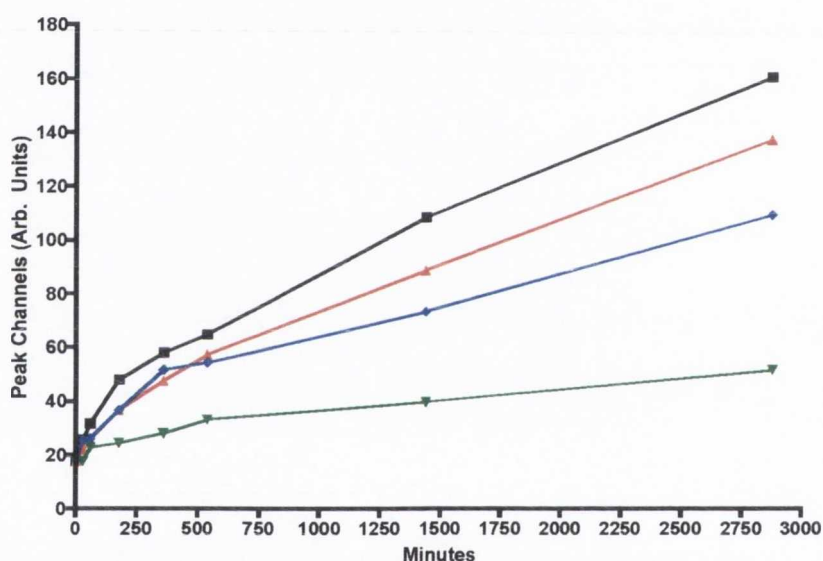


Figure 4.6 Cellular uptake of 74-77 by K562 cells. Cells were treated with 74 (1.0 μM , ■), 75 (1.0 μM , ▲), 76 (1.0 μM , ▼) and 77 (1.0 μM , ◆) for various times at 37 °C in the presence of 5% CO_2 . Each point at the graph represents a mean from three separate experiments.

In summary, these results demonstrated the rapid uptake of the Ru(II)-1,8-naphthalimide conjugates 74-77 by K562 cells, with the first signs of absorption being observed after 30 minutes. Furthermore, these results indicated that the linear conformation of 74 and 75 contributed to a more rapid uptake of these molecules. If these compounds were taken up by passive diffusion, then the difference between the linear and the wedged derivatives would be expected to arise from a difference in lipophilicity. However, to confirm if this is the case, further investigations into the lipophilicity of these compounds

needed to be carried out. In addition, other mechanism of absorption can not be excluded without further investigations. Investigation into the effects of the different substituents did not lead to any apparent conclusions. However, since these studies indicated that **74-77** were situated within K562 cells, it was decided to further confirm this observation by confocal microscopy. The results from these investigations are described in the following section.

4.2.2 Cellular Localisation studies of **74-77**

As discussed in Section 4.1, the localisation of a PDT agent is an important factor in estimating the extent of its cytotoxic activity and what signaling pathways it possibly might induce. For that reason, it was decided to investigate the localisation of **74-77** within the cell after 24 hours incubation. It was decided to use the adherent cervical cancer cell line, HeLa for this investigation, because they can be grown in a single layer on a chambered glass slide, and therefore would not need to be spun to the glass as for the K562 cells, which could potentially damage the cells. Furthermore, Dr. Ryan had previously shown that HeLa cells absorbed these compounds after 24 hours incubation in similar manner as was shown for K562 cells in Section 4.2.1.¹³⁵

The cells were incubated in a 6 well chambered glass slide for 24 hours before they were treated with **74-77** at 10 μ M concentration for a further 24 hours. Cells were counterstained with Hoechst 3342, the nuclear dye that was discussed in Section 2.2.2, before being fixed, and mounted with a cover slip. Both the nuclear stain, Hoechst 3342 and the corresponding Ru(II)-1,8-naphthalimide conjugates were excited with a diode laser at 405 nm wavelength. It had been shown that excitation of **74-77** at 450 nm in 10 mM phosphate buffer, resulted in a single emission band centered at 625 nm and more importantly, no emission was detected from the 1,8-naphthalimide moiety.¹³⁵ For that reason, the emission from Hoechst 3342 was detected by a 470-500 nm band pass filter, while the **74-77** were detected by a long pass filter at 650 nm. The resulting images from this investigation are shown in Figure 4.7, with the Hoechst 3342 nuclear dye shown in blue and the corresponding Ru(II)-1,8-naphthalimide conjugates shown in red.

These fluorescent images showed that **74-77** were situated at a similar site as the nuclear dye, Hoechst 3342 after 24 hours, indicating that these compounds did localise in the nucleus. These results correlated well with the uptake analysis in Section 4.2.1, where these compounds were found within cells after 24 hours.

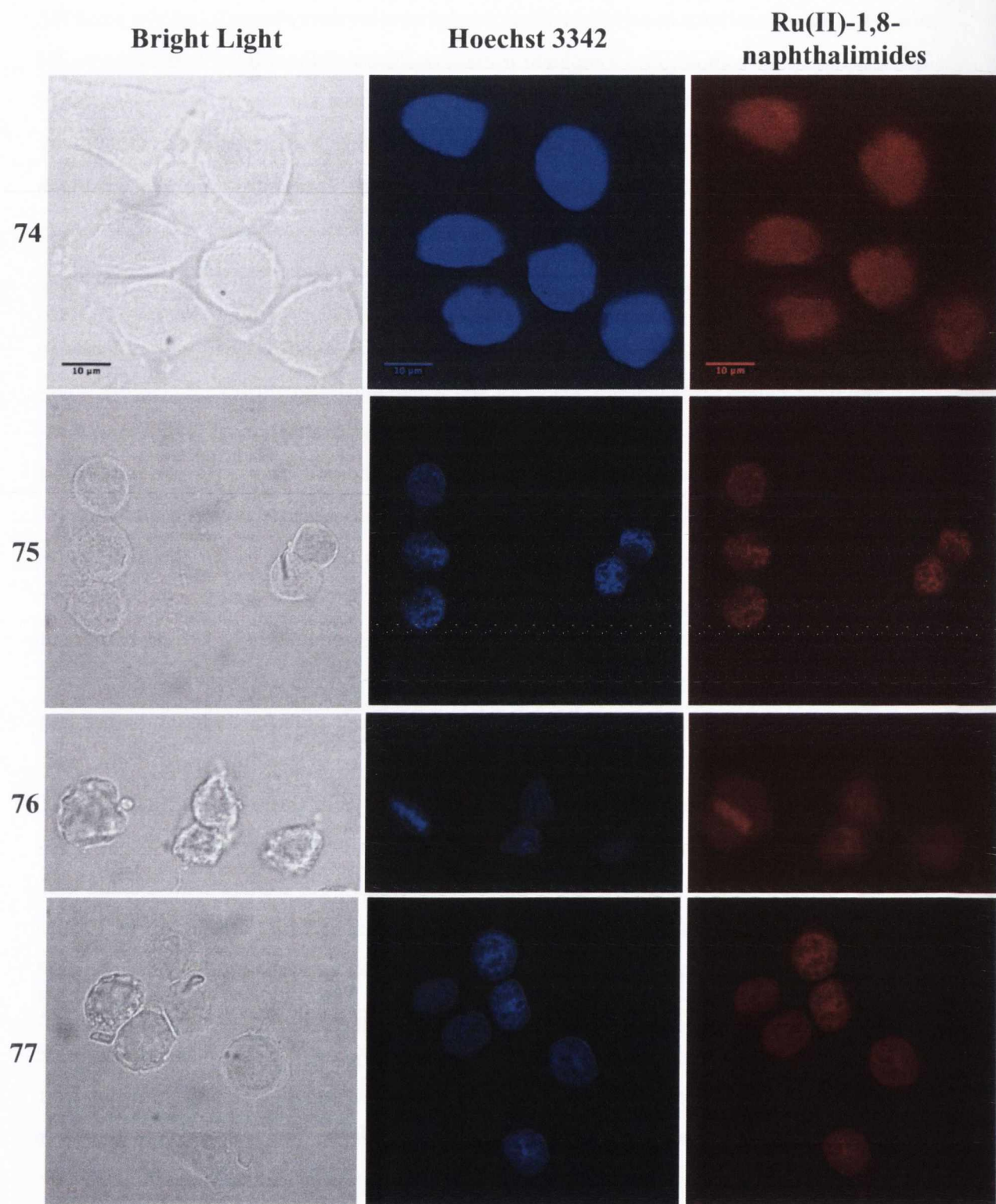


Figure 4.7 Bright light and confocal laser scanning microscopy images of HeLa cells treated with 74-77 and stained with Hoechst 3342. Cells were incubated with 74-77 at 10 μ M concentration for 24 hours before their nucleus was stained with Hoechst 3342 (0.5 μ M) for 15 minutes. The left panel shows the bright light images of the investigated cells. The middle panel shows the Hoechst 3342 nuclear stain (Ex. 405 nm / Em. 470-500 nm). The right panel shows compounds 74-77 (Ex. 405 nm / Em > 650 nm).

Furthermore, a considerable amount of fluorescence arising from the 4-nitro wedged derivative **76** was also detected in the cytoplasm after 24 hours, while the other derivatives were mainly shown to localise in the nucleus. These results were also in an agreement with the uptake analysis in Section 4.2.1, where **76** showed the slowest uptake as well as the lowest fluorescent intensity after 24 hours. Consequently, these results also suggest that the increase in fluorescence after 24 and 48 hours incubation as indicated from the uptake studies discussed in Section 4.2.1, might occur from the binding of **74-77** to DNA.

4.2.3 Summary

The results discussed in this section have shown that the Ru(II)-1,8-naphthalimide conjugates **74-77** were rapidly taken up by K562 cells and furthermore, that the linear configuration of these complexes might be responsible for the observed differences in uptake. Confocal microscopy analysis confirmed the presence of **74-77** within HeLa cells after 24 hours. Moreover, they indicated that these compounds localised mainly in the nucleus. This is, to the best of our knowledge, the first example of a Ru(II) polypyridyl complex in nucleus of a cell without electroporation, and thus represents a considerable milestone within this research field.

In summary, these results established that despite the known hydrophilicity of the Ru(bpy)₃²⁺ fragment, the combination with a more lipophilic 1,8-naphthalimide unit vastly improved their cellular uptake. In addition, these molecules were shown to bind their cellular target, DNA within cells, which was highly promising for the further development of these complexes as PDT agents. However, the next step in the biological investigation was to determine the effects **74-77** had on the growth of K562 cells, both without and with irradiation. The results from these studies are discussed in the next section.

4.3 Cytotoxicity and Phototoxicity of **74-77**

As discussed in *Section 1.4.1.1.1* in *Chapter 1*, the platinum complex cisplatin **4** has been widely used for the treatment of many cancers. However, because of its high toxicity and undesirable side effects, there has been a steadily growing interest in complexes with a different metal, such as ruthenium. Several cisplatin-like ruthenium containing complexes have been shown to exhibit good activity in screening studies, displaying activity similar to cisplatin. The ruthenium metal and ruthenium complexes have also been coupled with known photosensitisers such as porphyrin to improve their uptake,¹⁸⁹ in a similar manner as

was demonstrated for **74-77** in the last section, where these compounds were shown to be situated within K562 cells after 24 hours by flow cytometry and fluorescent microscopy analysis. These results, along with the observed phototoxicity results obtained by Dr. Ryan^{135,136} lead to further investigation into the effects that **74-77** have on the growth of cells in the presence and absence of light irradiation.

The cytotoxic and phototoxic investigations were carried out by using the MTT assay, as was described in detail in *Section 2.2* in *Chapter 2*. Briefly, K562 cells were incubated with either vehicle (RPMI medium) or various concentrations of **74-77** at 37 °C in the presence of 5% CO₂ for 24 hours, which had been shown by fluorescent microscopy to be sufficient length of time for these compounds to enter the cell nucleus. These cells were then irradiated at > 450 nm using a Xenon lamp at an irradiance of 6 MW/cm², which was measured by a photometer, to give light doses of 2, 4 and 8 J/cm², respectively. It has to be noted that stronger doses of light, up to 18 J/cm² doses have been used for PDT¹⁵⁹ however, these relatively low dosage were selected due to the low irradiance of the lamp, which increase the amount of time these cells were out of the ideal growth conditions at 37 °C in the presence of 5% CO₂. In addition, a 5% NaNO₂ filter was used to exclude light at wavelengths lower than 390 nm. A photograph of the experimental setup is shown in Figure 4.8.

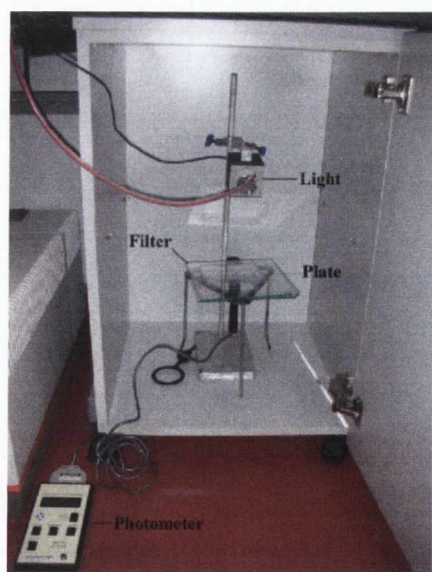


Figure 4.8 The irradiation system that was used for the investigation of the phototoxicity of **74-77**.

Cells were then incubated for a further 24 or 48 hours before being analysed using the MTT assay as described in *Section 2.2* in *Chapter 2.2*. The reason for the different “waiting” period was to give the cells time to recover from the effects of the irradiation, and therefore get a full indication of the strength of the PDT treatment with **74-77**. For determination of the cytotoxicity, the absorbance values from each of the treated wells were compared to the values of controls cells that were incubated without complexes. Phototoxicity was determined by comparing the values from irradiated cells that were treated with complexes and irradiated cells that were untreated.

All experiments were conducted in triplicate for each concentration and these experiments were repeated twice for more accurate results. The corresponding results for

the cytotoxicity and phototoxicity after 24 hours incubation post irradiation are shown in Figure 4.9 and the corresponding EC₅₀ values are summarised in Table 4.2. As before, the EC₅₀ value represents the concentration that is needed to exert 50% cytotoxicity when compared to the vehicle-treated control.

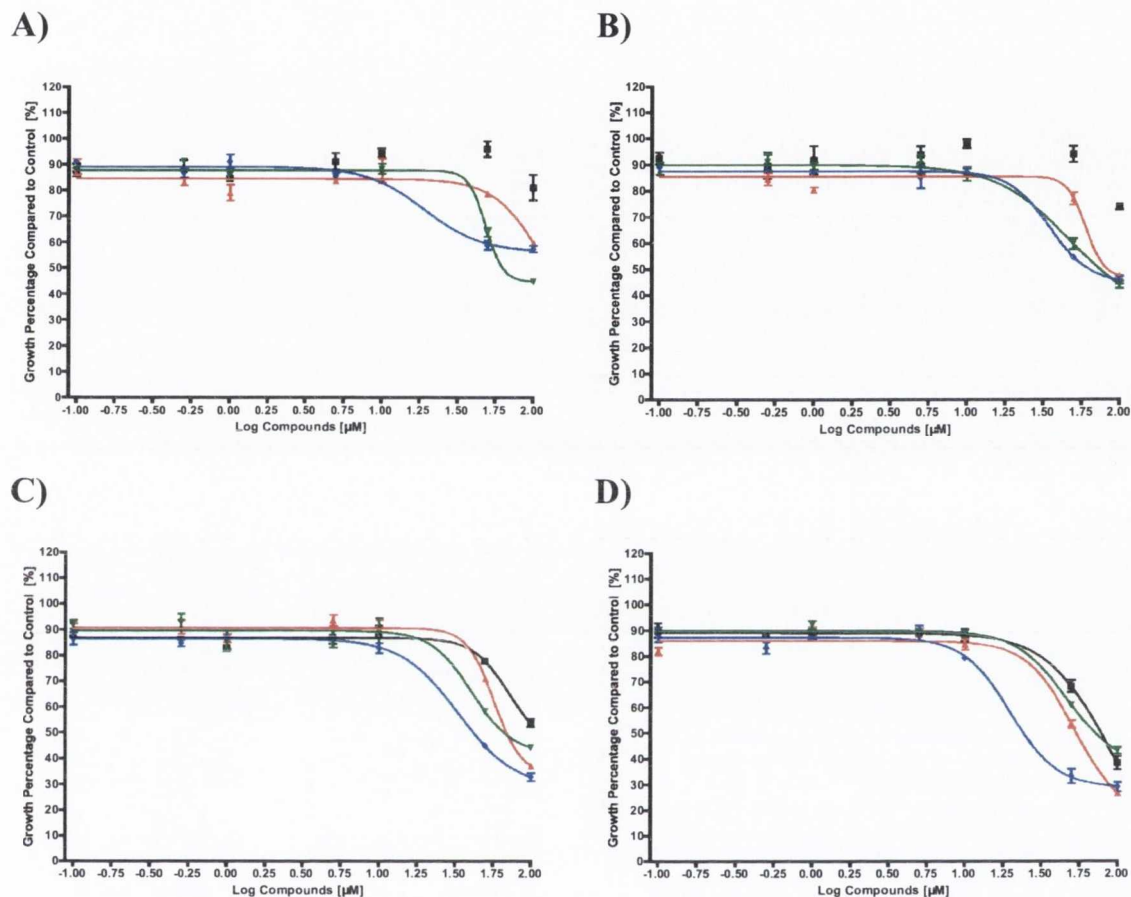


Figure 4.9 *In vitro* cyto- and phototoxicity of 74-77 against K562 cells after 24 hours incubation post irradiation. **A)** Dark controls, **B)** 2 J/cm², **C)** 4 J/cm² and **D)** 8 J/cm². Cells were treated with 74 (■), 75(▼), 76(▲) and 77(◆).

As shown in Figure 4.9 A and Table 4.2, the results from the cytotoxicity (without irradiation) showed that the wedged 4-nitro derivative **76** showed the highest cytotoxicity in the dark. These results correlated well with the DNA binding studies conducted by Dr. Ryan, where it was shown that **76** showed the most affinity for DNA in a cell-free system. This indicated that **76** was strongly bound to DNA and thus interfered with important cellular processes such as DNA duplication and protein expression. The other derivatives however, showed minimal toxicity without irradiation, exhibiting EC₅₀ values that were higher than 100 μM. These results were in contradiction to the uptake studies discussed in Section 4.2.1, where **76** was shown to have delayed uptake compared to the other

derivatives. These observations indicated that the differential exposure periods shown by these compounds were not responsible for the difference in cytotoxicity. Although this behaviour could not be explained, similar behaviour has been reported with different Ru(II) polypyridyl complexes, where the cytotoxicity did not exhibit any apparent correlation with the uptake.¹⁹⁰ As shown in Table 4.2, the highest phototoxicity was shown by the wedged 4-amino derivative **77** with an EC₅₀ value of 66.5 μ M indicating a 34% increase (>100 μ M \rightarrow 66.5 μ M) upon 2 J/cm² irradiation of these compounds. The linear 4-amino derivative showed the second highest cytotoxic increase upon irradiation with 2 J/cm², with more than 14% increase (> 100 μ M \rightarrow 86.5 μ M). However, no apparent changes were exhibited upon irradiation with the 4-nitro derivatives **74** and **76**. These results correlated well with the results from the DNA photocleavage obtained by Dr. Ryan, where the 4-amino derivatives **75** and **77** showed considerable photocleavage activity, while the 4-nitro derivatives **74** and **76** showed much less activity, as shown in Table 4.1.

Table 4.2 Summary of EC₅₀ values (μ M) for 74-77 after irradiation with different light doses after 24 hours post irradiation. Each value represents a mean calculated from a single experiment done in triplicate (\pm SEM)

	74	75	76	77
0 J/cm²	> 100	> 100	71.2 (\pm 6.9)	> 100
2 J/cm²	> 100	86.5 (\pm 8.3)	74.0 (\pm 7.5)	66.5 (\pm 9.2)
4 J/cm²	> 100	69.2 (\pm 3.3)	63.6 (\pm 9.5)	41.7 (\pm 2.3)
8 J/cm²	73.1 (\pm 4.4)	53.4 (\pm 4.0)	69.6 (\pm 8.4)	24.4 (\pm 3.0)

Similar results were obtained with 4 J/cm² light dose, where the phototoxicity was the highest for the 4-amino derivatives **75** and **77**, resulting in an increase of 31% and 58%, respectively over the 2 J/cm² treatment, while the 4-nitro derivatives showed minimal increase. As shown in Table 4.2, this trend was further maintained at 8 J/cm², where the 4-amino derivatives **75** and **77** were highly effective against the growth of K562 cells upon photoactivation, while the corresponding 4-nitro derivatives **74** and **76** showed considerably less phototoxicity at 8 J/cm² light dose. As discussed before, these analyses were in agreement with the data obtained by photocleavage assay conducted by Dr. Ryan, where the 4-amino derivatives were shown to be the most active photocleavers.

The mechanism of action of **74-77** was believed to involve induction of oxidative stress, resulting from the production of reactive oxygen species by these compounds. Therefore, to determine if cells could recover from the oxidative stress and carry on with

proliferation, phototoxicity studies were carried out 48 hours after irradiation. This investigation would also give information about the cyto- and phototoxicity over a longer time period. K562 cells were treated as before, with **74-77** at 10 μM concentration for 24 hours before irradiation with the different light doses. The results are shown in Figure 4.10 and summarised in Table 4.3.

As expected, the results showed that the cytotoxicity of **74-77** in dark after 72 hours incubation was higher than after 48 hours, especially for the wedged derivatives **76** and **77** that exhibited EC_{50} values of 57.6 μM and 50.6 μM , respectively. These results were in agreement with the DNA binding affinity studies conducted by Dr. Ryan, where these compound were shown to have the highest binding affinity, as detailed in Table 4.1.

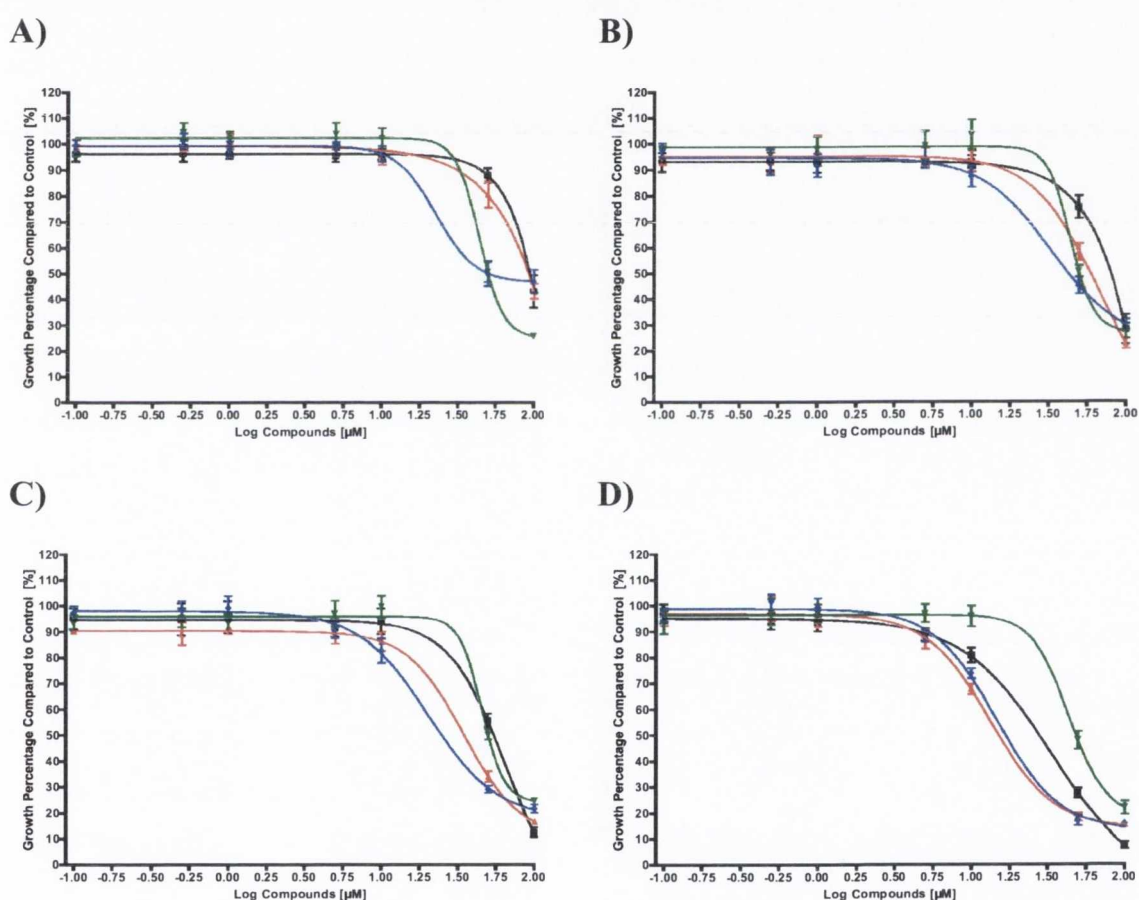


Figure 4.10 *In vitro* cyto- and phototoxicity of **74-77** against K562 cells after 48 hours incubation post irradiation. **A)** Dark controls, **B)** 2 J/cm^2 , **C)** 4 J/cm^2 and **D)** 8 J/cm^2 . Cells were treated with **74** (■), **75** (▼), **76** (▲) and **77** (◆).

As shown in Figure 4.10 **B**, incubation for 48 hours resulted in an increase in phototoxicity, upon irradiation with 2 J/cm^2 light dose. The 4-amino derivatives **75** and **77** were shown to induce the most phototoxicity at this light dose, resulting in a 33% and 26%

increase, respectively when compared to the 24 hours incubation period after irradiation. Similar observations were made at the 4 J/cm² and 8 J/cm² light doses, where all compounds except for **76** showed an increase in phototoxicity after 48 hours incubation period compared to the 24 hours waiting period.

Table 4.3 Summary of EC₅₀ values (μM) for 74-77 after irradiation with different light doses after 48 hours post irradiation. Each value represents a mean calculated from a three independent experiments done in triplicate (±SEM)

	74	75	76	77
0 J/cm²	70.61 (±1.473)	80.55 (±2.916)	57.63 (±3.885)	50.61 (±2.139)
2 J/cm²	74.28 (±7.375)	58.29 (±3.242)	59.57 (±4.632)	49.08 (±5.500)
4 J/cm²	53.24 (±2.522)	36.45 (±3.389)	56.96 (±2.421)	30.99 (±2.390)
8 J/cm²	29.78 (±1.631)	19.94 (±1.371)	53.59 (±3.416)	21.71 (± 1.113)

Additionally, the 4-amino derivatives **75** and **77** were found to be the most phototoxic of these compounds, showing EC₅₀ values of 20 μM and 22 μM, respectively after 8 J/cm² irradiation. The observed decrease in cell numbers between 24 and 48 hours waiting time indicated that upon photoactivation, compounds **74**, **76** and **77** induced a delayed cellular death. It has been reported that the release of cytochrome c is delayed upon PDT treatment¹⁹¹, resulting in a delay in apoptosis induction. Furthermore, the abnormal Bcr-Abl protein has been shown to exert its anti-apoptotic effect by blocking the activity of Bcl-2 pro-apoptotic proteins, which could further explain the delay in cellular death.¹⁷⁰ It is worth noting that the wedged 4-nitro derivative **76** showed considerable cytotoxicity in dark that did not change upon photoactivation, similar results as were obtained 24 hours post irradiation. The possible explanation for this behaviour by **76** might involve the structural effects this compound has on the mechanism of DNA damage, seeing that this compound is believed to act in a Type I reaction manner, by oxidising the DNA bases directly.¹³⁵

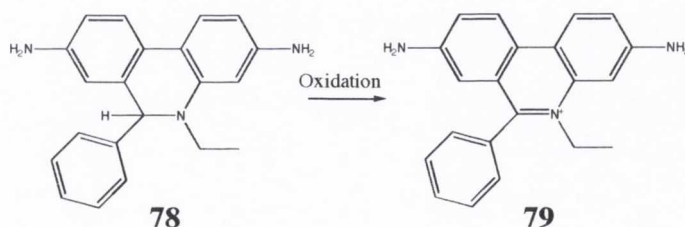
In summary, these results showed that **74-77** were cytotoxic to K562 cells after 72 hours incubation and more importantly compounds **74**, **76** and **77** were shown to be more cytotoxic upon photoactivation. Furthermore, these results correlated well with results from the DNA binding and photocleavage studies carried out by Dr. Ryan, where it was shown that the wedged derivatives had the highest affinity for DNA and that the 4-amino derivatives possessed the most phototoxicity. In the same study, it was shown that the

damage to DNA by **75** and **77** involved the formation of singlet oxygen and possibly other reactive oxygen species (ROS). It was therefore deemed necessary to investigate the formation of ROS within cells upon photodynamic treatment with **74-77**. The results from the subsequent study will be described in detail in the next section.

4.4 Formation of ROS in Cells after Treatment with 74-77

As discussed in Section 4.2, most photosensitising agents are shown to utilise the Type II reaction mechanism, by forming singlet oxygen, which reacts rapidly to the nearest environment, causing cellular damage. The 4-amino derivatives **75** and **77** displayed more efficient photocleavage efficiency of the DNA in D₂O solution than in H₂O solution, indicating that singlet oxygen was an important reactive species in the damage induced to DNA.^{135,136} Furthermore, as discussed in Section 4.3, **74-77** were shown to reduce the number of cells upon photoactivation. To investigate if the mechanism of photoactivity in cells would involve the formation of ROS, the flow cytometry system depicted in Figure 2.6 in Chapter 2 was used. These results could be used to correlate the activity within cells to the results from DNA photoactivity in a cell free system obtained by Dr. Ryan.

The studies were carried out by using dihydroethidium (DHEH) **78**, which has been used to detect the formation of ROS, such as singlet oxygen and superoxide.¹⁹² Compound **78** shows a blue fluorescence in the cytoplasm until oxidation, when it is turned into ethidium **79**, which emits red fluorescence upon intercalation into DNA.



To determine if compounds **74-77** induced the formation of ROS upon photoactivation, K562 cells were treated with either a vehicle (RMPI medium) or 10 μM concentrations of **74-77** for 24 hours before they were irradiated with 8 J/cm² light dose and incubated for further 48 hours after irradiation. Similar samples were prepared for dark controls, where cells were incubated with **74-77** at 10 μM concentration for 72 hours. Before the cells were analysed by flow cytometry, **78** was added to cells and incubated for 15 minutes. The fluorescence arising from **79** binding to DNA was detected using the FL-2

channel as was discussed in *Chapter 2* and the production of ROS was detected as an increase in fluorescence. Furthermore, the fluorescence arising from **74-77** at 10 μM concentration did not interfere with the fluorescence from **79**. The plots obtained from each compound and controls were put together and an example of results are shown in *Figure 4.11 A and B*, for dark controls and 8 J/cm^2 light dose, respectively. These assays were repeated twice for reproducibility and the summary from the repeated experiments can be found in *Figure A3.2* in *Appendix 3*. Furthermore, the mean of ROS production from these three experiments was determined and is shown in *Figure 4.12*, showing the standard error of mean.

As shown in *Figure 4.11 A* and *4.12* these compounds exhibited a small increase in ROS formation after 24 hours incubation in the absence of light irradiation. This can be visualised in *Figure 4.10*, where the left side of the black solid line indicates healthy cells with minimal formation of ROS. However, the right side of this line represents the population of cells that have increased fluorescence, which arises from the oxidation of **78** and the subsequent intercalation of **79** into DNA. Interestingly, compound **76** did not show any ROS formation in the absence of light irradiation despite being the most cytotoxic compound as was discussed in *Section 4.6*. These results indicated that this compound might exert its biological activity through a different mechanism than the other Ru(II)-1,8-naphthalimide derivatives.

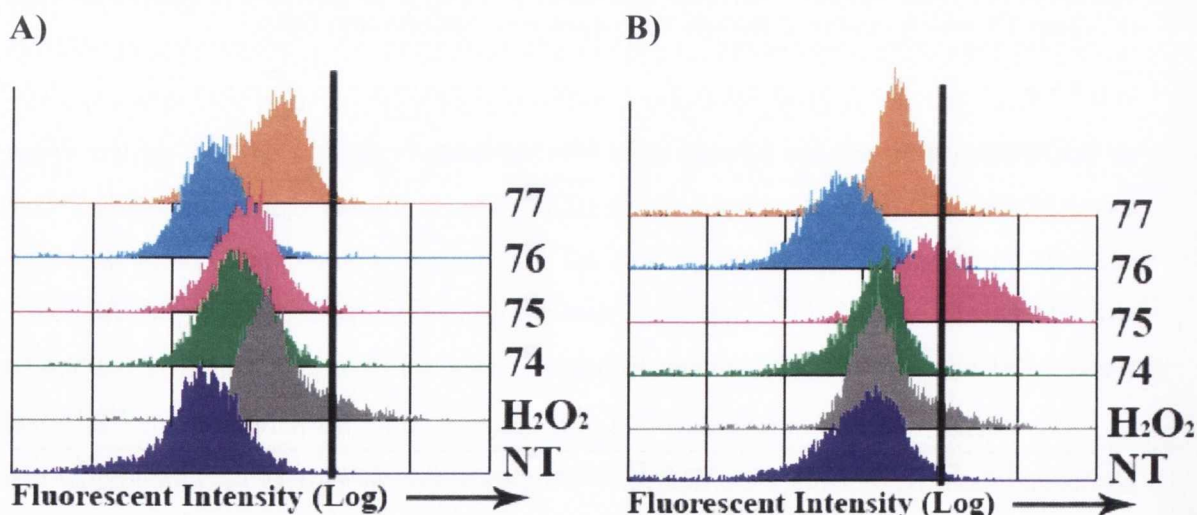


Figure 4.11 Formation of ROS in K562 cells treated with **74-77** **A)** in the dark and **B)** irradiation with 8 J/cm^2 light dose. Cells were either left untreated (\blacksquare), treated with **74** (10 μM , \blacksquare), **75** (10 μM , \blacksquare), **76** (10 μM , \blacksquare) and **77** (10 μM , \blacksquare) for 24 hours before irradiation. Cells were analyzed 48 hours after irradiation. Cells were also treated with H_2O_2 (2 mM, \blacksquare) for 5 minutes as a positive control. The solid line is for guideline purposes only, the right side indicating the increase in ROS production.

As shown in Figure 4.11 **B** and Figure 4.12, there was a minimal increase in ROS formation upon 8 J/cm² irradiation light dose in untreated cells. The linear 4-amino derivative **76** showed the highest increase of the Ru(II)-1,8-naphthalimide conjugates, while the corresponding wedged derivative **77** showed the second highest formation. These results were in correlation with the phototoxicity analyses that were discussed in Section 4.6, where the 4-amino derivatives showed the highest increase in cell reduction upon photoactivation, suggesting that the mechanism of phototoxicity exerted by these compounds involved the production of ROS. Although it was not possible to determine if the observed production of ROS was arising from the photoactivation of these compounds or from the induction of apoptosis, the latter seemed likely, especially due to the short lifetime of these reactive oxygenated species. The 4-nitro derivatives showed similar trends as was obtained from the phototoxicity studies, where the linear derivative **74** showed minimum increase in cytotoxicity upon irradiation and the wedged 4-nitro derivative **76** showed small or no changes after irradiation.

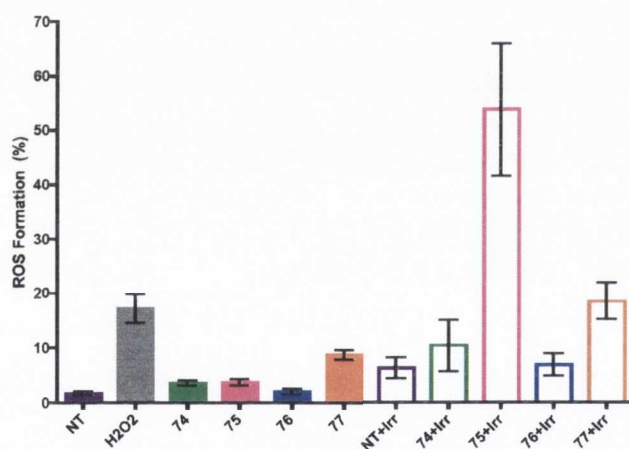


Figure 4.12 Summary of ROS production in K562 cells after treatment with 74-77. Cells were treated with **74** (10 μ M, \blacksquare), **75** (10 μ M, \blacksquare), **76** (10 μ M, \blacksquare) and **77** (10 μ M, \blacksquare) for 24 hours before they were irradiated (open bars) or left in the dark (solid bars). Vehicle-treated cells are indicated with purple (\blacksquare) and cells treated with 2 mM H₂O₂ are represented by a grey solid bar.

In summary, the 4-amino derivatives **75** and **77** showed the highest induction of ROS formation, as was shown for the phototoxicity studies, confirming the importance of the 4-amino substituents on the 1,8-naphthalimide chromophore. Compound **76** showed limited induction of ROS, indicating that this compound might work by a different mechanism or that this compound might be unable to form ROS, suggesting that the cytotoxicity of this

compound stemmed only from its efficient DNA binding, rather than the photoinduced DNA cleavage. However, these results also indicated that **74**, **75** and **77** induced ROS formation, possibly by promoting apoptosis. Further studies were needed to determine if **74-77** produce ROS species that is responsible for the observed cellular death. To examine the effects that these compounds had on the DNA, cellular growth and initiation of apoptosis, the cell cycle of cells treated with **74-77** were analysed by flow cytometry. The results from the corresponding investigations are discussed in next section.

4.5 The Effects on the Cell Cycle after Treatment with 74-77

As discussed in *Section 1.2.1* in *Chapter 1*, growth of cells is tightly regulated by the cell cycle, which ensures that each phase is carried out in the correct order and that cells with damaged DNA will not be allowed to proliferate unchecked. As discussed in the aforementioned sections in this chapter, compounds **74-77** were shown to reduce cell numbers in culture and furthermore, were believed to induce ROS production, possibly through the induction of apoptosis. Therefore, it was decided to investigate the effects of these compounds on the cell cycle and as discussed in *Section 2.5* in *Chapter 2*, the potential of these compounds to induce apoptosis.

The cell cycle analysis was carried out by using flow cytometry, as discussed in *Section 2.5* in *Chapter 2*. Briefly, K562 cells were treated either with vehicle (RPMI medium) or with **74-77** at 10 μM concentration for 24 hours before they were irradiated with 4 J/cm^2 or 8 J/cm^2 light doses by using the irradiation system depicted in Figure 4.7. The irradiated cells were incubated for 48 hours before they were subjected to propidium iodide staining and subsequent flow cytometry analysis, as was discussed in *Section 2.5* in *Chapter 2*. Investigations were conducted in triplicate for reproducibility and an example of results for 4 J/cm^2 and 8 J/cm^2 light doses are shown in Figure 4.13 **A** and **B**, respectively. The repeats from the two other experiments can be found in *Figure A3.3* in *Appendix 3*. Furthermore, the percentage of cells situated in each phase of the cell cycle is summarised in Table 4.4 and Table 4.5 for 4 J/cm^2 and 8 J/cm^2 , respectively.

As shown in Figure 4.13 **A** and Table 4.4, irradiation with 4 J/cm^2 light doses lead to a minimal increase in cells that are situated in G_2/M phase of the cell cycle, indicating that irradiation at 450 nm wavelength promoted DNA damage, resulting in the G_2/M block and activation of the DNA repair mechanism. Similar observations have been shown following treatment with ionising radiation.¹⁹³ Furthermore, this light dose was shown to induce apoptosis to a small population of cells that were incubated in the absence of **74-77**.

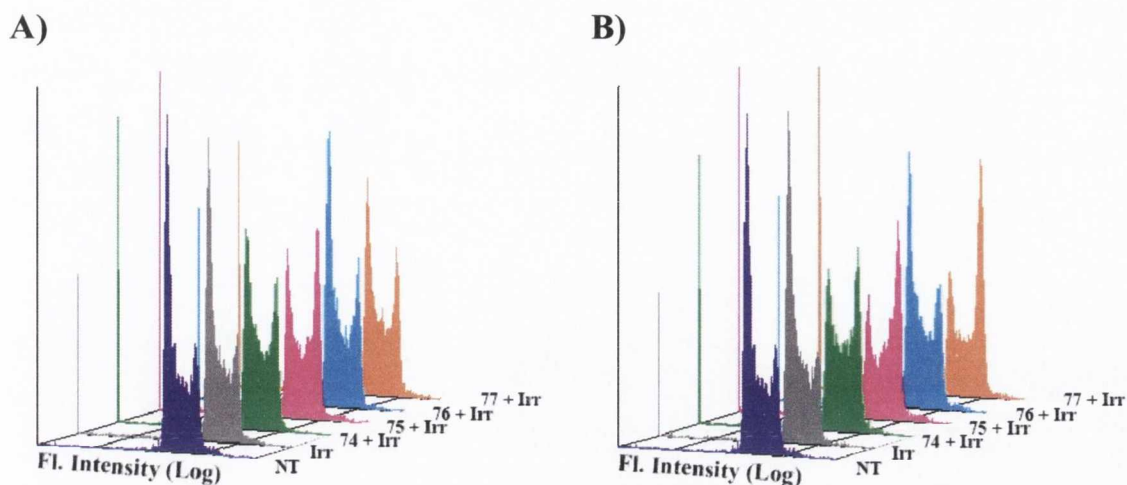


Figure 4.13 Cell cycle analysis of K562 cells irradiated with **A) 4 J/cm²** and **B) 8 J/cm²**. Cells were either left untreated (■) or treated with **74** (10 µM, ■), **75** (10 µM, ■), **76** (10 µM, ■) and **77** (10 µM, ■), respectively for 24 hours before irradiation. Cells were analysed 48 hours after irradiation. Untreated, irradiated cells are indicated with a solid gray plot (■).

However, in the presence of **74-77** at 10 µM concentration, cells were arrested in the G₂/M phase to a larger extent than the untreated cells upon irradiation with 4 J/cm² light dose. Furthermore, as shown in Figure 4.13 **B** and Table 4.4, the linear 4-amino derivative **75** induced the highest amount of G₂/M blocked cells, in correlation with what had been shown when investigating the formation of ROS, as discussed in Section 4.4. The treatment with **74-77** also showed a considerable induction of apoptosis, especially by the wedged 4-amino derivative **77**, which showed 10% apoptosis. These results were in agreement with the cytotoxicity results discussed in Section 4.3, where **77** was shown to be the most phototoxic at this light dose. In addition, a similar overall trend was obtained as for the phototoxicity investigation, where the 4-amino derivatives **75** and **77** were shown to be more phototoxic than the 4-nitro derivatives **74** and **76**.

Table 4.4 Cell cycle analysis of K562 cells untreated or treated with **74-77** and irradiated with 4 J/cm². Values indicated in the text are shown in red.

	NT	NT+Irr	74	75	76	77
Sub-G₁	5.01 (±0.3)	5.71 (±0.4)	8.63 (±0.4)	8.64 (±0.3)	5.74 (±0.1)	10.1 (±0.1)
G₁	52.3 (±0.6)	48.9 (±0.6)	40.6 (±0.4)	32.1 (±0.4)	46.1 (±1.0)	40.7 (±0.4)
S	24.7 (±0.3)	26.6 (±0.5)	29.9 (±0.1)	26.0 (±0.4)	27.1 (±0.6)	25.0 (±0.8)
G₂/M	15.6 (±0.5)	17.1 (±0.4)	21.2 (±0.1)	32.0 (±0.1)	20.9 (±0.6)	22.4 (±0.3)

These results indicated that the mechanism of cell reduction by **74-77** was possibly apoptosis, which was induced by arresting cells in the G₂/M phase of the cell cycle. Furthermore, as discussed in Section 1.2.1 in Chapter 1, the G₂/M checkpoint has been shown to be activated upon DNA damage and in light of these results, it is possible that these compounds might photocleave DNA within cells.

As shown in Figure 4.13 **B** and Table 4.5, the effects were more pronounced with a 8 J/cm² light dose, indicating that the treatments with **74-77** were irradiation-dependant. Although a similar trend was obtained as for the 4 J/cm² treatment where the 4-amino derivatives were shown to induce the highest extent of G₂/M arrest, the wedged 4-amino derivative **77**, not the linear 4-amino derivative **75**, induced the highest percentage of G₂/M arrested cells at 8 J/cm² or about 38%. This could be explained by analysing the observed induction of apoptosis, where the linear 4-amino derivative **75** promoted the highest percentage of apoptosis at 16%. These results could further be indicative of the more severe DNA damage induced by **75** than with compound **77**, leading to an earlier arrest in G₂/M and more rapid induction of apoptosis. The wedged 4-nitro derivative **76** did not show any significant difference between light doses (21% vs. 22%), which correlated well with the phototoxicity results and the investigations into the formation of ROS, as discussed in Section 4.3 and Section 4.4 respectively, where this compounds did not show improved activity upon irradiation.

Table 4.5 Cell cycle analysis of K562 cells untreated or treated with 74-77 and irradiated with 8 J/cm². Values indicated in the text are shown in red.

	NT	NT+Irr	74	75	76	77
Sub-G₁	5.01 (±0.3)	5.75 (±0.1)	9.03 (±0.1)	16.3 (±0.1)	6.97 (±0.1)	12.7 (±0.2)
G₁	52.3 (±0.6)	50.8 (±0.1)	32.3 (±0.2)	22.8 (±0.3)	42.7 (±0.4)	25.7 (±0.3)
S	24.7 (±0.3)	27.8 (±0.3)	30.2 (±0.6)	27.6 (±0.1)	27.5 (±0.6)	21.3 (±0.1)
G₂/M	15.6 (±0.5)	15.1 (±0.3)	26.9 (±0.3)	29.9 (±0.5)	21.8 (±0.2)	38.2 (±0.8)

In summary, the cell cycle analyses revealed significant changes between untreated cells and cells that were treated with **74-77**. Upon light irradiation, cells treated with **74-77** were shown to be arrested in the G₂/M phase of the cell cycle, which resulted in apoptosis. These results also confirmed the conclusions from both cytotoxicity studies and investigation of ROS formation discussed in Section 4.3 and Section 4.4, respectively where the 4-amino derivatives were shown to be superior to the 4-nitro derivatives. These

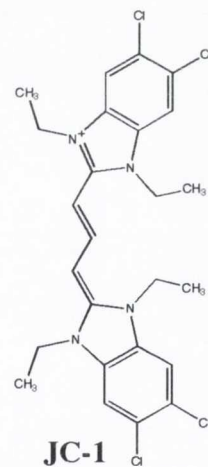
results indicated that the mechanism of phototoxicity by **74-77** was initiated by DNA photocleavage, resulting in DNA strand breaks and an arrest in G₂/M. However, further investigation is needed to confirm if this is in fact the case. After establishing that these compounds affected the cell cycle and induced apoptosis, it was decided to investigate the effects these compounds had on the mitochondrial membrane. The results from the resulting studies are discussed in the next section.

4.6 Changes in the Mitochondrial Membrane Potential Induced by 74-77

As discussed in *Section 1.2.2* in *Chapter 1*, the mitochondria plays a major role in the induction of apoptosis. Upon apoptotic stimuli, pro-apoptotic members of the Bcl-2 family relocate to the mitochondria, where they induce mitochondrial outer membrane permeabilisation, releasing pro-apoptotic protein and cofactors that lead to the activation of caspases.²³ Furthermore, various photosensitising agents have been shown to strongly influence the mitochondrial membrane potential, by forming ROS that in turn attacks the mitochondrial associated proteins and disrupt their normal function.

Compounds **74-77** were shown to localise in the nucleus after 24 hours and they induced a G₂/M block as was discussed in *Section 4.2.2* and *4.5*, respectively. These aforementioned results indicated that these compounds photocleaved DNA within cells, possibly activating DNA damage checkpoint proteins and ultimately resulting in apoptosis *via* the mitochondrial mediated pathway, which was discussed in *Section 1.2.2* in *Chapter 1*. Furthermore, it is expected that a small fraction of compounds **74-77** might be located in the cytoplasm upon irradiation, which would possibly influence the mitochondrial membrane potential, leading to apoptosis. For that reason, the effects of these compounds on the mitochondrial membrane potential were investigated by using the flow cytometry system shown in *Section 2.2* in *Chapter 2*.

For the investigation into the effects **74-77** had on the mitochondrial membrane potential, a cationic dye JC-1 was used. This dye localises in the mitochondria, possibly because of its positive charge and when the dye reaches critical concentrations within the small mitochondrial intermembrane space, it forms fluorescent orange aggregates. However, upon the loss of mitochondrial membrane potential, these aggregates are released into the cytoplasm where they form green fluorescent monomers that are easily differentiated from the orange fluorescence arising from healthy cells with intact



mitochondria. The fluorescence difference is detected by channels FL-1 and FL-2 on the flow cytometry system shown in *Figure 2.6*.

Studies were carried out on K562 cells that were either treated with vehicle (RPMI medium) or with **74-77** at 10 μM concentrations for 24 hours before cells were irradiated with 8 J/cm^2 light doses and incubated for a further 48 hours. Simultaneously, cells were kept in the dark for 72 hours. The detected fluorescence from the FL-1 and FL-2 detectors were plotted for each sample and an example of corresponding plots are shown in *Figure 4.14* and *Figure 4.15* for the dark and the irradiated treatments, respectively. These investigations were repeated and the resulting plots can be found in *Figures A3.5* and *A3.6* in *Appendix 3*. Furthermore, the summary of these results can be found in *Figure 4.16*.

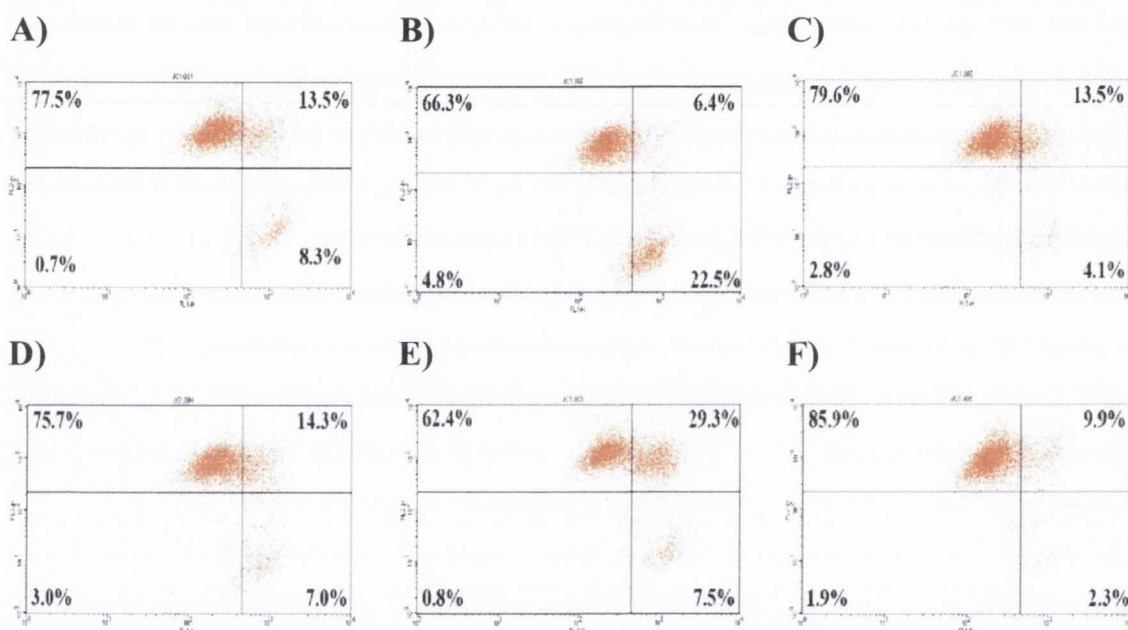


Figure 4.14 Flow cytometry plots of K562 cells treated with **74-77** in the dark. Cells were incubated with **A)** vehicle (RPMI medium), **B)** Etoposide (100 μM), **C)** **74** (10 μM), **D)** **75** (10 μM), **E)** **76** (10 μM) and **F)** **77** (10 μM) for 72 hours at 37 $^{\circ}\text{C}$ in the presence of 5% CO_2 before they were analysed by flow cytometry as described in the text.

The results for the dark controls in *Figure 4.14* indicated that three different populations of cells were observed on these plots. First, the upper left grid represented cells that exhibited both green and red fluorescence, indicating that presence of JC-1 in both the cytoplasm and the mitochondria. These were counted as a healthy cell population. Secondly, the cell population that had increased green fluorescence, shown in the upper right grid in the plots in *Figure 4.13*. Similar behaviour has been seen with staurosporine treated HL-60 cells upon apoptosis induction.¹⁹⁴ It was concluded in the same study, that

cells could contain both depolarised mitochondria and healthy mitochondria. For that reason, the upper right grid represented cells that have depolarised mitochondria. Finally, the lower grids corresponded to cells that lost the orange fluorescence, indicating that most of the mitochondria had depolarised, resulting in the release of the orange fluorescent aggregates into the cytoplasm, forming green fluorescent monomers of JC-1. As shown in Figure 4.14 A, the untreated control contained a small fraction of cells that had depolarised mitochondria. This was expected due to the fact that these samples had been allowed to grow at 37 °C in the presence of 5% CO₂ for 72 hours and might have been overgrown at that stage. The positive control, etoposide **58** displayed an induction of cells exhibiting a complete loss of mitochondrial membrane potential or nearly 30% as can be seen in Figure 4.14 B. The cells that were treated with **74-77** at 10 μM concentration, shown in Figures 4.14 C-F indicated that these compounds did not induce any major changes to mitochondrial potential, although treatment with compound **76** showed an increase in the number of cells with partially depolarised mitochondria compared to the untreated control. These results were in correlation with the cytotoxicity studies discussed in Section 4.3, where it was shown that **76** was the most cytotoxic compound in the absence of light. Other compounds except for **76** showed a similar percentage of cells with healthy mitochondria as the dark control. However, as shown in Figure 4.15 B, the mitochondrial membrane potential was affected upon irradiation with 8 J/cm² light dose.

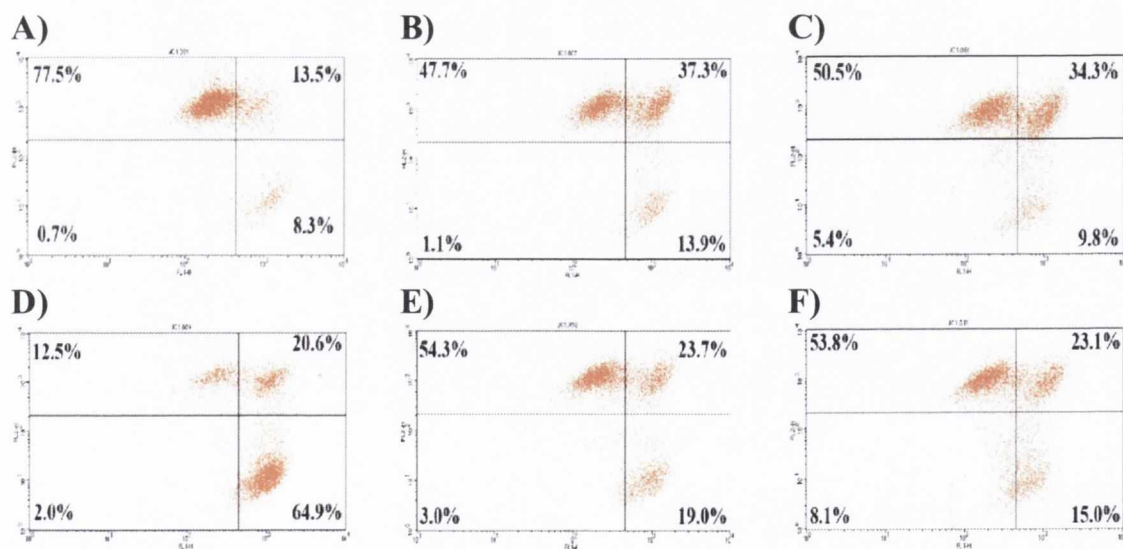


Figure 4.15 Flow cytometry plots of K562 cells treated with **74-77** and irradiated with 8 J/cm². Cells were incubated with A) vehicle (RPMI medium) in the dark, B) Etoposide (100 μM), C) **74** (10 μM), D) **75** (10 μM), E) **76** (10 μM) and F) **77** (10 μM) for 72 hours at 37 °C in the presence of 5% CO₂ before they were irradiated with 8 J/cm² light dose. The cells were then incubated for 48 hours before being analysed by using flow cytometry as described in the text.

This was expected, since it had been shown that irradiation caused DNA damage, which resulted in the loss of mitochondrial membrane potential and the subsequent induction of apoptosis. Irradiation in the presence of **74-77** at 10 μM concentration greatly affected the mitochondrial membrane potential as shown in Figure 4.15 C-F. The linear 4-amino derivative **75** showed the highest percentage of cells with a complete loss of mitochondrial membrane potential, as represented by the lower grids in Figure 4.15 D. These results are in agreement with the cytotoxicity and the ROS production studies discussed in Section 4.2 and 4.3, respectively, where this compound was shown to be the most cytotoxic and induce the highest percentage of ROS. Furthermore, these results also indicated the rapid apoptosis induction by these compounds compared to the other Ru(II)-1,8-naphthalimide derivatives, similar to what was observed when analysing the cell cycle studies. As shown in Figure 4.16, treatment with **74** upon irradiation resulted in an increase in cells with partially depolarised mitochondria, which might indicate that longer incubation time might be needed after irradiation to allow the cells to carry out apoptosis by this compound. However, the wedged derivatives **76** and **77** showed similar results as the irradiated control.

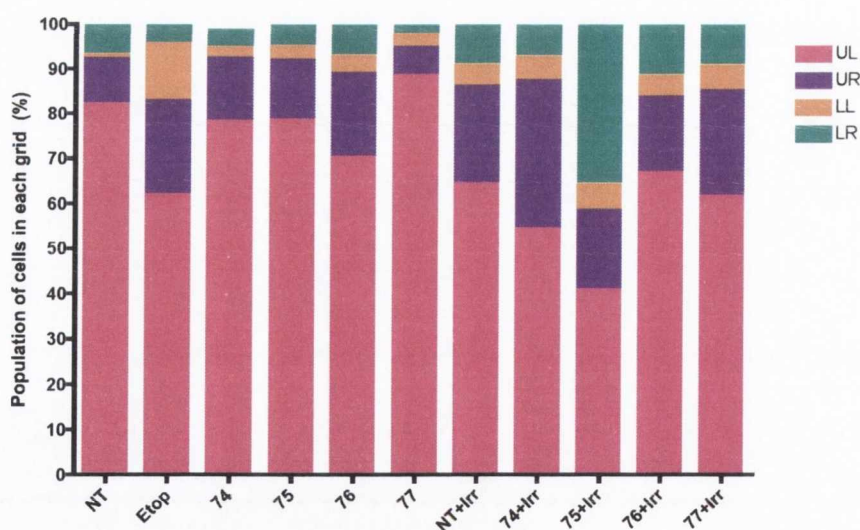


Figure 4.16 Summary of the results obtained from the flow cytometry analysis of the mitochondrial membrane potential after treatment with **74-77** in presence and absence of 8 J/cm^2 light. UL represents the upper left grid and corresponds to healthy cells. The upper right (UR) grid correlates to cells with partially depolarised mitochondria and the lower grids (LL and LR) represents cells that exhibited complete loss of the mitochondrial membrane potential. Each stacked bar corresponds to a mean from two individual experiments.

In summary, these results have shown that **74-77** induced the depolarisation of the mitochondria upon irradiation with 8 J/cm^2 . Furthermore, these results were in good correlation with the results obtained from the ROS production, where it was concluded that the ROS production was most likely a consequence of apoptosis induction. These results support that, and furthermore, they also indicate that these compounds only induced minimal changes to the mitochondrial membrane potential in absence of light. As for the aforementioned studies, the linear 4-amino derivative **75** showed the highest induction of depolarised mitochondria, indicating the potential of this compound for further development as a PDT agent.

4.7 Conclusion and Future Studies

In this chapter, the biological effects of novel Ru(II)-1,8-naphthalimide compounds **74-77** were investigated and their potential as PDT agents was discussed. As detailed in Section 4.2.1, these compounds were shown to be effectively transferred over the cellular membrane, despite their hydrophilic Ru(II) component. The lipophilic 1,8-naphthalimide moiety was believed to be responsible for the observed uptake, similar to that which had been shown for other Ru(II) complexes, where the more lipophilic complexes were able to enter cells.¹⁸⁸ Furthermore, these results also suggested that the linear, *para* configuration lead to more rapid uptake, possibly because of a difference in lipophilicity to the wedged, *meta* configured derivatives **76** and **77**. Further studies into the lipophilicity are needed to confirm this observation. In addition, compounds **74-77** showed increased fluorescence within cells after 24 and 48 hours incubation, indicating that these compounds were bound to a cellular target. These results were confirmed by confocal microscopy discussed in Section 4.2.2, where it was shown that these compounds entered the nucleus after 24 hours.

As discussed in Section 4.3, these compounds were shown to induce limited cytotoxicity in the dark after 48 hours incubation. However, they were shown to reduce cell numbers in culture upon irradiation at 450 nm, which suggested that these compounds were activated within the cells. Furthermore, these studies showed that the phototoxicity of **74-77** was more apparent when the cells were incubated for longer time periods after irradiation. These results suggested that the cells were unable to recover from the damage exerted by compounds **74-77**. Furthermore, these results suggested that the mechanism of cell death was delayed, possibly due to the presence of abnormal Bcr-Abl protein that has been shown to induce Bcl-2, an anti-apoptotic protein discussed in Section 1.2.2. However, further studies are needed to confirm if this is the case. Interestingly, the trend obtained for

the phototoxicity was in correlation with DNA photocleavage studies by Dr. Ryan, where the 4-amino derivatives **75** and **77** were shown to be the most efficient photocleavers.

As discussed in Section 4.4, compound **75** induced the highest production of ROS after 8 J/cm² irradiation, which indicated that apoptosis induction might happen earlier than with treatment of other derivatives. The ROS formation was not believed to arise directly from the photoactivation of **74-77**, due to the 48 hours incubation after irradiation and the fact that most ROS have a short lifetime. To investigate if the mechanism of action by **74-77** involved ROS formation, short incubation is preferential before the cells would be analysed on the flow cytometry system. The cell cycle investigations, which were discussed in Section 4.5 showed that **74-77** induced a G₂/M block after irradiation at 8 J/cm², indicating that these compounds could possibly induce DNA damage and furthermore, this G₂/M arrest was followed by apoptosis. A similar trend was observed for the cytotoxicity studies, where the 4-amino derivatives **75** and **77** were shown to be superior than the 4-nitro derivatives **74** and **76**.

Finally, as described in Section 4.6, the mitochondrial membrane potential was affected by the photoactivation of compounds **74-77**. Furthermore, the linear 4-amino derivative **75** showed the greatest increase in cells that had completely lost their mitochondrial membrane potential, which indicated that this compound induced the apoptosis effect in a more rapid fashion. However, other compounds showed an increase in cell population that had partially depolarised mitochondria, indicating that a longer incubation time after irradiation might be needed to see the full phototoxic effect of these compounds.

In conclusion, these investigation have shown the potential of Ru(II)-1,8-naphthalimides as PDT agents. Future studies will be directed to the effect that photoactivation of these complexes has on the nuclear material, by using assays such as the comet assay, which can be used to detect DNA strand cleavage within cells. Furthermore, the phototoxicity of these compounds will be investigation in hypoxic cells, where less oxygen is expected to lead to decreased phototoxicity.

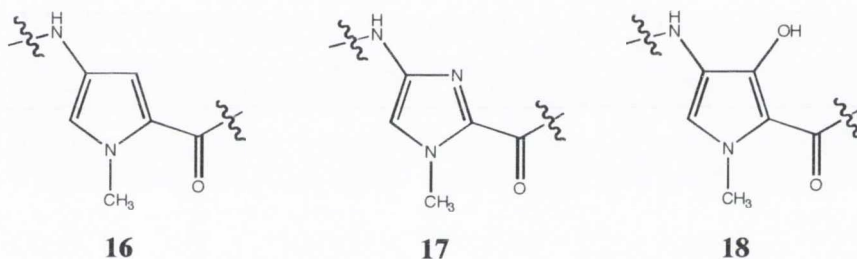
This PhD project involved the biological testing of numerous 1,8-naphthalimide compounds, which have been discussed in detail in Chapter 2, Chapter 3 and Chapter 4. However, it also involved the chemical synthesis of novel pyridine minor groove binders and the results from those studies will be described in the next chapter.

5 The Synthesis of Pyridine Based Minor Groove Binders

5.1 Introduction

As discussed in *Chapter 1 (Section 1.4.1.1.4)*, proteins utilise the minor and major grooves to interact specifically with the DNA duplex, by forming hydrogen bond arrays with the edges of the DNA base pairs. Furthermore, advances in the understanding how a normal cell transforms into a cancerous cell have revealed that DNA rearrangements such as point mutations and translocations affect either the expression of, or the biochemical function, of specific genes.¹⁹⁵ Therefore, the design of synthetic ligands that target predetermined DNA sequences could possibly offer a potential approach for the regulation of gene expression.¹²⁴

There are several drug classes that are able to recognise specific sequences of DNA.¹⁹⁵ As discussed in *Chapter 1 (Section 1.4.1.1.4)*, the pyrrole-imidazole polyamides **16-18** have been highly successful, in binding to DNA with a subnanomolar affinity that is comparable to those of transcriptional regulatory proteins.



As discussed in *Chapter 1 (Section 1.4.1.1.4)*, pairs of **16**, **17** and **18** were able to distinguish the four Watson-Crick base pairs, where **17/16** and **16/17** recognized **G:C** from **C:G**, respectively and **18/16** distinguished **T:A** from **A:T** base pairs. It was also found that by linking antiparallel polyamide dimers with a short alkyl chain, single oligomers were afforded that folded into hairpins within the minor groove of DNA. Furthermore, the introduction of a chiral amine in the middle of the alkyl chain was shown to increase the binding affinity of such structures and prevent the molecule from binding in a reverse fashion.¹²⁴ Such preferential hydrogen-based binding to DNA, by a linked antiparallel dimer containing **16-18**, is shown in Figure 5.1 **B**.¹⁹⁶ In addition to the hairpin motif, various different binding shapes have been explored, such as cycles and dimers.¹⁹⁶ However, due to synthetic difficulties and poor cellular uptake of these different binding motifs, the hairpin configuration has been the most extensively used to date.¹⁹⁶ However, polyamides based on **16-17** have been shown to suffer from several limitations including

the degradation of the polyamides and the overcurvature of the polyamides with respect to DNA. Therefore, investigations into the use of different heterocyclic recognition elements was initiated, which lead to the incorporation of the benzimidazole analogues **19-21** into such DNA binding motifs.

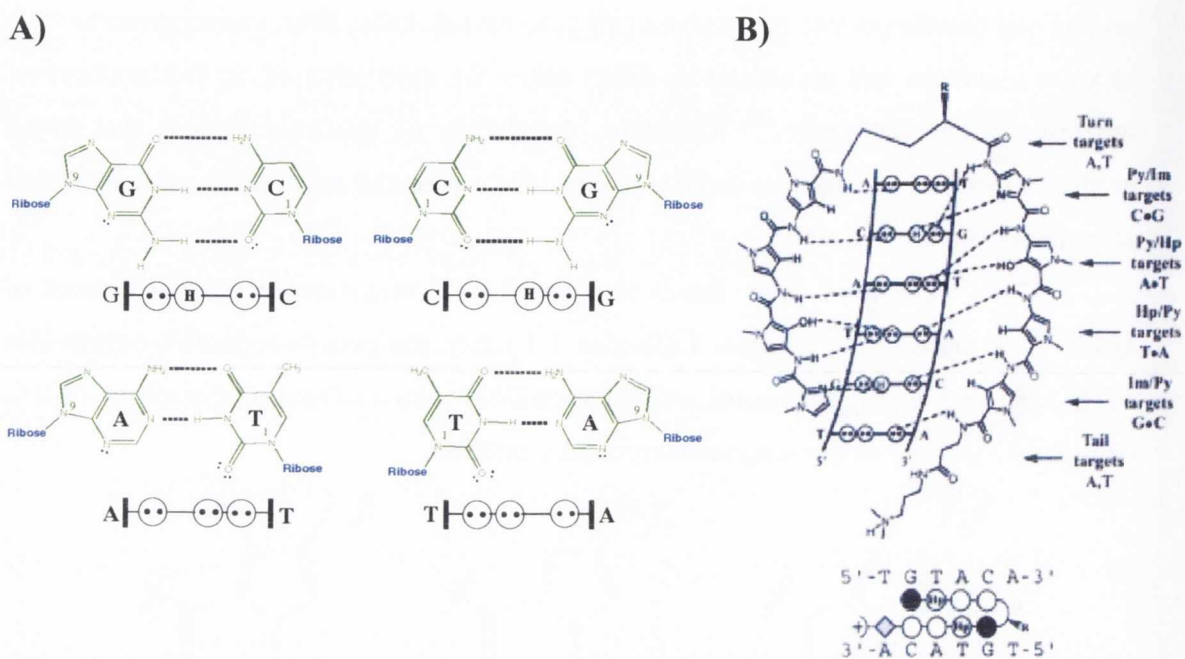
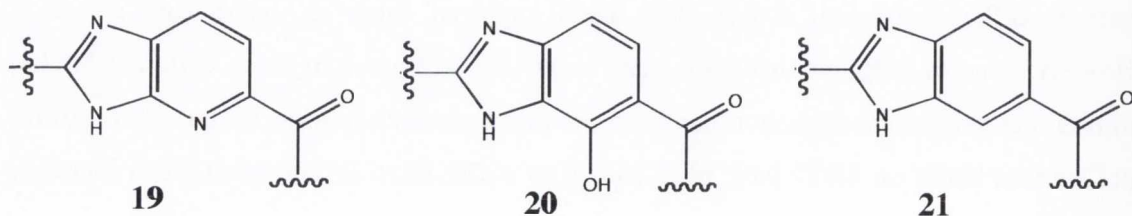


Figure 5.1 A) Chemical structure of the Watson-Crick base pairs. Circle with two dots indicates a hydrogen bond acceptor while a circle with an H indicates a hydrogen bond donor. B) Chemical structure of a pyrrole polyamide with the putative hydrogen bonds to the DNA minor groove. The pairing rules for the 5-membered heterocycles are also shown.¹⁹⁶

The resulting benzimidazole bicyclic ring structures presented an edge that had similar readout to the 5-membered heterocyclic polyamides **16-18**. In addition, they had a curvature that was closer to the shape of the DNA minor groove. These modified structures also showed a higher degree of rigidity, and consequently a lower degree of inherent curvature, which played a significant role in the increased affinity and specificity observed by the bicyclic ring structures **19-21** over their 5-membered heterocyclic counterparts.¹⁹⁶



Furthermore, these the bicyclic moieties have a greater aromatic surface area and hydrophobicity that possibly may alter the DNA-ligand interactions and consequently improve cellular uptake.¹⁹⁶ As discussed in *Chapter 1* (Section 1.4.1.1.4), these polyamides have been used to target specific sequences in cell culture, such as the HRE (Hypoxia-responsive element) and NF- κ B binding sequences.^{129,197}

5.1.1 The Objectives of This Research

With the above results in mind, the aim of the research described in this chapter was to develop novel pyridine based polyamides. It was anticipated that the 6-membered aromatic systems, shown in Figure 5.2 **A**, may adopt the necessary crescent shape that potentially could improve recognition of DNA over the 5-membered heterocyclic rings. Moreover, as shown in Figure 5.2 **B**, the pyridine nitrogen and the amide hydrogen were anticipated to form hydrogen bonds to the NH₂ group and lone pair electrons of the **G**, **C** base pairs, respectively in a similar manner to the imidazole **17** and the bicyclic system **19**.

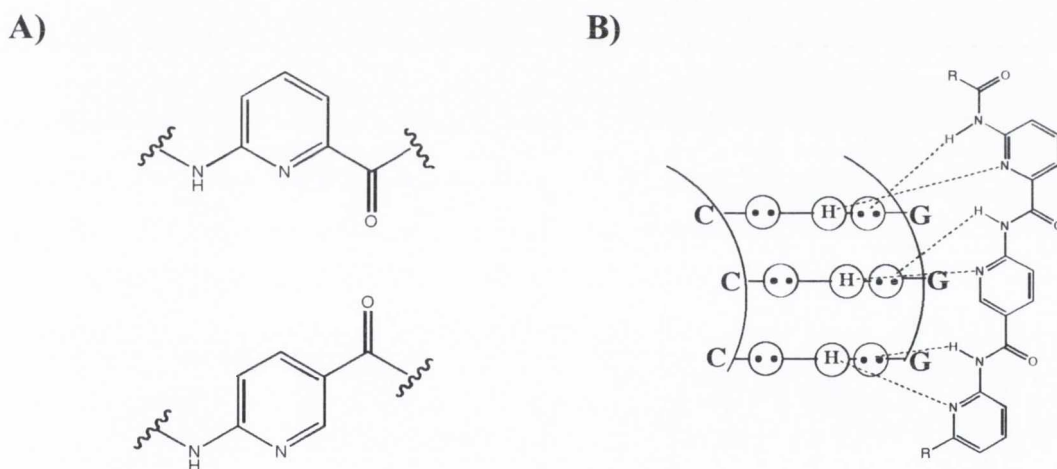


Figure 5.2 **A)** The 6-membered pyridine aromatic systems. **B)** Chemical structure of a pyridine polyamide, showing the potential hydrogen bonds to the DNA minor groove.

The synthetic strategy for the development of these pyridine polyamides is shown in Figure 5.3 and involved the formation of an amino protected pyridine carboxylic acid building block that would then be coupled to a carboxylic acid protected pyridine amine. The resulting di-peptide would then be either deprotected at the amino or the carboxylic acid terminus, followed by a second peptide coupling, increasing the polyamide by one unit at a time in either direction. This strategy could also be employed with the aim of doubling

the length of the polyamide chain, by coupling an amine deprotected di- or tri-peptide derivative with a corresponding carboxylic acid derivative. Finally, upon when reaching the desired polyamide length, the ends could be functionalised by different groups to increase the water solubility or the DNA binding affinity of the polyamide.

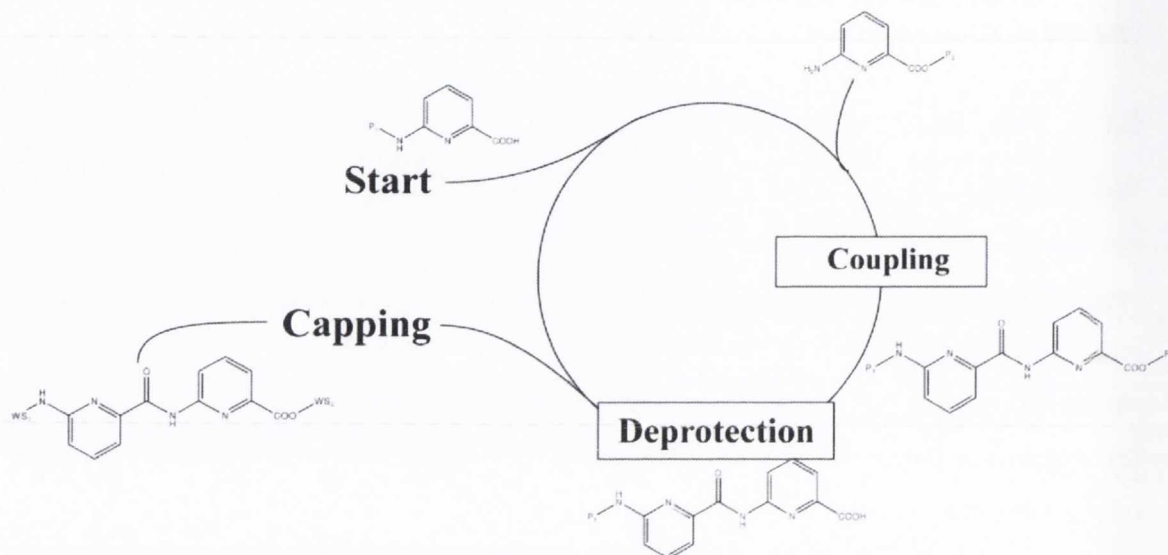


Figure 5.3 The generic synthetic strategy of peptide coupling.

The first section of this chapter describes the synthesis of the pyridine amino acid units, which are necessary building blocks for the polyamide synthesis shown in Figure 5.3. Such synthesis commenced using the commercially available 2-amino-6-picoline **80** as a starting material. Subsequent protection of the amino group with different protecting groups, such as acetic anhydride or di-*tert* butyl dicarbonate (Boc). Secondly, different oxidations conditions were investigated for the transformation of the methyl group in 2-amino-6-picoline at the sixth position of the pyridine ring to a carboxyl group.

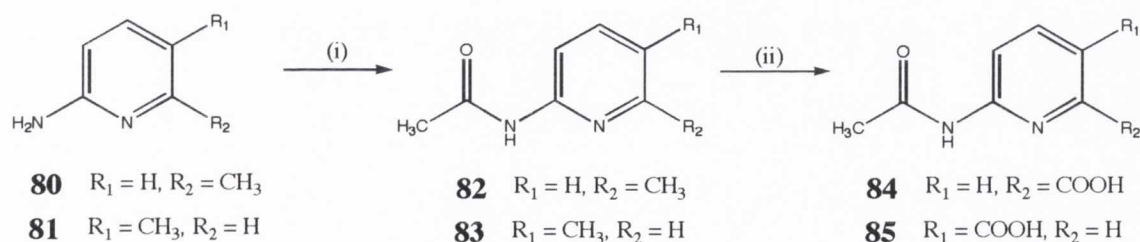
The second section of this chapter discusses the successful synthesis of pyridine di- and tri-peptides, which was achieved after various different synthetic routes were attempted. Such approaches included; *i*) the formation of an acid chloride of pyridine carboxylic acid and the subsequent condensation with **80** to form an amide bond and *ii*) the use of peptide coupling reagents, such as dicyclocarboddimide (DCC) and 1-ethyl-3-(3-dimethylaminopropyl) carbodiimide hydrochloride (EDCI) under different experimental conditions. In addition, various attempts to elongate the pyridine peptide chain will be discussed. The results from these synthetic attempts will be discussed in the following sections. These amino acids units consisted of either amino or carboxylic acid protected pyridines and the results from these investigations will be discussed in next section.

5.2 The Synthesis of the Amino and Carboxylic Acid Based Pyridine Building Blocks 84-85 and 94-95

5.2.1 Synthesis of Amino Protected Pyridine Carboxylic Acid Derivatives

A two-step synthesis for the *N*-acetyl-2-amino-6-picolinic acid had previously been published by Schmuch *et al.*¹⁹⁸, where the first step involved the protection of the 2-amino group of the commercially available 2-amino-6-picoline **80** with acetic anhydride. This reaction was carried out by stirring in toluene overnight at 95 °C after which the solvent was removed under reduced pressure to give off-white crystals. Similarly, 2-amino-5-picoline **81** was protected using identical conditions to give the corresponding *N*-acetyl derivative **83**. Compounds **82** and **83** were synthesised in 95% and 89% yields, respectively without the need for further purification.

The next step in this synthesis involved the oxidation of the methyl group to the corresponding carboxylic acid, using two equivalents of potassium permanganate (KMnO₄) in the presence of sodium hydroxide (NaOH). After refluxing the reaction mixture in water overnight, the manganese(IV) oxide was collected by filtration and the volume of the filtrate was reduced. The solution was then acidified to pH 4, by addition of concentrated HCl and the resulting white precipitate was collected by filtration and dried to give the *N*-acetyl-picolinic acid derivatives **84** and **85** in 62% and 45% yields, respectively. Both **84** and **85** were characterised using conventional methods, ¹H and ¹³C NMR as well with ESMS and IR analysis to confirm their purity.



Scheme 5.1 Synthesis of **84** and **85**. Reagents and conditions: (i) Acetic anhydride, toluene, 95 °C, (ii) KMnO₄, NaOH, H₂O, reflux.

The ¹H NMR spectrum (DMSO-d₆, 400 MHz) of **84** is shown in Figure 5.4. The amide proton (**A**) appears as a singlet at 10.8 ppm and the aromatic region between 8.26 and 7.72 ppm consists of two doublets (**B** and **D**) and one triplet (**C**) all integrating for one proton and the methyl group appeared as a singlet (**E**) at 2.1 ppm. The ¹H NMR spectrum

also showed the presence of water in the sample, but the reoccurring problem in the synthesis of these compounds was their tendencies to be hydroscopic. However, drying these products under reduced pressure in the presence of P_2O_5 was sufficient enough to dry these samples before they were used in further synthesis.

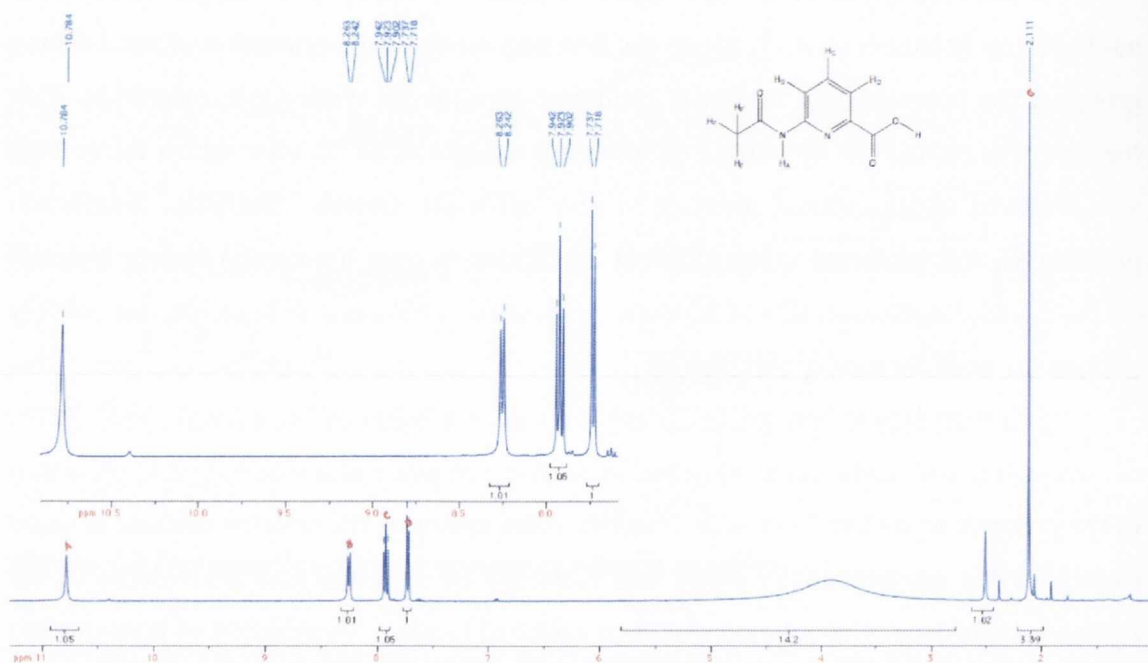
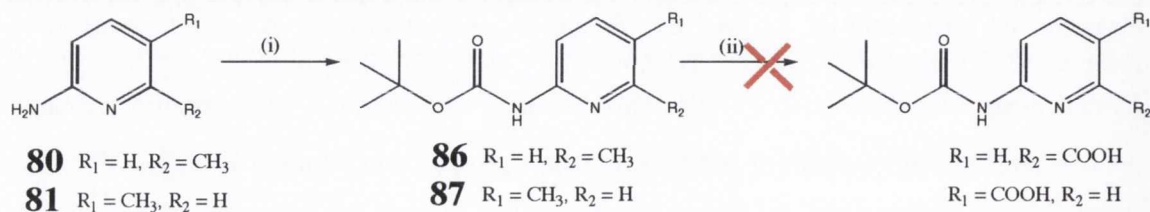


Figure 5.4 The 1H NMR spectrum ($DMSO-d_6$, 400 MHz) of **84**.

Although the *N*-acetyl-picolinic acids **84** and **85** were obtained in good yields, it was decided to investigate other amino protecting groups that would possibly be more labile than the acetyl group. This was important for the future development of the polyamides, because the elongation of the peptide chain would involve the coupling of the free amine to the carboxylic acid, as discussed in Section 5.1.

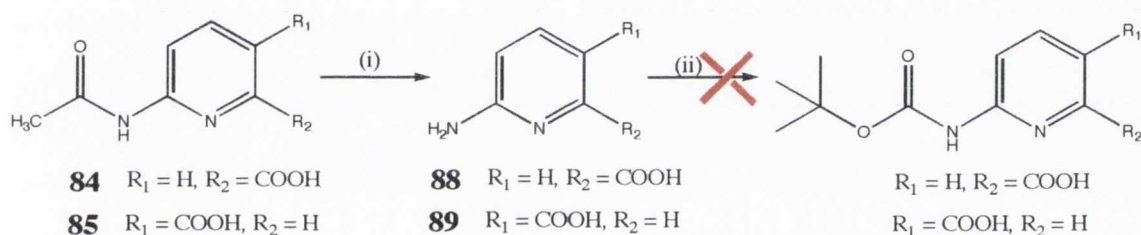
The first approach considered involved using Boc anhydride as an amino protecting group as depicted in Scheme 5.2, as the removal of the Boc protecting group is normally carried out under rather mild acidic conditions.



Scheme 5.2 The synthetic route for the formation of the Boc-protected amino picolinic acid. Reagents and conditions: (i) Boc Anhydride, 60 °C, (ii) $KMnO_4$, NaOH, H_2O , reflux.

Reaction of Boc anhydride with **80** and **81** and stirring at 60 °C overnight, resulted in the formation of **86** and **87** in 89% and 98% yields, respectively after purification by column chromatography on flash silica using hexane as an eluent. However, the following step, which involved the oxidation of the methyl group to the corresponding carboxylic acid with KMnO_4 was unsuccessful (according to ^1H NMR) under similar conditions as were used for the synthesis of **84** and **85**. A possible reason for the unreactivity may be due to the insolubility of **86** and **87** in basic and neutral aqueous solutions. Consequently, different mixtures of solvents were used, such as the use of 50/50 MeOH/ H_2O or MeCN/ H_2O . However, these modifications only resulted in the recovery of the starting materials according to ^1H NMR analysis.

As a result, another synthetic approach was also investigated, which involved the oxidation of the methyl group of **84** and **85** prior to protection of the amino group as shown in Scheme 5.3.

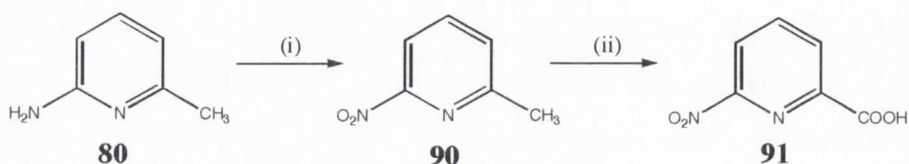


Scheme 5.3 The synthetic route for the Boc-protected amino picolinic acid through 2-amino-picolinic acid. Reagents and conditions: (i) 10% NaOH, reflux, (ii) Boc Anhydride, NEt_3 , DMF, 60 °C.

This approach involved removing the acetyl protecting group of **82** and **83**, by refluxing these derivatives in 10% aqueous sodium hydroxide solution for 6 hours. The resulting solution was then cooled in an ice bath and acidified to pH 4 using concentrated HCl. The resulting beige solid was washed with water and diethyl ether to give the pyridine amino acid **88** and **89** in 58% and 46% yields, respectively. However, due to the insolubility of **88** and **89** in organic solvents, the further syntheses of the target molecules were not carried out.

The third approach involved the transformation of the amino group of **80** (Figure 5.4) into a nitro group, which could serve as a synthetic equivalent to a protected amino group. The nitro group could possibly be reduced back to the amino functionality by catalytic hydrogenation. This approach has previously been used in the synthesis of short imidazole

polyamides, discussed in Section 5.1.¹⁹⁹ The oxidation of 2-amino-6-picoline has been reported by Wiley *et al.*²⁰⁰ using concentrated and fuming sulphuric acid (H_2SO_4) in the presence of hydrogen peroxide (H_2O_2). Furthermore, the oxidation of the corresponding 2-nitro-6-picolinic acid was published by Brown *et al.*²⁰¹ using KMnO_4 in a similar manner to the formation of **84** and **85** above. The synthetic strategy for the formation of 2-nitro-6-picolinic acid is shown in Scheme 5.4.



Scheme 5.4 Synthesis of 2-nitro-picolinic acid **91**. Reagents and conditions: (i) H_2SO_4 , 35% H_2O_2 / 30% Fuming H_2SO_4 , 10-20 °C, (ii) KMnO_4 , H_2O , 90 °C.

The 2-amino-picoline **80** was dissolved in concentrated H_2SO_4 and the solution was cooled to 15 °C. A mixture of 35% H_2O_2 and 30% fuming H_2SO_4 was added dropwise to the reaction and the temperature was maintained at 15 °C for three hours. After 48 hours stirring at room temperature, the reaction was poured onto ice and the solution was neutralised with concentrated NaOH solution. The aqueous solution was extracted with diethyl ether and the organic phase was dried and then removed under reduced pressure, resulting in the isolation of the expected 2-nitro-6-picoline **90** in 63% yield. The successful formation of this compound was confirmed by NMR analysis and ESMS.

The oxidation of the methyl group to the corresponding carboxylic acid was carried out in a similar manner to that described for the *N*-acetyl derivatives **82** and **83**, using KMnO_4 in H_2O . As before, the manganese(IV) oxide was filtered off and the aqueous solution was reduced *in vacuo* and acidified to pH 4, which gave precipitation of the desired product 2-nitro-6-picolinic acid **91** in 10% yield.

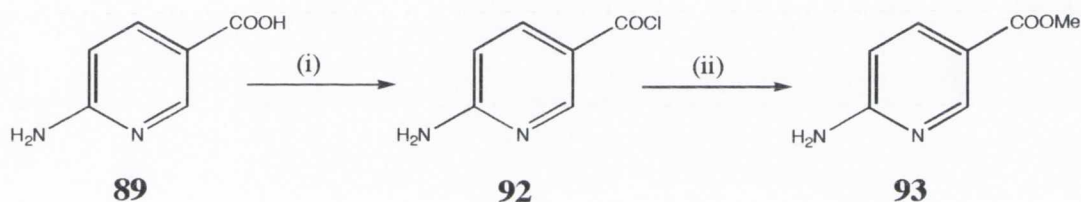
After successfully synthesising three derivatives of an amino protected pyridine carboxylic acids, namely compounds **84**, **85** and **91**, it was decided to investigate the synthesis of a carboxylic acid protected pyridine amine. These results will be discussed in the next section.

5.2.2 Synthesis of Carboxylic Acid Protected Pyridine Amine Derivatives

The main object of the investigation discussed in this section was to synthesise 2-amino-picolinic esters from the *N*-acetyl derivatives **84** and **85**, which were successfully synthesised in Section 5.2.1. This would involve the hydrolysis of the acetyl protecting

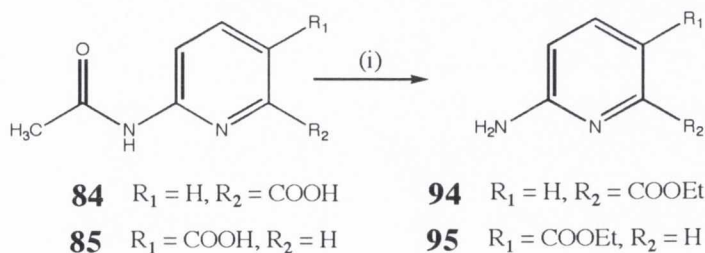
group and the subsequent protection of the carboxylic acid group, as methyl and ethyl esters.

The formation of a methyl ester was achieved *via* the formation of an acid chloride as shown in Scheme 5.5. The hydrolysis of the acetyl group was achieved by simply refluxing the *N*-acetyl-picolinic acids **84** and **85** in 10% NaOH overnight to give the 2-aminopicolinic acids **88** and **89** in 58% and 46% yield, respectively. Compound **89** was then partially dissolved in chloroform and oxalyl chloride was added at room temperature. This reaction mixture was stirred at room temperature over 4 days at 45 °C before the solvent and the excess oxalyl chloride were removed under reduced pressure to give the desired acid chloride **92**, which was dried under vacuum before further use. Methanol was added dropwise to the acid chloride at 0 °C and upon complete addition, the solution was refluxed at 80 °C overnight under argon. The solvent was removed and the corresponding methyl ester was obtained in 35% yield. The synthetic route is depicted in Scheme 5.5 and the full characterisation of **93** can be found in Chapter 6.



Scheme 5.5 The synthesis of 2-amino-5-picolinic ester **93**. Reagents and conditions: (i) Oxalyl chloride, CHCl_3 , 45 °C, (ii) MeOH, reflux.

Despite successfully synthesising the amino picolinic ester **93** through acid chloride formation, it was decided to investigate other ways that would improve overall yields. A synthetic route to the ethyl ester **94** has been published by Selwood and coworkers²⁰² involving the one-pot hydrolysis and ester formation of the *N*-acetyl derivatives **84** and **85**, shown in Scheme 5.6.



Scheme 5.6 The synthesis of 2-amino-5-picolinic esters **94** and **95**. Reagents and conditions: (i) H_2SO_4 , EtOH, reflux.

This method was adopted here, and the *N*-acetyl derivatives **84** and **85** were dissolved in a 3:20 mixture of H₂SO₄ and ethanol and the resulting solutions were refluxed for five hours under argon. The mixtures were then cooled in an ice bath and basified with NH₄⁺_(aq). The aqueous layers were then extracted with ethyl acetate, dried over MgSO₄ and the organic solvent was removed under reduced pressure, to give **94** and **95** in 50% and 51% yields, respectively. The ¹H NMR spectrum of **95** in DMSO-*d*₆ (400 MHz) is shown in Figure 5.5, and demonstrates the successful synthesis of this compound where the amine protons appear as a singlet (C) at 6.8 ppm and the proton at the sixth position of the pyridine ring resonates downfield (A) at 8.5 ppm. The pyridine proton in the fourth position (B) appears as a doublet of doublets at 7.8 ppm. Finally, the signals pertaining to the ethyl protons appear as a quartet (E) and a triplet (F) for CH₂ and CH₃, at 4.2 ppm and 1.3 ppm, respectively.

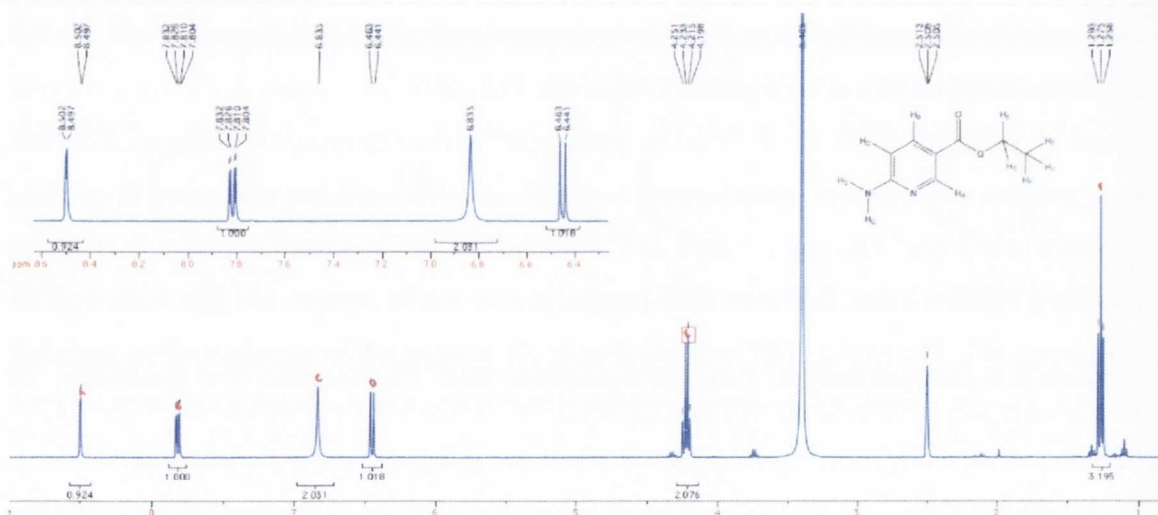


Figure 5.5 The ¹H NMR spectrum (DMSO-*d*₆, 400 MHz) of **95**.

5.2.3 Summary

This section described the successful synthesis of the basic pyridine building blocks, the *N*-acetyl-picolinic acids and 2-amino-picolinic esters **84-85** and **94-95**, respectively. As discussed in Section 5.1, these molecules were required for the synthesis of the pyridine-based polyamides. Therefore, investigations into the use of various different peptide coupling procedures were subsequently carried out and the results from these investigations are discussed in the next section.

5.3 Pyridine Polyamide Synthesis

5.3.1 The Synthesis of Di-Peptides and Symmetrical Tri-Peptides

As discussed in Section 5.2, the synthesis of the *N*-acetyl-2-amino-picolinic acid derivatives **82** and **84** was achieved in considerably good yields. The next step towards the constructing the polyamide, involved coupling these two derivatives to 2-amino-picolinic ethyl esters **94** and **95**. Because the three-step synthesis of **94** and **95**, was achieved relatively low overall yields, it was initially decided to use the 2-amino-picoline derivatives **80** and **81** for preliminary synthetic investigations. Furthermore, the product from this reaction could be further utilised for instance; *i*) as a capping agent as discussed in Section 5.1 and *ii*) the methyl group could be potentially oxidised to the corresponding carboxylic acid in a manner described above.

The first attempt towards the formation of a di-peptide involved the preparation of an acid chloride *in situ*, followed by reaction with 2-amino-6-picoline under Schotten-Baumann conditions, as shown in Figure 5.6 A. This synthetic strategy was proven successful for **96**, by reacting 2,6-pyridine diacid chloride *in situ* with 2-amino-6-picoline **80**, which after aqueous base workup gave **96** in 23% yield.

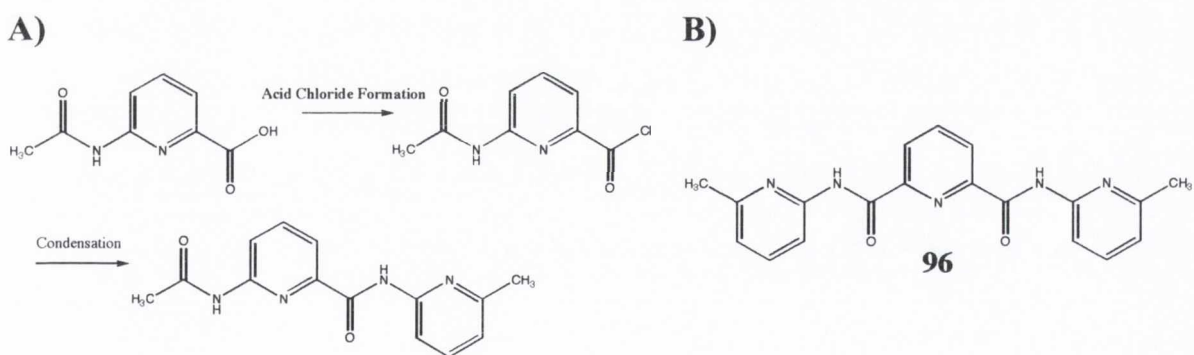


Figure 5.6 A) The synthetic strategy used for the formation of di-peptide. B) The tri-pyridine peptide **96**.

However, when the amino protected carboxylic acids **84** and **85** were reacted with thionyl chloride and subsequently condensed with **80**, in a similar manner to **96**, only the starting materials were recovered according to ^1H NMR analysis. This indicated that the acid chloride was not formed *in situ*, possibly because of the insolubility of **82** and **83** in heated thionyl chloride. Consequently, different conditions to that used for **96** were thus

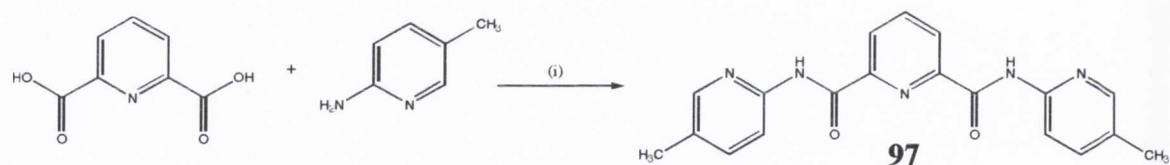
employed, by varying the reaction time, solvent and chlorinating agents. However, as listed in Table 5.1, these attempts were unsuccessful.

Table 5.1 Conditions investigated for the formation of the *N*-acetyl-picolinic acid chloride.

Attempt	Reaction Conditions	Result
1	SOCl ₂ , reflux, 5 hours	Unsuccessful by ¹ H NMR
2	SOCl ₂ , CHCl ₃ , reflux, 12 hours	Unsuccessful by ¹ H NMR
3	SOCl ₂ , CH ₂ Cl ₂ , 45 °C, 12 hours	Unsuccessful by ¹ H NMR
4	SOCl ₂ , DMF, 110 °C, 12 hours	Unsuccessful by ¹ H NMR
5	Oxalyl Chloride, reflux, 3 hours	Unsuccessful by ¹ H NMR
6	SOCl ₂ , DMF, 55 °C, 72 hours	Unsuccessful by ¹ H NMR

The next synthetic strategy involved the use of the peptide coupling reagents, dicyclohexylcarbodiimide (DCC) and 1-ethyl-3-(3-dimethylaminopropyl) carbodiimide hydrochloride (EDCI). The mechanism for this coupling involves the rapid formation of an *O*-acylisourea under ambient conditions, which is followed by nucleophilic attack of the amino group, ultimately forming the amide bond.

Firstly, investigate the compatibility of these reagents with pyridine compounds, they were initially reacted with the commercially available 2,6-pyridine-dicarboxylic acid to form the tripyridine peptide **97**, as shown in Scheme 5.7.

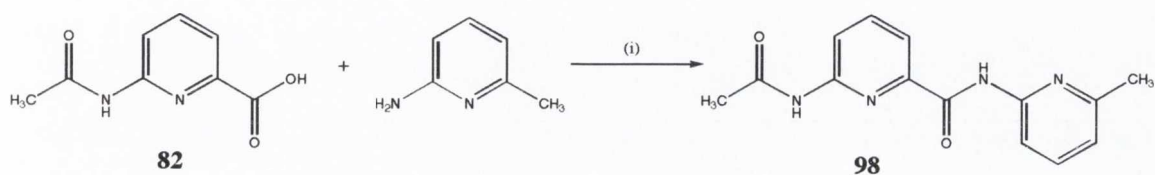


Scheme 5.7 Synthesis of the tri-peptide 97. Reagents and conditions: (i) DCC, HOBT, DMAP, 1:10 DMF/CH₂Cl₂, room temperature.

The general procedure involved adding DCC to a solution containing 2,6-pyridine dicarboxylic acid, HOBT, 2-amino-picoline and dimethylaminopyridine in a mixture of DMF/CH₂Cl₂ (1/10) at 0 °C. The resulting mixture was then stirred at room temperature for 24 hours, after which the dicyclohexyl urea was found to precipitate out of solution, indicating the completion of the reaction. The precipitate was collected by filtration and the solvent was removed under reduced pressure to give **97** in 13% yield after recrystallisation

from EtOAc. The full characterisation of **97** by ^1H , ^{13}C NMR and IR spectroscopy can be found in Chapter 6.

Having demonstrated the successful synthesis of **97**, the coupling of the *N*-acetyl derivative **82** to 2-amino-6-picoline **80** was carried out using the same procedure as discussed above and shown in Scheme 5.8.



Scheme 5.8 The synthesis of the di-peptide **98**. Reagents and conditions: (i) DCC, HOBT, DMF, room temperature.

Compound **82**, 2-amino-picoline and HOBT were dissolved in DMF, due to the insolubility of **82** in most organic solvents. This reaction was then stirred for 24 hours at room temperature, followed by cooling to 4 °C in an attempt to fully precipitate the dicyclohexyl urea. After removing any residues of the urea by filtration, the desired product was obtained in 14% yield as a white solid after recrystallisation from EtOAc.

The ^1H NMR spectrum (DMSO- d_6 , 400 MHz) of **98** is shown in Figure 5.7, and clearly shows the two amide hydrogens, which appear as singlets at 10.91 and 10.23 ppm, respectively. Furthermore, the aromatic region consists of four doublets and two triplets pertaining to the pyridine rings while the methyl groups are observed as singlets at 2.43 and 2.20 ppm, respectively.

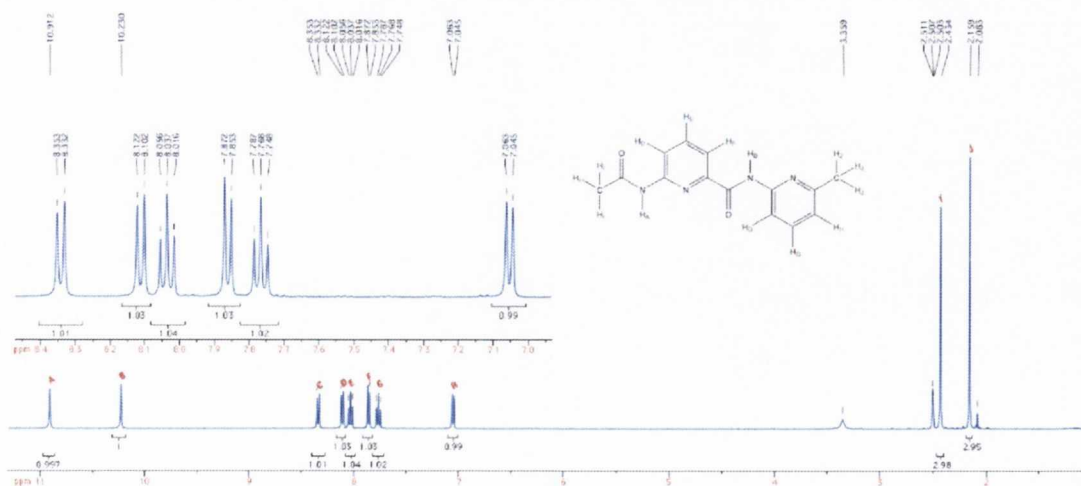


Figure 5.7 The ^1H NMR spectrum (DMSO- d_6 , 400 MHz) of **98**.

Using similar synthetic protocol, three other pyridine di-peptides **98-101** were also successfully synthesised using these same coupling reagents (DCC and EDCI) after overnight reaction at room temperature. They were all fully characterised by ^1H , ^{13}C NMR, ESMS and IR spectroscopy. Nevertheless, ESMS analysis displayed a peak at 315.1717, which corresponds to the $\text{M}+\text{H}^+$ ion for the derivative **102**, which indicated that the 2-amino-6-picoline reacted with DCC and gave rise to a stable product. A possible reason for the observed unreactivity could be a result of the poor solubility of **81** in most organic solvents.

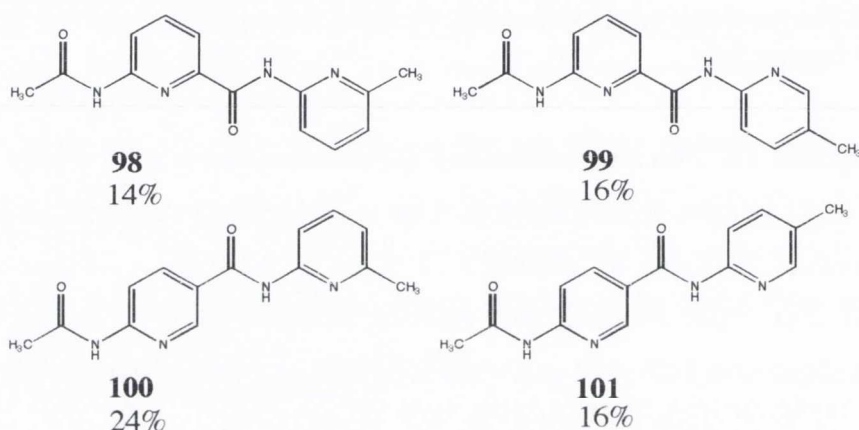
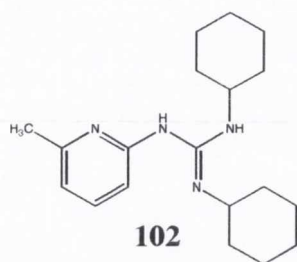
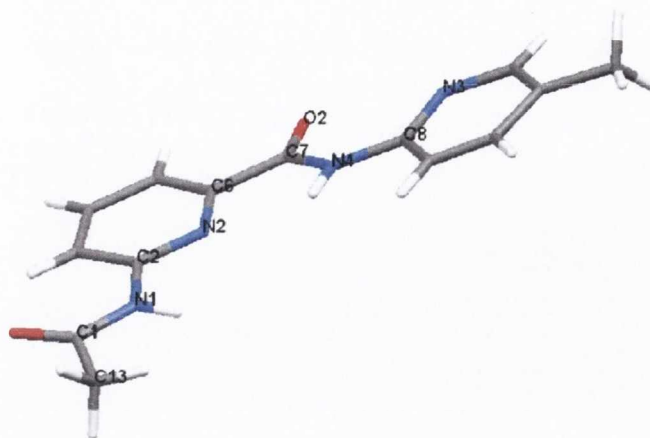


Figure 5.8 The pyridine di-peptides **98-101** and their corresponding yields.

Crystals of the di-pyridine derivative **99** were grown in DMSO. These crystals were suitable for X-ray diffraction analysis, which was carried out by Dr. McCabe in the School of Chemistry, Trinity College Dublin and the resulting crystal structure is shown in Figure 5.9. Furthermore, the list of bond lengths and bond angles corresponding to this structure can be found in Table 4.1A in Appendix 4. As shown in Figure 5.9 A, the pyridine units are anti to each other in the solid state. This would perhaps indicate that while in solution, the nitrogen (N3) of the 2,5-substituted pyridine ring would not be able to interact with the bases of DNA and the aromatic hydrogen (H9) would be expected to be set deeply in the minor groove and hence sterically clashing with the NH_2 of **G** and **C**. This would further indicate that the 2,5 pyridine substitution afforded binding specificity for **A**, by introducing a steric hindrance with the carbonyl group of **T**, in a similar manner to netropsin and distamycin, that were discussed in Chapter 1. However, further studies into the DNA binding of **99** are needed to confirm if this is indeed the case.

A)



B)



Figure 5.9 Crystal structure of 99. **A)** A view along the *b* axis and, **B)** a view through the pyridine (*N2* nitrogen) plane. Carbon atoms are represented by grey colour, hydrogens atoms with white, oxygens atoms with red and finally, nitrogen atoms with blue.

As shown in Figure 5.9 **B**, upon viewing the crystal structure through the 2,6-substituted pyridine plane, the second pyridine appears slightly twisted out of plane. The angle between the planar pyridine units is equal to the sum of three torsion angle deviations in the bonds that connect the pyridine units: $-7.3^\circ + 4.7^\circ + 0.2^\circ = -2.4^\circ$. These torsion angles are indicated by a red colour in Figure 5.10, where the negative torsion angles indicate counter clockwise rotation of the most distant end of the investigated bond. In a similar manner, the pyrrole ring planes in netropsin have been reported to have an angle of 20° to one another.¹¹⁶ The difference between the pyrrole and the pyridine units is believed to arise from the non-planarity of the pyrrole units, which is ascribed to the steric clash between the pyrrole CH and the adjacent amide group.¹¹⁶ In addition, the rise per DNA base pair is found to be around 33° and therefore, these pyridine units would not have the correct curvature to fit DNA. However, it has been previously that the angle between the pyrrole rings of pyrrole polyamides is increased upon binding within the minor groove.¹¹⁶

Therefore, further investigations are needed to fully confirm that the pyridine based polyamides fit the concave structure of the DNA minor groove.

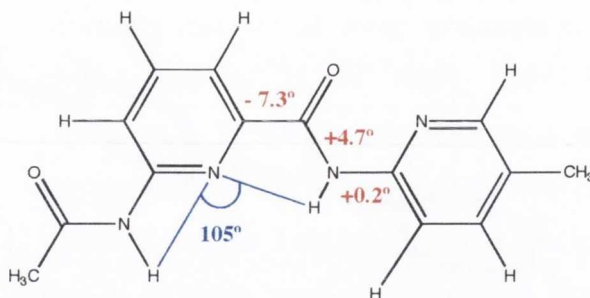


Figure 5.10 Flattened drawing of the crystal structure of **99**. Red numbers alongside bonds are torsional deviations from the planarity about these bonds. Positive torsion angles indicate clockwise rotation for the most distant end of a bond when sighting along the bond. Blue numbers indicate the angle between the amide nitrogens.

In addition, as shown in Figure 5.10, the angle formed between the amide hydrogens is 105° , suggesting that repeated units of the 2,6-substituted pyridines would span 360° after nearly 5 repeating units ($360^\circ/75^\circ = 4.8$), while DNA has about 10 base pairs per turn.¹⁸ Although these results are based on the solution structure of **99**, these results indicated that the pyridine polyamides could be overcurved in relation to DNA. However, as mentioned earlier, both these angles and the distortion angles could change upon binding in the minor groove as have been shown for netropsin.¹¹⁶

With the above assumption in mind, the cytotoxicity of di-peptide **98** against K562 cells was determined by MTT proliferation assay. Cells were incubated with **98** for 48 hours before determining the numbers of cells by the MTT assay, as was discussed in Section 2.3 in Chapter 2. The absorbance was plotted against the concentration of **98**, which is shown in Figure 5.11.

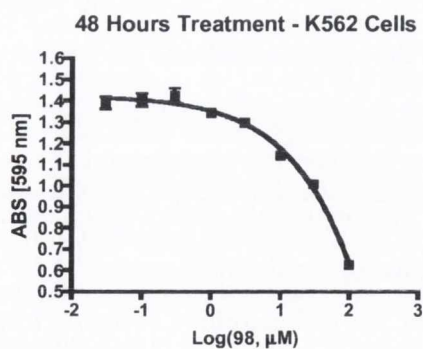
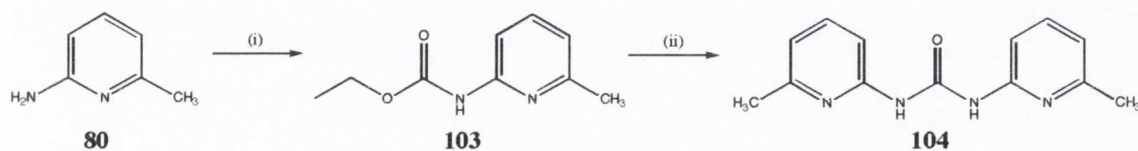


Figure 5.11 The cytotoxicity profile for di-peptide **98** against K562 cells. Each point on the graph represents the mean obtained from a triplicate experiment (\pm Standard error).

Compound **98** was shown to reduce cell numbers at relatively high doses and the EC_{50} value was found to be 82 μ M. This result indicated that the di-peptide was able to cross the cell membrane of treated cells and induce cellular death at high concentrations. However, further investigations are needed to fully establish the basis of the observed cytotoxicity and the extent of cellular uptake.

In addition to compound **98-101**, other di-peptide motifs were also synthesised that may potentially display a different kind of binding in comparison to **98-101**. First, the pyridine units were coupled together by an urea moiety as shown in Scheme 5.9.



Scheme 5.9 The synthesis of the urea coupled pyridine di-peptide **104**. Reagents and conditions: (i) Ethyl chloroformate, pyridine, 0 °C, (ii) **80**, pyridine, reflux.

The synthesis was achieved from the commercially available 2-amino-6-picoline **80**, which was reacted with ethyl chloroformate at room temperature overnight. The reaction mixture was then poured onto ice and the resulting precipitate was collected by filtration, giving rise to the formation of ethyl 6-methylpyridinyl-2-carbamate **103** in 71% yield. No further purification was necessary. Compound **103** was then refluxed in a pressure tube with **80** in pyridine. The reaction mixture was allowed to stir for three days after which the solvent was evaporated under reduced pressure and the crude material taken up into toluene, which resulted in the formation of a grey precipitate, which was shown to be the expected urea compound **104** in 44% yield according to ^1H NMR analysis.

The ^1H NMR spectrum (DMSO- d_6 , 400 MHz) of **104** is shown in Figure 5.12, and clearly demonstrates the C_2 -symmetry of this molecule. The amide protons were observed as a broad peak at 10.4 ppm (A), possibly because of the formation of an intramolecular hydrogen bond between one of the amide protons and the non-adjacent pyridine nitrogen atom.²⁰³ This equilibrium also affected the protons at the third position in the pyridine ring (C), giving rise to a broad NMR signal for these protons. As expected, the other two pyridine protons were observed as a triplet (B) and a doublet (D) at 7.65 and 6.91 ppm, respectively, whereas the methyl protons (E) resonate as a singlet at 2.43 ppm.

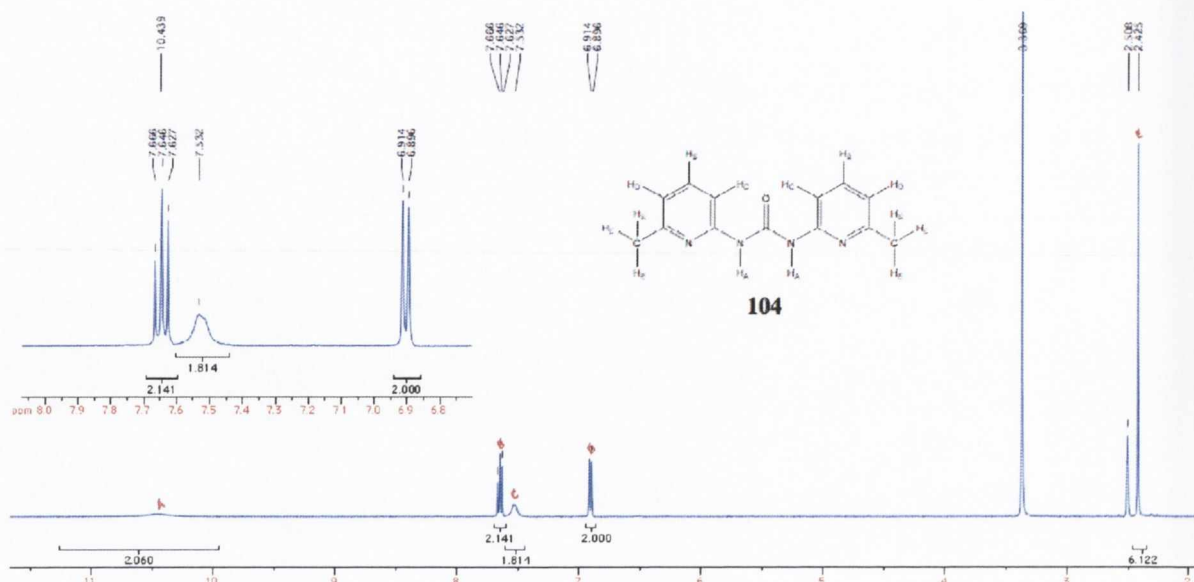
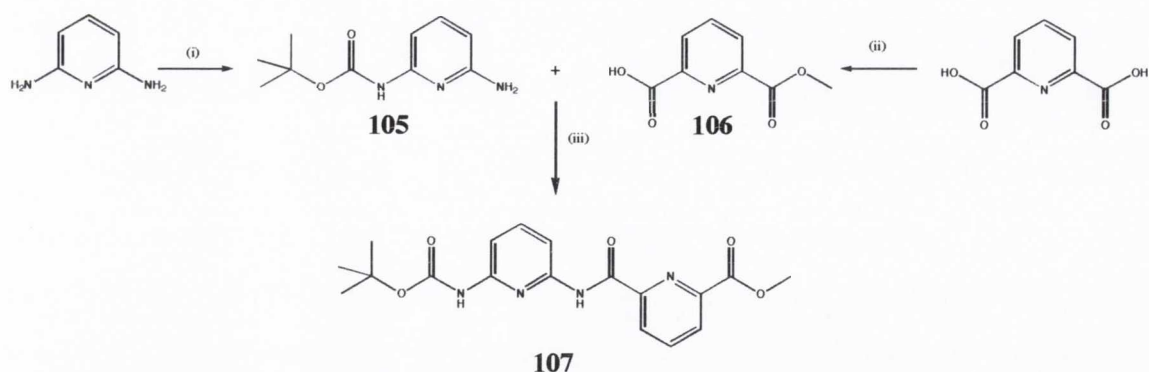


Figure 5.12 The ^1H NMR spectrum ($\text{DMSO-}d_6$, 400 MHz) of **104**.

This urea motif of **104** represents a different hydrogen-bonding surface to the dipeptides **98-101** synthesised above, where it was anticipated that they would specifically bind to **A** in the minor groove. These urea-based systems however, offer the possibility of four hydrogen bonds to the base pairs of DNA. Furthermore, the urea moiety itself could potentially show preferential binding to **T**, in a similar manner as the hydroxypyrrole shown in Figure 5.1. However, further investigations need to be carried out to establish if this system shows any sequence specificity in binding.

Another di-peptide motif was synthesised according to Scheme 5.10, where the 2,6-diaminopyridine was coupled with 2,6-pyridine carboxylic acid. The synthesis commenced with a mono-protection of the commercially available 2,6-diamino pyridine with Boc-anhydride.²⁰⁴ This reaction was carried out in THF at 60 °C for 24 hours and the product was obtained in 49% yield after purification by column chromatography on flash silica (10/90 EtOAc/ CH_2Cl_2). The full characterisation of **107** by ^1H , ^{13}C NMR and IR spectroscopy can be found in Chapter 6. The commercially available 2,6-pyridine dicarboxylic acid was also mono-protected by refluxing it in a mixture of methanol and water in the presence of H_2SO_4 for 15 minutes followed by stirring at room temperature overnight.²⁰⁵ The aqueous solution was neutralised by the addition of concentration HCl and extracted with chloroform to remove the di-substituted methyl ester and then further acidified and extracted with chloroform. This resulted in the formation of the monoester **106** as a white solid in 26% yield, according to ^1H NMR analysis.



Scheme 5.10 The synthesis of di-peptide **107**. Reagents and conditions: (i) Boc anhydride, THF, room temperature, (ii) H_2SO_4 , MeOH/ H_2O , reflux for 15 minutes, room temperature overnight, (iii) DCC, HOBT, Et_3N , THF, room temperature.

As for the synthesis of compounds **98-101**, the mono-protected **105** and **106** were coupled together by using the same peptide coupling reagents, where compounds **105**, **106** and HOBT were dissolved in THF and DCC and triethylamine were added to this solution at 0 °C. The reaction mixture was then stirred overnight at room temperature, after which the solvent was removed under reduced pressure and the resulting residues were purified by column chromatography using flash silica (40/60 EtOAc/ CH_2Cl_2), giving the di-peptide **107** as a white solid in 27% yield. The full characterisation of **107** can be found in Chapter 6.

The 1H NMR spectra of **107** is shown in Figure 5.13 (DMSO- d_6 , 400 MHz). The amide protons resonates as sharp singlets (A and B) at 10.1 and 9.98 ppm, while the

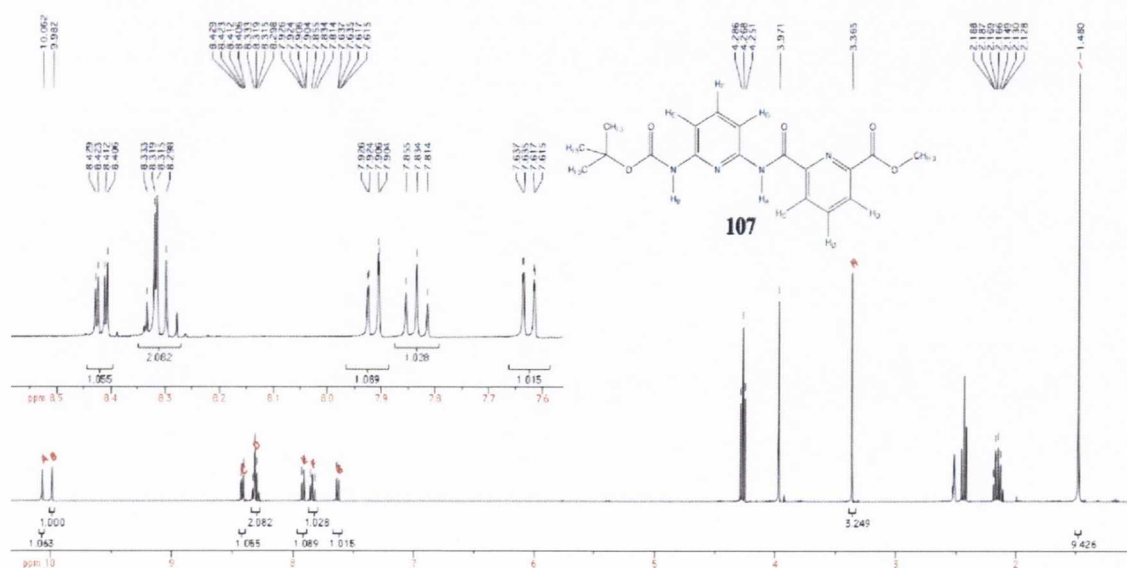


Figure 5.13 The 1H NMR spectrum (DMSO- d_6 , 400 MHz) of **107**.

aromatic region shows that the protons from the 2,6-dicarboxylic acid unit are further downfield than the 2,6-diamino unit. The methyl protons from the methyl ester and the Boc group are observed as singlets at 3.4 and 1.5 ppm, indicated by **H** and **I**, respectively.

Crystals of **107** were obtained by slow evaporation of methanol and they were found to be suitable for X-ray diffraction analysis, which was carried out by Dr. McCabe. The resulting crystal structure of **107** is shown in Figure 5.14. In contrast to the crystal structure of **98** shown in Figure 5.9, the crystal structure of **107** shows that both pyridine nitrogens (N2 and N4) faced inwards. Although the structure could possibly be different in solution to the solid state, this indicates that the di-peptide **107** could preferentially target **G** sequences, by i) forming hydrogen bonds between the pyridine nitrogen and the NH₂ of **G** and by ii) the amide hydrogen and the lone pair of the **G** base.

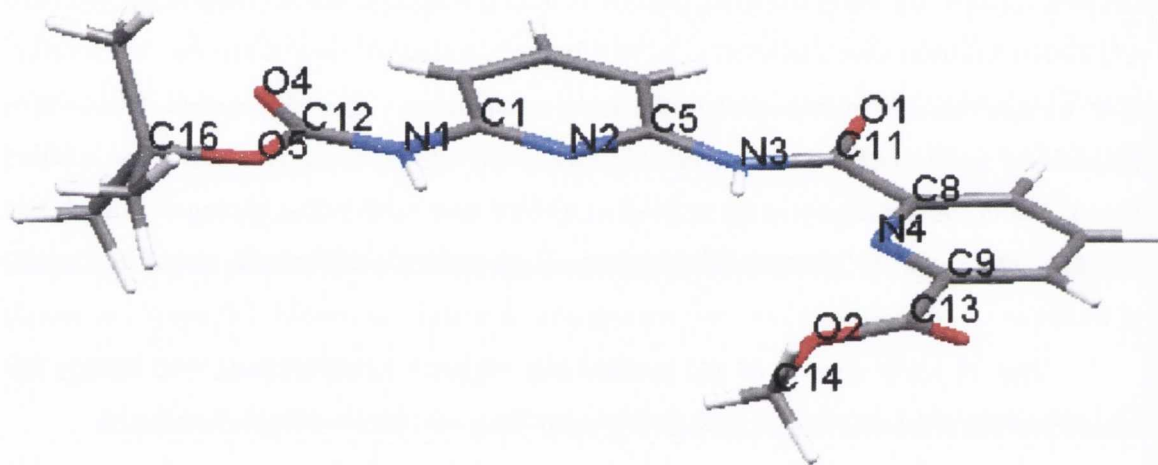


Figure 5.14 A view of the crystallographic *b** axis of **107**.

As for the crystal structure of **98**, the angle between the relatively planar pyridine aromatic rings was calculated from the three torsion angles that connect the pyridine units: $-1.28^\circ - 0.56^\circ + 1.48^\circ = -0.36^\circ$. This resulted in a small rise between the pyridine units. Selected bond lengths, angles and torsion angles can be found in *Table A4.2* in *Appendix 4*. Furthermore, as shown in Figure 5.15 the angle formed between the two amide protons is 130° . These results indicate that this configuration of the 2,6-diaminopyridine units would span 360° after 7 units ($360^\circ / 50^\circ = 7.2$).

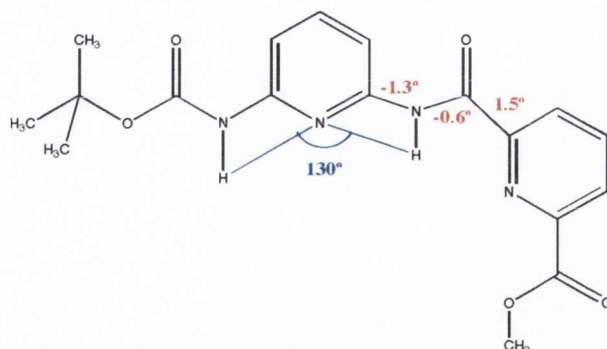
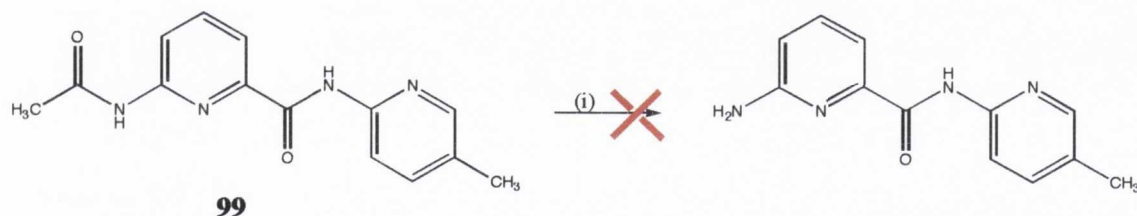


Figure 5.15 Flattened drawing of the crystal structure of **107**. Red numbers alongside bonds are torsional deviations from the planarity about these bonds. Positive torsion angles indicate clockwise rotation for the most distant end of a bond when sighting along the bond. Blue numbers indicate the angle between the amide nitrogen atoms.

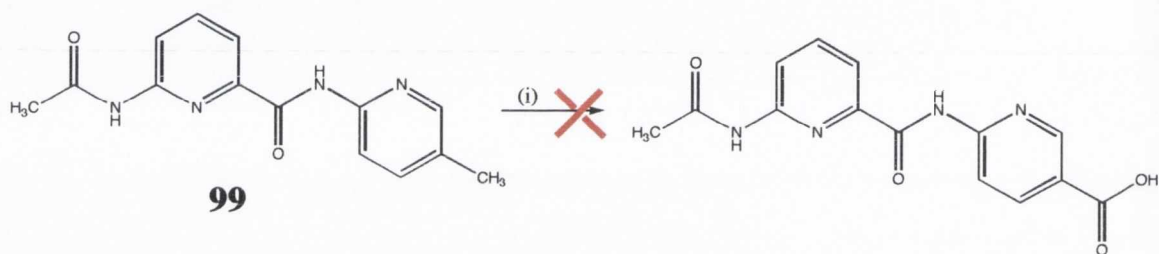
After successfully synthesising di-peptides **98-101**, **104** and **107**, attempts were carried out to develop tri-peptides, containing **98-101**. As previously discussed at the beginning of this section, the synthesis involved deprotecting either the amino end of the di-peptide or to oxidise the methyl group to a carboxylic acid. As shown in Scheme 5.11, in an attempt to remove the *N*-acetyl protecting group, the di-peptide **99** was refluxed in an equal mixture of concentrated HCl and H₂O overnight.



Scheme 5.11 The proposed removal of the *N*-acetyl protecting group. Reagent and conditions: 1:1 concentrated HCl/H₂O, reflux.

The reaction mixture was then neutralised by the addition of concentrated NaOH and subsequently extracted with EtOAc. Upon removal of the organic solvent under reduced pressure, a white solid was obtained. However, according to ¹H NMR analysis, the presence of only a triplet and two doublets in the aromatic region between 8.0-7.1 ppm, indicated that the harsh acidic conditions cleaved the amide bond and thus the 2,6-substituted pyridine unit was obtained. Due to time restraints, milder acidic conditions were not further investigated for the synthesis of this target molecule.

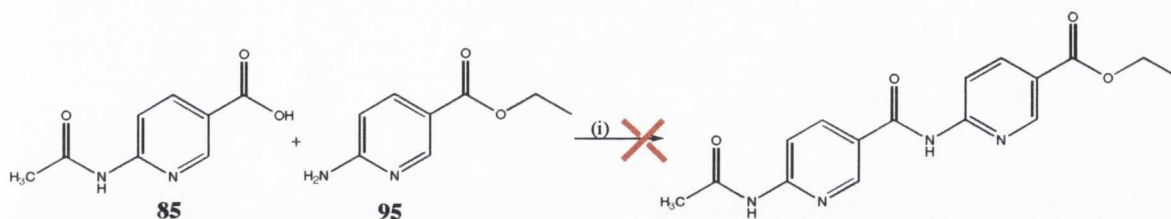
The oxidation of the methyl group of compound **99** was also carried out in a similar manner as for compounds **84** and **85** by using KMnO_4 as shown in Scheme 5.12. However, the di-peptide **99** was shown to be insoluble in water and continuous addition of NaOH was needed to dissolve **99**. The resulting solution was heated at $90\text{ }^\circ\text{C}$ and KMnO_4 was gradually added over a range of 15 minutes. However, the solution remained purple in colour after refluxing overnight. Furthermore, there were no apparent signs of manganese(IV), which indicated that the oxidation reaction had not taken place. The use of different oxidising reagents were also investigated, such as K_2CrO_7 that can be employed under more acidic conditions. However, these reaction conditions did not show the formation of the carboxylic acid group according to ^1H NMR. Consequently, the methyl group in **99** was unable to undergo oxidation.



Scheme 5.12 The proposed oxidation of **99**. Reagents and conditions: (i) KMnO_4 , NaOH , H_2O , reflux.

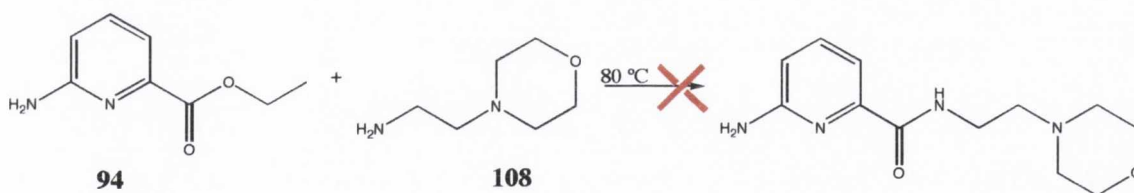
However, at this stage of the investigation, it was decided to synthesise a different di-peptide by coupling the 2-amino-picolinic acid esters **94** and **95** to an *N*-acetyl-2-aminopicolinic acid derivatives **84** and **85**. This would yield a ester protected di-peptide that would potentially be deprotected under milder conditions than those previously attempted. Similar reactions as for the synthesis of di-peptides **98-101** were employed, by using coupling reagents DCC and EDCI in the presence of HOBt. Compounds **85** and **95** were dissolved in THF along with HOBt and DMAP as depicted in Scheme 5.13. The procedure involved adding EDCI to this solution of at $0\text{ }^\circ\text{C}$ and the reaction was allowed to stir overnight at room temperature. A precipitate formed after overnight reaction that was filtered off. The solvent was removed under reduced pressure and the residue was redissolved in CH_2Cl_2 . The organic phase was washed with water and saturated NaHCO_3 , resulting in a yellow solid, identified as compound **95** by ^1H NMR analysis (DMSO- d_6 , 400 MHz). Furthermore, the precipitate that crashed out of the reaction mixture was also identified as compound **85** by ^1H NMR analysis (DMSO- d_6 , 400 MHz). These results suggested that the insolubility of **85** in THF was the cause of the apparent absence of di-

peptide formation. However, due to time restraints, this work could not be continued any further.



Scheme 5.13 The proposed coupling of **85** and **95**. Reagents and conditions: (i) EDCI, HOBt, DMAP, THF, room temperature.

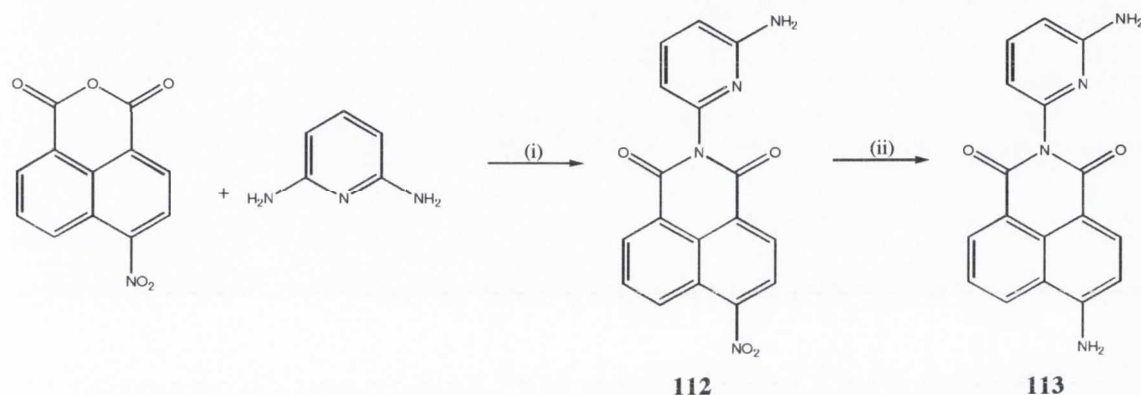
As discussed in Section 5.1, the ultimate objective of this research was to cap these pyridine polyamides with molecules that could enhance water solubility or to increase their binding affinity with DNA. The first approach taken, shown in Scheme 5.14, involved heating compound **94** with 4-(2-aminoethyl)morpholine **108** at 80 °C overnight. The reaction was then poured onto ice and stirred, resulting in a precipitate, which was collected. However, ^1H NMR analysis of this precipitate only showed the presence of unreacted **94**, indicating that higher temperature and longer reaction time might be required for the formation of the target molecule.



Scheme 5.14 The proposed synthesis of a morpholine-based pyridine derivative.

Similarly, when the 2,6-dimethyl pyridine ester **109** was treated with 2-aminoethanol **110** at 100 °C in toluene, this resulted in the formation of the pyridine mono-ester **111** after purification by column chromatography using flash silica (5/95 MeOH/CH₂Cl₂) in 5% yield. The benefit of the alcohol moiety is that it could be functionalised with a protonated group, thus enhancing water solubility and DNA binding affinity as discussed above.

diaminopyridine with 4-nitro-1,8-naphthalic anhydride in pyridine and refluxing the reaction mixture for 12 hours. Upon completion of the reaction, the solution was cooled and then poured into water to give a pale yellow precipitate, which was filtered and washed with methanol and water. This gave rise to the successful formation of **112** in 94% yield, without the need for further purification. The full characterisation of this compound by ^1H , ^{13}C and IR spectroscopy can be found in the experimental Chapter 6.



Scheme 5.16 The synthesis of **112** and **113**. Reagents and conditions: (i) Pyridine, reflux, (ii) 10% Pd/C, 3 Atm.

Following this, the catalytic hydrogenation of **112** to form the corresponding 4-amino-1,8-naphthalimide derivative was carried out overnight in DMF using 10% Pd/C over 4 Atm H_2 . This resulted in the formation of the amino derivative **113** in quantitative yield and in good purity according to ^1H NMR analysis (DMSO- d_6 , 400 MHz). Unfortunately, due to time restraints biological investigation of these compounds could not be carried out.

5.4 Conclusion and Future Studies

In this chapter, many different approaches for synthesising pyridine building blocks and pyridine-based polyamides were discussed. Section 5.2, described the successful synthesis of the proposed building blocks for the polyamide synthesis, namely the amino protected pyridine carboxylic acid derivatives **84** and **85** and the carboxylic acid protected pyridine derivatives **94** and **95**.

In Section 5.3, compounds **84** and **85** were coupled with 2-amino-picoline derivatives to give the di-peptides **98-101**, by using conventional peptide coupling reagents, DCC and EDCI. The apparent insolubility of the *N*-acetyl-2-amino-picolinic acid

derivatives **84** and **85** was believed to be responsible for the relatively low yields obtained. Nonetheless, a crystal structure of **99** indicated that the pyridine units were opposite to each other, with one nitrogen from the pyridine ring facing inwards and the other one outwards. This indicated that these types of di-peptides could potentially offer a specific interaction to A base due to the steric clash between the hydrogen from the pyridine and the carboxyl group from T. Furthermore, the other pyridine unit could potentially be used to bind the NH₂ of the G base. This speculative binding by **99** to DNA is shown in Figure 5.17 A. However, it has to be noted that the crystal structure represents the lowest energy conformation in a solid structure.

In addition to these results, other binding motifs were synthesised that would offer a different mode of binding to DNA. The urea-based di-pyridine **104** was synthesised in considerably good yields from 2-amino-6-picoline. This binding motif could potentially bind to T, through the urea bond between the pyridine units as depicted in Figure 5.17 B.

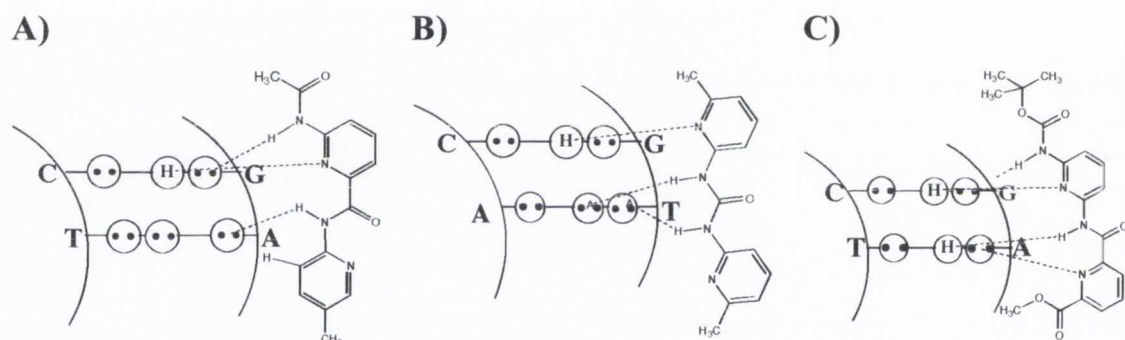


Figure 5.17 The proposed binding of A) di-peptide **99**, B) urea based di-pyridine **104** and C) di-peptided **107**.

The third di-peptide motif **107**, was synthesised by connecting 2,6-diaminopyridine and 2,6-pyridine carboxylic acid. Compound **107** was obtained by using DCC as a coupling reagent, in a similar manner to the synthesis of **98-101**. The crystal structure of **107** showed that the pyridine units faced the same way and both nitrogen atoms were available to hydrogen bond to minor groove of DNA. Furthermore, this binding motif potentially offers specific interactions with two neighbouring G bases as shown in Figure 5.17 C.

In conclusion, the results discussed in this chapter show that the pyridine unit could potentially be used to target specific sequences of DNA. Furthermore, these pyridine derivatives have also been shown to be compatible with numerous capping moieties, such as the 1,8-naphthalimide chromophore that could increase the binding affinity of the

polyamide units. However, future studies will include DNA binding studies of these dipeptides, by using UV/Vis spectroscopy and T_m studies. In addition, investigation into different means of elongating the pyridine peptide chain will be undertaken.

6 Experimental Procedures

6.1 Biological Assay

6.1.1 Cell Lines and Compounds

All cell lines were obtained from the American Type Culture Collection. HL-60 and K562 cells were cultured in RPMI-1640 medium with Glutamax-1™ (GIBCO # 61870) supplemented with 10% fetal bovine serum, 20 U/mL penicillin and 50 µg/mL streptomycin. HeLa Cells were cultured in Dulbecco's Modified Eagle's Medium (DMEM, GIBCO # 31966) with same supplements as above. All cells were maintained in 5% CO₂ at 37 °C.

6.1.2 Investigation of the Cell Morphology¹⁹²

Cells (1×10^6) were seeded in the presence or absence of a drug for an indicated amount of time. A part of them (about 20000 cells) were centrifuged on a glass slide (700 rpm, 2 minutes) and dried. Then they were fixed using 90% EtOH and again allowed to dry. Next, the cytoplasm was stained using haemotoxylin and after drying the nucleus was stained with eosin, washed with water and dried before investigating using a bright light microscope.

6.1.3 Toxicity Studies Using the MTT Survival Assay

The effects from various concentrations of compounds on the proliferation of the HL60, K562 and HeLa cells were assessed using the MTT proliferation assay Kit I (Roche). Cells were seeded at a density of 1×10^6 for HL-60 cells or 1×10^4 for K562 and HeLa cells in a 96 well microplate. They were then incubated at 37 °C in the presence of 5% CO₂ for 24 hours before being incubated with selected medium (RPMI with FCS and penicillin-streptomycin or DMSO) or the various concentration of the investigated compound. After a specific incubation period, the MTT reagent was added and the micro plate was further incubated for 4 hours. Next, solubilisation solution was added and the micro plate was incubated for another 4 hours before measuring the spectrophotometrical absorbance using a micro plate ELISA plate reader. The absorbance wavelength used was at 595 nm and the reference filter was at 690 nm. To determine the EC₅₀ values, the results were then analyzed with Prism GraphPad software (San Diego), using sigmoidal dose-response analysis parameters. Furthermore, the cytotoxic parameters GI₅₀, TGI and LD₅₀,

were used to calculate the percentage growth inhibition at each of the concentrations using equations 2.1 or 2.2,

$$Ti \geq Tz, (Ti-Tz)/(C-Tz) \times 100\% \quad (\text{Eq. 2.1})$$

or

$$Ti < Tz, (Ti-Tz)/Tz \times 100\% \quad (\text{Eq. 2.2})$$

where **Ti** is the absorbance from wells that holds treated cells, **Tz** is the absorbance from cells at the time of treatment and **C** is the absorbance from cells that were treated with corresponding vehicles.

6.1.4 Phototoxicity Studies Using the (MTT) Survival Assay

Cells were seeded in a 96-well plate (1×10^5 cells per well) and incubated at 37 °C in a 5% CO₂ incubator for 24 hours before being treated with varying concentrations of PDT agents (from 0.01 μM to 100 μM). The cells were then incubated again at 37 °C in a 5% incubator for 24 hours before being subjected to irradiation with a Xenon lamp (Hamamatsu, Model C2577). Irradiation doses were 2 J/cm², 4 J/cm² and 8 J/cm² as measured with a radiometer (International Light, Model IL1400A). Cells were incubated for 24 or 48 hours at 37 °C in the presence of 5 % CO₂ before they were assessed for cell viability using a standard MTT assay kit as described in Section 6.1.3. Every experiment had controls; cells treated with PDT agents but not irradiated and cells irradiated but not treated with PDT agents. The phototoxicity was determined by comparing the effects of the drug to the effects from untreated cells upon irradiation. The data was analysed using Prism GraphPad Software (San Diego), using a sigmoidal dose-response analysis parameters.

6.1.5 Flow Cytometry Studies of Cellular Uptake¹⁴⁸

Cells were seeded in a 24 well plate (5×10^4 cells per well) and incubated at 37 °C in the presence of 5% CO₂ for 24 hours before being treated with corresponding agent. At various times (15 min, 30 min, 60 min, 9 hours, 24 hours and 48 hours), cells were collected and washed three times with PBS. Samples were analyzed by flow cytometry (BD FACSCalibur System), using the FL-2 or FL-3 channels to detect fluorescence and the highest peak in the emission channel was recorded. The data was further analyzed with CellQuest software.

6.1.6 Flow Cytometry Studies of Mitochondrial Membrane Potential¹⁹²

Cells were seeded in a 6 well plate (2.5×10^5 cells per well) and incubated at 37 °C in the presence of 5% CO₂ for 24 hours before being treated with 10 μM of PDT agents. The cells were then incubated along with the PDT agents for 24 hours at 37 °C in the presence of 5% CO₂ before being irradiated with a Xenon lamp (Hamamatsu, Model C2577) to give 8 J/cm² light dose. After irradiation, cells were incubated for either 24 or 48 hours. Cells were stained with JC-1 (final concentration 2 μM) and samples incubated for 30 minutes at 37 °C in the presence of 5% CO₂. Cells were then collected and centrifuged (1300 rpm for 3 minutes) and washed twice with PBS. Samples were centrifuged again and resuspended in FACSFlow solution (500 μL) before being analysed by flow cytometry (BD FACSCalibur system). The fluorescence intensity was detected by the FL-2 channel and the data was further analysed using the CellQuest software.

6.1.7 Flow Cytometry Studies of Reactive Oxygen Species¹⁹²

Cells were seeded in a 6 well plate (2.5×10^5 cells per well) and incubated at 37 °C in the presence of 5% CO₂ for 24 hours before being treated with 10 μM of PDT agents that were discussed in *Chapter 4*. The cells were then incubated along with the PDT agents for 24 hours at 37 °C and in the presence of 5% CO₂ before being irradiated. Irradiation doses were 4 J/cm² and 8 J/cm². After irradiation, cells were incubated for a further 48 hours. Cells were stained with dihydroethidium (final concentration 2 μM) and samples incubated for 20 minutes at 37 °C in the presence of 5% CO₂. Cells were then collected and centrifuged (1300 rpm for 3 minutes) and washed twice with PBS. Samples were centrifuged again and resuspended in FACSFlow solution (500 μL) before being analysed by flow cytometry (BD FACSCalibur system) using the software CellQuest. The fluorescence intensity in FL-2 was collected.

6.1.8 Confocal Laser Scanning Microscopy

Cells (1×10^4 cells per well) were seeded in a 8 chambered slide (LAB-TEK) and incubated for 24 hours at 37 °C in the presence of 5% CO₂. Cells were then incubated with 10 μM of the investigated compound as discussed in *Chapters 3 and 4* for 24 hours. As discussed in *Chapter 3*, K562 cells were centrifuged to a glass slide and then fixed with 90% EtOH. A coverslip was mounted onto the glass slide. In *Chapter 4*, HeLa cells were incubated with Hoechst 33342 (0.5 μM) for 15 minutes before the excess probe was

removed and the cells washed with PBS. Cells were then fixed with Cellfix (BD BioScience) for 35 minutes. Cells were then washed once with PBS and mounting fluid and a coverslip was placed onto the glass slide.

Image analysis were performed on a LSM510 Laser Scanning Microscopy (Zeiss) using a 63x magnification. Compounds **68-70**, discussed in *Chapter 3*, were excited at 488 nm by an argon laser and their fluorescence was detected by a 500-530 nm bandpass filter. Compounds **74-77**, discussed in *Chapter 4*, were excited at 405 nm by a diode laser and their fluorescence emission was detected by a 650 nm longpass filter. Hoechst 3342 was excited at 405 nm and its fluorescence was detected by a 470-500 bandpass filter.

6.1.9 Cell Cycle Analysis Using Flow Cytometry¹⁹²

Cells were treated with compounds for either 24 or 48 hours in a 6 well plate. At the desired time, untreated and drug-treated cells were harvested by centrifugation, rinsed with PBS (1 mL) and fixed with 90 % ethanol (2.5 mL) for 30 minutes at 4 °C. After washes with PBS, the cells were stained with propidium iodide (final concentration 25 µg/mL) and treated with RNase (25 µL) for 30 minutes at 37 °C. The cells were then analysed by flow cytometry (BD FACSCalibur System) and the fluorescence from propidium iodide bound to DNA was detected by the FL-2 detector. The data obtained was further analysed using the CellQuest software.

6.1.10 Immunoblotting

HL-60 cells (1×10^4) were incubated in the absence or presence of a drug for 24 hours. They were then harvested by centrifugation (1300 rpm, 3 minutes, 25 °C) and resuspended in ice cold PBS and centrifuged again (1300 rpm, 3 minutes, 25 °C). They were resuspended in RIPA lysis buffer (Pierce Biotechnology) and kept on ice for 20 minutes. They were then harvested by centrifugation again (12000 rpm, 20 minutes, 4 °C) and the supernatant retained and kept at -70 °C until needed. Protein concentration was measured using the Bradford method. Cell lysates containing equal amount of protein (20 µg/µL) were boiled in a SDS sample buffer for 5 minutes before loading on a 10% SDS-polyacrylamide gel. Gels were run in a running buffer for about 1 hour at 200 V or until the ladder reached the end. Then proteins were transferred to a PVDF membrane in a transfer buffer overnight at 30 V or for 45 minutes at 100 V. Membranes were then activated with methanol and washed for 5 minutes in deionised water. They were then blocked with a 5% dry milk in PBS solution containing 0.05% Tween 20 (PBS-T) for 1 hour and washed three

times with PBS-T before being incubated with specific antibodies against PARP-1 overnight at 4 ° C. After washing three times with PBS-T, PARP-1 was incubated with anti-mouse HRP-labeled secondary mouse antibody (Oncogene). The membrane was washed again with PBS-T and then incubated with a chemiluminescent substrate (Supersignal, Pierce) for 15 minutes before the membrane was exposed to an X-ray film. The film was subsequently developed using a developer (AGFA).

6.2 General Chemical Techniques

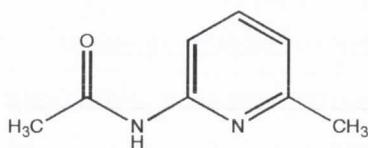
6.2.1 General

All NMR spectra were recorded using a Brüker DPX-400 Avance spectrometer, operating at 400.13 MHz for ^1H NMR and 100.6 MHz for ^{13}C NMR, or a Brüker AV-600 spectrometer, operating at 600.1 MHz for ^1H NMR and 150.2 MHz for ^{13}C NMR. Shifts are referenced relative to the internal solvent signals. Electrospray mass spectra were recorded on a Micromass LCT spectrometer, running Mass Lynx NT V 3.4 on a Waters 600 controller connected to a 996 photodiode array detector with HPLC-grade methanol or acetonitrile. High resolution mass spectra were determined by a peak matching method, using leucine Enkephalin, (Tyr-Gly-Gly-Phe-Leu), as the standard reference ($m/z = 556.2771$). Melting points were determined using an IA9000 digital melting point apparatus. Infrared spectra were recorded on a Perkin Elmer Spectrum One FT-IR spectrometer fitted with a Universal ATR Sampling Accessory. X-Ray diffraction studies were carried out by Dr. Thomas McCabe (School of Chemistry, Trinity College Dublin) using a Brüker SMART APEX single crystal CD diffractometer. Elemental analysis was conducted at the Microanalytical Laboratory, School of Chemistry and Chemical Biology, University College Dublin. However, it has to be noted the researcher had difficulties obtaining elemental analysis due to the hygroscopic nature of the compounds synthesised during this p.H.D work.

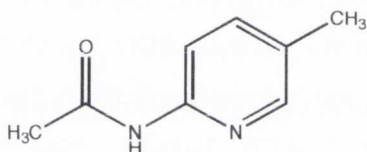
6.2.2 Materials

All reagents and solvents were purchased commercially and used without further purification unless otherwise stated. Anhydrous solvents were prepared using standard procedures, according to Vögel, with distillation under argon prior to each use. Chromatographic columns were run using Silica gel 60 (230 – 400 mesh ATSM). Analytical TLC was performed using Merck Kieselgel 60 F₂₅₄ silica gel plates.

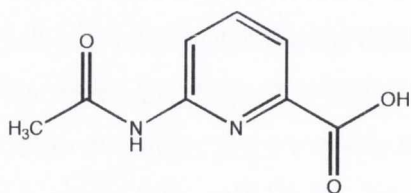
6.3 Synthesis and Characterisation of Compounds Described in Chapter 5

***N*-acetyl-2-amino-6-picoline (82)¹⁹⁸**

2-Amino-6-picoline (10 g, 92 mmol) was dissolved in toluene and acetic anhydride (17 mL, 184 mmol) was added to the solution. The reaction mixture was heated at 95 °C for 4 hours. The excess acetic anhydride and the solvent were then evaporated under reduced pressure. The desired product was obtained as a white solid (13 g, 89 mmol, 96%) after recrystallisation from methanol. m.p. 65-67 °C (Ref. 62 °C); ¹H NMR δ_H (400 MHz, CDCl₃): 10.4 (1H, br s, NH), 8.15 (1H, d, *J* = 8.5 Hz, Ar-H), 7.66 (1H, t, *J* = 8.5, 7.6 Hz, Ar-H), 6.90 (1H, d, *J* = 7.1 Hz, Ar-H), 2.45 (3H, s, Ar-CH₃), 2.15 (3H, s, COCH₃); ¹³C NMR δ_C (100 MHz, CDCl₃): 169.4, 156.6, 151.8, 138.6, 118.6, 110.4, 23.7, 21.2; Accurate MS (m/z) Calculated: 173.0698 (M+Na)⁺, Found: 173.0691; IR ν_{max} (cm⁻¹): 3240 (NH), 1699 (CO-NH).

***N*-acetyl-2-amino-nicoline (83)**

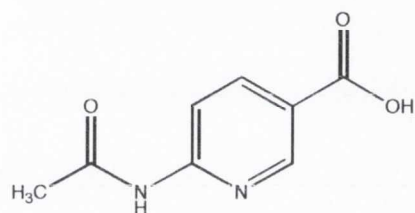
2-Amino-6-picoline (2.0 g, 19 mmol) was dissolved in toluene and acetic anhydride (4.5 mL, 47 mmol) was added to the solution. The reaction mixture was heated at 95 °C overnight. The excess acetic anhydride and the solvent were then evaporated under reduced pressure. The desired product was obtained as a yellowish coloured needles (2.5 g, 17 mmol, 89%) after recrystallisation from EtOAc. m.p. 60-62 °C; ¹H-NMR δ_H (400 MHz; CDCl₃): 10.1 (1H, s, NH), 8.23 (1H, d, *J* = 8.8 Hz, Ar-H), 7.93 (1H, dd, *J* = 1.4; 0.6 Hz, Ar-H), 7.60-7.57 (1H, m, Ar-H), 2.29 (3H, s, Ar-CH₃), 2.13 (3H, s, CH₃-CO) ¹³C NMR δ_C (100 MHz; CDCl₃): 169.4, 149.6, 145.6, 140.1, 128.9, 114.3, 24.4, 17.8; Accurate MS (m/z) Calculated: 151.0878 (M+H)⁺, Found: 151.0871; IR ν_{max} (cm⁻¹): 3008 (NH), 1694 (s, C=O).

***N*-acetyl-2-amino-6-picolinic acid (84)¹⁹⁸**

NaOH (0.95 g, 24 mmol) and compound **82** (5.00 g, 23.8 mmol) were dissolved in H₂O (20 mL). To this solution KMnO₄ (17 g, 36 mmol) was added in small increments over 2 hours. The reaction was allowed to stir overnight at 90 °C. The reaction was then filtered through a sinter funnel and washed

with hot H₂O. The solvent was reduced to about 1/3 and the resulting solution was first acidified to pH \approx 1.5 using concentrated HCl and then basified to pH \approx 4 using saturated NaHCO₃. White crystals (2.6 g, 15 mmol, 62%) were obtained after filtration and recrystallisation with CH₂Cl₂. m.p. 213-216 °C (ref., 216 °C); ¹H NMR δ_{H} (400 MHz, DMSO-d₆): 10.8 (1H, br s, NH), 8.76 (1H, d, J = 8.5 Hz, Ar-H), 7.92 (1H, t, J = 8.1, 8.0 Hz, Ar-H), 7.74 (1H, d, J = 7.6 Hz, Ar-H), 2.14 (3H, s, CH₃); ¹³C NMR δ_{C} (100 MHz, DMSO-d₆): 169.8, 165.9, 152.1, 146.9, 139.4, 120.1, 116.9, 23.9; Accurate MS (m/z) Calculated: 203.0431 (M+Na)⁺, Found: 203.0433; IR ν_{max} (cm⁻¹): 3217 (NH), 2980 (OH), 1723 (C=O), 1692 (CO-NH).

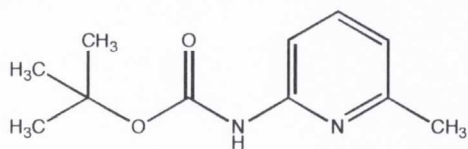
N-acetyl-2-amino-5-picolinic acid (85)



Compound **83** (2.2 g, 15 mmol) was dissolved in H₂O (20 mL). To this solution KMnO₄ (6.3 g, 40 mmol) was added in small increments over 2 hours. The reaction was allowed to stir overnight at 90 °C. The reaction was then filtered through a sinter funnel and washed with

hot H₂O. The solvent was reduced to about 1/3 and the resulting solution was first acidified to pH \approx 1.5 using concentrated HCl and then basified to pH \approx 4 using saturated NaHCO₃. White crystals (1.2 g, 6.6 mmol, 45%) were obtained after filtration and recrystallisation with CH₂Cl₂. m.p. 216-218 °C; ¹H-NMR δ_{H} (400 MHz; DMSO-d₆): 10.6 (1H, s, NH), 8.71-8.70 (1H, m, Ar-H), 8.10 (1H, dd, J = 8.5; 2.2 Hz, Ar-H), 7.95 (1H, d, J = 8.4 Hz, Ar-H), 2.08 (3H, s, CH₃-CO); ¹³C NMR δ_{C} (100 MHz, DMSO-d₆): 169.6, 165.6, 151.8, 145.9, 140.0, 120.8, 116.0, 23.7; IR ν_{max} (cm⁻¹): 3268 (NH), a 2981 (OH), 1723 (C=O).

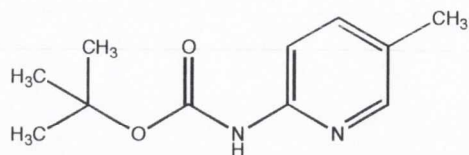
(6-Methyl-pyridin-2-yl)-carbamic acid tert-butyl ester (86)^{206,207}



2-Amino-6-picoline (1.1 g, 10 mmol) and di-*tert*-butyl-dicarbonate (3.3 g, 15 mmol) were stirred overnight at 60 °C. The reaction was cooled down and the product was obtained as a clear liquid. (1.8 g, 8.9 mmol, 89%) after purification using chromatography silica column and hexane as the eluent. ¹H NMR δ_{H} (400 MHz, CDCl₃): 7.93 (1H, br s, NH), 7.71 (1H, d, J = 8.4 Hz, Ar-H), 7.53 (1H, t, J = 7.8 Hz, Ar-H), 6.78 (1H, d, J = 7.6 Hz, Ar-H), 2.42 (3H, s, Ar-CH₃), 1.48 (9H, s, C(CH₃)₃), ¹³C NMR δ_{C} (100 MHz, CDCl₃): 156.2, 152.0, 150.7, 146.3, 138.1, 117.5, 108.6, 84.7, 80.3, 27.8,

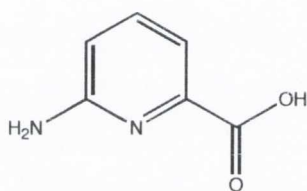
27.0; Accurate MS (m/z) Calculated: 231.1120 ($M+Na$)⁺, Found: 231.1109; IR ν_{\max} (cm^{-1}): 3384 (NH), 1697 (C=O).

(5-Methyl-pyridin-2-yl)-carbamic acid tert-butyl ester (87)



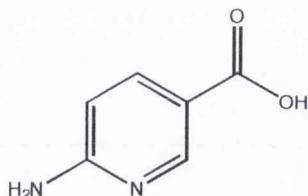
87 was prepared using the same procedure as for **86**. The product was obtained as a white crystalline solid (1.7 g, 8.2 mmol, 98 %). m.p. 130-132 °C; ¹H NMR δ_{H} (400 MHz, CDCl_3), 9.27 (1H, s, NH), 8.90 (1H, s, Ar-H), 7.91 (1H, d, $J = 8.4$ Hz, Ar-H), 7.50 (1H, dd, $J = 8.4, 2.00$ Hz, Ar-H), 2.27 (3H, s, Ar- CH_3), 1.56 (9H, s, $\text{C}(\text{CH}_3)_3$); ¹³C NMR δ_{C} (100 MHz, CDCl_3); 149.5, 148.5, 146.9, 138.5, 126.7, 111.5, 84.7, 82.4, 80.1, 27.9, 27.4; Accurate MS (m/z) Calculated: 209.1288 ($M+H$)⁺, Found: 209.1290; IR ν_{\max} (cm^{-1}): 3172 (NH), 1716 (C=O).

6-aminopicolinic acid (88)²⁰⁸



84 (6.0 g, 33 mmol) was dissolved in 10 % aqueous NaOH. The resulting solution was heated to reflux for 6 hours. Afterward, it was cooled in an ice bath and acidified to a pH of 4-5 by adding concentrated HCl. The resulting white precipitate was filtered and washed with cold water and ether to give a white solid (2.7 g, 19 mmol, 58%). m.p. 319-321 °C (Ref. 320 °C); ¹H NMR δ_{H} (400 MHz, $\text{D}_2\text{O}/\text{NaOD}$): 7.49 (1H, t, $J = 7.8$ Hz, Ar-H), 7.11 (1H, d, $J = 7.6$ Hz, Ar-H), 6.64 (1H, d, $J = 8.0$ Hz, Ar-H); ¹³C NMR δ_{C} (400 MHz, $\text{D}_2\text{O}/\text{NaOD}$): 172.3, 157.92, 151.08, 138.81, 113.81, 111.52; IR ν_{\max} (cm^{-1}): 3361 (NH_2), 1700 (s, C=O).

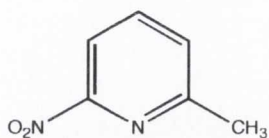
6-aminonicotinic acid (89)²⁰⁹



85 (2.0 g, 11 mmol) was dissolved in 10% aqueous NaOH and the resulting solution was refluxed for 6 hours. The solution was then cooled in an ice bath and acidified with concentrated HCl to a pH \approx 4. The resulting white precipitate was filtered off and washed with ether, which was dried in vacuo over P_2O_5 (0.7 g, 5 mmol, 46%). m.p. 245-247 °C (Ref. 244-246 °C); ¹H NMR δ_{H} (400 MHz, $\text{D}_2\text{O}/\text{NaOD}$): δ 8.30 (1 H, d, $J = 2.0$ Hz, Ar-H), 7.82 (1 H, dd, $J = 8.6$ Hz, 2.2 Hz, Ar-H), 6.53 (1 H, d, $J = 8.8$ Hz, Ar-H); ¹³C NMR δ_{C} (100 MHz, $\text{D}_2\text{O}/\text{NaOD}$): 173.6, 159.9, 148.6,

139.0, 121.4, 108.2; IR ν_{\max} (cm^{-1}): 3275 (m, C-NH₂), 2982 (m, CO-OH), 1664 (s, C-CO-OH).

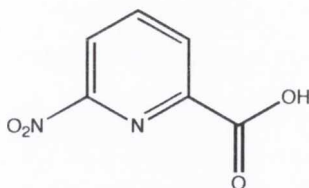
2-nitro-6-picoline (90)²⁰⁰



2-amino-6-picoline (3.0 g, 28 mmol) was dissolved in concentrated H₂SO₄ (10 mL) and the temperature was maintained at 15 °C. A mixture of 35% hydrogen peroxide (15 mL) and 30% fuming H₂SO₄ (50 mL) was added and the temperature maintained at 15 °C

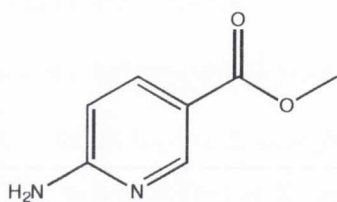
for 3 hours. The mixture was then stirred for further 48 hours at room temperature. The reaction was poured onto ice (200 mL) and the solution was neutralized with concentrated NaOH. The solution was extracted with diethyl ether (4 x 50 mL) and the organic solvent was dried with MgSO₄. Evaporation of the solvent resulted in a yellow solid (2.4 g 18 mmol, 63 %). m.p. 111-113 °C (Ref. 113-114 °C); ¹H NMR δ_{H} (400 MHz, CDCl₃): 8.08 (1H, d, *J* = 8.0 Hz, Ar-H), 7.94 (1H, t, *J* = 7.8 Hz, Ar-H), 7.56 (1H, d, *J* = 7.6 Hz, Ar-H), 2.71 (3H, s, CH₃). ¹³C NMR δ_{C} (400 MHz, CDCl₃): 158.8, 139.4, 134.7, 128.6, 114.6, 23.8; Accurate MS (*m/z*) Calculated: 151.0878 (M+H)⁺, Found: 151.0871; IR ν_{\max} (cm^{-1}): 1537 (NO₂), 1356 (NO₂).

2-nitro-picolinic acid (91)²⁰¹

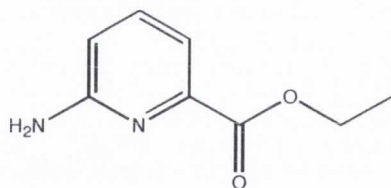


Compound **90** (1.3 g, 9.1 mmol) and water were heated to 90 °C and treated with KMnO₄ (2.4 g, 15 mmol) over a period of one hour. The reaction mixture was allowed to reflux overnight. The resulting brown solution was filtered and the filtrate reduced to

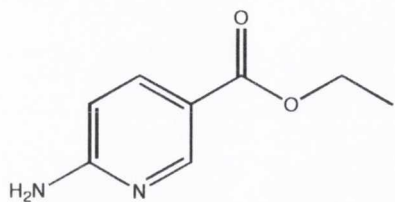
about a third under reduced pressure. The resulting solution was extracted with diethyl ether to recover unreacted starting material. The pH of the aqueous solution was set to ~ 4 using concentrated H₂SO₄ and the precipitate was filtered off and dried resulting in a white precipitate (0.16, 0.95 mmol, 10%). m.p. 168-170 °C (Ref. 168 °C); ¹H NMR δ_{H} (400 MHz, CDCl₃): 8.65 (1H, dd, *J* = 7.6; 0.8 Hz, Ar-H), 8.57 (1H, dd, *J* = 8.0; 0. Hz, Ar-H), 8.38 (1H, t, *J* = 8.0 Hz, Ar-H); ¹³C NMR (400 MHz, CDCl₃): δ 164.50, 156.02, 147.62, 142.52, 130.24, 121.31; Accurate MS (*m/z*) Calculated: 191.0077 (M+H)⁺, Found: 191.0069; IR ν_{\max} (cm^{-1}): 2888 (OH), 1699 (C=O), 1540 (NO₂), 1268 (NO₂).

Methyl 6-aminonicotinate (93)

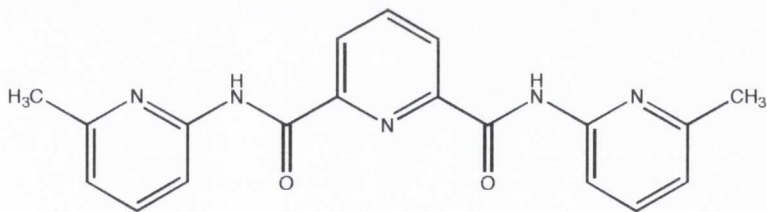
A round bottom flask, fitted with a drying tube was charged with **89** (0.50 g, 3.6 mmol), which was partially dissolved in CHCl_3 . Excess oxalyl chloride was added at room temperature and the reaction mixture was stirred for 2 hours at room temperature and then heated at 45 °C for 4 days. The solvent was evaporated under reduced pressure and the residue was dried under vacuum for 1 hour. Methanol was added to this solid material and this solution was refluxed overnight. The solvent was removed and the residue was suspended in a mixture of water (25 mL) and saturated sodium bicarbonate (20 mL). The aqueous suspension was then extracted with diethyl ether and the ether extracts were dried over anhydrous MgSO_4 . The solution was concentrated and crystals formed overnight (0.19 g, 1.3 mmol, 35%). m.p 151-153 °C; ^1H NMR δ_{H} (400 MHz, DMSO-d_6): 8.49 (1H, d, $J = 2.0$ Hz, Ar-H), 7.82 (1H, dd, $J = 8.8$; 2.4 Hz, Ar-H), 6.86 (2H, s, NH_2), 6.46 (1H, d, $J = 8.8$ Hz, Ar-H), 3.75 (3H, s, CH_3); ^{13}C NMR 165.8, 162.4, 151.0, 137.7, 113.3, 107.2, 51.5; IR ν_{max} (cm^{-1}): 3384 (NH_2), 3145 (Aliphatic CH), 1691 ($\text{C}=\text{O}$), 1592 (Pyridine).

Ethyl 6-aminopicolinate (94)²⁰²

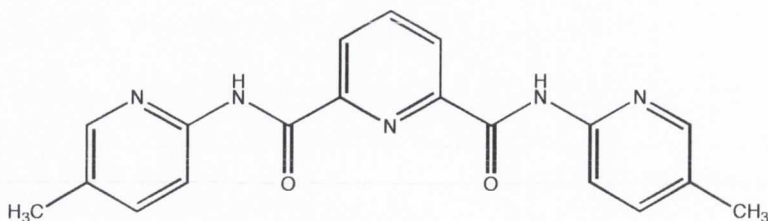
84 (1.0 g, 5.6 mmol) was dissolved in a mixture of H_2SO_4 (3 mL) in 98 % EtOH (20 mL) and the reaction was allowed to reflux overnight. The cooled mixture was then basified with aqueous ammonia and extracted with EtOAc (3 x 20 mL). The organic layer was dried over MgSO_4 , filtered and evaporated to yield white crystals (0.46 g, 2.8 mmol, 50% yield). m.p.144-145 °C; ^1H NMR δ_{H} (400 MHz, DMSO-d_6): 7.52 (1 H, t, $J = 7.8$ Hz, Ar-H), 7.18 (1 H, d, $J = 7.2$ Hz, Ar-H), 6.66 (1 H, d, $J = 8.4$ Hz, Ar-H), 6.32 (2 H, s, NH_2), 4.26 (2 H, q, $J = 7.2$ Hz, CH_2), 1.28 (3 H, t, $J = 7.0$ Hz, Ar-H); ^{13}C NMR δ_{C} (400 MHz, DMSO-d_6): 165.3, 159.6, 145.8, 137.8, 113.2, 112.3, 61.2, 15.1; Accurate MS (m/z) Calculated: 167.0818 ($\text{M}+\text{H}$)⁺, Found: 167.0821; IR ν_{max} (cm^{-1}): 3410 (NH_2), 1686 ($\text{C}=\text{O}$), 1265 ($\text{O}-\text{CH}_2$).

Ethyl 6-aminonicotinate (95)

85 (0.90 g, 4.9 mmol) was dissolved in a mixture of H₂SO₄ (3 mL) in EtOH (20 mL). This reaction was refluxed overnight. The reaction was cooled and then basified with aqueous ammonia. The aqueous layer was then extracted with ethyl acetate (3 x 20 mL) and the organic layer dried over MgSO₄, filtered and the solvent removed under reduced pressure resulting in white solid (0.42 g, 2.5 mmol, 51% yield). m.p. 143-145 °C; ¹H NMR δ_H (400 MHz, DMSO-d₆): 8.50 (1 H, d, *J* = 2.0 Hz, Ar-H), 7.82 (1 H, dd, *J* = 8.8, 2.4 Hz, Ar-H), 6.84 (2 H, s, NH₂), 6.45 (1 H, d, *J* = 8.8 Hz, Ar-H), 4.22 (2 H, q, *J* = 7.2, CH₂), 1.28 (3 H, t, *J* = 7.0, CH₃); ¹³C NMR δ_C (400 MHz, DMSO-d₆): 165.2, 162.4, 150.8, 137.7, 113.5, 107.2, 59.9, 14.3; Accurate MS (*m/z*) Calculated: 167.827 (M+H)⁺, Found: 167.0821; IR ν_{max} (cm⁻¹): 3409 (NH₂), 1689 (C=O), 1269 (O-CH₂)

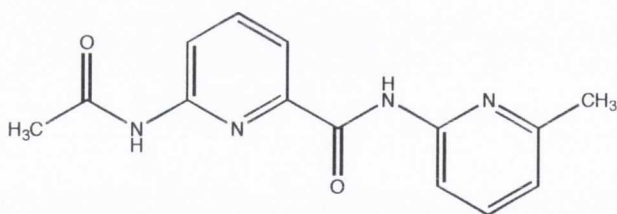
***N,N*-bis(6-methylpyridin-2-yl)pyridine-2,6-dicarboxamide (96)**

The diacid chloride (0.50 g, 3.0 mmol) was formed *in situ* with excess of 2M oxalyl chloride in distilled CH₂Cl₂. The remaining oxalyl chloride was removed and the resulting residue was partly dissolved in CH₂Cl₂ and added to an ice cooled solution of 2-amino-6-picoline (0.81 g, 2.5 mmol) that had been dissolved in CH₂Cl₂. The reaction was then stirred overnight at room temperature. This mixture was extracted with 0.1 M NaOH solution and the organic layer dried over MgSO₄ and filtered. The solvent was then evaporated *in vacuo* and then dried under reduced pressure. The dried solid was recrystallised from EtOAc to give the product as a solid (0.24 g, 0.69 mmol, 23%). m.p. 229-230 °C (REF.); ¹H NMR δ_H (400 MHz, DMSO-d₆): 11.7 (2H, s, CO-NH-Ar), 8.38 (2H, d, *J* = 7.6 Hz, Ar-H), 8.28 (1H, t, *J* = 7.8 Hz, Ar-H), 8.14 (2H, d, *J* = 8.4 Hz, Ar-H), 7.80 (2H, t, *J* = 7.8 Hz, Ar-H), 7.11 (2H, d, *J* = 7.2 Hz, Ar-H), 2.52 (6H, s, Ar-CH₃); ¹³C NMR δ_C (400 MHz, DMSO-d₆): 162.90, 156.8, 151.0, 149.1, 139.7, 138.7, 125.9, 119.6, 112.0, 23.6; Accurate MS (*m/z*) Calculated: 348.1446 (M+H)⁺, Found: 348.1461; IR ν_{max} (cm⁻¹): 3255 (CO-NH-Ar), 1689 (NH-CO-Ar).

***N,N*-bis(5-methylpyridin-2-yl)pyridine-2,6-dicarboxamide (97)**

2,6-dicarboxylic acid (0.50 g, 3.0 mmol), 2-amino-5-picoline (0.81 g, 7.5 mmol), HOBt (0.49 g, 3.6 mmol) and DMAP (0.92 g,

7.5 mmol) were cooled in an ice bath and a mixture of 1/10 DMF/ CH₂Cl₂ was added. This reaction was then stirred overnight at room temperature under argon. The reaction was filtered through celite and the filtrate was concentrated *in vacuo*. The resulting solid was recrystallised from EtOAc and the product was obtained as a white solid (0.13 g, 0.38 mmol, 13%). m.p. 220-221 °C; ¹H NMR δ_H (600 MHz, DMSO-d₆): 11.76 (2H, s, CO-NH-Ar), 8.39 (2H, d, *J* = 7.8 Hz, Ar-H), 8.33 (2H, s, Ar-H), 8.29 (2H, t, *J* = 7.8 Hz, Ar-H), 8.22 (2H, d, *J* = 8.4 Hz, Ar-H), 7.74 (2H, dd, *J* = 8.4; 1.2 Hz, Ar-H), 2.33 (6H, s, CH₃); ¹³C NMR δ_H (150 MHz, DMSO-d₆): 162.9, 149.7, 149.4, 148.1, 140.0, 139.0, 129.6, 126.0, 114.8, 17.7; Accurate MS (m/z) Calculated: 348.1456 (M+H)⁺, Found: 348.1461; IR ν_{max} (cm⁻¹): 3314 (NH), 1692 (C=O).

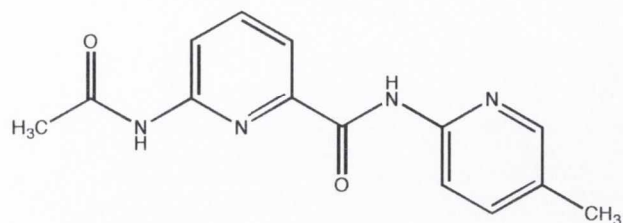
6-Acetylamino-pyridine-2-carboxylic acid (6-methyl-pyridin-2-yl)-amide (98)

Compound **84** (0.28 g, 1.57 mmol) along with 2-amino-6-picoline (0.21 g, 1.88 mmol) and HOBt (0.25 g, 1.84 mmol) were dissolved in DMF. To this solution DCC (0.35 g, 1.67 mmol) was

added at 0 °C. The reaction was stirred overnight under argon at room temperature. The reaction mixture was then kept at 4 °C for 3 hours before filtering it through celite. The solvent was evaporated under reduced pressure and the product was obtained as a white solid dried (0.06 g, 0.22 mmol, 14%) that was dried under high vacuum. m.p. 205-207 °C; ¹H NMR δ_H (400 MHz, DMSO-d₆): 10.9 (1H, s, Ar-NH-CO-Ar), 10.2 (1H, s, Ar-NH-CO-CH₃), 8.34 (1H, d, *J* = 8.4 Hz, Ar-H), 8.11 (1H, d, *J* = 8.0 Hz, Ar-H), 8.03 (1H, t, *J* = 8.0 Hz, Ar-H), 7.86 (1H, d, *J* = 7.6 Hz, Ar-H), 7.77 (1H, t, *J* = 7.8 Hz, Ar-H), 7.05 (1H, d, *J* = 7.2 Hz; Ar-H), 2.43 (3H, s, CO-CH₃), 2.16 (3H, s, Ar-CH₃); ¹³C NMR δ_c (100 MHz, DMSO-d₆), 169.6, 161.6, 157.0, 151.0, 150.0, 146.8, 140.4, 139.0, 119.5, 117.0, 116.9,

110.0, 24.0, 23.6; Accurate MS (m/z) Calculated: 271.1190 (M+H)⁺, Found: 271.1195; IR ν_{\max} (cm⁻¹): 3354 (NH), 3251 (NH), 1689 (C=O), 1668 (C=O), 1449 (Pyridine).

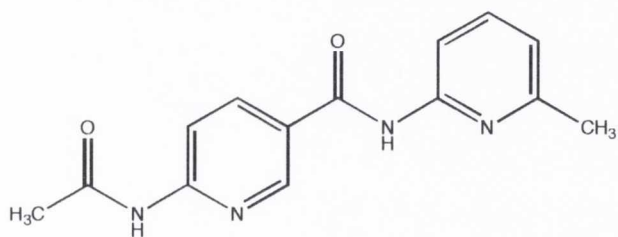
6-acetamido-*N*-(5-methylpyridin-2-yl)picolinamide (99)



84 (0.61 g, 3.4 mmol), 2-amino-5-picoline (0.44 g, 4.1 mmol) and HOBT (0.15 g, 4.0 mmol) were dissolved in DMF. DCC (0.76 g, 3.7 mmol) was dissolved in CH₂Cl₂ and added at 0 °C

under argon. The reaction mixture was stirred for 2 hours and then additional DCC (0.38 g, 1.8 mmol) was added and the reaction allowed to stir overnight at room temperature. The reaction mixture was then filtered through celite and the filtrate was evaporated under reduced pressure. After purification by silica flash column chromatography eluting with 20% EtOAc/ CH₂Cl₂, the product was obtained as a white solid (0.15 g, 0.56 mmol, 16%). m.p. 204-206 °C; ¹H NMR δ_{H} (400 MHz, DMSO-d₆): 10.9 (1H, s, NH-CO-Pyr), 10.4 (1H, s, CO-NH-Me), 8.34 (1H, d, *J* = 8.0 Hz, Ar-H), 8.24 (1H, s, Ar-H), 8.20 (1H, d, *J* = 8.4 Hz, Ar-H), 8.06 (1H, t, *J* = 8.0 Hz, Ar-H), 7.87 (1H, d, *J* = 7.6 Hz, Ar-H), 7.73 (1H, dd, *J* = 8.4; 2.0 Hz, Ar-H), 2.30 (3H, s, Ar-CH₃), 2.16 (3H, s, CH₃-CO); ¹³C NMR δ_{C} (400 MHz, DMSO-d₆): 169.6, 161.4, 156.6, 151.0, 148.2, 146.8, 140.5, 139.0, 119.5, 117.0, 116.9, 110.0, 24.0, 23.6; IR ν_{\max} (cm⁻¹): 3354 (NH), 3252 (NH), 1689 (C=O), 1668 (C=O).

6-acetamido-*N*-(6-methylpyridin-2-yl)nicotinamide (100)

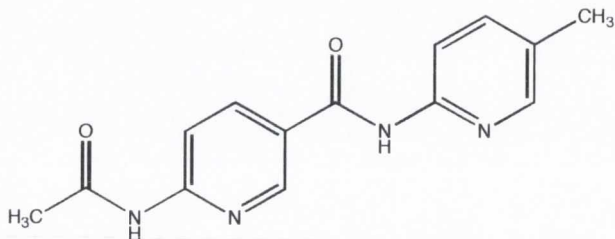


To a stirred solution of **85** (0.18 g, 1.0 mmol), 2-amino nicoline (0.12 g, 1.1 mmol) and HOBT (0.17 g, 1.3 mmol) was suspended in DMF and, DCC (0.26 g, 1.3 mmol) and triethylamine were

added and stirred for 30 minutes at 0–4 °C under argon and then at room temperature overnight. The reaction was filtered through celite and the solvent was evaporated under reduced pressure. After purification by silica flash column chromatography eluting with 20% EtOAc/CH₂Cl₂ → 50% EtOAc/CH₂Cl₂ the product was obtained as a white solid. (0.06 g, 0.24 mmol, 24% yield). m.p 217-218 °C; ¹H NMR δ_{H} (400 MHz, DMSO-d₆): 10.9 (1 H, s, Ar-NH-CO-Pyr), 10.2 (1 H, s, Ar-NH-CO-Me), 8.34 (1 H, d, *J* = 8.4 Hz, Ar-H), 8.11 (1 H, d, *J* = 8.0 Hz, Ar-H), 8.0.3 (1 H, t, *J* = 8.0 Ar-H), 7.86 (1 H, d, *J* = 7.6 Hz, Ar-

H), 7.77 (1 H, t, $J = 8.0$ Hz, Ar-H), 7.05 (1 H, d, $J = 7.2$ Hz, Ar-H), 2.43 (3 H, s, Ar-CH₃), 2.16 (3 H, s, CH₃-CO); ¹³C NMR δ_C (400 MHz, DMSO-d₆): 170.0, 161.6, 157.0, 151.0, 150.0, 146.8, 140.3, 139.0, 119.5, 117.2, 116.9, 110.0, 24.0, 23.6; Accurate MS (m/z) Calculated: 293.1008 (M+Na)⁺, Found: 293.1014; IR ν_{max} (cm⁻¹): 3355 (NH), 3251 (NH), 1689 (C=O), 1668 (C=O), 1447 (pyridine).

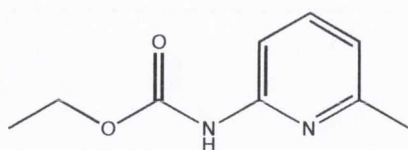
6-acetamido-*N*-(5-methylpyridin-2-yl)nicotinamide (101)



85 (0.18 g, 1.0 mmol), 2-amino-5-picoline (0.15 g, 1.0 mmol) and HOBt (0.15 g, 1.1 mmol) was weighed out and dried under reduced pressure before dissolved in dry THF (10 mL) and cooled in an ice bath for

30 minutes. EDCI·HCl (0.21 g, 1.1 mmol) was added and stirred for further 30 minutes at 0 °C and then stirred overnight at R.T. The solvent was removed and the solid dried under reduced pressure before CH₂Cl₂ was added. The mixture was washed three times with saturated NaHCO₃ and the organic layer was dried over MgSO₄, filtered and evaporated to give white crystals (0.04 g, 0.16 mmol, 16% yield); m.p 216-217 °C; ¹H NMR δ_H (400 MHz, DMSO-d₆): 10.84 (1H, s, CO-NH-Pyr), 10.83 (1H, s, CO-NH-Me), 8.93 (1H, d, $J = 2.4$ Hz, Ar-H), 8.37 (1H, dd, $J = 8.8; 2.8$ Hz, Ar-H), 8.22 (1H, s, Ar-H), 8.16 (1H, d, $J = 8.8$ Hz, Ar-H), 8.08 (1H, d, $J = 8.4$ Hz, Ar-H), 7.67 (1H, dd, $J = 8.4; 2.0$ Hz, Ar-H), 2.29 (3H, s, Ar-CH₃), 2.14 (3H, s, CH₃-CO); ¹³C NMR δ_C (400 MHz, DMSO-d₆): δ 169.8, 163.9, 154.2, 149.9, 148.3, 147.7, 138.5, 138.1, 128.9, 125.0, 114.3, 112.0, 24.1, 17.4; Accurate MS (m/z) Calculated: 293.1008 (M+Na)⁺, Found: 293.1014; IR ν_{max} (cm⁻¹): 3355 (NH), 3251 (NH), 1689 (C=O), 1668 (C=O), 1449 (Pyridine).

Ethyl 6-methyl-2-pyridinyl-carbamate (103)²¹⁰

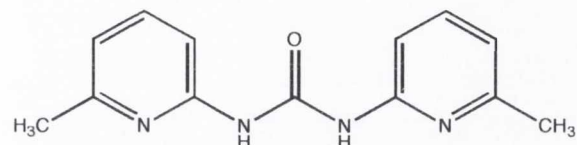


2-amino-6-picoline (3.03 g, 28 mmol) was dissolved under argon in dry pyridine (≥ 99%, 5.0 mL) and ethyl chloroformate (3.5 mL, 36.5 mmol) was added at 0 °C.

This solution was stirred overnight at 0 °C. The reaction mixture was then poured into ice-water and the white precipitate (3.6 g, 20 mmol, 71% yield) was collected and dried over P₂O₅. m.p 59-61 °C; ¹H NMR δ_H (400 MHz, DMSO-d₆): 9.98 (1 H, s, NH), 7.63 (2H, d, $J = 4.0$ Hz, Ar-H), 6.89 (1H, t, $J = 4.0$ Hz, Ar-H), 4.11

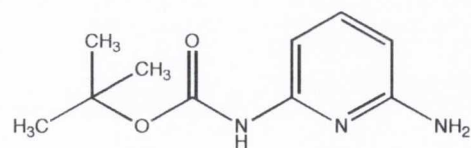
(2H, q, $J = 7.0$ Hz, O-CH₂-CH₃), 2.36 (3H, s, Ar-CH₃), 1.21 (3H, t, $J = 7.0$ Hz, CH₃); ¹³C NMR δ_C (400 MHz, DMSO-d₆): δ 156.3, 153.6, 151.5, 138.4, 117.8, 109.2, 60.3, 23.6, 14.5; Accurate MS (m/z) Calculated: 181.0978 (M+H)⁺, Found: 181.0977; IR ν_{max} (cm⁻¹): 3182 (NH), 2980 (Aliphatic CH), 1724 (C=O), 1581 (Aromatic), 1534 (CO-NH-Ar), 1082 (CH₂-O-CO).

1,3-bis(6-methyl-2-pyridyl)urea (104)

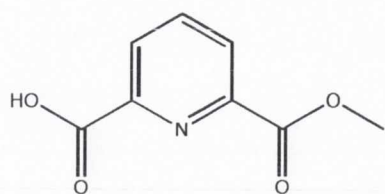


2-amino-6-picoline (0.53 g, 4.9 mmol) and **103** (0.59, 3.3 mmol) were dissolved with pyridine (10 mL) in a pressure tube and heated at reflux for three days. The solvent removed and the remaining precipitate was recrystallised from toluene, resulting in a crystalline gray solid (0.35 g, 1.4 mmol, 44%). m.p. 185-187 °C (Ref. 186-187); ¹H NMR δ_H (400 MHz, DMSO-d₆): 10.4 (2H, br s, NH), 7.65 (2H, t, $J = 7.8$ Hz, Ar-H), 7.53 (2H, s, Ar-H), 6.91 (2H, d, $J = 7.2$ Hz, Ar-H), 2.42 (6H, s, CH₃); ¹³C NMR δ_C (400 MHz, DMSO-d₆): 156.0, 151.9, 138.7, 117.3, 109.1, 23.76; Accurate MS (m/z) Calculated: 265.1055 (M+Na)⁺, Found: 265.1065; IR ν_{max} (cm⁻¹): 3181 (NH), 2980 (Aliphatic CH), 1723 (C=O).

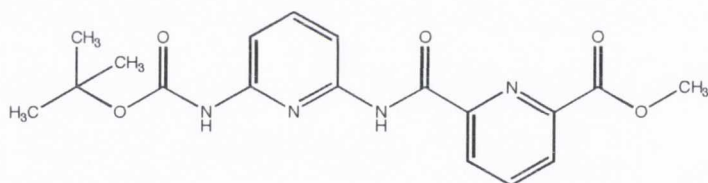
tert-butyl 6-aminopyridin-2-ylcarbamate (**105**)²⁰⁴



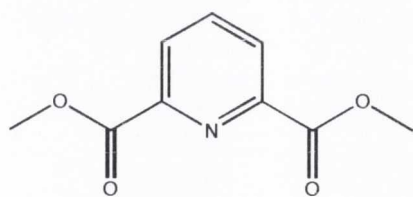
2,6-diaminopyridine (1.5 g, 14 mmol) was recrystallised from hot CHCl₃ and was dissolved in THF. To this solution, Boc (3.0 g, 14 mmol) dissolved in THF was added dropwise at room temperature. The reaction was allowed to proceed under heating (60 °C) for 24 hours. The solvent was removed and the resulting residue was purified by silica flash column chromatography (10% EtOAc/CHCl₃) giving the product as a white solid (1.4 g, 6.7 mmol, 49%). m.p. 125-127 °C (Ref. 125-128 °C); ¹H NMR δ_H (400 MHz, CDCl₃): 7.44 (1H, t, $J = 8.0$ Hz, Ar-H), 7.25 (1H, d, $J = 8.0$ Hz, Ar-H), 7.19 (1H, s, NH) 6.19 (1H, d, $J = 8.0$ Hz, Ar-H), 4.34 (2H, s, NH₂), 1.53 (9H, s, (CH₃)₃); ¹³C NMR δ_H (100 MHz, CDCl₃): 156.7, 151.9, 150.0, 139.5, 102.5, 101.1, 80.3, 27.9; IR ν_{max} (cm⁻¹): 3417 (NH₂), 3384 (NH), 1697 (C=O), 1151 (CO-O).

6-(methoxycarbonyl) picolinic acid (106)²⁰⁵

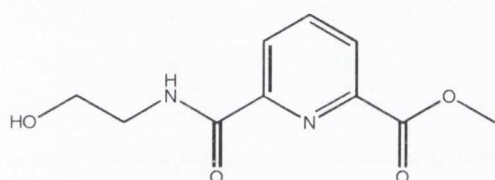
A mixture of pyridine-2,6-dicarboxylic acid (10 g, 60 mmol), water (50 mL), MeOH (50 mL) and H₂SO₄ (5 mL) was refluxed for 15 minutes and then stirred at room temperature overnight. The solution was poured into 500 mL of saturated NaHCO₃ and extracted with CHCl₃. The organic layer was dried over MgSO₄. Evaporation of the CHCl₃ gave the bis ester **109** (34.0 g, 20 mmol, 34%). The aqueous phase was acidified with concentrated HCl and extracted with CHCl₃ (3 x 15 mL) and the organic layer dried over MgSO₄. Evaporation of the CHCl₃ gave a white solid (2.8 g, 16 mmol, 26%). m.p. 148-150 °C (Ref. 147-148 °C); ¹H NMR δ_H (400 MHz, CDCl₃): 8.45 (1H, dd, *J* = 8.0; 0.8 Hz, Ar-H), 8.39 (1H, dd, *J* = 8.0; 0.8 Hz, Ar-H), 8.16 (1H, t, *J* = 8.0 Hz, Ar-H), 4.07 (3H, s, CH₃); ¹³C NMR δ_C (400 MHz, CDCl₃): 164.22, 163.62, 146.46, 139.68, 128.81, 128.11, 126.91, 53.24; Accurate MS (*m/z*) Calculated: 204.0271 (M+Na)⁺, Found: 204.0273; IR ν_{max} (cm⁻¹): 2842 (OH), 1716 (C=O), 1693 (C=O), 1135 (O-CH₃)

Methyl 6-(6-(*tert*-butoxycarbonylamino)pyridin-2-ylcarbamoyl)picolinate (107)

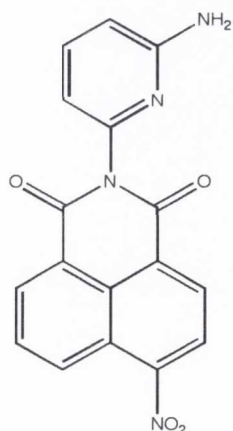
To a stirred solution of **105** (0.50 g, 2.4 mmol) and **106** (0.50 g, 2.8 mmol) and HOBT (0.38 g, 2.8 mmol) were suspended in THF. Triethylamine (0.5 mL, 2.6 mmol) and DCC (0.55 g, 2.4 mmol) were added to this solution at 4 °C and under argon. This reaction was stirred at 4 °C for 15 minutes and then overnight at room temperature. The reaction was filtered and the solvent was removed under reduced pressure. The reaction mixture was dried and then suspended in CH₂Cl₂. The residue was separated by silica flash column chromatography (4% EtOAc/CH₂Cl₂) resulting in the product as a white solid (0.24 g, 0.64 mmol, 27%). m.p. 153.2-154.0 °C; ¹H NMR δ_H (400 MHz, DMSO-*d*₆): 10.1 (1H, s, NH), 9.98 (1H, s, NH), 8.42 (1H, dd, *J* = 6.8; 2.4 Hz, Ar-H), 8.33-8.30 (2H, m, 2 x Ar-H), 7.92 (1H, dd, *J* = 8.0; 2.0 Hz, Ar-H), 7.83 (1H, t, *J* = 7.8 Hz, Ar-H), 7.63 (1H, dd, *J* = 8.0; 0.8 Hz, Ar-H), 3.37 (3H, s, CH₃), 1.48 (9H, s, (CH₃)₃); ¹³C NMR δ_C (100 MHz, DMSO-*d*₆): 178.3, 164.6, 153.1, 152.0, 149.2, 141.1, 128.7, 126.0, 109.0, 107.4, 80.1, 68.8, 53.4, 28.5, 27.9, 22.2; IR ν_{max} (cm⁻¹): 3344 (NH₂), 1693 (C=O).

Dimethyl-pyridine-2,6-dicarboxylate (109)²⁰⁵

For synthesis see compound **106**. m.p. 109-110 °C; ¹H NMR δ_H (400 MHz, CDCl₃): 8.30 (2H, d, *J* = 7.6 Hz, 2 x Ar-H), 8.03 (1H, t, *J* = 7.8 Hz, Ar-H), 4.00 (6H, s, 2 x CH₃); ¹³C NMR δ_C (400 MHz, CDCl₃): 164.6, 147.7, 138.0, 127.6, 52.8; Accurate MS (m/z) Calculated: 218.0435 (M+Na)⁺, Found: 218.0429; IR ν_{max} (cm⁻¹): 2968 (Aliphatic CH), 1724 (C=O), 1243 (O-CH₃).

Methyl 6-(2-hydroxyethylcarbamoyl)picolinate (111)²¹¹

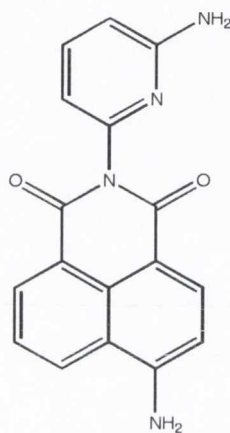
A solution of compound **109** (1.02 g, 5.3 mmol) and 2-aminoethanol (0.32 mL, 5.3 mmol) in toluene (10 mL) was heated at 100 °C for 30 minutes and the reaction was filtered hot through a filter funnel to remove unreacted starting material. The filtrate was concentrated under reduced pressure and the residue was separated by silica column chromatography (5% MeOH/CH₂Cl₂) to give a white precipitate (0.05 g, 0.23 mmol, 4.3%). m.p. 97-99 °C; ¹H NMR δ_H (400 MHz, CDCl₃): 8.86 (1H, s, NH), 8.31 (1H, d, *J* = 7.6 Hz, Ar-H), 8.15 (1H, d, *J* = 7.6 Hz, Ar-H), 7.96 (1H, t, *J* = 7.6 Hz, Ar-H), 4.00 (3H, s, O-CH₃), 3.93 (2H, s, CH₂), 3.70 (3H, s, CH₂-CH₃); ¹³C NMR δ_C (400 MHz, CDCl₃): 165.2, 164.2, 150.4, 146.1, 138.5, 127.1, 125.6, 61.8, 53.1, 42.6; Accurate MS (m/z) Calculated: 247.0700 (M+Na)⁺, Found: 247.0695; IR ν_{max} (cm⁻¹):

2-(6-aminopyrid-2-yl)-4-nitro-1,8-naphthalimide (112)

A solution of 4-nitro-1,8-naphthalic anhydride (0.35 g, 1.4 mmol) and 2,6-diaminopyridine (0.16 g, 1.4 mmol) was refluxed in pyridine (10 mL) overnight. The solution was then cooled and poured into water to give a pale yellow precipitate of the imide. The precipitate was filtered and washed with methanol and water to give a dark brown solid (0.44 g, 1.3 mmol, 94%). m.p. 324-325 °C; ¹H NMR δ_H (600 MHz, DMSO-d₆) 8.66 (1H, d, *J* = 8.0 Hz, Naph-H7), 8.42 (1H, d, *J* = 6.6 Hz, Naph-H2), 8.18 (1H, d, *J* = 8.8 Hz, Naph-H5), 7.68 (1H, t, *J* = 8.0 Hz, Naph-H6) 7.53 (1H, t, *J* = 7.7 Hz, Ar-H) 7.47 (1H, br s, NH) 6.88 (1H, d, *J* = 8.8 Hz, Naph-H3), 6.51 (1H, d, *J* = 8.0 Hz, Ar-H), 6.50 (2H, d, *J* = 7.3 Hz, Ar-H), 6.06 (2H,

br s, NH₂); ¹³C NMR δ_C (100 MHz, DMSO-d₆) 163.2, 162.4, 160.6, 149.9, 147.7, 139.6, 132.3, 132.3, 130.6, 130.3, 129.3, 124.7, 123.3, 111.3, 108.5; Accurate MS (m/z) Calculated: 357.0609 (M+Na)⁺, Found: 357.0600; IR ν_{max} (cm⁻¹): 3448 (NH₂), 1710 (C=O), 1524 (NO₂), 1343 (NO₂).

2-(6-aminopyrid-2-yl)-4-amino-1,8-naphthalimide (112)



Compound **112** (0.14 g, 0.43 mmol) was hydrogenated in DMF in the presence of 10% Pd/C. The reaction mixture was subjected to 3 Atm H₂ for 24 hours. The reaction was filtered through a celite plug and the solvent removed under reduced pressure to give the product as a brown solid (0.13 g, 0.42 mmol, 98%). m.p. 389 °C decomp.; ¹H NMR δ_H (600 MHz, DMSO-d₆) 8.76 (1H, d, *J* = 8.0 Hz, Naph-H), 8.58 – 8.66 (3H, m, Naph-H) 8.59 (1H, t, *J* = 8.0 Hz, Naph-H6) 8.14 (1H, t, *J* = 8.0 Hz, Ar-H) 6.64 (2H, d, *J* = 7.3 Hz, Ar-H) 6.65 (2H, d, *J* = 8.8 Hz, Ar-H), 6.18 (2H, br s, NH₂); δ_C (100 MHz, DMSO-d₆): 164.1, 163.2, 160.2, 153.3, 148.9, 139.3, 134.2, 131.3, 130.6, 129.8, 124.1, 122.4, 119.9, 119.9, 111.4, 108.5, 107.9; Accurate MS (m/z) Calculated: 305.1052 (M+Na)⁺, Found: 305.1039; IR ν_{max} (cm⁻¹): 3376 (NH₂), 1678 (C=O), 1581 (NH₂).

7 References

7.1 References

- (1) Ferlay, J.; Autier, P.; Boniol, M.; Heanue, M.; Colombet, M.; Boyle, P. *Ann Oncol* **2007**, *18*, 581-92.
- (2) Quinn, M. J.; d'Onofrio, A.; Moller, B.; Black, R.; Martinez-Garcia, C.; Moller, H.; Rahu, M.; Robertson, C.; Schouten, L. J.; La Vecchia, C.; Boyle, P. *Ann Oncol* **2003**, *14*, 1148-52.
- (3) Berrino, F.; De Angelis, R.; Sant, M.; Rosso, S.; Bielska-Lasota, M.; Coebergh, J. W.; Santaquilani, M. *Lancet Oncol* **2007**, *8*, 773-83.
- (4) Hussey, G. Ph.D. Thesis, Trinity College, 2004.
- (5) Gillespie, L. J. Ph.D. Thesis, Trinity College, 2007.
- (6) Veale, E. B. Ph.D. Thesis, Trinity College, 2007.
- (7) Ruddon, R. W. *Cancer biology*; 4th ed.; Oxford University Press: New York ; Oxford, 2007.
- (8) Knudson, A. G., Jr. *Cancer Res* **1985**, *45*, 1437-43.
- (9) Knudson, A. G., Jr. *Proc Natl Acad Sci U S A* **1971**, *68*, 820-3.
- (10) Renan, M. J. *Mol Carcinog* **1993**, *7*, 139-46.
- (11) Foulds, L. *Cancer Res* **1954**, *14*, 327-39.
- (12) Nowell, P. C. *Science* **1976**, *194*, 23-8.
- (13) Hanahan, D.; Weinberg, R. A. *Cell* **2000**, *100*, 57-70.
- (14) Forbes, I. J.; Leong, A. S. Y. *Essential oncology of the lymphocyte*; Springer-Verlag: London, 1987.
- (15) Corn, P. G.; El-Deiry, W. S. *Bioessays* **2002**, *24*, 83-90.
- (16) Sherr, C. J. *Harvey Lect* **2000**, *96*, 73-92.
- (17) Sandal, T. *Oncologist* **2002**, *7*, 73-81.
- (18) Alberts, B. *Molecular biology of the cell*; 5th ed.; Garland Science: New York ; Abingdon, 2008.
- (19) Pardee, A. B. *Science* **1989**, *246*, 603-8.
- (20) Fingert, H. J.; Pu, A. T.; Chen, Z. Y.; Googe, P. B.; Alley, M. C.; Pardee, A. B. *Cancer Res* **1988**, *48*, 4375-81.
- (21) Alison, M. *The cancer handbook*; 2nd ed.; John Wiley & Sons: Chichester, 2007.
- (22) Kerr, J. F.; Wyllie, A. H.; Currie, A. R. *Br J Cancer* **1972**, *26*, 239-57.
- (23) Elmore, S. *Toxicol Pathol* **2007**, *35*, 495-516.
- (24) Fink, S. L.; Cookson, B. T. *Infect Immun* **2005**, *73*, 1907-16.
- (25) Formigli, L.; Papucci, L.; Tani, A.; Schiavone, N.; Tempestini, A.; Orlandini, G. E.; Capaccioli, S.; Orlandini, S. Z. *J Cell Physiol* **2000**, *182*, 41-9.
- (26) Leist, M.; Single, B.; Castoldi, A. F.; Kuhnle, S.; Nicotera, P. *J Exp Med* **1997**, *185*, 1481-6.
- (27) Nishimura, Y.; Lemasters, J. J. *Cell Death Differ* **2001**, *8*, 850-8.
- (28) Zong, W. X.; Thompson, C. B. *Genes Dev* **2006**, *20*, 1-15.
- (29) Majno, G.; Joris, I. *Am J Pathol* **1995**, *146*, 3-15.
- (30) Creavin, T. *Drug Discov Today* **2004**, *9*, 628.
- (31) Zong, W. X.; Ditsworth, D.; Bauer, D. E.; Wang, Z. Q.; Thompson, C. B. *Genes Dev* **2004**, *18*, 1272-82.
- (32) Kurosaka, K.; Takahashi, M.; Watanabe, N.; Kobayashi, Y. *J Immunol* **2003**, *171*, 4672-9.
- (33) Locksley, R. M.; Killeen, N.; Lenardo, M. J. *Cell* **2001**, *104*, 487-501.
- (34) Huang, B.; Eberstadt, M.; Olejniczak, E. T.; Meadows, R. P.; Fesik, S. W. *Nature* **1996**, *384*, 638-41.

- (35) Eck, M. J.; Ultsch, M.; Rinderknecht, E.; de Vos, A. M.; Sprang, S. R. *J Biol Chem* **1992**, *267*, 2119-22.
- (36) Gruss, H. J.; Dower, S. K. *Blood* **1995**, *85*, 3378-404.
- (37) Jones, E. Y.; Stuart, D. I.; Walker, N. P. *Prog Clin Biol Res* **1990**, *349*, 321-7.
- (38) Tartaglia, L. A.; Ayres, T. M.; Wong, G. H.; Goeddel, D. V. *Cell* **1993**, *74*, 845-53.
- (39) Medema, J. P.; Scaffidi, C.; Kischkel, F. C.; Shevchenko, A.; Mann, M.; Krammer, P. H.; Peter, M. E. *Embo J* **1997**, *16*, 2794-804.
- (40) Griffith, T. S.; Lynch, D. H. *Curr Opin Immunol* **1998**, *10*, 559-63.
- (41) Schulze-Osthoff, K.; Ferrari, D.; Los, M.; Wesselborg, S.; Peter, M. E. *Eur J Biochem* **1998**, *254*, 439-59.
- (42) Vermeulen, K.; Van Bockstaele, D. R.; Berneman, Z. N. *Ann Hematol* **2005**, *84*, 627-39.
- (43) Muschen, M.; Warskulat, U.; Beckmann, M. W. *J Mol Med* **2000**, *78*, 312-25.
- (44) Shin, M. S.; Kim, H. S.; Lee, S. H.; Park, W. S.; Kim, S. Y.; Park, J. Y.; Lee, J. H.; Lee, S. K.; Lee, S. N.; Jung, S. S.; Han, J. Y.; Kim, H.; Lee, J. Y.; Yoo, N. J. *Cancer Res* **2001**, *61*, 4942-6.
- (45) Tepper, C. G.; Seldin, M. F. *Blood* **1999**, *94*, 1727-37.
- (46) Johnstone, R. W.; Ruefli, A. A.; Lowe, S. W. *Cell* **2002**, *108*, 153-64.
- (47) Garrido, C.; Galluzzi, L.; Brunet, M.; Puig, P. E.; Didelot, C.; Kroemer, G. *Cell Death Differ* **2006**, *13*, 1423-33.
- (48) Du, C.; Fang, M.; Li, Y.; Li, L.; Wang, X. *Cell* **2000**, *102*, 33-42.
- (49) Verhagen, A. M.; Ekert, P. G.; Pakusch, M.; Silke, J.; Connolly, L. M.; Reid, G. E.; Moritz, R. L.; Simpson, R. J.; Vaux, D. L. *Cell* **2000**, *102*, 43-53.
- (50) Zou, H.; Henzel, W. J.; Liu, X.; Lutschg, A.; Wang, X. *Cell* **1997**, *90*, 405-13.
- (51) Chinnaiyan, A. M. *Neoplasia* **1999**, *1*, 5-15.
- (52) Hill, M. M.; Adrain, C.; Duriez, P. J.; Creagh, E. M.; Martin, S. J. *Embo J* **2004**, *23*, 2134-45.
- (53) Slee, E. A.; Adrain, C.; Martin, S. J. *J Biol Chem* **2001**, *276*, 7320-6.
- (54) Enari, M.; Sakahira, H.; Yokoyama, H.; Okawa, K.; Iwamatsu, A.; Nagata, S. *Nature* **1998**, *391*, 43-50.
- (55) Sakahira, H.; Enari, M.; Nagata, S. *Nature* **1998**, *391*, 96-9.
- (56) Levine, A. J. *Cell* **1997**, *88*, 323-31.
- (57) Golub, T. R.; Slonim, D. K.; Tamayo, P.; Huard, C.; Gaasenbeek, M.; Mesirov, J. P.; Coller, H.; Loh, M. L.; Downing, J. R.; Caligiuri, M. A.; Bloomfield, C. D.; Lander, E. S. *Science* **1999**, *286*, 531-7.
- (58) Hunter, T. *J Clin Invest* **2007**, *117*, 2036-43.
- (59) Nowell, P. C.; Hungerford, D. A. *J Natl Cancer Inst* **1960**, *25*, 85-109.
- (60) Gilliland, D. G.; Jordan, C. T.; Felix, C. A. *Hematology Am Soc Hematol Educ Program* **2004**, 80-97.
- (61) Degos, L.; Linch, D. C.; Löwenberg, B. *Textbook of malignant haematology*; 2nd ed.; Taylor & Francis: London, 2005.
- (62) Belfield, G. P.; Delaney, S. J. *Biochem Soc Trans* **2006**, *34*, 313-6.
- (63) Weinstein, I. B. *Science* **2002**, *297*, 63-4.
- (64) Vabmus, H. E.; Bishop, J. M.; Vogt, P. K. *Journal of Molecular Biology* **1973**, *74*, 613-626.
- (65) Capdeville, R.; Buchdunger, E.; Zimmermann, J.; Matter, A. *Nat Rev Drug Discov* **2002**, *1*, 493-502.
- (66) Fausel, C. *J Manag Care Pharm* **2007**, *13*, 8-12.
- (67) Felsher, D. W. *Nat Rev Cancer* **2003**, *3*, 375-80.

- (68) Mahon, F. X.; Deininger, M. W.; Schultheis, B.; Chabrol, J.; Reiffers, J.; Goldman, J. M.; Melo, J. V. *Blood* **2000**, *96*, 1070-9.
- (69) Weisberg, E.; Griffin, J. D. *Blood* **2000**, *95*, 3498-505.
- (70) von Bubnoff, N.; Schneller, F.; Peschel, C.; Duyster, J. *Lancet* **2002**, *359*, 487-91.
- (71) Gorre, M. E.; Mohammed, M.; Ellwood, K.; Hsu, N.; Paquette, R.; Rao, P. N.; Sawyers, C. L. *Science* **2001**, *293*, 876-880.
- (72) Warrell, R. P., Jr.; Maslak, P.; Eardley, A.; Heller, G.; Miller, W. H., Jr.; Frankel, S. R. *Leukemia* **1994**, *8*, 929-33.
- (73) Degos, L.; Wang, Z. Y. *Oncogene* **2001**, *20*, 7140-5.
- (74) Mc Gee, M. M.; Campiani, G.; Ramunno, A.; Fattorusso, C.; Nacci, V.; Lawler, M.; Williams, D. C.; Zisterer, D. M. *J Pharmacol Exp Ther* **2001**, *296*, 31-40.
- (75) Greene, L. M.; Kelly, L.; Onnis, V.; Campiani, G.; Lawler, M.; Williams, D. C.; Zisterer, D. M. *J Pharmacol Exp Ther* **2007**, *321*, 288-97.
- (76) Watson, J. D.; Crick, F. H. *Nature* **1953**, *171*, 737-8.
- (77) Hannon, M. J. *Chem Soc Rev* **2007**, *36*, 280-95.
- (78) Leonard, G. A.; Hunter, W. N. *J Mol Biol* **1993**, *234*, 198-208.
- (79) Coste, F.; Malinge, J. M.; Serre, L.; Shepard, W.; Roth, M.; Leng, M.; Zelwer, C. *Nucleic Acids Res* **1999**, *27*, 1837-46.
- (80) Brabec, V.; Boudny, V.; Balcarova, Z. *Biochemistry* **1994**, *33*, 1316-22.
- (81) Brabec, V.; Reedijk, J.; Leng, M. *Biochemistry* **1992**, *31*, 12397-402.
- (82) Allday, M. J.; Inman, G. J.; Crawford, D. H.; Farrell, P. J. *Embo J* **1995**, *14*, 4994-5005.
- (83) Chu, G. *J Biol Chem* **1994**, *269*, 787-90.
- (84) Kelland, L. R. *Drugs* **2000**, *59 Suppl 4*, 1-8; discussion 37-8.
- (85) Lerman, L. S. *J Mol Biol* **1961**, *3*, 18-30.
- (86) Waring, M. *J Mol Biol* **1970**, *54*, 247-79.
- (87) Waring, M. J. *Humangenetik* **1970**, *9*, 234-6.
- (88) Hunter, C. A. *J Mol Biol* **1993**, *230*, 1025-54.
- (89) Luedtke, N. W.; Hwang, J. S.; Nava, E.; Gut, D.; Kol, M.; Tor, Y. *Nucleic Acids Res* **2003**, *31*, 5732-40.
- (90) Nuss, M. E.; Marsh, F. J.; Kollman, P. A. *J. Am. Chem. Soc.* **1979**, *101*, 825-833.
- (91) Gago, F. *Methods* **1998**, *14*, 277-92.
- (92) Stevenson, K. A.; Yen, S. F.; Yang, N. C.; Boykin, D. W.; Wilson, W. D. *J Med Chem* **1984**, *27*, 1677-82.
- (93) Braña, M. F.; Ramos, A. *Curr Med Chem Anticancer Agents* **2001**, *1*, 237-55.
- (94) Andersson, B. S.; Beran, M.; Bakic, M.; Silberman, L. E.; Newman, R. A.; Zwelling, L. A. *Cancer Res* **1987**, *47*, 1040-4.
- (95) Hsiang, Y. H.; Jiang, J. B.; Liu, L. F. *Mol Pharmacol* **1989**, *36*, 371-6.
- (96) Braña, M. F.; Cacho, M.; Gradillas, A.; de Pascual-Teresa, B.; Ramos, A. *Curr Pharm Des* **2001**, *7*, 1745-80.
- (97) Innocenti, F.; Iyer, L.; Ratain, M. J. *Drug Metab Dispos* **2001**, *29*, 596-600.
- (98) Rosell, R.; Carles, J.; Abad, A.; Ribelles, N.; Barnadas, A.; Benavides, A.; Martin, M. *Invest New Drugs* **1992**, *10*, 171-5.
- (99) Felder, T. B.; McLean, M. A.; Vestal, M. L.; Lu, K.; Farquhar, D.; Legha, S. S.; Shah, R.; Newman, R. A. *Drug Metab Dispos* **1987**, *15*, 773-8.
- (100) Allen, S. L.; Kolitz, J. E.; Lundberg, A. S.; Capizzi, R. L.; Budman, D. R. *J Clin Oncol (Meeting Abstracts)* **2006**, *24*, 6584-.
- (101) Brana, M. F.; Castellano, J. M.; Moran, M.; Perez de Vega, M. J.; Romerdahl, C. R.; Qian, X. D.; Bousquet, P.; Emling, F.; Schlick, E.; Keilhauer, G. *Anticancer Drug Des* **1993**, *8*, 257-68.

- (102) Gallego, J.; Reid, B. R. *Biochemistry* **1999**, *38*, 15104-15.
- (103) Cobb, P. W.; Degen, D. R.; Clark, G. M.; Chen, S. F.; Kuhn, J. G.; Gross, J. L.; Kirshenbaum, M. R.; Sun, J. H.; Burris, H. A., 3rd; Von Hoff, D. D. *J Natl Cancer Inst* **1994**, *86*, 1462-5.
- (104) Cholody, W. M.; Kosakowska-Cholody, T.; Hollingshead, M. G.; Hariprakash, H. K.; Michejda, C. J. *J Med Chem* **2005**, *48*, 4474-81.
- (105) Kosakowska-Cholody, T.; Cholody, W. M.; Monks, A.; Woynarowska, B. A.; Michejda, C. J. *Mol Cancer Ther* **2005**, *4*, 1617-27.
- (106) Kelly, J. M.; Tossi, A. B.; McConnell, D. J.; OhUigin, C. *Nucleic Acids Res* **1985**, *13*, 6017-34.
- (107) Novakova, O.; Kasparkova, J.; Vrana, O.; van Vliet, P. M.; Reedijk, J.; Brabec, V. *Biochemistry* **1995**, *34*, 12369-12378.
- (108) Barton, J. K.; Danishefsky, A.; Goldberg, J. *J. Am. Chem. Soc.* **1984**, *106*, 2172-2176.
- (109) Kumar, C. V.; Barton, J. K.; Turro, N. J. *J. Am. Chem. Soc.* **1985**, *107*, 5518-5523.
- (110) Satyanarayana, S.; Dabrowiak, J. C.; Chaires, J. B. *Biochemistry* **1992**, *31*, 9319-9324.
- (111) Felsenfeld, G.; Davies, D. R.; Rich, A. *J. Am. Chem. Soc.* **1957**, *79*, 2023-2024.
- (112) Moser, H. E.; Dervan, P. B. *Science* **1987**, *238*, 645-50.
- (113) Maher, L. J., 3rd; Dervan, P. B.; Wold, B. *Biochemistry* **1992**, *31*, 70-81.
- (114) Maher, L. J., 3rd; Wold, B.; Dervan, P. B. *Science* **1989**, *245*, 725-30.
- (115) Dervan, P. B. *Bioorg Med Chem* **2001**, *9*, 2215-35.
- (116) Kopka, M. L.; Yoon, C.; Goodsell, D.; Pjura, P.; Dickerson, R. E. *Proc Natl Acad Sci U S A* **1985**, *82*, 1376-80.
- (117) Kopka, M. L.; Yoon, C.; Goodsell, D.; Pjura, P.; Dickerson, R. E. *J Mol Biol* **1985**, *183*, 553-63.
- (118) Patel, D. J. *Proc Natl Acad Sci U S A* **1982**, *79*, 6424-8.
- (119) Luscombe, N. M.; Laskowski, R. A.; Thornton, J. M. *Nucleic Acids Res* **2001**, *29*, 2860-74.
- (120) Pelton, J. G.; Wemmer, D. E. *Proc Natl Acad Sci U S A* **1989**, *86*, 5723-7.
- (121) Lacy, E. R.; Le, N. M.; Price, C. A.; Lee, M.; Wilson, W. D. *J Am Chem Soc* **2002**, *124*, 2153-63.
- (122) Seeman, N. C.; Rosenberg, J. M.; Rich, A. *Proc Natl Acad Sci U S A* **1976**, *73*, 804-8.
- (123) Kielkopf, C. L.; Bremer, R. E.; White, S.; Szewczyk, J. W.; Turner, J. M.; Baird, E. E.; Dervan, P. B.; Rees, D. C. *J Mol Biol* **2000**, *295*, 557-67.
- (124) White, S.; Szewczyk, J. W.; Turner, J. M.; Baird, E. E.; Dervan, P. B. *Nature* **1998**, *391*, 468-71.
- (125) Kielkopf, C. L.; White, S.; Szewczyk, J. W.; Turner, J. M.; Baird, E. E.; Dervan, P. B.; Rees, D. C. *Science* **1998**, *282*, 111-5.
- (126) Urbach, A. R.; Szewczyk, J. W.; White, S.; Turner, J. M.; Baird, E. E.; Dervan, P. B. *J. Am. Chem. Soc.* **1999**, *121*, 11621-11629.
- (127) White, S.; Turner, J. M.; Szewczyk, J. W.; Baird, E. E.; Dervan, P. B. *J. Am. Chem. Soc.* **1999**, *121*, 260-261.
- (128) Urbach, A. R.; Love, J. J.; Ross, S. A.; Dervan, P. B. *J Mol Biol* **2002**, *320*, 55-71.
- (129) Nickols, N. G.; Jacobs, C. S.; Farkas, M. E.; Dervan, P. B. *ACS Chem Biol* **2007**, *2*, 561-71.
- (130) Olenyuk, B. Z.; Zhang, G. J.; Klco, J. M.; Nickols, N. G.; Kaelin, W. G., Jr.; Dervan, P. B. *Proc Natl Acad Sci U S A* **2004**, *101*, 16768-73.
- (131) Underiner, T. L.; Ruggeri, B.; Gingrich, D. E. *Curr Med Chem* **2004**, *11*, 731-45.

- (132) Renneberg, D.; Dervan, P. B. *J Am Chem Soc* **2003**, *125*, 5707-16.
- (133) Doss, R. M.; Marques, M. A.; Foister, S.; Chenoweth, D. M.; Dervan, P. B. *J Am Chem Soc* **2006**, *128*, 9074-9.
- (134) Briehn, C. A.; Weyermann, P.; Dervan, P. B. *Chemistry* **2003**, *9*, 2110-22.
- (135) Ryan, G. J., Trinity College, 2008.
- (136) Ryan, G. J.; Quinn, S.; Gunnlaugsson, T. *Inorg. Chem.* **2008**, *47*, 401-403.
- (137) Flores, L. V.; Staples, A. M.; Mackay, H.; Howard, C. M.; Uthe, P. B.; Sexton, J. S., 3rd; Buchmueller, K. L.; Wilson, W. D.; O'Hare, C.; Kluza, J.; Hochhauser, D.; Hartley, J. A.; Lee, M. *Chembiochem* **2006**, *7*, 1722-9.
- (138) Jantz, D.; Amann, B. T.; Gatto, G. J., Jr.; Berg, J. M. *Chem Rev* **2004**, *104*, 789-99.
- (139) Gatto, B.; Zagotto, G.; Sissi, C.; Cera, C.; Uriarte, E.; Palu, G.; Capranico, G.; Palumbo, M. *J Med Chem* **1996**, *39*, 3114-22.
- (140) Guelev, V.; Lee, J.; Ward, J.; Sorey, S.; Hoffman, D. W.; Iverson, B. L. *Chem Biol* **2001**, *8*, 415-25.
- (141) Saito, I.; Takayama, M.; Kawanishi, S. *J. Am. Chem. Soc.* **1995**, *117*, 5590-5591.
- (142) Phelan, C. M. Ph.D. Thesis, Trinity College, 2003.
- (143) Blais, C. *Postdoctoral Report*, 2005.
- (144) Neoptolemos, J. P.; Stocken, D. D.; Friess, H.; Bassi, C.; Dunn, J. A.; Hickey, H.; Beger, H.; Fernandez-Cruz, L.; Dervenis, C.; Lacaine, F.; Falconi, M.; Pederzoli, P.; Pap, A.; Spooner, D.; Kerr, D. J.; Buchler, M. W. *N Engl J Med* **2004**, *350*, 1200-10.
- (145) Hodgkiss, R. J.; Middleton, R. W.; Stratford, M. R.; Del Buono, R. *Biochem Pharmacol* **1987**, *36*, 1483-7.
- (146) Hodgkiss, R. J.; Jones, G. W.; Long, A.; Middleton, R. W.; Parrick, J.; Stratford, M. R.; Wardman, P.; Wilson, G. D. *J Med Chem* **1991**, *34*, 2268-74.
- (147) Givan, A. L. *Flow cytometry : first principles*; 2nd ed.; Wiley-Liss: New York ; Chichester, 2001.
- (148) Puckett, C. A.; Barton, J. K. *J Am Chem Soc* **2007**, *129*, 46-7.
- (149) Pleuvry, B. J. *Anaesthesia & intensive care medicine* **2005**, *6*, 135-138.
- (150) Hartsel, S. C. E. C., WI, US), Lewis, David E. (Eau Claire, WI, US); WISYS TECHNOLOGY FOUNDATION, INC. (614 Walnut Street, Madison, WI, US): United States, 2006.
- (151) Safaei, R.; Katano, K.; Larson, B. J.; Samimi, G.; Holzer, A. K.; Naerdemann, W.; Tomioka, M.; Goodman, M.; Howell, S. B. *Clin Cancer Res* **2005**, *11*, 756-67.
- (152) Mosmann, T. *J Immunol Methods* **1983**, *65*, 55-63.
- (153) Alley, M. C.; Scudiero, D. A.; Monks, A.; Hursey, M. L.; Czerwinski, M. J.; Fine, D. L.; Abbott, B. J.; Mayo, J. G.; Shoemaker, R. H.; Boyd, M. R. *Cancer Res* **1988**, *48*, 589-601.
- (154) Zhu, H.; Huang, M.; Yang, F.; Chen, Y.; Miao, Z. H.; Qian, X. H.; Xu, Y. F.; Qin, Y. X.; Luo, H. B.; Shen, X.; Geng, M. Y.; Cai, Y. J.; Ding, J. *Mol Cancer Ther* **2007**, *6*, 484-95.
- (155) Sinha, B. K.; Strong, J.; Gibson, N. W.; Kalyanaraman, B. *Biochem Pharmacol* **1985**, *34*, 3845-52.
- (156) Froelich-Ammon, S. J.; Osheroff, N. *J Biol Chem* **1995**, *270*, 21429-32.
- (157) Vögtle, F.; Alfter, F.; Boyd, G. V. *Fascinating molecules in organic chemistry*; Wiley: Chichester, 1992.
- (158) Spielman, M. A. *J. Am. Chem. Soc.* **1935**, *57*, 583-585.
- (159) Larson, S. B.; Wilcox, C. S. *Acta Crystallographica Section C* **1986**, *42*, 224-227.
- (160) Valík, M.; Strongin, R. M.; Král, V. *Supramolecular Chemistry* **2005**, *17*, 347-367.
- (161) Tatibouet, A.; Demeunynck, M.; Andraud, C.; Collet, A.; Lhomme, J. *Chemical Communications* **1999**, 161-162.

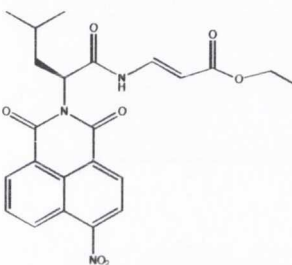
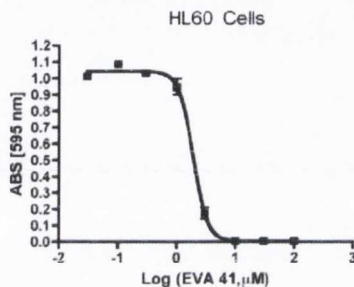
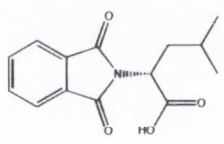
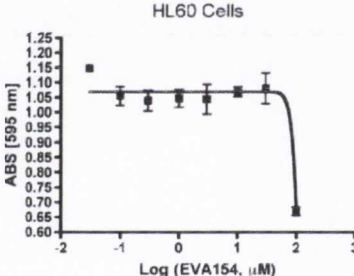
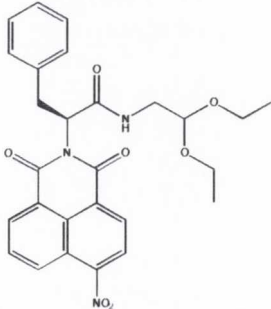
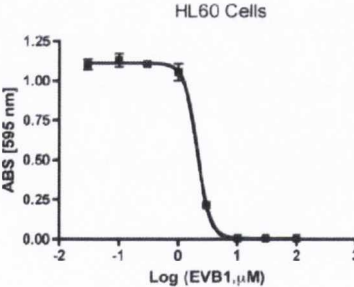
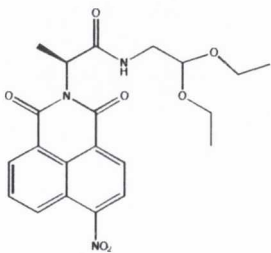
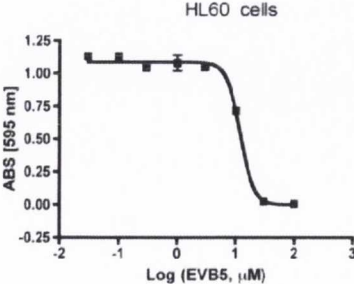
- (162) Yashima, E.; Akashi, M.; Miyauchi, N. *Chemistry Letters* **1991**, *20*, 1017-1020.
- (163) Bailly, C.; Laine, W.; Demeunynck, M.; Lhomme, J. *Biochem Biophys Res Commun* **2000**, *273*, 681-5.
- (164) Baldeyrou, B.; Tardy, C.; Bailly, C.; Colson, P.; Houssier, C.; Charmantay, F.; Demeunynck, M. *Eur J Med Chem* **2002**, *37*, 315-22.
- (165) Valík, M.; Malina, J.; Palivec, L.; Foltýnová, J.; Tkadlecová, M.; Urbanová, M.; Brabec, V.; Král, V. *Tetrahedron* **2006**, *62*, 8591-8600.
- (166) Braña, M. F.; Castellano, J. M.; Roldan, C. M.; Santos, A.; Vazquez, D.; Jimenez, A. *Cancer Chemother Pharmacol* **1980**, *4*, 61-6.
- (167) Li, Z. G.; Yang, Q.; Qian, X. H. *Bioorganic & Medicinal Chemistry Letter*: **2005**, *15*, 3143-3146.
- (168) Deprez, N. R.; McNitt, K. A.; Petersen, M. E.; Brown, R. G.; Lewis, D. E. *Tetrahedron Letters* **2005**, *46*, 2149-2153.
- (169) Kuzelova, K.; Grebenova, D.; Pluskalova, M.; Marinov, I.; Hrkal, Z. *J Photochem Photobiol B* **2004**, *73*, 67-78.
- (170) Ritke, M. K.; Rusnak, J. M.; Lazo, J. S.; Allan, W. P.; Dive, C.; Heer, S.; Yaowich, J. C. *Mol Pharmacol* **1994**, *46*, 605-11.
- (171) Mijatovic, T.; Mahieu, T.; Bruyere, C.; De Neve, N.; Dewelle, J.; Simon, G.; Dehoux, M. J.; van der Aar, E.; Haibe-Kains, B.; Bontempi, G.; Decaestecker, C.; Van Quaquebeke, E.; Darro, F.; Kiss, R. *Neoplasia* **2008**, *10*, 573-86.
- (172) Ross, W. E. *Biochem Pharmacol* **1985**, *34*, 4191-5.
- (173) Slunt, K. M.; Grace, J. M.; Macdonald, T. L.; Pearson, R. D. *Antimicrob Agents Chemother* **1996**, *40*, 706-9.
- (174) Bjornstl, M.; Osheroff, N. *DNA topology protocols*; Humana: Totowa, N.J., 1997.
- (175) Storl, K.; Burckhardt, G.; Lown, J. W.; Zimmer, C. *FEBS Lett* **1993**, *334*, 49-54.
- (176) Xu, Y. C.; Bremer, H. *Nucleic Acids Res* **1997**, *25*, 4067-71.
- (177) Jori, G. *Journal of Photochemistry and Photobiology B: Biology* **1996**, *36*, 87-93.
- (178) Moor, A. C. *J Photochem Photobiol B* **2000**, *57*, 1-13.
- (179) Oleinick, N. L.; Morris, R. L.; Belichenko, I. *Photochem Photobiol Sci* **2002**, *1*, 1-21.
- (180) Oleinick, N. L.; Evans, H. H. *Radiat Res* **1998**, *150*, S146-56.
- (181) Evans, H. H.; Horng, M. F.; Ricanati, M.; Deahl, J. T.; Oleinick, N. L. *Photochem Photobiol* **1997**, *66*, 690-6.
- (182) Agarwal, M. L.; Clay, M. E.; Harvey, E. J.; Evans, H. H.; Antunez, A. R.; Oleinick, N. L. *Cancer Res* **1991**, *51*, 5993-6.
- (183) Triesscheijn, M.; Baas, P.; Schellens, J. H.; Stewart, F. A. *Oncologist* **2006**, *11*, 1034-44.
- (184) Gallagher, W. M.; Allen, L. T.; O'Shea, C.; Kenna, T.; Hall, M.; Gorman, A.; Killoran, J.; O'Shea, D. F. *Br J Cancer* **2005**, *92*, 1702-10.
- (185) Erkkila, K. E.; Odom, D. T.; Barton, J. K. *Chem. Rev.* **1999**, *99*, 2777-2796.
- (186) Fleisher, M. B.; Waterman, K. C.; Turro, N. J.; Barton, J. K. *Inorg. Chem.* **1986**, *25*, 3549-3551.
- (187) Law, J. C.; Ritke, M. K.; Yalowich, J. C.; Leder, G. H.; Ferrell, R. E. *Luk Res* **1993**, *17*, 1045-50.
- (188) Puckett, C. A.; Barton, J. K. *J. Am. Chem. Soc.* **2007**, *129*, 46-47.
- (189) Schmitt, F.; Govindaswamy, P.; Zava, O.; Suss-Fink, G.; Juillerat-Jeanneret, L.; Therrien, B. *J Biol Inorg Chem* **2008**.
- (190) Novakova, O.; Kasparkova, J.; Vrana, O.; van Vliet, P. M.; Reedijk, J.; Brabec, V. *Biochemistry* **1995**, *34*, 12369-78.

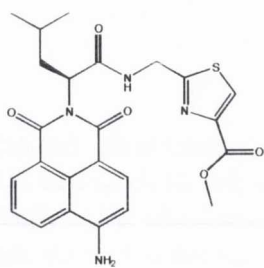
- (191) Chiu, S.; Evans, H. H.; Lam, M.; Nieminen, A.; Oleinick, N. L. *Cancer Lett* **2001**, *165*, 51-8.
- (192) Hughes, D.; Mehmet, H. *Cell proliferation & apoptosis*; BIOS Scientific: Oxford, 2003.
- (193) Higginbottom, K.; Cummings, M.; Newland, A. C.; Allen, P. D. *Br J Haematol* **2002**, *119*, 956-64.
- (194) Salvioli, S.; Dobrucki, J.; Moretti, L.; Troiano, L.; Fernandez, M. G.; Pinti, M.; Pedrazzi, J.; Franceschi, C.; Cossarizza, A. *Cytometry* **2000**, *40*, 189-97.
- (195) Bailly, C.; Chaires, J. B. *Bioconjug Chem* **1998**, *9*, 513-38.
- (196) Dervan, P. B.; Doss, R. M.; Marques, M. A. *Curr Med Chem Anticancer Agents* **2005**, *5*, 373-87.
- (197) Chenoweth, D. M.; Poposki, J. A.; Marques, M. A.; Dervan, P. B. *Bioorg Med Chem* **2007**, *15*, 759-70.
- (198) Schmuck, C.; Machon, U. *Chemistry-a European Journal* **2005**, *11*, 1109-1118.
- (199) Wade, W. S.; Mrksich, M.; Dervan, P. B. *J. Am. Chem. Soc.* **1992**, *114*, 8783-8794.
- (200) Wiley, R. H.; Hartman, J. L. *J. Am. Chem. Soc.* **1951**, *73*, 494-494.
- (201) Brown, E. V. *J. Am. Chem. Soc.* **1954**, *76*, 3167-3168.
- (202) Selwood, D. L.; Brummell, D. G.; Budworth, J.; Burtin, G. E.; Campbell, R. O.; Chana, S. S.; Charles, I. G.; Fernandez, P. A.; Glen, R. C.; Goggin, M. C.; Hobbs, A. J.; Kling, M. R.; Liu, Q.; Madge, D. J.; Meillerais, S.; Powell, K. L.; Reynolds, K.; Spacey, G. D.; Stables, J. N.; Tatlock, M. A.; Wheeler, K. A.; Wishart, G.; Woo, C. K. *J. Med. Chem.* **2001**, *44*, 78-93.
- (203) Lüning, U.; Kühn, C.; Uphoff, A. *European Journal of Organic Chemistry* **2002**, *2002*, 4063-4070.
- (204) Kolomiets, E.; Berl, V.; Lehn, J.-M. *Chemistry - A European Journal* **2007**, *13*, 5466-5479.
- (205) Johansen, J. E.; Christie, B. D.; Rapoport, H. *J. Org. Chem.* **1981**, *46*, 4914-4920.
- (206) Miller, W. H.; Alberts, D. P.; Bhatnagar, P. K.; Bondinell, W. E.; Callahan, J. F.; Calvo, R. R.; Cousins, R. D.; Erhard, K. F.; Heerding, D. A.; Keenan, R. M.; Kwon, C.; Manley, P. J.; Newlander, K. A.; Ross, S. T.; Samanen, J. M.; Uzinskas, I. N.; Venslavsky, J. W.; Yuan, C. C. K.; Haltiwanger, R. C.; Gowen, M.; Hwang, S. M.; James, I. E.; Lark, M. W.; Rieman, D. J.; Stroup, G. B.; Azzarano, L. M.; Salyers, K. L.; Smith, B. R.; Ward, K. W.; Johanson, K. O.; Huffman, W. F. *J. Med. Chem.* **2000**, *43*, 22-26.
- (207) Pitts, W. J.; Wityak, J.; Smallheer, J. M.; Tobin, A. E.; Jetter, J. W.; Buynitsky, J. S.; Harlow, P. P.; Solomon, K. A.; Corjay, M. H.; Mousa, S. A.; Wexler, R. R.; Jadhav, P. K. *J. Med. Chem.* **2000**, *43*, 27-40.
- (208) Brown, E. V.; Moser, R. J. *J. Org. Chem.* **1971**, *36*, 454-457.
- (209) Ramesh, R. R.; Krishna, M. S.; Jayarama, R. S. *Tetrahedron Letters* **2003**, *44*, 4133-4135.
- (210) Ulrich Lüning, C. K. A. U. *European Journal of Organic Chemistry* **2002**, *2002*, 4063-4070.
- (211) Nishiyama, H.; Soeda, N.; Naito, T.; Motoyama, Y. *Tetrahedron: Asymmetry* **1998**, *9*, 2865-2869.

Appendices

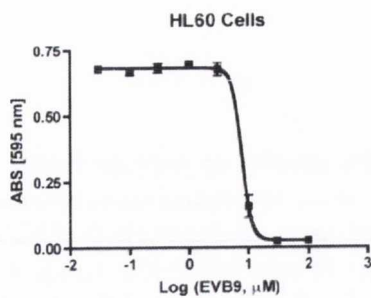
Appendix 1

Table A1.1 Cytotoxicity studies of peptide based 1,8-naphthalimide compounds. HL-60, K562 and HeLa cells were incubated with representative compounds for 24 hours or 48 hours at seven different concentrations (100, 33, 10, 3.3, 1, 0.3, 0.1 and 0.03 μM). Each concentration was done in triplicate. The amount of cells was then quantified using the MTT assay as discussed in Section 2.3 in Chapter 2 and the corresponding EC_{50} value was determined from the graph. The EC_{50} value refers to the concentration of a compound, which induces a response halfway between the baseline and the maximum. The range in brackets shows 95% confidence intervals.

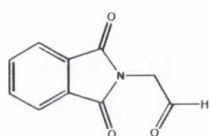
Compound	Code	Dose-Response Curve	EC_{50} Value
	EVA41	 <p>HL60 Cells</p>	1.90 μM (1.72-2.11)
	EVA154	 <p>HL60 Cells</p>	139 μM
	EVB1	 <p>HL60 Cells</p>	2.08 μM (1.86-2.34)
	EVB5	 <p>HL60 cells</p>	11.9 μM (10.3-13.7)



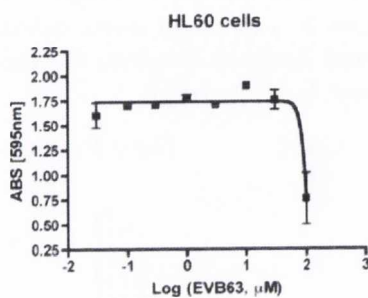
EVB9



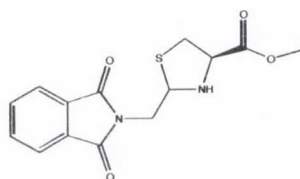
7.73 μM



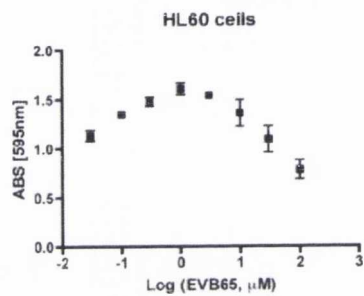
EVB63



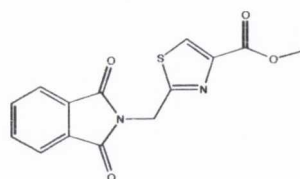
108 μM



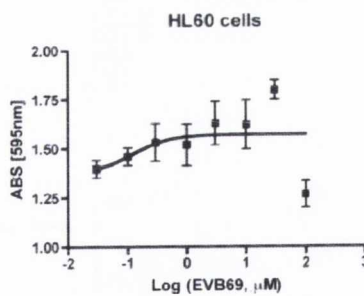
EVB65



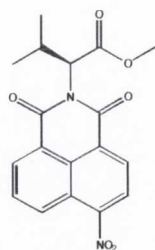
> 100 μM



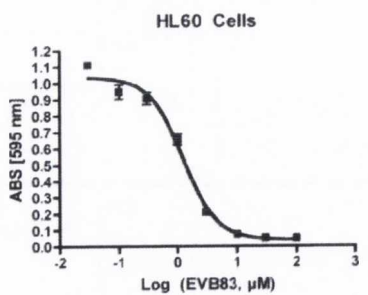
EVB69



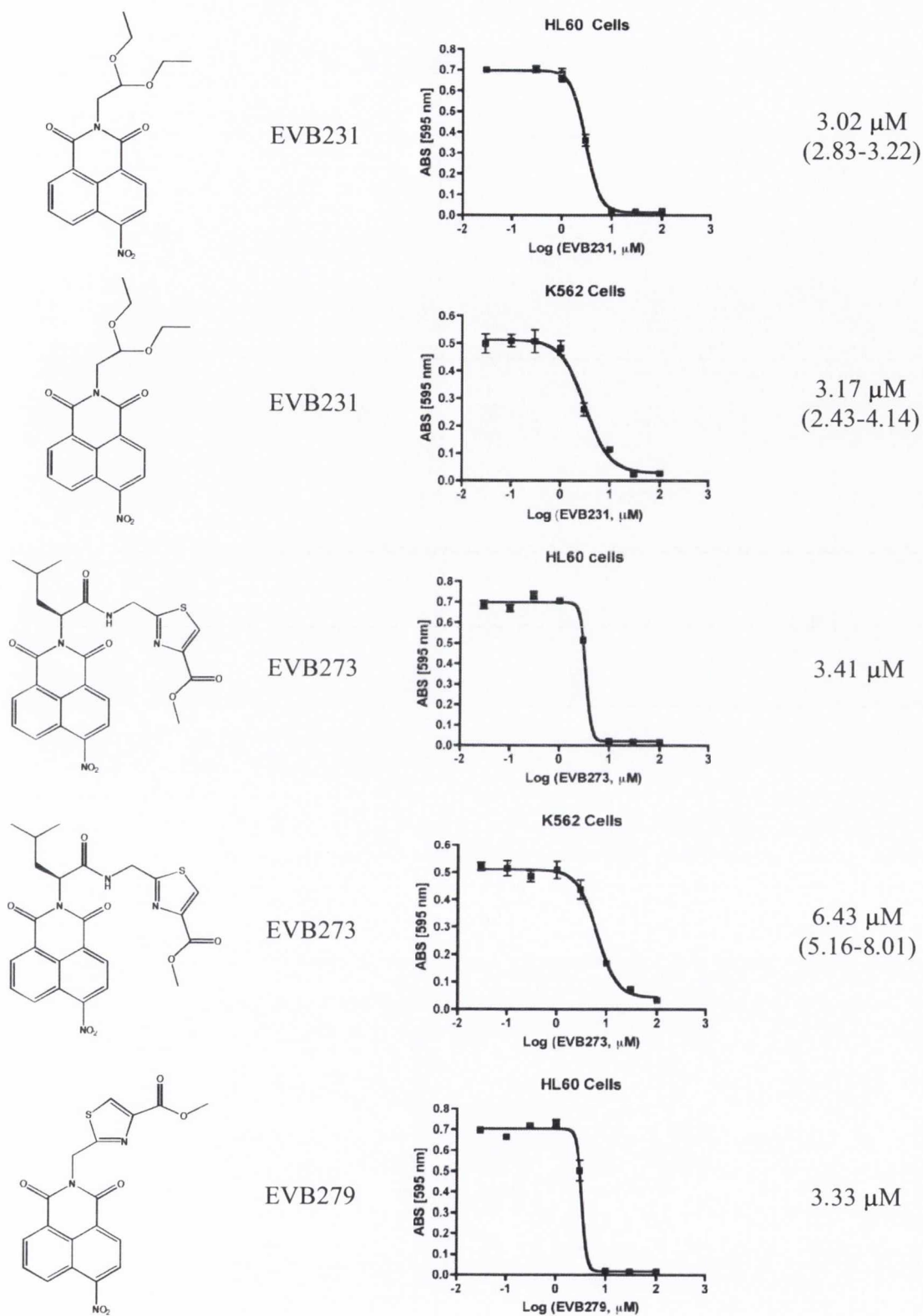
> 100 μM

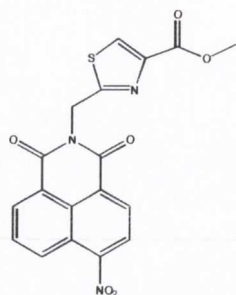


EVB83

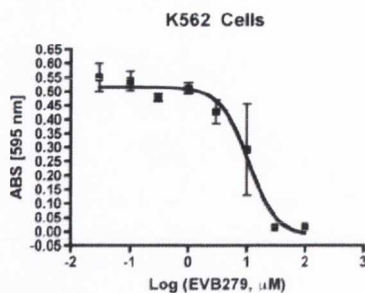


1.24 μM
(1.02 – 1.51)

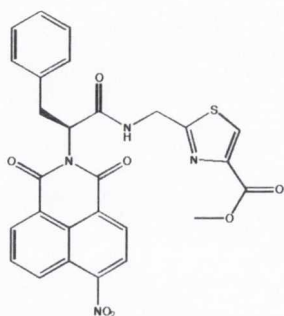




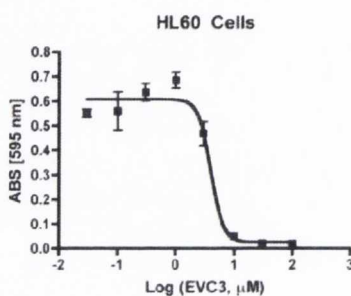
EVB279



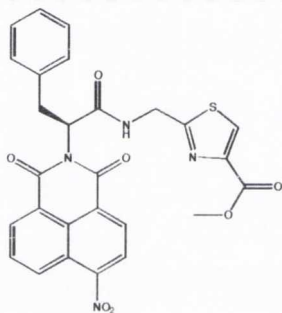
10.5 μM
(5.53-20.0)



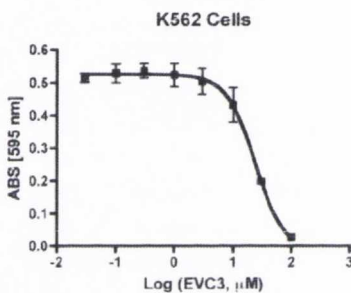
EVC3



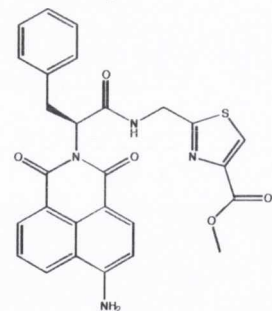
4.01 μM
(2.43-6.61)



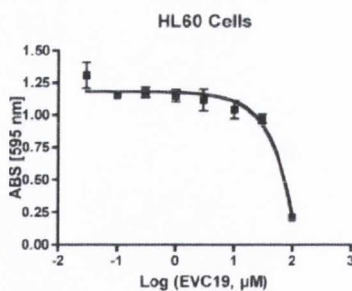
EVC3



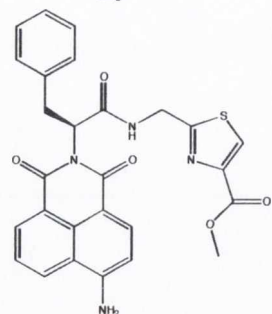
23.5 μM
(16.3-33.7)



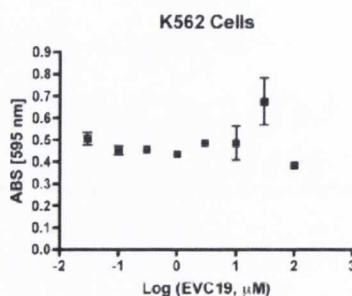
EVC19



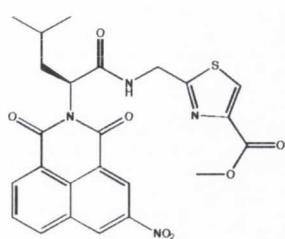
> 100 μM



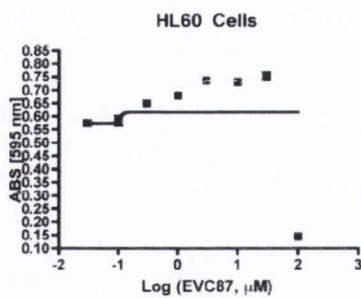
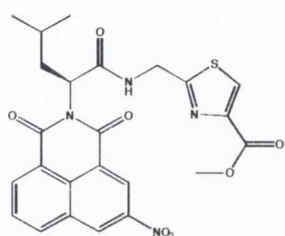
EVC19



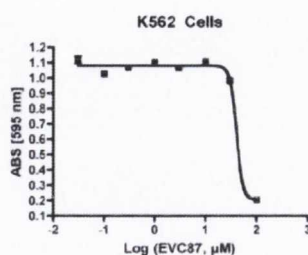
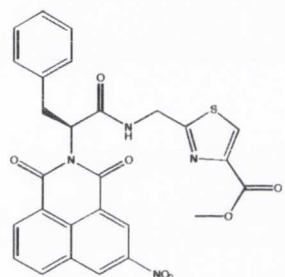
>100 μM



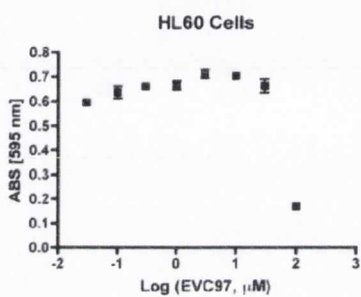
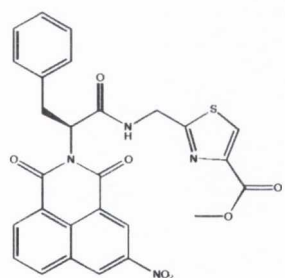
EVC87

> 100 μM 

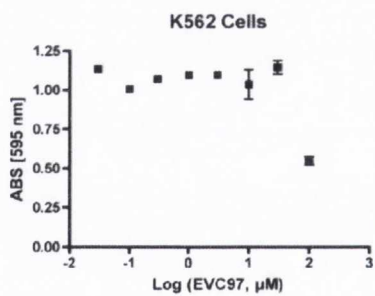
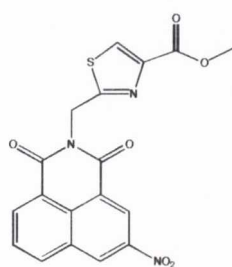
EVC87

> 100 μM 

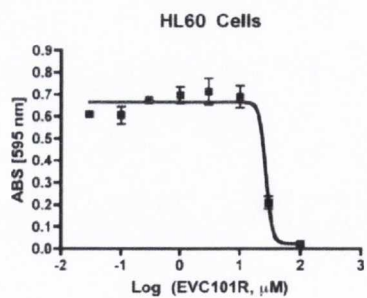
EVC97

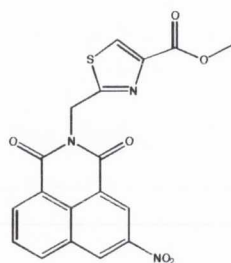
> 100 μM 

EVC97

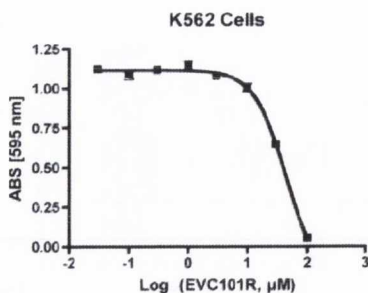
>100 μM 

EVC101R

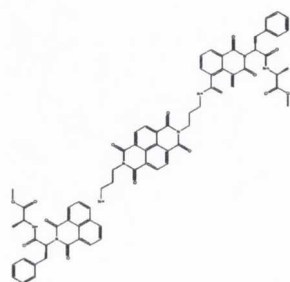
26.9 μM



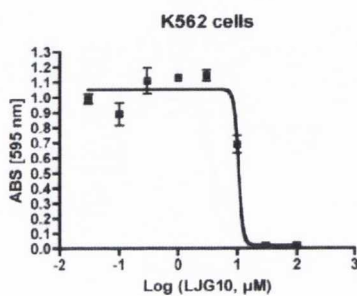
EVC101R



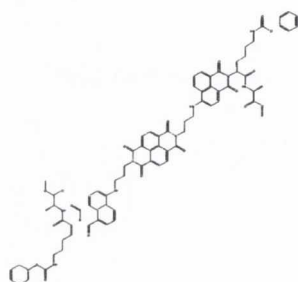
34.5 μM



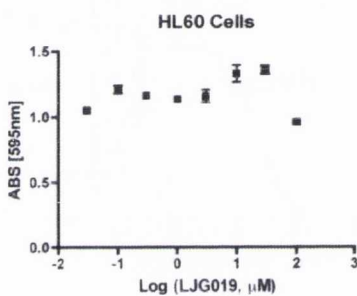
LJG010



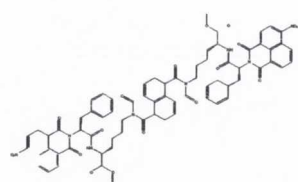
10.3 μM



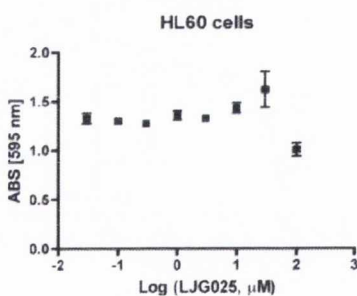
LJG019



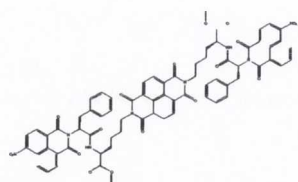
> 100 μM



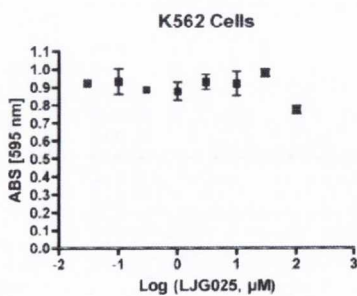
LJG025



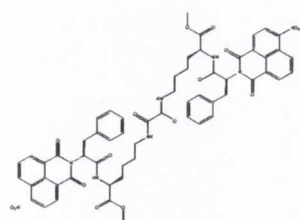
> 100 μM



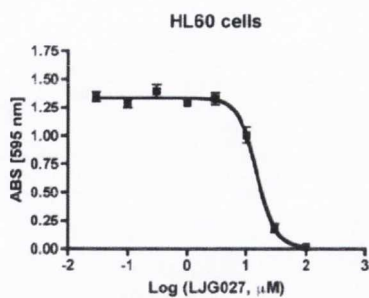
LJG025



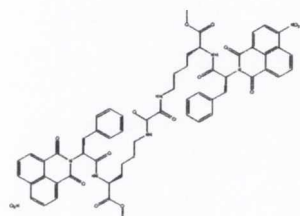
>100 μM



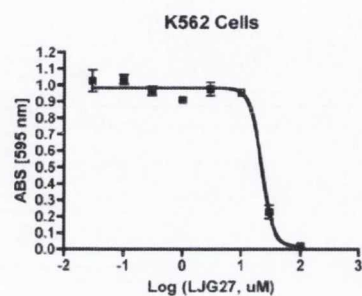
LJG027



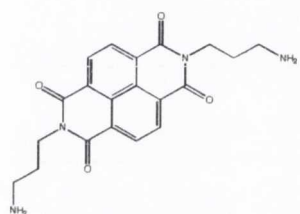
15.0 μM
(12.7-17.7)



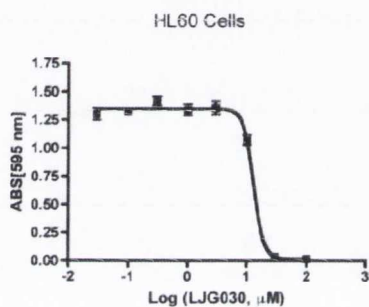
LJG027



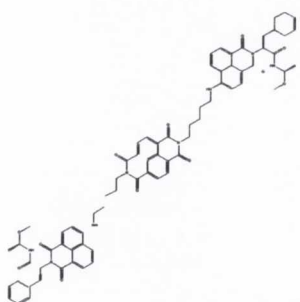
22.5 μM
(17.9-28.1)



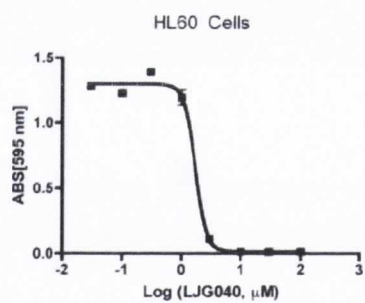
LJG030



13.0 μM
(9.47-17.9)



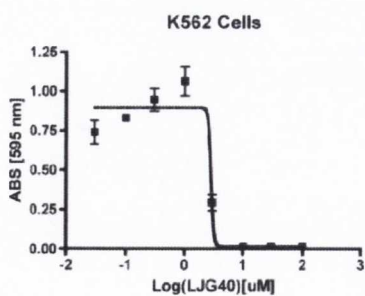
LJG040



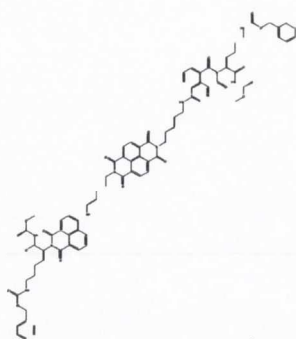
1.72 μM
(1.49-1.98)



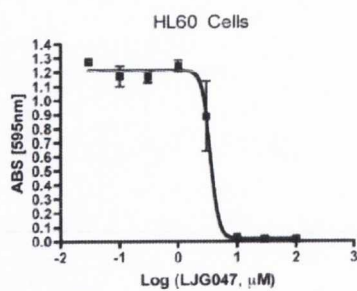
LJG040



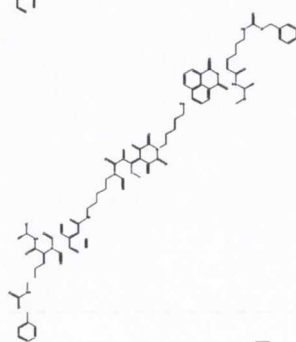
2.88 μM



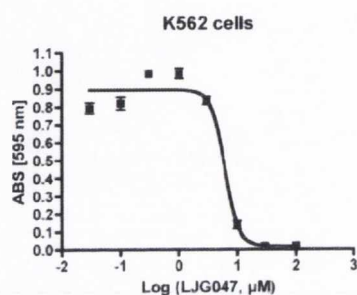
LJM182



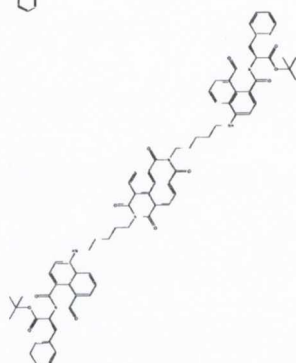
3.50 μM
(0.456-26.9)



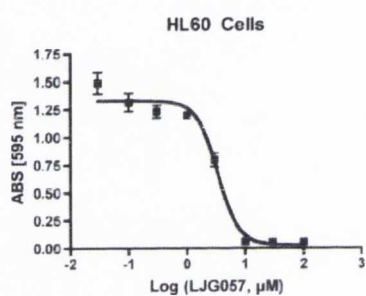
LJM182



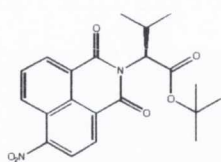
10.5 μM



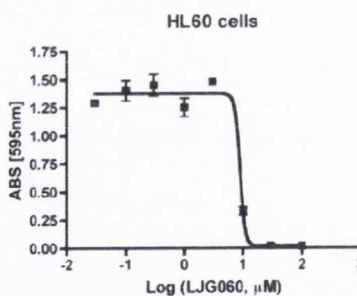
LJM182



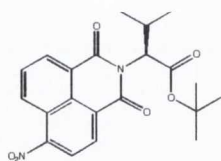
3.37 μM
(2.72 – 4.17)



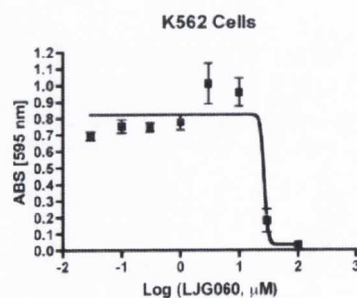
LJM182



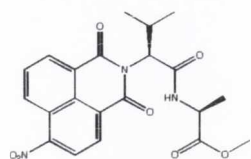
8.88 μM



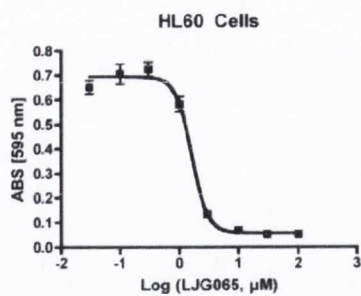
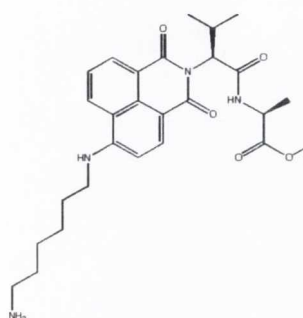
LJM182



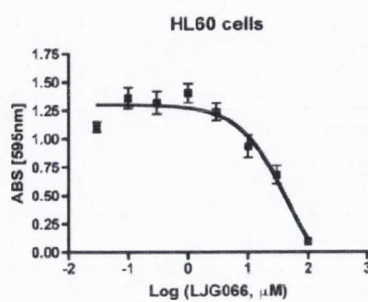
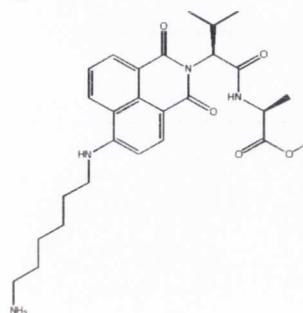
27.1 μM



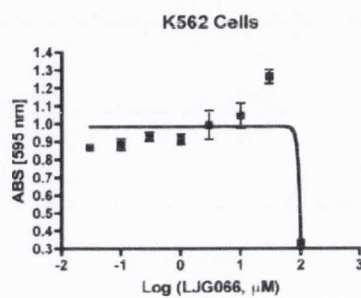
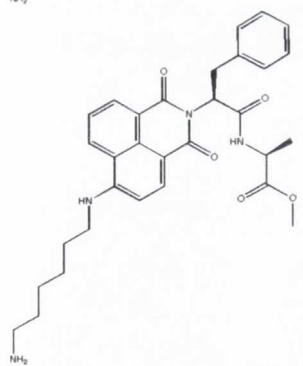
LJM065

1.62 μM
(1.38 – 1.91)

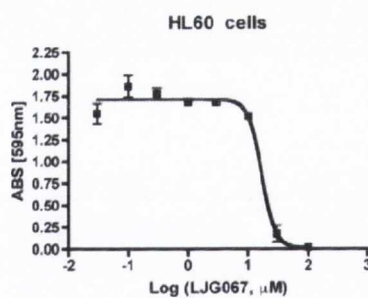
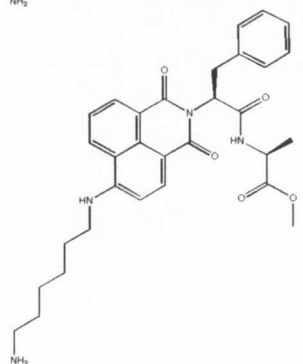
LJM066

46.2 μM 

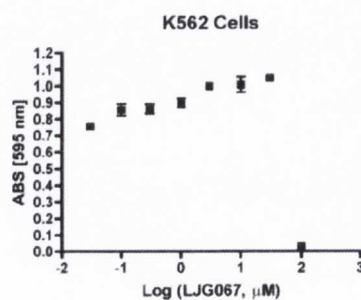
LJM066

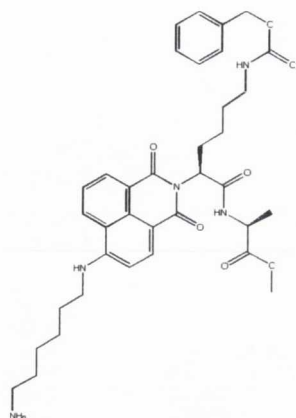
> 100 μM 

LJM067

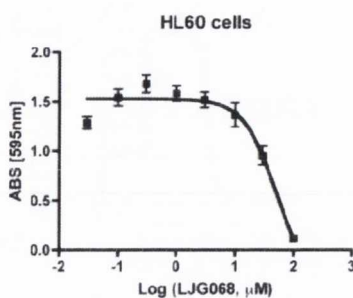
16.8 μM 

LJM067

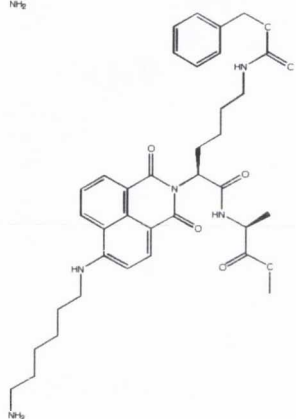
>100 μM



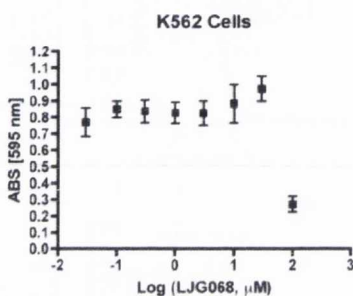
LJM068



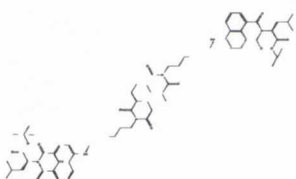
52.1 μM



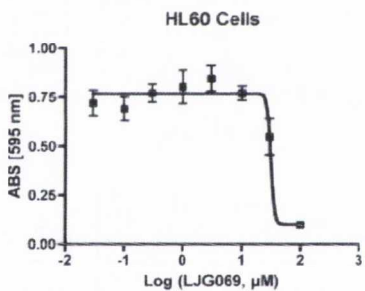
LJM068



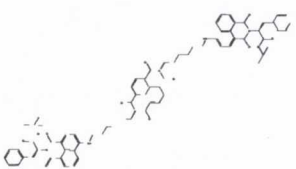
>100 μM



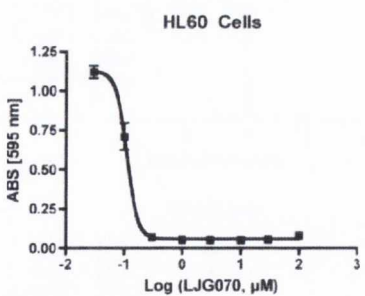
LJM069



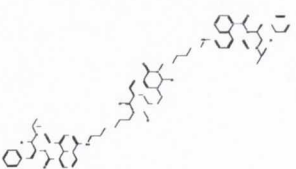
31.6 μM



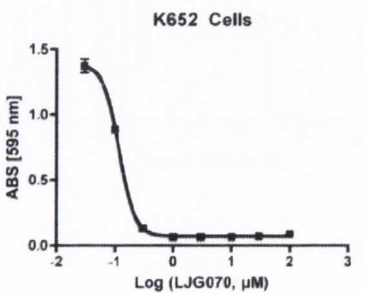
LJM070



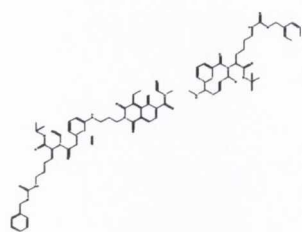
0.110 μM
(0.100 - 0.127)



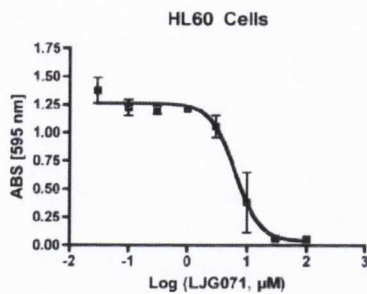
LJM070



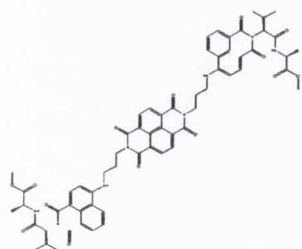
0.117 μM
(0.111 - 0.123)



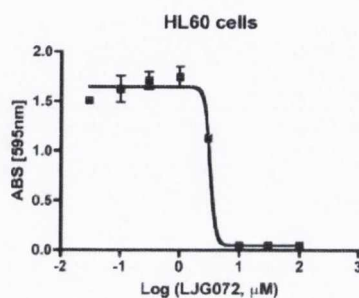
LJM071



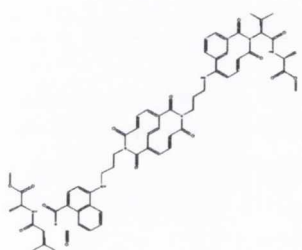
6.37 μM
(4.13 – 9.83)



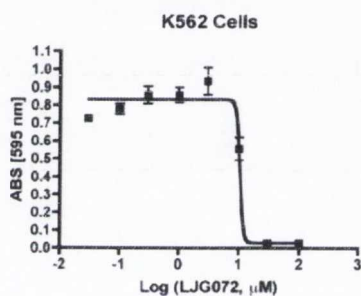
LJM072



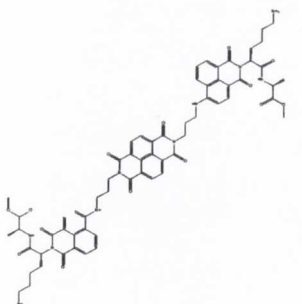
3.24 μM



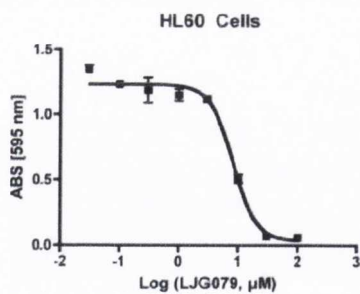
LJM072



10.4 μM



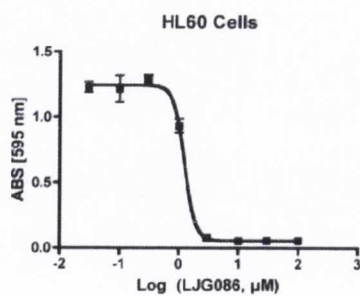
LJM079



8.18 μM
(6.79 – 9.87)



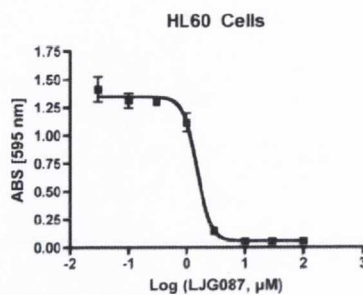
LJM086



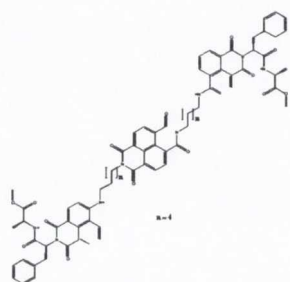
1.25 μM
(0.975 – 1.60)



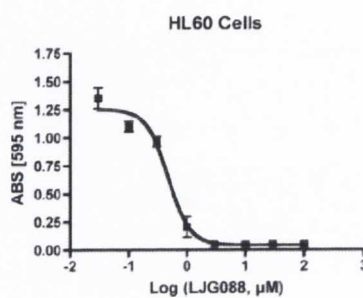
LJM151



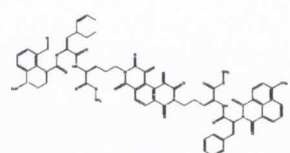
1.51 μM
(1.25 – 1.83)



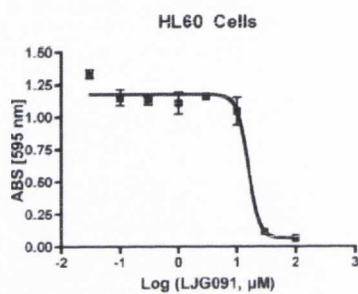
LJM152



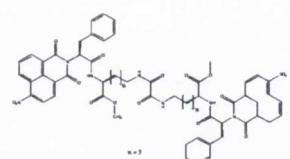
0.469 μM
(0.372–0.590)



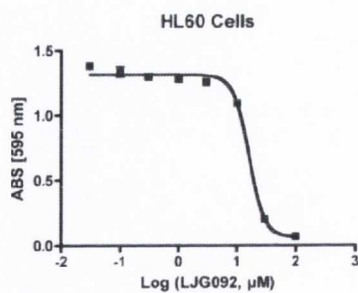
LJM153



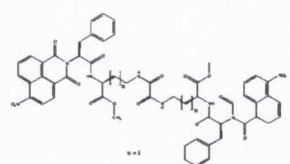
15.6 μM
(10.7 – 22.7)



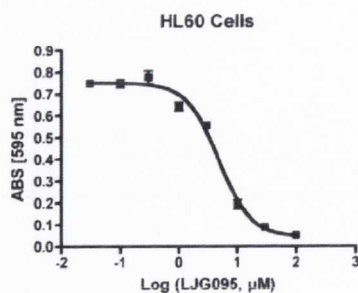
LJM154



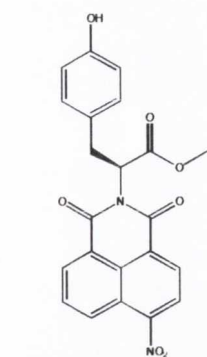
16.0 μM
(14.3 – 18.0)



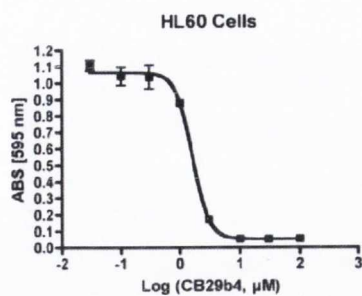
LJM155



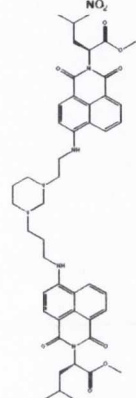
4.82 μM
(3.95 – 5.87)



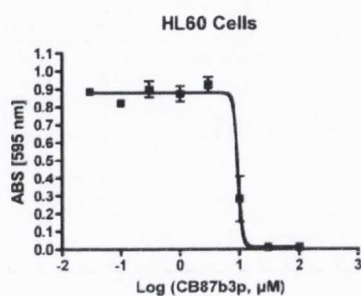
CB29b4



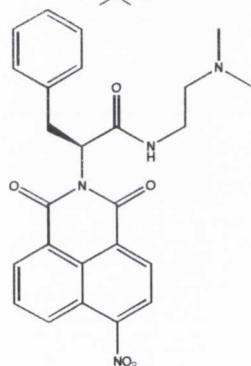
1.60 μM
(1.38 – 1.84)



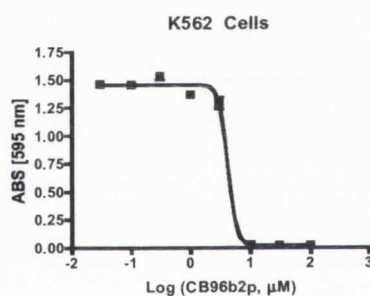
CB87b3p



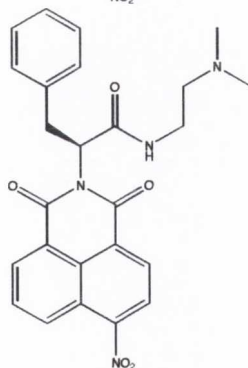
9.37 μM



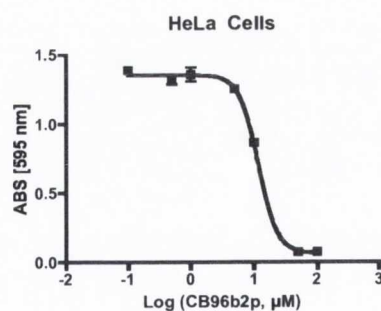
CB96b2p



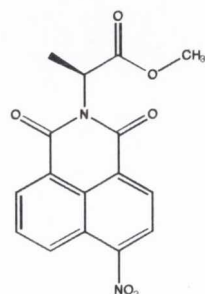
4.22 μM
(2.49-7.15)



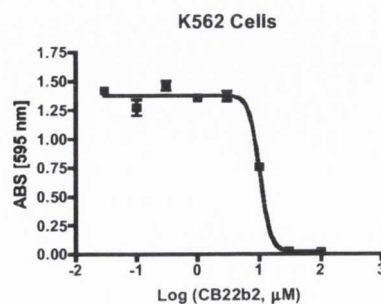
CB96b2p



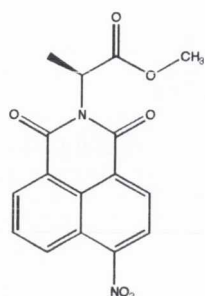
11.8 μM



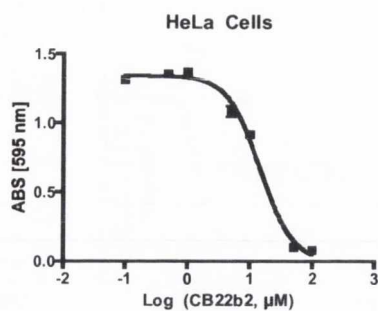
CB22b2



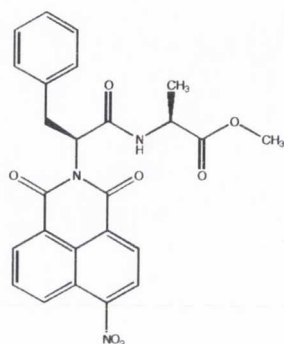
10.3 μM
(9.00-11.9)



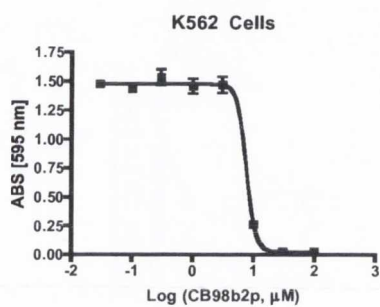
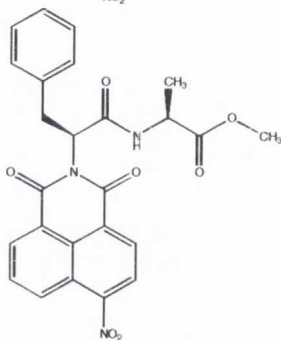
CB22b2



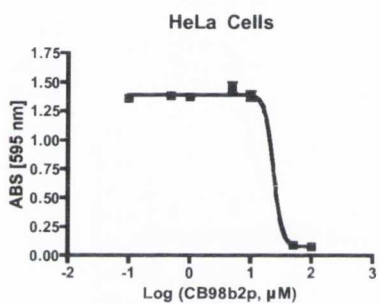
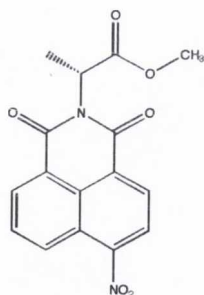
14.4



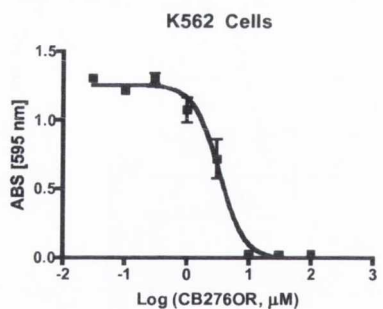
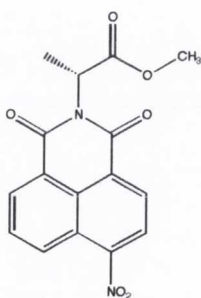
CB98b2p

7.95 μM
(4.52-12.4)

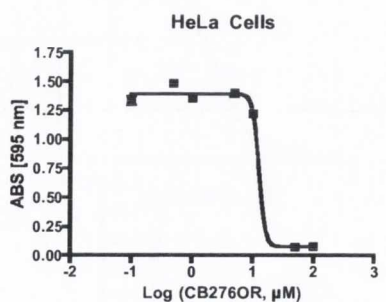
CB98b2p

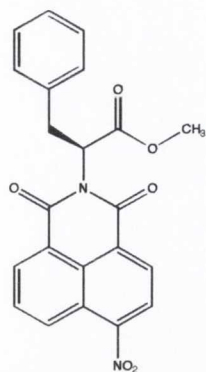
23.3 μM 

CB276OR

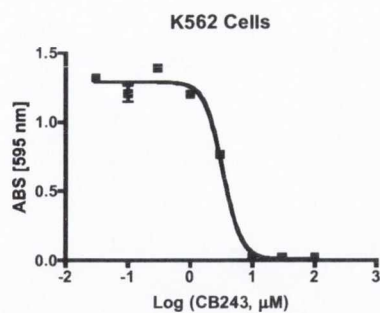
3.22 μM
(2.56-4.05)

CB276OR

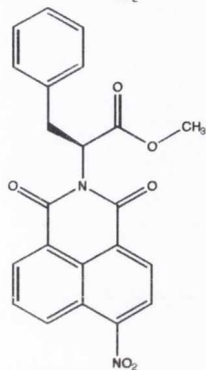
12.5 μM



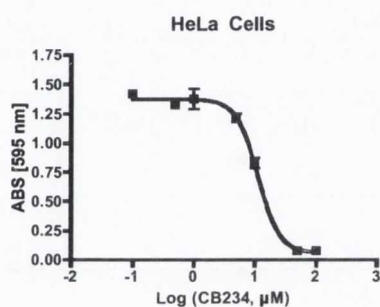
CB243



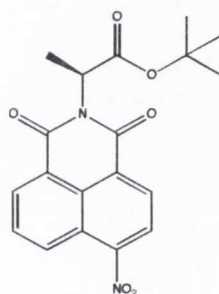
3.36 μM
(2.99-3.77)



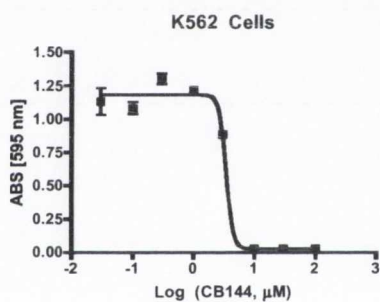
CB243



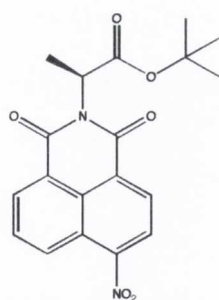
11.5 μM



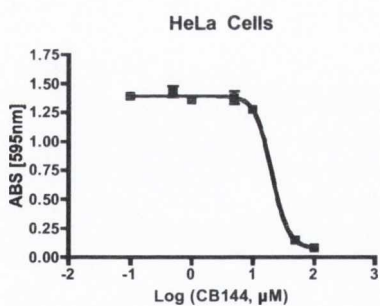
CB144



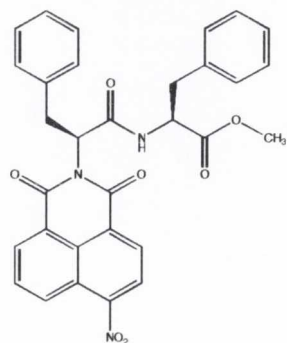
3.44 μM



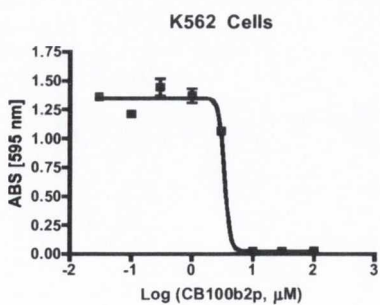
CB144



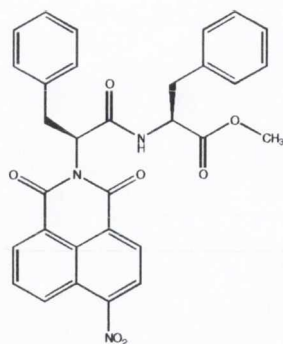
20.7 μM



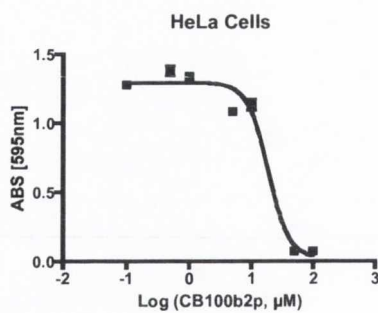
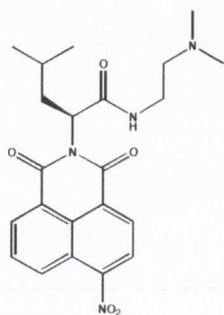
CB100b2p



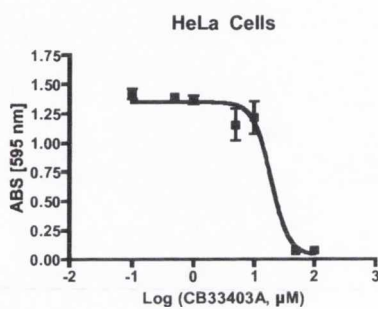
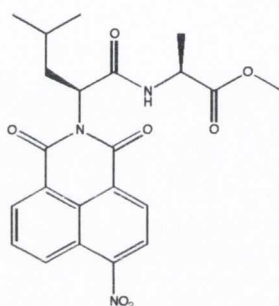
3.45 μM



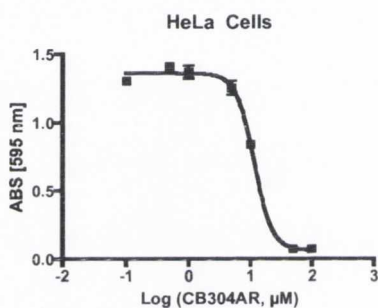
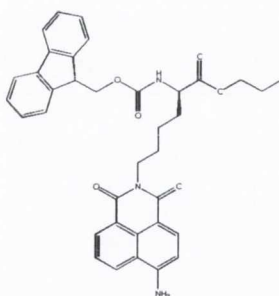
CB100b2p

18.6 μM 

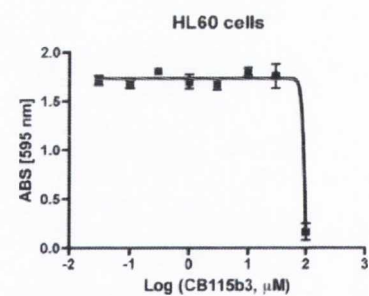
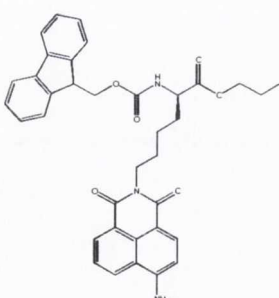
CB33403a

19.0 μM 

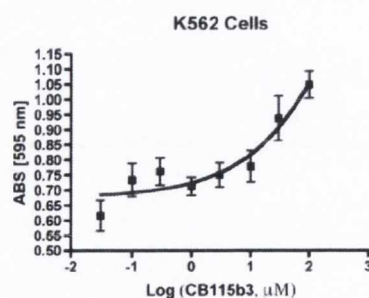
CB304ar

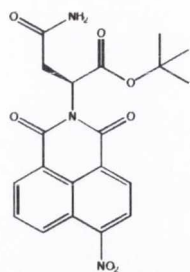
11.4 μM 

CB115b3

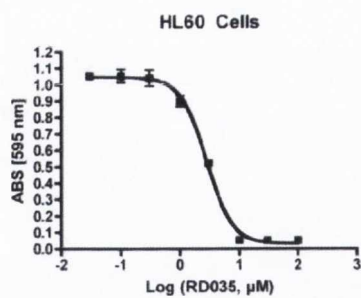
>100 μM 

CB115b3

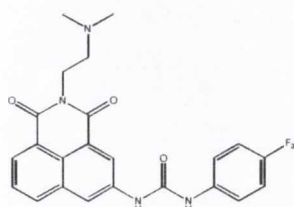
>100 μM



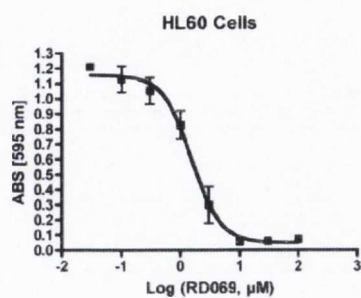
RD035



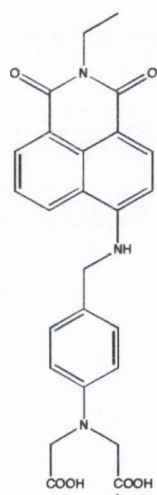
2.78 μM
(2.44 – 3.16)



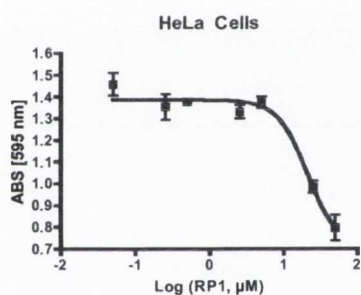
RD069



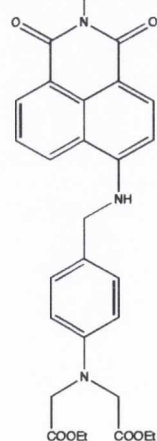
1.54 μM
(1.14 – 2.07)



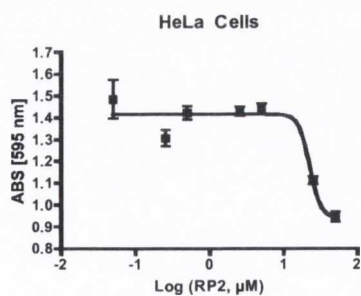
RP1



21.3 μM



RP2



22.6 μM

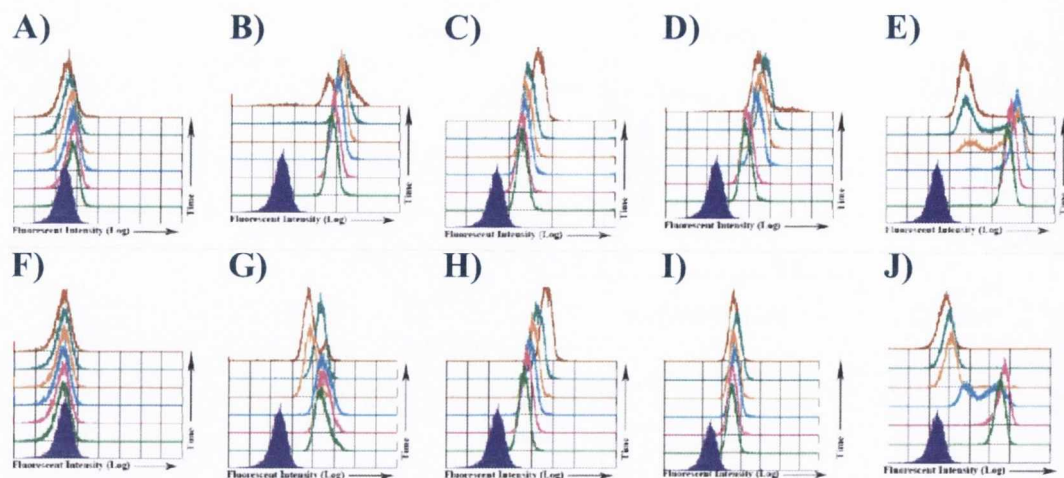


Figure A1.1 Plots of emitting fluorescence intensity from HL-60 cells. HL-60 cells were treated with $0.5 \mu\text{M}$ A, F) 47, B, G) 48, C, H) 49, D, I) 50 and E, J) 51 30 min. (—), 60 min. (—), 3 hours (—), 6 hours (—), 9 hours (—) and 24 hours (—). Untreated cells are shown as a solid purple peak. (Section 2.2.1, Chapter 2)

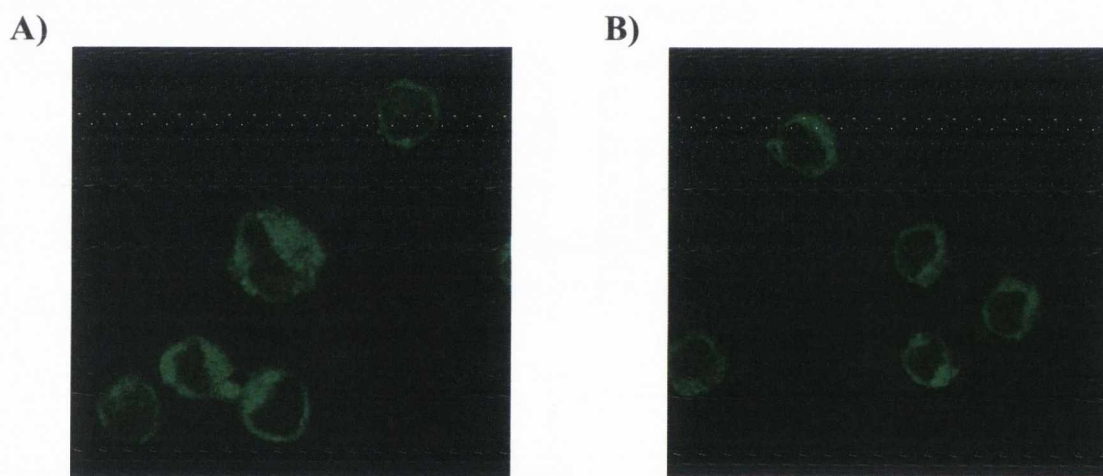


Figure A1.2 Confocal images of HL60 cells after 24 hours treatment with A) 47 and B) 51. Cells were treated with compounds for 24 hours. Prior to visualization, excess compound was washed off by rinsing in PBS three times. The cells were then spun to a glass slide, fixed and mounted. Compounds were excited by a 488 nm argon laser and 50-530 nm band pass filter was used to detect the fluorescence. The slides were investigated at magnification $\times 63$. (Section 2.2.2, Chapter 2)

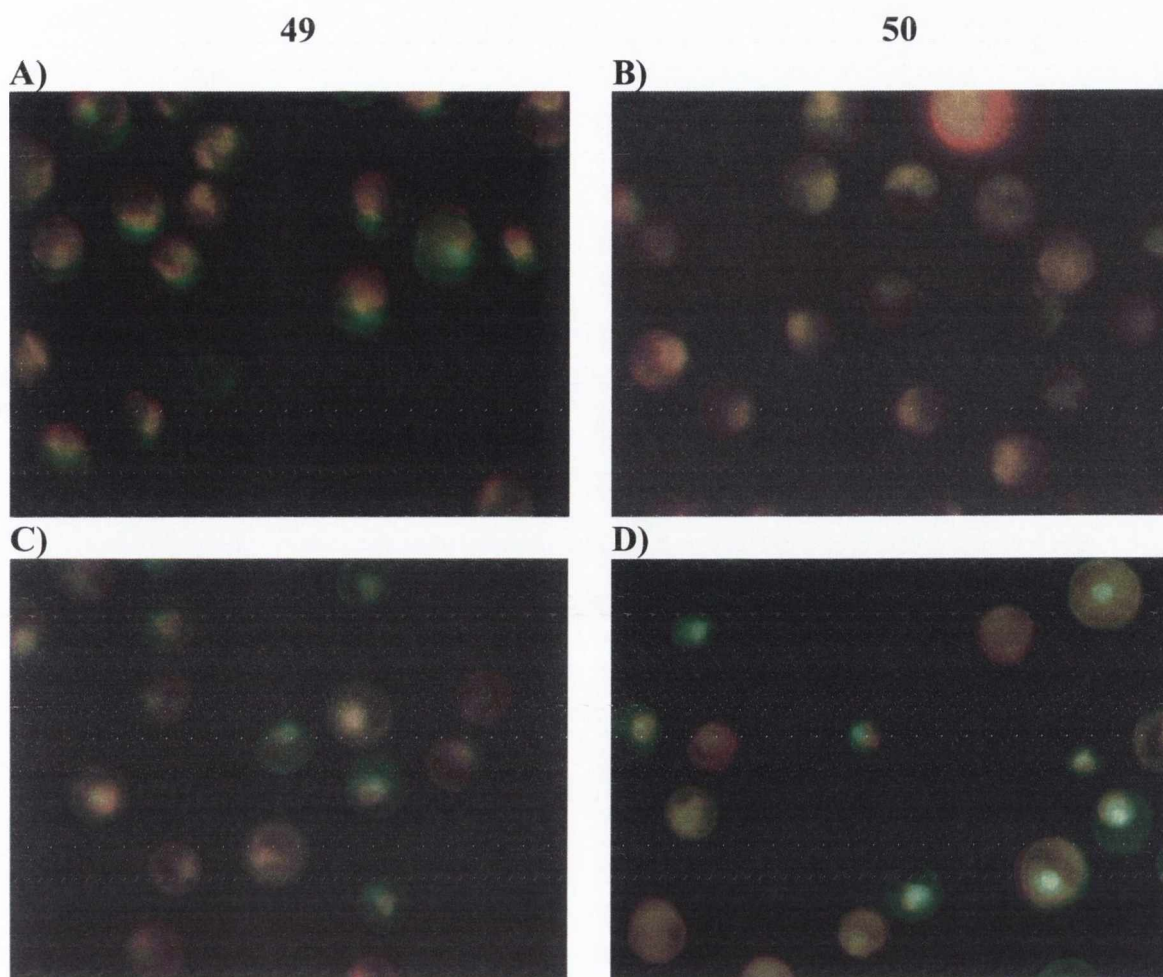


Figure A1.3 Overlaid images from colocalization studies of compounds 49 and 50. HL-60 cells were incubated with compounds 49 and 50 at $1.0 \mu\text{M}$ concentration (green) for 24 hours and counterstained with **A-B**) Mitotracker Red for mitochondria detection (500 nM) and **C-D**) NBD C_6 -ceramide ($5 \mu\text{M}$) for the detection of the Golgi complex. The slides were investigated at magnification $\times 60$ under a fluorescent microscope. (Section 2.2.2, Chapter 2)

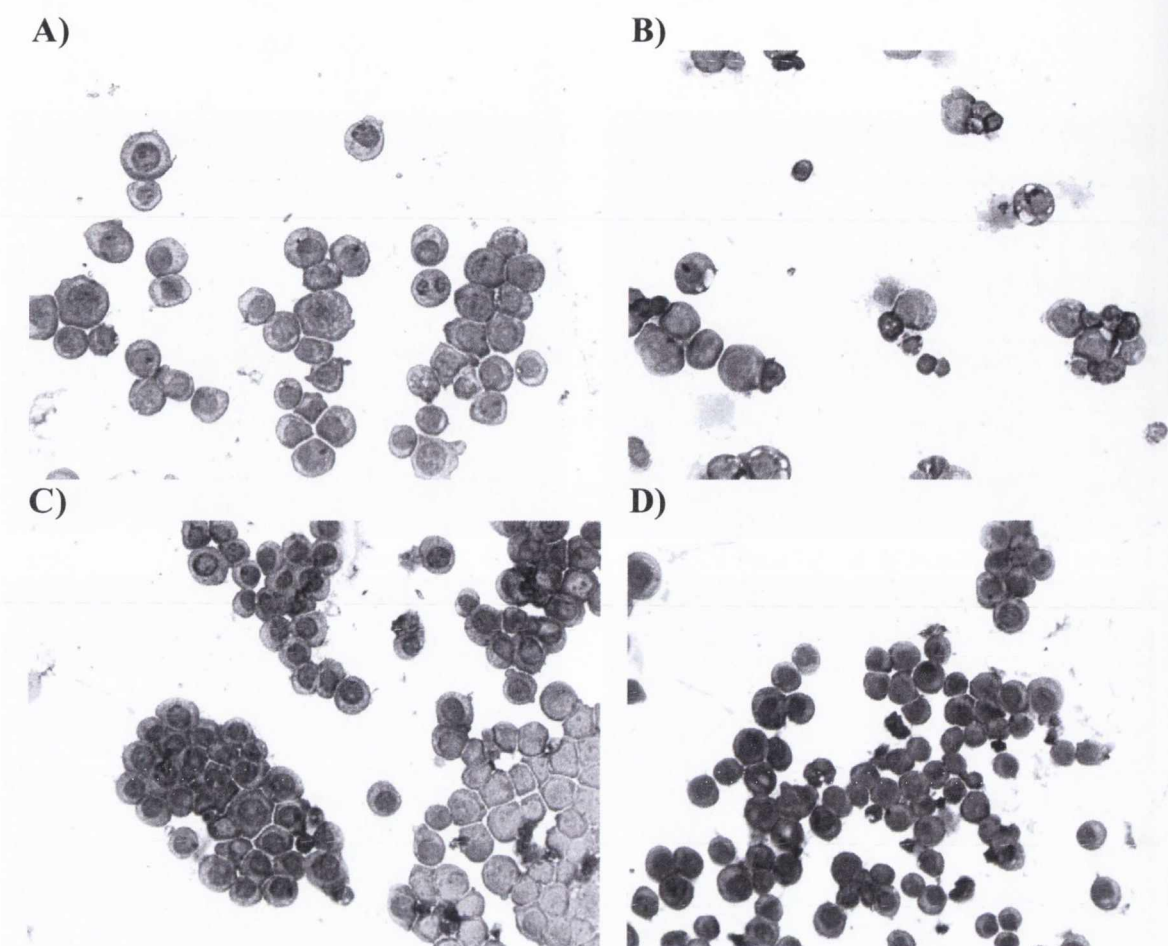


Figure A1.4 Haematoxylin and eosin staining of HL-60 cells treated with A) 47, B) 48, C) 49 and D) 50 for 24 hours. (Section 2.4.1, Chapter 2)

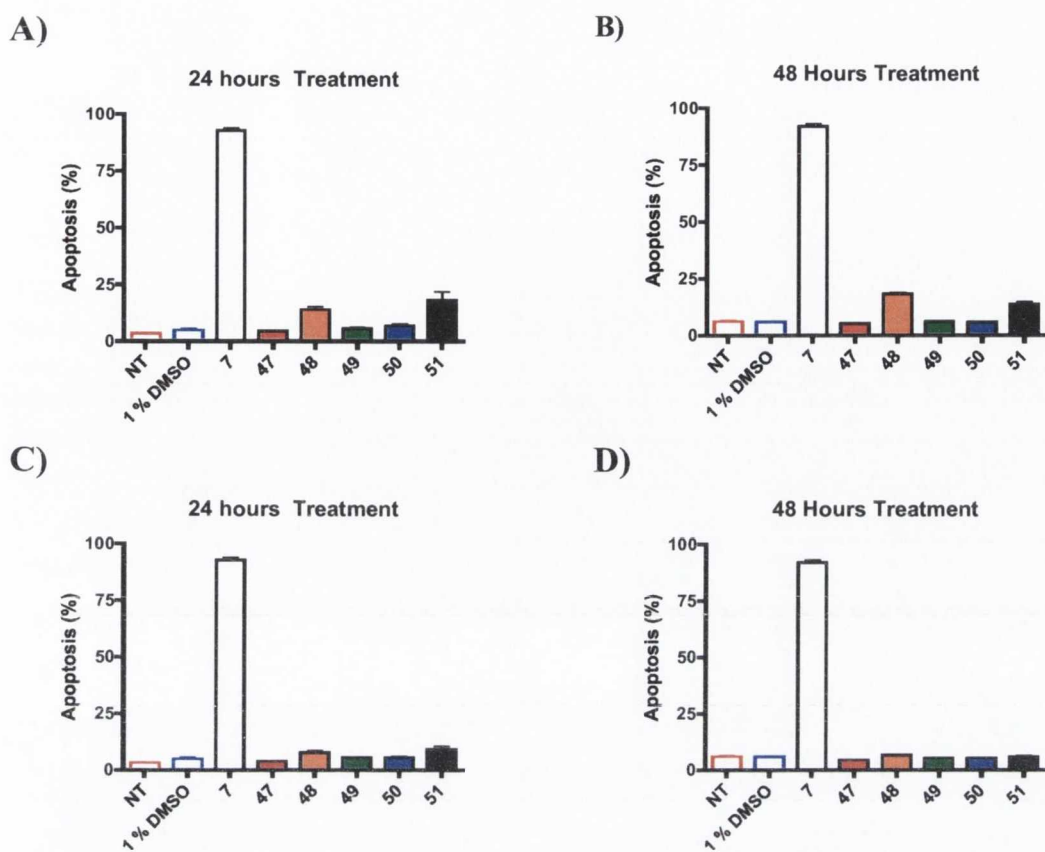


Figure A1.5 Morphological changes in HL-60 cells by treatment of peptide derivatives. HL-60 cells were treated with **A, B)** 1.0 μ M **C, D)** 0.5 μ M for 24 or 48 hours as indicated. The percentage of apoptosis induced by 1 % DMSO (\square), 7 (1.0 μ M, \square), 47 (\blacksquare), 48 (\blacksquare), 49 (\blacksquare), 50 (\blacksquare) and 51 (\blacksquare). Untreated cells are shown as \square . Each graph represents three separate experiments. (Section 2.4.1, Chapter 2)

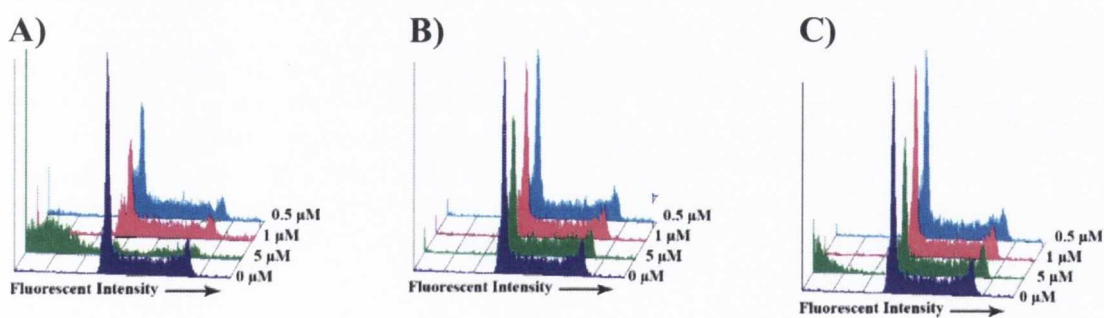


Figure A1.6 Cell cycle analysis on HL-60 cells after treatment with compounds A) 48, B) 49 and C) 50 after 24 hours. HL-60 cells were treated with compounds 48-50 for 24 hours before analysis on the flow cytometry. The solid purple histogram represents untreated cells. Other colors are indicative of concentrations, 5.0 μ M (\blacksquare), 1.0 μ M (\blacksquare) and 0.5 μ M (\blacksquare). (Section 2.5, Chapter 2)

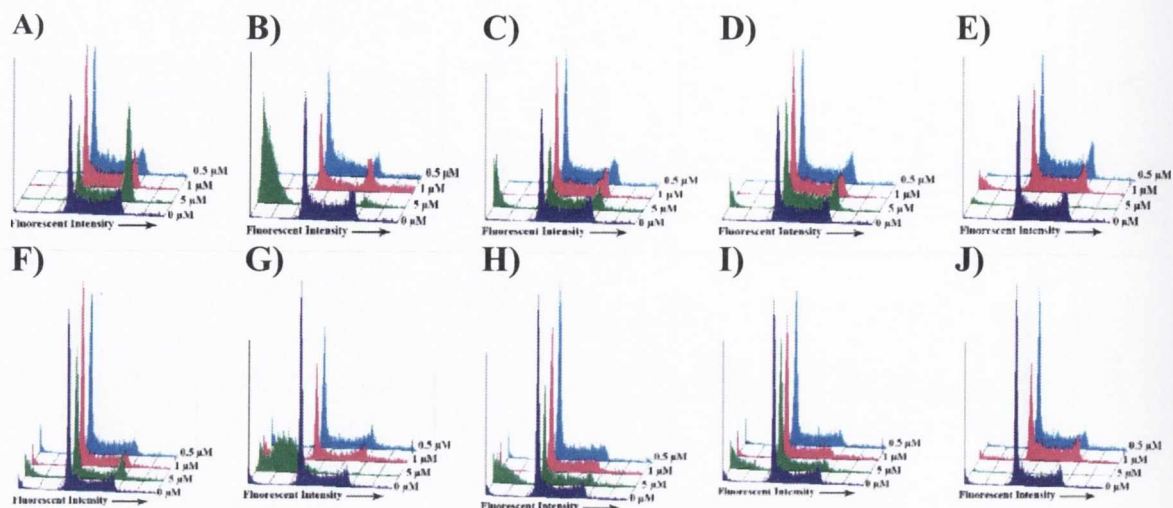


Figure A1.7 Cell cycle analysis on HL-60 cells after treatment with compounds 47-51 after 24 hours. HL-60 cells were treated with compounds 48-50 at three concentration, 5.0 μM (■), 1.0 μM (■) and 0.5 μM (■) for 24 hours before analysis on the flow cytometry. The solid purple histogram represents untreated cells. (Section 2.5, Chapter 2)

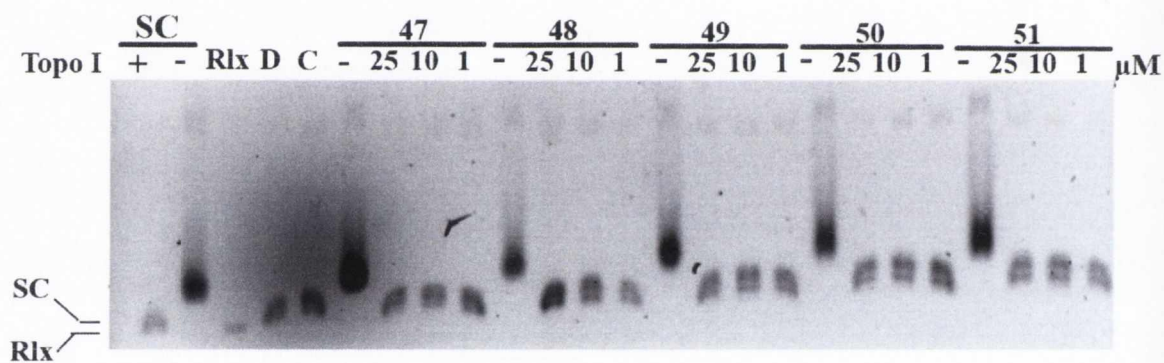


Figure A1.8 Topoisomerase I in the presence of EtBr/SYBr green. Compounds were incubated with a supercoiled plasmid (0.5 μg) and Topo I (5 units), at three different concentrations (25, 10 and 1 μM) as indicated above each lane. Lanes labeled - represent reactions done in the absence of Topo I. Lane D represents the effects of 1 % DMSO and Rlx indicates the position of the relaxed DNA. Lane C represents the effects of a Topo I poison (Camptothecin, 100 μM) and finally the Topo I, + and Topo I, - represents the reactions done in presence and in absence of Topo I, respectively. (Section 2.6, Chapter 2)

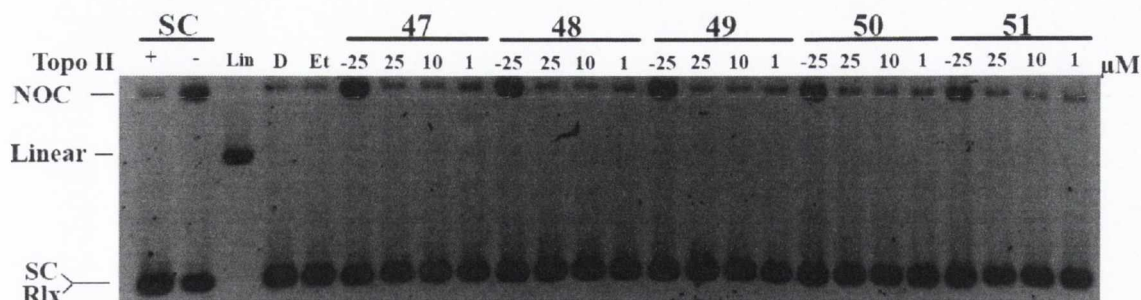


Figure A1.9 Topoisomerase I in the absence of EtBr/SYBr green. Compounds were incubated with a supercoiled plasmid (0.5 μg) and Topo II (5 units), at three different concentrations (25, 10 and 1 μM) as indicated above each lane. Lanes labeled - represent reactions done in the absence of Topo II. Lane D represents the effects of 1 % DMSO and Lin indicates the position of the linear marker. Lane C represents the effects of a Topo II poison (Etoposide, 100 μM) and finally the Topo II, + and Topo II, - represents the reactions done in presence and in absence of Topo II, respectively. (Section 2.6, Chapter 2)

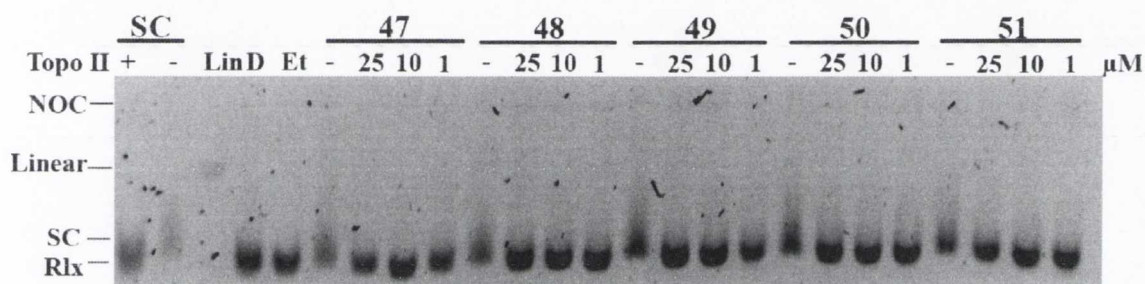


Figure A1.10 Topoisomerase I in the presence of EtBr/SYBr green. Compounds were incubated with a supercoiled plasmid (0.5 μg) and Topo II (5 units), at three different concentrations (25, 10 and 1 μM) as indicated above each lane. Lanes labeled - represent reactions done in the absence of Topo II. Lane D represents the effects of 1 % DMSO and Lin indicates the position of the linear marker. Lane C represents the effects of a Topo II poison (Etoposide, 100 μM) and finally the Topo II, + and Topo II, - represents the reactions done in presence and in absence of Topo II, respectively. (Section 2.6, Chapter 2)

Appendix 2

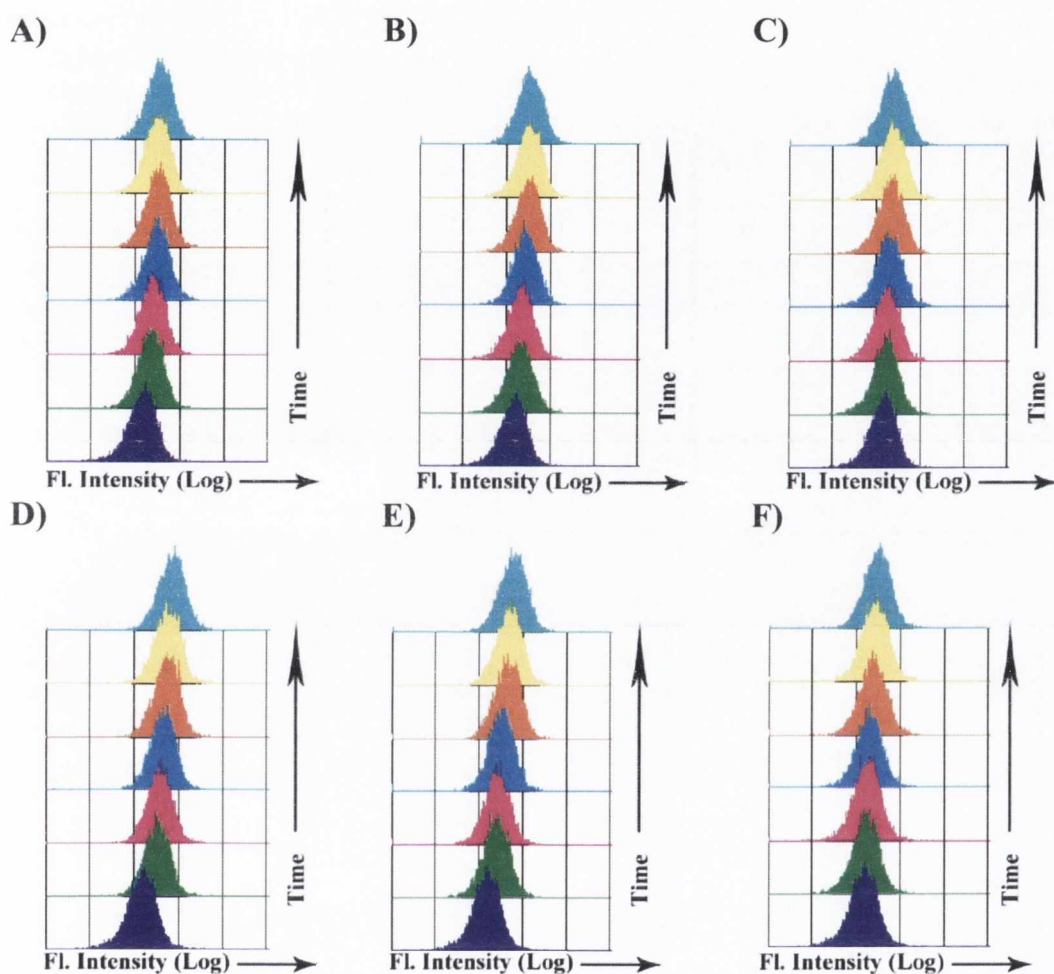
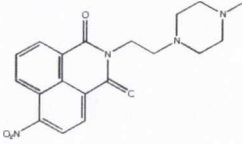
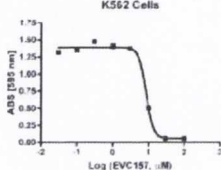
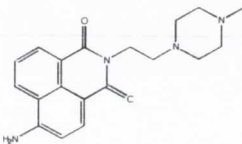
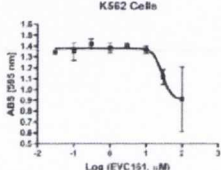
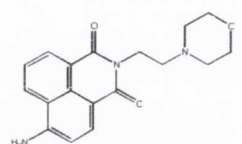
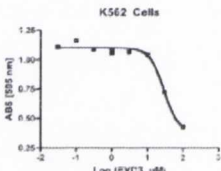
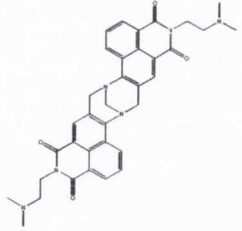
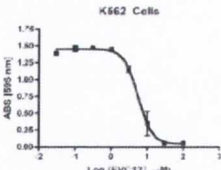
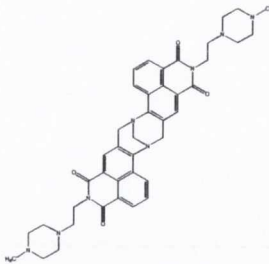
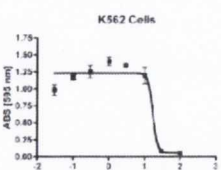
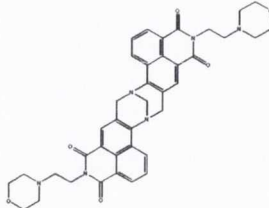
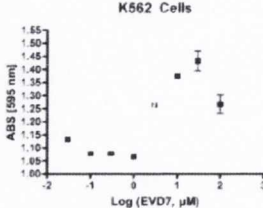
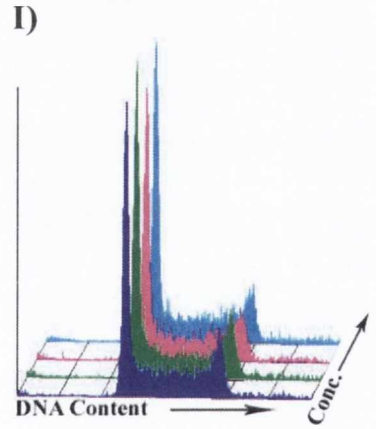
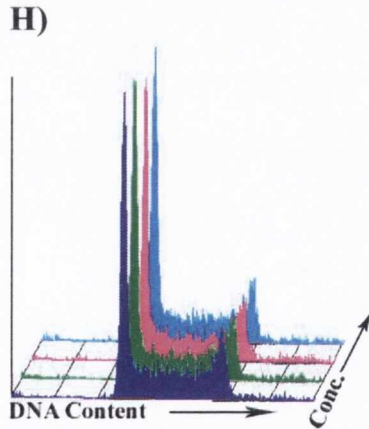
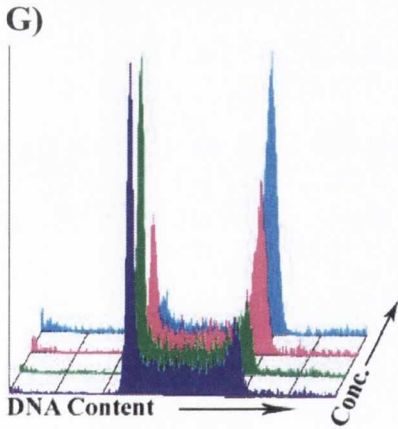
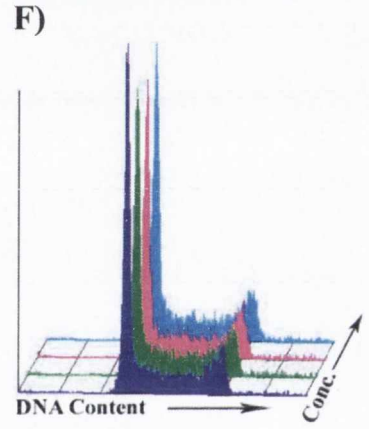
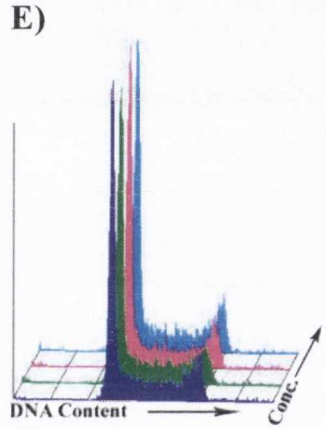
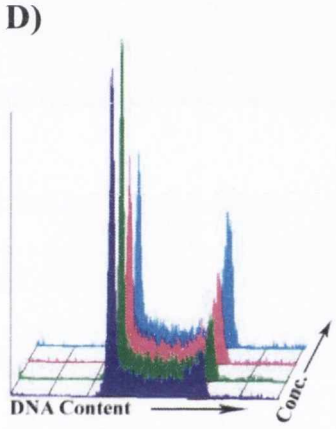
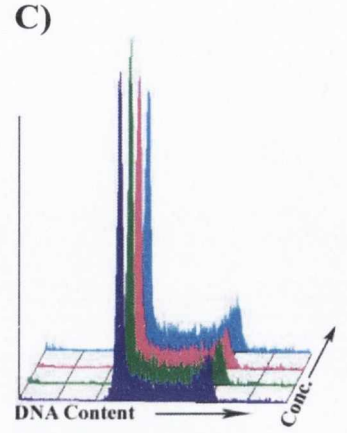
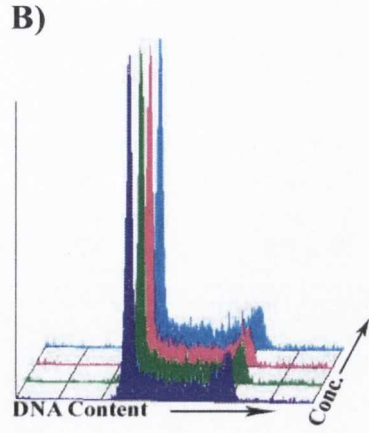
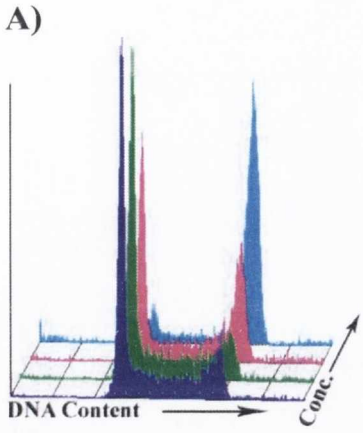


Figure A2.1 Plots of the emitting fluorescence intensity from HL-60 cells. Cells treated with **A,D** 68 (1.0 μM), **B, E** 69 (1.0 μM), **C, F** 70 (1.0 μM) for 30 min. (■), 60 min. (■), 3 hours (■), 6 hours (■), 9 hours (■) and 24 hours (■). Untreated cells are shown as a solid purple peak. (Section 3.2, Chapter 3)

Table A2.1 Cytotoxicity studies of Tröger's base compounds and their precursors in K562 cells. K562 cells were incubated with representative compounds for 24 hours or 48 hours at seven different concentrations (100, 33, 10, 3.3, 1, 0.3, 0.1 and 0.03 μM). Each concentration was done in triplicate. The amount of cells was then quantified using the MTT assay as discussed in Section 2.3 in Chapter 2 and the corresponding EC_{50} value was determined from the graph. The EC_{50} value refers to the concentration of a compound, which induces a response halfway between the baseline and the maximum. The range in brackets shows 95% confidence intervals.

	EVC157		8.543 μM (7.266 – 10.05)
	EVC161		28.08 μM (14.27 – 55.22)
	EVD3		28.67 μM (24.10 – 34.11)
	EVC127		5.537 μM (4.397 – 6.972)
	EVC183		17.00 μM (6.916 – 41.77)
	EVD7		> 100 μM



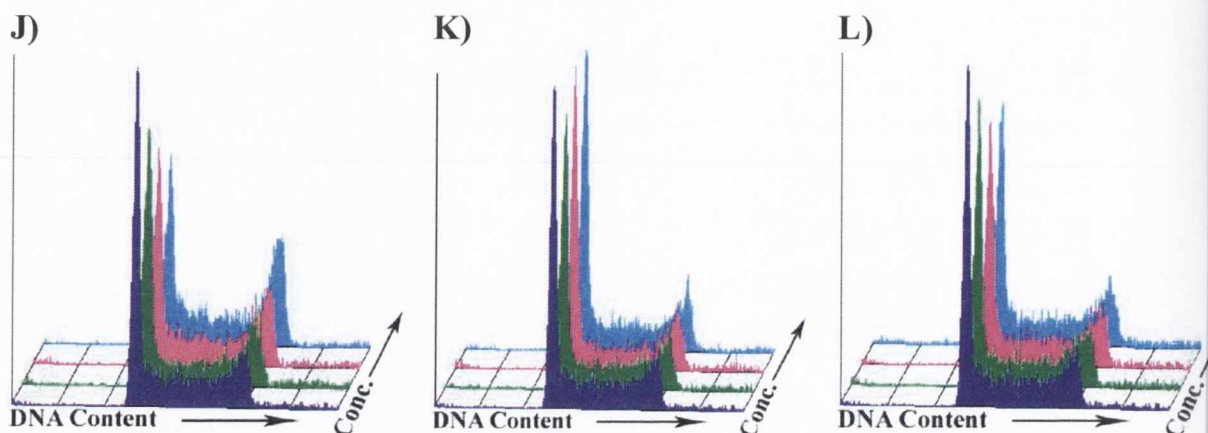
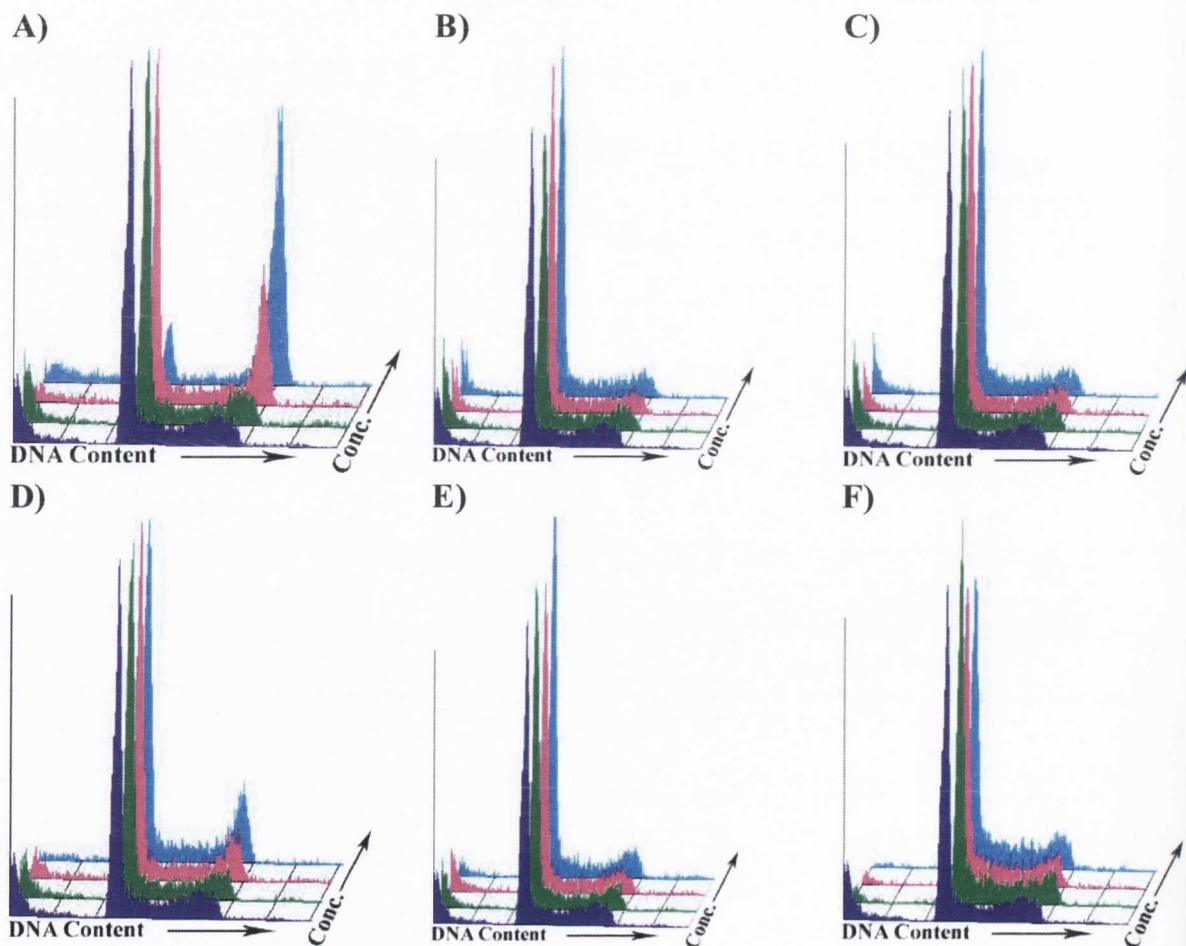
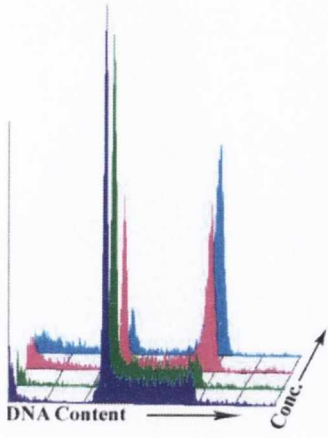


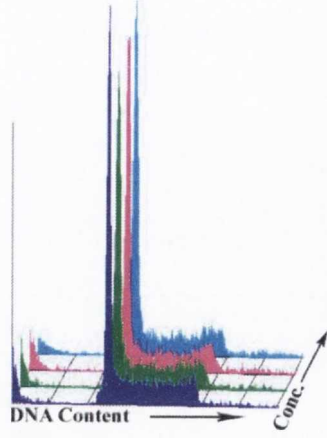
Figure A2.2 Cell cycle analysis of precursors 65-67 and Tröger's bases 68-70 after 24 hours treatment. HL-60 cells were incubated with the 4-amino 1,8-naphthalimides **A, G)** 65, **B, H)** 66 and **C, I)** 67 and the tröger's bases **D, J)** 68, **E, K)** 69 and **F, L)** 70 at three concentrations 10 μM (■), 5.0 μM (■) and 1.0 μM (■) for 24 hours. The vehicle-treated cells are shown as a purple solid peak. (Section 3.4, Chapter 3)



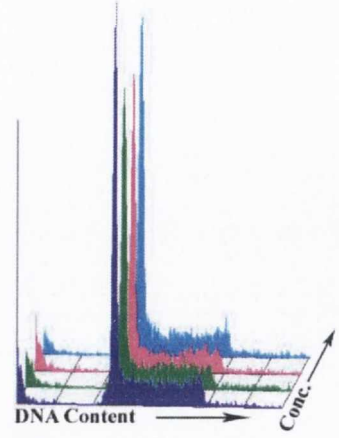
G)



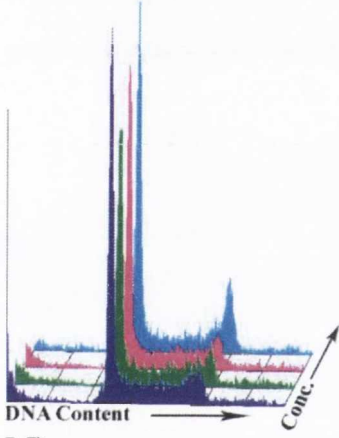
H)



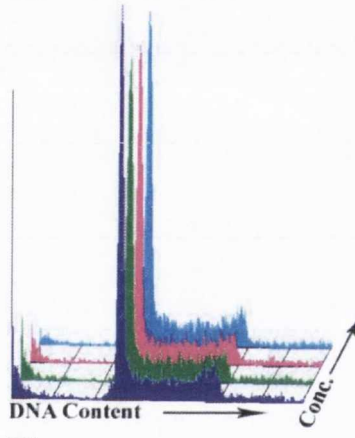
I)



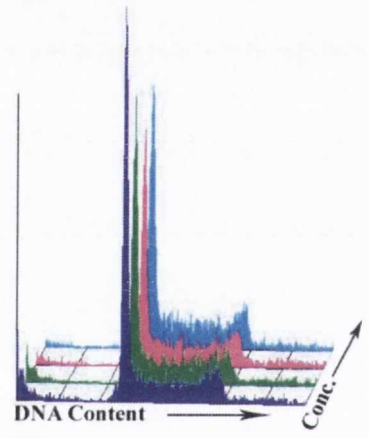
J)



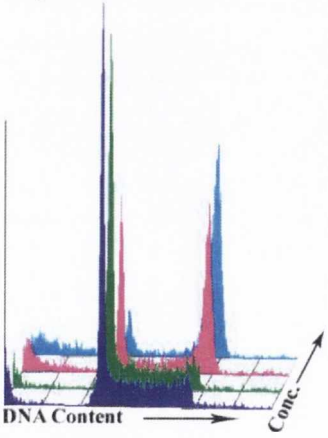
K)



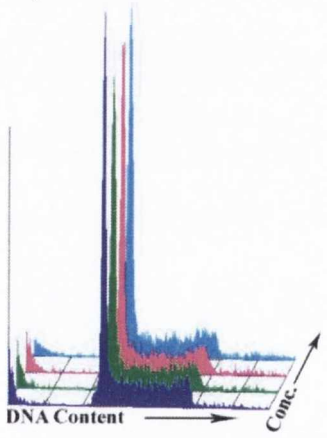
L)



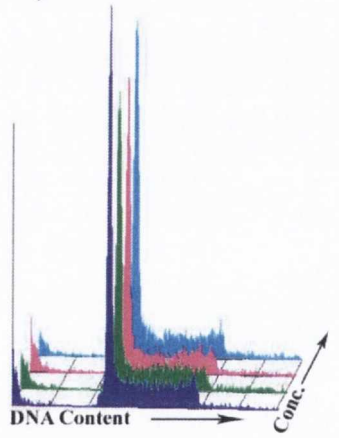
M)



N)



O)



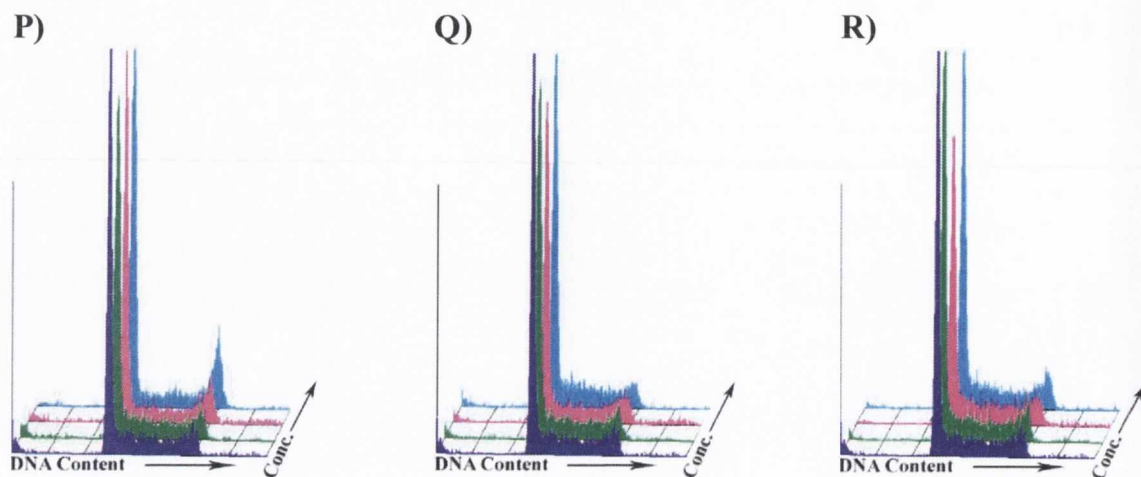


Figure A2.3 Cell cycle analysis of precursors 65-67 and Tröger's bases 68-70 after 48 hours treatment. HL-60 cells were incubated with the 4-amino 1,8-naphthalimides **A, G, M) 65, B, H, N) 66** and **C, I, O) 67** and the tröger's bases **D, J, P) 68, E, K, Q) 69** and **F, L, R) 70** at three concentrations 10 μM (■), 5.0 μM (■) and 1.0 μM (■) for 48 hours. The vehicle-treated cells are shown as a purple solid peak. (Section 3.4, Chapter 3)

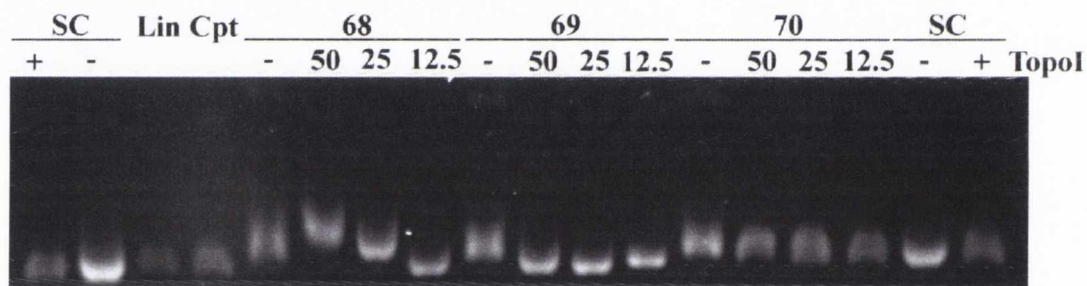


Figure A2.4 Topo I analysis of compounds 68-70 at 50, 25 and 12.5 μM concentrations in the presence of SYBr green. Compounds were incubated with a supercoiled plasmid (0.5 μg) and Topo I (5 units), at three different concentrations (50, 25 and 12.5 μM) as indicated above each lane. Lanes labeled -25 represent reactions done in the absence of Topo I. Lin indicates the position of the linear marker. Lane Cpt represents the effects of a Topo I poison (Camptothecin, 100 μM) and finally the Topo I, + and Topo I, - represents the reactions done in presence and in absence of Topo I, respectively. (Section 3.5, Chapter 3)

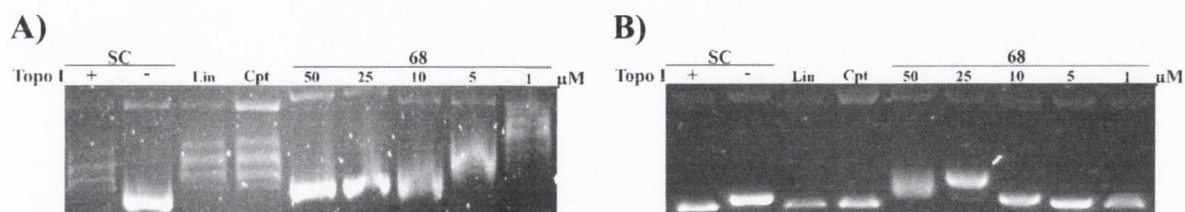


Figure A 2.5 Topo I analysis of 68 at 50, 25, 10, 5 and 1 μM concentrations in the A) absence of SYBr green and B) presence of SYBr green. Compound 68 was incubated with a supercoiled plasmid (0.5 μg) and Topo I (5 units), at five different concentrations (50, 25, 10, 5 and 1 μM) as indicated above each lane. Lin indicates the position of the linear marker. Lane Cpt represents the effects of a Topo I poison (Camptothecin, 100 μM) and finally the Topo I, + and Topo I, - represents the reactions done in presence and in absence of Topo I, respectively. (Section 3.5, Chapter 3)

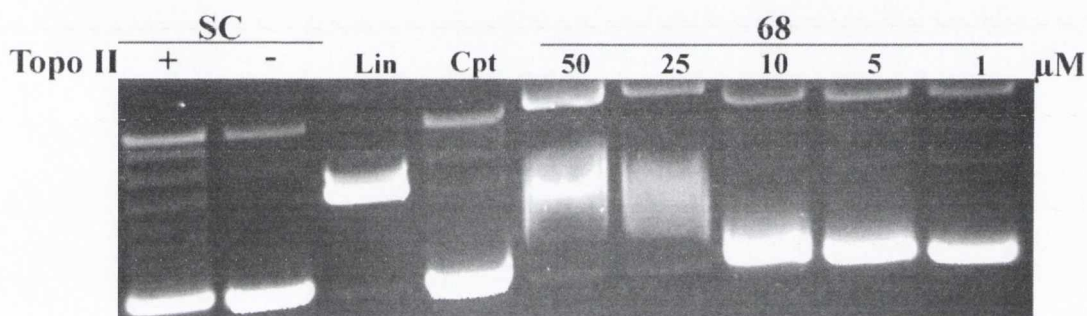


Figure A 2.6 Topo I analysis of 68 at 50, 25, 10, 5 and 1 μM concentrations in the absence of SYBr. Compound 68 was incubated with a supercoiled plasmid (0.5 μg) and Topo I (5 units), at five different concentrations (50, 25, 10, 5 and 1 μM) as indicated above each lane. Lin indicates the position of the linear marker. Lane Cpt represents the effects of a Topo I poison (Camptothecin, 100 μM) and finally the Topo I, + and Topo I, - represents the reactions done in presence and in absence of Topo I, respectively. (Section 3.5, Chapter 3)

Appendix 3

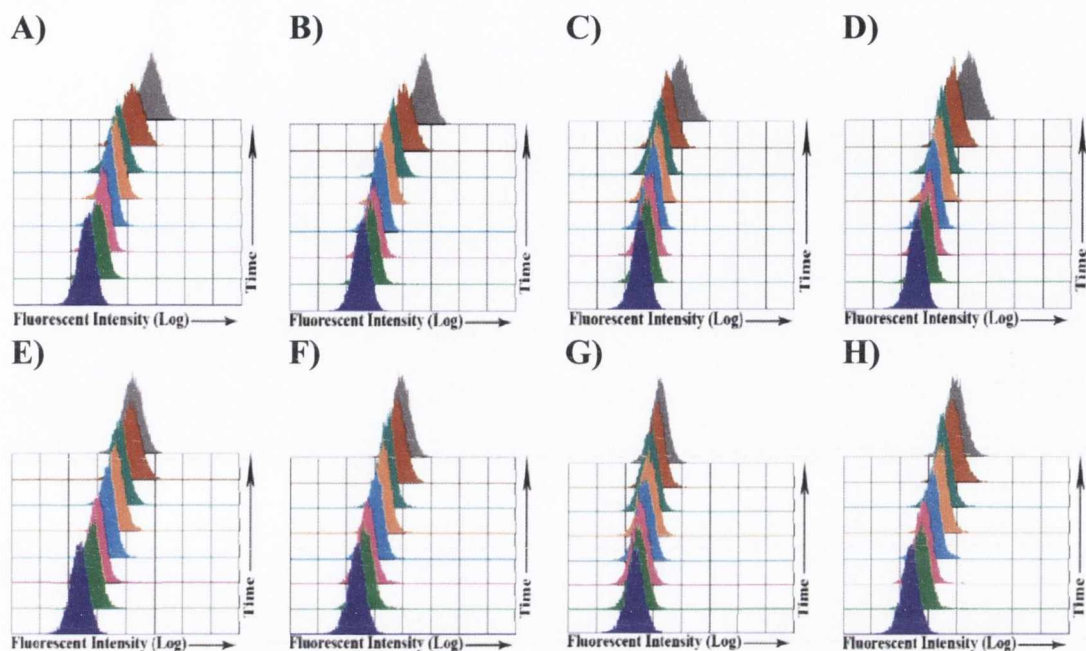


Figure A3.1 Plots of emitting fluorescence intensity from K562 cells. Cells were treated with **A and E** 74 (1.0 μM), **B and F** 75 (1.0 μM), **C and G** 76 (1.0 μM) and **D and H** 77 (1.0 μM) for 30 min. (■), 60 min. (■), 3 hours (■), 6 hours (■), 9 hours (■), 24 hours (■) and 48 hours (■). Untreated cells are shown as a solid purple peak. (Section 4.2.1, Chapter 4)

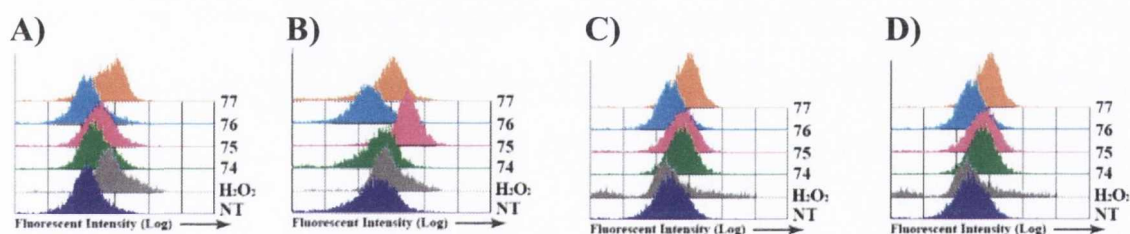


Figure A3.2 Formation of ROS in K562 cells treated with 74-77 **A and C** in the dark and **B and D** irradiation with 8 J/cm^2 light dose. Cells were either left untreated (■), treated with 74 (10 μM , ■), 75 (10 μM , ■), 76 (10 μM , ■) and 77 (10 μM , ■) for 24 hours before irradiation. Cells were analyzed 48 hours after irradiation. Cells were also treated with H_2O_2 (2 mM, ■) for 5 minutes as a positive control. (Section 4.4, Chapter 4).

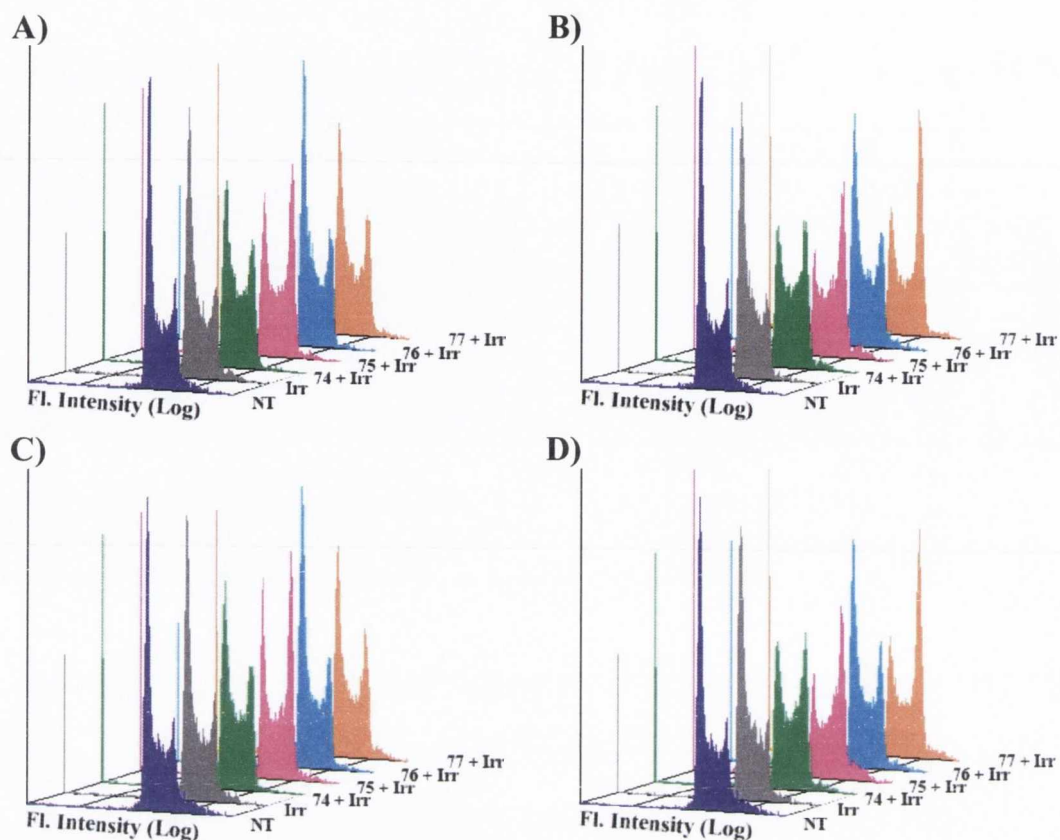


Figure A3.3 Cell cycle analysis of K562 cells irradiated with A and C) 4 J/cm^2 and B and D) 8 J/cm^2 . Cells were either left untreated (■), treated with 74 ($10 \mu\text{M}$, ■), 75 ($10 \mu\text{M}$, ■), 76 ($10 \mu\text{M}$, ■) and 77 ($10 \mu\text{M}$, ■) for 24 hours before irradiation. Cells were analyzed 48 hours after irradiation. Untreated, irradiated cells are indicated with a solid gray plot (■).

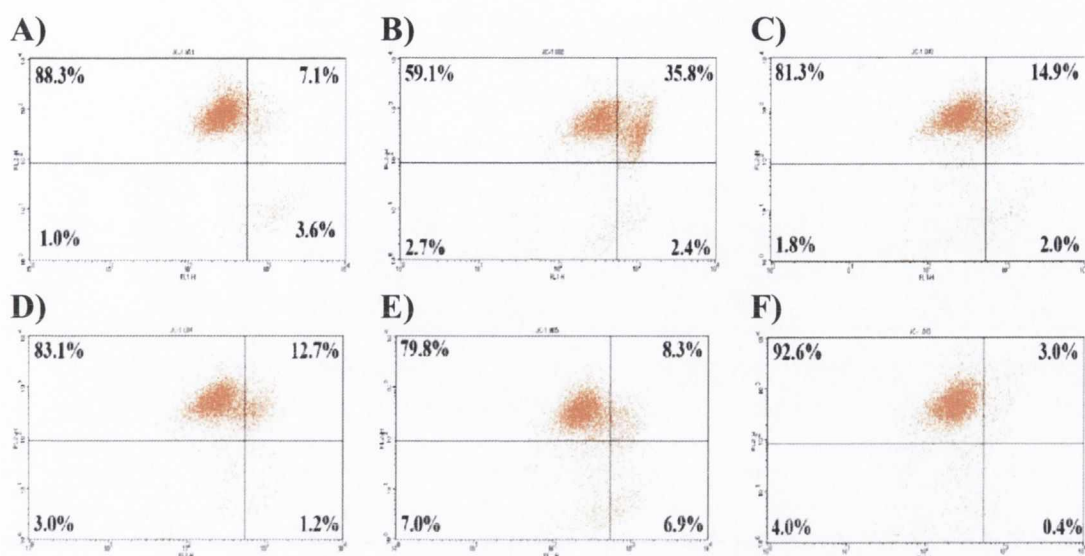


Figure A3.4 Flow cytometry plots of K562 cells treated with 74-77 in the dark. Cells were incubated with **A)** vehicle (RPMI medium), **B)** Etoposide (100 μ M), **C)** 74 (10 μ M), **D)** 75 (10 μ M), **E)** 76 (10 μ M) and **F)** 77 (10 μ M) for 72 hours at 37 $^{\circ}$ C in the presence of 5% CO₂ before they were analysed by flow cytometry as described in Section 4.6 in Chapter 4.

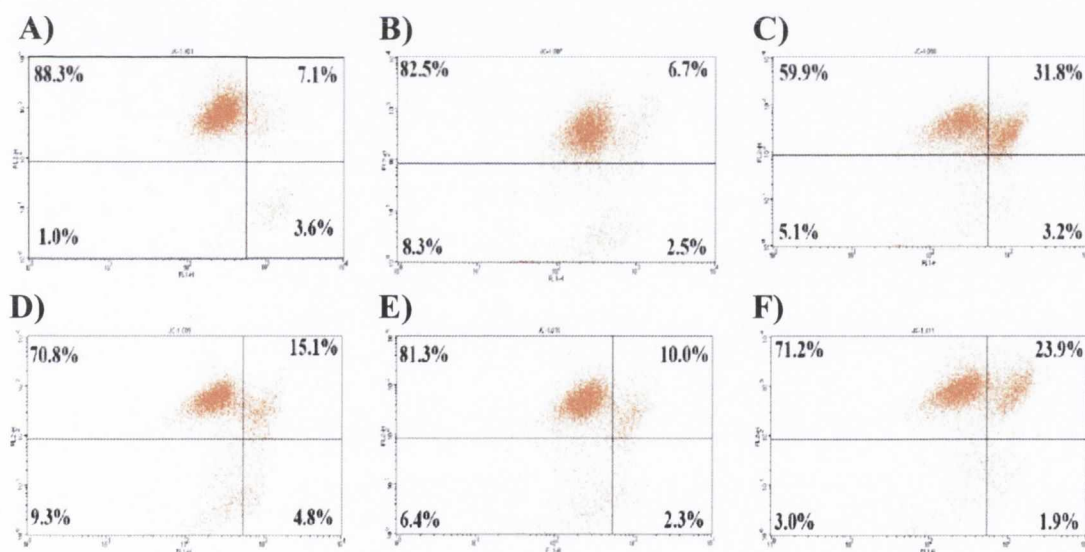


Figure A3.5 Flow cytometry plots of K562 cells treated with 74-77 and irradiated with 8 J/cm². Cells were incubated with **A)** vehicle (RPMI medium) in the dark, **B)** vehicle, **C)** 74 (10 μ M), **D)** 75 (10 μ M), **E)** 76 (10 μ M) and **F)** 77 (10 μ M) for 72 hours at 37 $^{\circ}$ C in the presence of 5% CO₂ before they were irradiated with 8 J/cm² light dose. The cells were then incubated for 48 hours before being analysed by using flow cytometry as described in the text.

Appendix 4

Table A4.1 Selected bond lengths and angles for 99. This data was obtained from analysis of the CIF files using Mercury®.

Bond	Length (Å)	Bond	Angle (deg)
C1 N1	1.344	O1 C1 N1	123.52
N1 C2	1.402	H4 N4 C7	114.04
C2 N2	1.329	H1 N1 C2	115.39
N2 C6	1.339	N1 C2 N2	112.79
C6 C7	1.504	N2 C6 C7	116.09
N4 C8	1.409	O2 C7 N4	124.76
H1 N2	2.333	H4 N4 C8	113.97
N2 H4	2.135	H9 C9 C8	120.98
H4 H9	2.086	N4 C8 N3	121.79
O2 N3	2.950		
O1 H3	2.302		

Table A4.2 Selected bond lengths and angles for 107. This data was obtained from analysis of the CIF files using Mercury®.

Bond	Length (Å)	Bond	Angle (deg)
C16 O5	1.467	H1 C1 N2	89.26
O5 C12	1.346	C16 O5 C12	121.24
C12 O4	1.208	O5 C12 O4	126.22
C12 N1	1.366	C12 N1 C1	127.22
N1 C1	1.40	N1 C1 N2	112.4
C1 N2	1.339	N2 C5 N3	118.9
N2 C5	1.344	N3 C11 O1	125.84
C5 N3	1.397	O1 C11 C8	121.1
N3 C11	1.357	N4 C9 C13	117.9
C11 O1	1.221	C13 O2 C14	114.76
C11 C8	1.512	O2 C13 O3	124.6
N4 C9	1.338		
C9 C13	1.50		
C13 O3	1.211		
C13 O2	1.323		
O2 C14	1.452		